ELECTROMIGRATION TIME-TO-FAILURE

ANALYSIS USING A LUMPED ELEMENT MODEL

by

Wan Sazaley Wan Ismail

A Doctoral Thesis

**Submitted in partial fulfilment of the requirements
for the award of the Degree of Doctor of Philosophy
of Loughborough University**

June 2001

ABSTRACT

This thesis presents a theoretical and computer simulation of Electromigration behaviour in the Integrated Circuit (ICs') interconnection , with a particular emphasis on the analysis of the Time to Failure (TTF) produced through the Lumped Element model .

The current and most accepted physical model for Electromigration is the Stress Evolution Model which forms the basis for the development of the current Lumped Element Model. For early failures, and ignoring transport through the grain bulk, the problem reduces to that of solving the equations for stress evolution equation on the complex grain boundary networks which make the cluster sections of the near-bamboo interconnect. The present research attempts to show that the stress evolution in a grain boundary cluster network mimics the time development of the voltage on an equivalent, lumped C-R-C Π electrical network. By solving the node voltage equation by a Matrix approach, the Time to Failure at a particular node along any complex grain boundary can be obtained when the local stress at the node reaches some threshold value. The present work also introduces the concept of the Signal or Elmore delay to estimate the Electromigration Time to Failure.

The models are applied to various grain boundary configurations including the single grain boundary, example of a complex grain boundary clusters and more realistic grain boundary structures. The current model is validated by comparing the results to those from existing literature. The current model enables the effect of the microstructural or geometrical properties on the Time to Failure to be analyse in greater detail. A log-normal distribution has been obtained by both the Lumped element model and the signal delay approximation method. The time-scale obtained for the Mean Time to Failure and the Deviation Time to Failure are within the range of the experimental results of existing references.

ACKNOWLEDGEMENT

The author would like to express gratitude and appreciation to his academic adviser, Dr. Vincent Dwyer, for his help on matters regarding with mathematical, mechanical and physical problems relating to the study. Also the author like to thank for his encouragement, guidance, support and most of all the belief in me to carry out this project succesfully.

Appreciation also goes to all the staffs in the International Electronics Reliability Institute (IERI), for all the friendship they provided. Many thanks also go to the IT technical staff for helping me on computer related problems. Also many thanks to secretary of the Electronic and Electrical Engineering department for research student, Miss Lynn for helping with administrative work.

The author is also extremely grateful to the Standards and Industrial Research Institute of Malaysia (SIRIM Berhad) for the award of a research studentship particularly En. Megat Ahmad Zaki for recommending and supporting the application.

Many thanks to the parents, Haji Wan Ismail Wan Sulaiman and Hajjah Zainab Sam Abdul Latiff for their love ,support and encouragement. Last and not least ,the wife Fadilah Din for her moral support, patience and love given throughout the period of this work and also to the three sons Wan Azmir, Wan Afiq and Wan Muhammad Ariff, who provided the cheerful moments whenever the time was tough during the project and writing of this thesis. It is to them this work is dedicated.

CONTENTS

iv

iii. The function file: imroot

B.2:   Single grain boundary with both ends blocked

i.   The script file: sg2ball.m

B.3:   An example of a typical complex grain boundary with one end has a

vacancy supply c_0 and the rest are blocked

i.   The script file: net1ball.m

B.4:   An example of a typical complex grain boundary with all ends blocked.

i.   The script file: net2ball.m

B.5:   Realistic interconnects

i.   The script file: vrnoittf.m
ii.   The function file: annealing.m
iii.   The function file: geometry.m
iv.   The function file: labgrain1.m
v.   The function file: labgrain2.m
vi.   The function file: conmtrix.m
vii.   The function file: lamda1.m
viii.   Thefunction file: grwth1.m
ix.   The function file: trisw1.m
x.   The function file: output.m
xi.   The function file: figvrnoi.m
xii.   The function file: lablenode.m
xiii.   The function file: slices2.m
xiv.   The function file: newgeometry.m
xv.   The function file: newnode.m
xvi.   The function file: vrttf.m
xvii.   The function file: vrmat4.m
xviii. The function file: vres3.m
xix.   The function file: vcmat3.m
xx.   The function file: vnoicap3.m
xxi.   The function file: vcrgmat.m
xxii.   The function file:vcrg3.m
xxiii. The function file:vumat3.m
xxiv.   The function file:elmore3.m

(note: the appendices above can be retrieved by Microsoft word)

Appendix C   Publication

Electromigration voiding in nanoindented, single crystal Al line

Journal of Applied Physics, 2001, Vol 89(5)

SYMBOLS AND NOMENCLATURE

(i)   **Units and Prefixes**

A	Ampere
^0C	Centigrade
cm	Centimetre
m	Metre
M	Mega(10^6)
Pa	Pascal
G	Giga(10^9)
eV	Electron-volt
k	Kilo(10^3)
Hz	Hertz
μ	Micro(10^{-6})

(ii)   **Principal Symbols used in model**

B	Elastic modulus of material
C	Capacitor
$\underset{=}{C}$	Capacitance matrix
C_A	Atomic concentration
C_v	Vacancy concentration
c_0	Initial vacancy concentration
c_{cr} or c^*	Critical vacancy concentration
D	Diffusion coefficient
D_A	Atomic diffusion coefficient
D_A^{GB}	Atomic diffusion coefficient along grain boundary
D_{eff}	Effective diffusion coefficient

D_v^{GB}	Vacancy diffusion coefficient along grain boundary
d	Grain size
e	Electron charge
$\underset{=}{G}$	Conductance matrix
$\underset{=}{R}$	Resistance matrix for signal delay
R_{rc}	Rate of resistance change
k	Boltzman's constant
T	Temperature
Q or E_A	Activation energy
J	Flux
J_A	Atomic flux
J_V	Vacancy flux
j	Current density
W	Line width
t_f	Failure time
t_{50}	Mean Time to Failure
T_D	Signal delay
T_{Di}	Signal delay at node i
N_v	Density of diffusing vacancies
N_v^c	Critical number of vacancies
v	Pseudo voltage
v_s	Supply voltage
Z^*	Effective charge of ion
θ	Tilt angle of grain boundary
ψ	Angle of orientation of grain boundary
σ	Stress
σ_{cr}	Critical stress

σ_{sd}	Standard deviation
δ	Width of grain boundary
∇	Gradient
μ_A	Atomic mobilities
μ_v	Vacancies mobilities
γ	Rate of recombination
α	Drift coefficient of electomigration
α_{eff}	Effective drift coefficient of electromigration
$\underline{r}$	Vector length along a grain boundary
s	Number of sections of CR network per grain boundary

(iii)　**Chemical Symbols**

Al	Aluminium
Cu	Copper
SiO_2	Silicon dioxide
Ti	Titanium
TiN	Titanium nitride
W	Tungsten

(iv)　**Abbreviations**

CDF	Cumulative distribution function
CMOS	Complementary metal oxide semiconductor
C-R-C-Π	Capacitor-resistor-capacitor network
DTTF	Deviation of Time to Failure
erf	Error function
erfc	Complementary error function
GB	Grain boundary
LGB	Longest path of the grain boundary

LN	Natural logarithm
MTTF	Median Time to Failure
MOS	Metal oxide semiconductor
RAM	Random access memory
SIA	Semiconductor Industry Association
SEM	Scanning electron microscopy
TTF	Time to Failure
TEM	Transmission electron microscopy

CHAPTER 1

OVERVIEW OF ELECTROMIGRATION AND AIMS OF THE STUDY

1.0   Introduction

Interconnection technology is one of the most critical areas in VLSI and ULSI fabrication. With the increasing complexity of VLSI and ULSI circuits, interconnections may take up almost 65% of the chip area, are therefore there is a growing concern that the reliability of the interconnections will be a major factor limiting the reliability of the chips[Ghate,1986].The predominant failure modes limiting the reliability of interconnects are electromigration, corrosion and the stress-induced formation of voids.[Ghate,1986]

Electromigration has been the subject of scientific study for about 140 years when it was first observed in 1861 by Geradin, the subject is still very much of interest to researchers whose work is often supported by major IC manufacturers.[Ho and Kwok ,1988],[Llyod,1994].The failure mechanism was identified shortly after the production of integrated circuits in early 1960s, and has been a major reliability issue with IC manufacturers ever since. The recent interest in electromigration is closely related to the ever-present goal of producing more circuit functions on a single chip where the technology has progress from small scale integration(SSI) to very large scale integration (VLSI).The latter, consisting of more than 10^6 devices per chip, is at present giving way to ultra large scale integration (ULSI).

The advancement of the IC technology is made possible by the ability to shrink the dimensions of some critical device features such as the interconnect size where the width of the aluminium interconnect (line width) has shrunk from several microns to 0.28 microns in 1998 ,currently it is 0.18 microns and by 2010, the line widths of 0.07 microns are projected[Ohring,1998],[SIA roadmap]. The continual circuit integration and scale reduction has a negative impact on IC reliability, since current densities and

device operating temperature increase which exacerbates the problems of electromigration[Malone and Hummel,1997].

1.1   The Electromigration Process

Electromigration refers to the migration of metal atoms due to the impact of moving electrons. It is also called electro-transport and is essentially a phenomenon of diffusion of atoms activated by the transfer of momentum from a stream of electrons in the presence of an electric field. It can also be referred as the mass transport of metal atoms due to the momentum exchange resulting from the collisions of the metal atoms with the current conduction electrons. The result is a net flux of metal atoms which generally migrate in the same direction as the current flux [Black,1969],[Sigsbee,1973],[[Ho and Kwok,1989]. This literature refers to the study conducted by Professor Huntington and co-workers in 1961 which also explains the mechanism of electromigration which are now widely used and accepted :-

A metal ion which has been thermally activated and is at its saddle point(lifted out of its potential well and is essentially free of the metal lattice), is acted on by two opposing forces in an electrically conducting single band metal. The two forces are:-

i) The electric field applied to the conductor will exert a force on the activated ion in a direction opposite to the electron flow.

ii) The rate of momentum exchange between the conducting electrons colliding with the activated metal ions will exert a force on the metal ion in the direction of the electron flow.

The force on the ion due to the electric field is quite small due to the shielding by electrons therefore, the dominating force is that of the 'electron wind'. As a result, activated metal ions which are upstream (in terms of electron flow) from a vacancy, have a higher probability of occupying the vacancy site than do other near neighbour

ions which surround the vacancy. Metal ions therefore, travel towards the positive end of the conductor. The displacement of metal ions creates vacancies which move toward the negative end. The vacancies condense to form voids while the ions condense at certain discontinuities to form dendrites, whiskers, or hillocks.

The formation of voids will reduce the effective cross-section of the metal lines and increase the current density. Increase in current density gives rise to localised heating which then creates a temperature gradient. As a result, electromigration occurs at an accelerated rate and causes line to open circuit. Whereas hillocks and whiskers can cause an electrical short circuit to the nearby conductors and even fracture the oxide layer surrounding the conductor. Hillock is a term applied to any perturbation or mass accumulation on a metal line due to electromigration or mechanical stresses. A whisker is a growth from the surface of a single crystal aluminium.[Sabnis,1990] Fig 1.0 shows the voids and hillocks taken from the reference of [Gangulee and D' Heurle,1973]

(a)   (b)
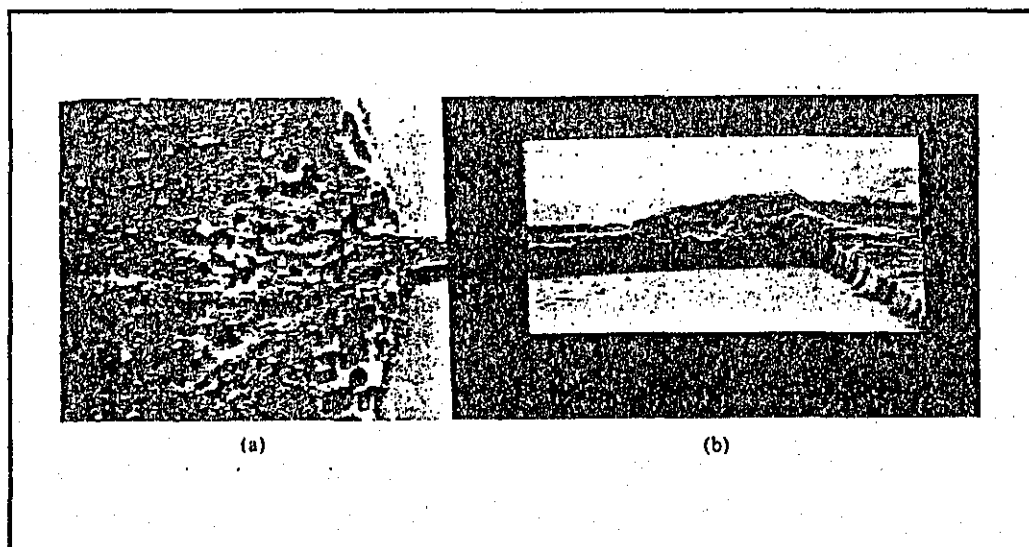
Fig 1.0 Scanning electron micrograph showing (a) the voids at the cathode end
and (b) hillocks near the anode end of Al interconnect.

1.2 History and overview of Electromigration

1.2.1 Early study on electromigration

The first observation of the atomic motion or diffusion in a metal conductor under the influence of an applied electric field was reported by Geradin in 1861 where the metals under study are molten alloys of lead-tin and mercury-sodium. It was not until much later in 1953 in a study on mass transport of Hume-Rothery alloys that Seith and Wever made the important observation relating to the nature of the driving force for electromigration. They found that the atomic motion is not determined solely by the electrostatic force imposed by the applied field but also depends on the direction of the motion of charge carriers. Later Seith introduce the idea of ' electron wind' to account for induced mass transport, an idea which laid the foundation for the basic understanding of electromigration[Ho and Kwok,1988]. They also introduced the 'marker motion' technique now known as 'vacancy flux' method to measure the induced mass transport which became one of the standard measurement of electromigration. The 'marker motion' technique used the displacement of the surface markers(scratches or indentations) along the length of a metal wire to measure the changes in the sample dimension as a result of the creation and annihilation of vacancies.[Ho and Kwok,1988].

The concept of the 'electron wind' driving force was first formulated by Fiks in 1959 and Huntington and Grone in 1961.They employed a 'ballistic' approach to treat the collision of the moving atom with the charge carriers. In their work, Huntington and Grone showed that, beside the initial and final states of charge carriers to be considered, the spatial variation of the force experienced by the moving atom has also to be considered in the collision process. This led to the idea that the 'electron wind' also depend on the type of defect and the atomic configuration of the migration path. The formulation of the driving force was a major contribution to the study of electromigration as it became possible then to probe directly the interaction of the mobile defects and the charge carriers.[Ho and Kwok,1988].

4

In the 1960s, research activities basically focused on the investigation of bulk materials. The interest in electromigration concentrated on self-electromigration in pure metals and later extended to alloys and liquid metals, work done by Huntington in1974 and Rigney in 1977 respectively.[Ho and Kwok,1988]

1.2.2 Study of the electromigration transport mechanism in thin conductor film

The interest in electromigration took a drastic turn in the late 1960s when it was identified as causing cracks in aluminium conductor lines in Integrated circuits (IC's). It was discovered that the electromigration was the cause of failure in the thin aluminium film where the opening up of holes or voids near the cathode was observed by using TEM.[Blech and Meieran,1969].Local thinning of the aluminium film was also observed by using TEM which was attributed to the lack of adherence of films to the substrate.[Rosenberg and Berenbaum,1968].

This finding resulted in many more research activities in studying electromigration in thin film conductors. Most of the studies in the late 60's and in 70's were aimed at the rather practical problem of conductor line failure, or the 'cracked stripe' problem in microelectronics integrated circuits. These studies were carried out in thin films prepared by evaporating metal atoms onto insulating substrate and at moderate temperatures of about half the absolute melting point. These studies show that electromigration occurs primarily along the grain boundaries based both on the observed low activation energy ($E_A \approx$ 0.5-0.6eV) while monitoring changes in electrical resistivity[Rosenberg and Berenbaum,1968] and also by direct electron microscopic observations ($E_A \approx$ 0.7±0.2 eV)[Blech and Meiren,1969].This low value of activation energy E_A is the evidence that the electromigration is the process of diffusion along grain boundaries. For lattice self-diffusion E_A is about 1.3eV[d'Heurle and Rosenberg,1973].The above results were supported by experiments on a single-crystal aluminium films which resulted in no indication of electromigration-induced failure[d'Heurle and Ames,1969].

5

1.2.3   Study of the cause of interconnect failure -flux divergence

Electromigration alone will not cause aluminium interconnects to fail. The failure also requires flux divergence where damage (e.g. voids or hillocks) are formed. Voids can grow and link together to cause electrical discontinuity in conductor lines which leads to open-circuit failure. Hillocks can also grow and extrude out materials to cause short-circuit failure between adjacent conductor lines. It can also break through the passivation or protective coating layers and lead to subsequent corrosion-induced failure.

The 'flux divergence' refers to the imbalance of atomic flux caused by inhomogenity of parameters controlling the diffusion process from, macroscopic design parameters, such as length and width, to microstructural features such as grain size distribution, film orientation and grain boundary characteristics. This aspect of electromigration damage has shifted the focus of the investigation to that of understanding electromigration at the level of structural defects in thin film materials.

Non-uniformity in the grain size at a junction between a fine and a coarse grained area, is a flux divergent site where hillock formation has been observed[Attardo and Rosenberg,1970]. The flux divergence occurs because the number of atoms migrating to the junction through the fine-grain side exceeds that migrating out of the junction through the coarse-grain side. Voids and hillock formation are frequently observed at grain boundary triple points where three or more grain boundaries are joined[Berenbaum,1970].

The present study of electromigration in very fine conductors derives from the development of very large-scale integrated (VLSI) circuits. The interconnects are not only small in dimensions, they are also assembled into a multilayed structure with a certain combination of conductors and insulators. The multilevel interconnect scheme is to keep the CR delay low (as CR delay depends on the length of interconnect) to provide the required speed performance. The linewidth of thin-film interconnects has

to be reduced to the submicron range in order to provide the required device density. The impact of scaling on the electromigration can give rise to two kinds of problems. One problem is due to increase in the current density and the other is from the reduction in device dimension. The current density will increase linearly with size reduction for FET devices (kj) and approximately with the square of the dimensional scaling for Bipolar devices ($k^2 j$), where k is the scaling factor and j is the unscaled current density[Dennard et al.,1974]. In addition to the effect of the driving force due to the increase in j, the $j^2 \rho$ increase in the Joule heating can raise the conductor temperature, making higher atomic diffusivity and enhanced electromigration. With the projected high current density in submicron metal lines, there is increasing concern over electromigration-induced failures. With the reduction in interconnect line width beyond the submicron range, the grain size has approached that of the line width (the so called bamboo structure). This constitutes a significant change in the microstructure of the conductor line and the behaviour of electromigration.

1.2.4 The development of electromigration failure models

A standard engineering test for electromigration is the lifetime test. This is an accelerated test in which a group of test structures is electrically stressed until all of the specimen 'fail', where the failure is identified as a complete loss of conduction or some critical increase in electrical resistance.The Time To Failure or TTF of electromigration-induced failure is generally considered to follow a log-normal distribution.[Agarwala et al.,1970],[Attardo and Rosemberg,1970], [Thompson and Cho,1986],[Attardo et al.,1971]. This result is based both on experimental findings and by computer model simulation.The median time to failure or t_{50} is the measure by which the electromigration reliability of a particular metallization scheme is compared to another for a given set of test conditions. The commonly used empirical model for the median time to failure ,t_{50}, is

$$t_{50} = \frac{A}{j^n} \exp\left(\frac{Q}{kT}\right) \qquad\qquad 1.1$$

where,

t_{50}= mean time to failure, A= a constant which contains a factor involving the cross-sectional area of film. j= current density, Q= an activation energy, k= Boltzmann's contant, T= film temperature,

which is popularly known as the 'Black's Equation[Black,1969]. Naturally activation energy, Q, is of particular interest, because being in the exponential, it has a heavy influence on t_{50}. Clearly increasing the activation energy will increase the t_{50}. Should the activation energy increase by 0.1eV, t_{50} will increase by a factor of 55 at room temperature and a factor of 20 at 125^0 C[Spitzer,1969]. The activation energy is the measure which determines the kind of diffusion or migration mechanism is taking place whether it is through surface, grain boundary or bulk(lattice).The exponent n is also a much debated issue because the studies conducted on thin films have not provided a consistent result.

Early experimental results[Black,1969],[d'Heurle,1971] account for values of n between 2 and 3 while there is some theoretical argument to support n=1[Sigsbee,1973] and n=2[[Black,1969],[Shatzkes and Lloyd,1986], [Trattles et al.,1994] .The most widely use value for n is 2 [Malone and Hummel,1997]

The model by Black is purely empirical and the accuracy lies in the fitting of parameters such as the value for n and Q. Lloyd argued that if there is no physical model, any values for the fitted parameters can be chosen and if there are changes in the failure mechanism between the stress conditions and use conditions, extrapolations will be invalid[Shatzkes and Lloyd,1986],[Lloyd,1994].

As a result [Lloyd et al., 1986,1994]developed a physical model which described the electromigration by a drift-diffusion mechanism of atoms or vacancies. In the Drift-diffusion model, the transportation of metal atoms may be alternatively be viewed as a drift-diffusion of vacancies c in a direction opposite to that of the atomic flux. The general drift-diffusion equation is given below is :-

$$J = D\frac{\partial c}{\partial x} - \frac{DZ*e\rho jc}{kT}$$

1.2

where J is the vacancy flux

D is the diffusion coefficient

c is the vacancy concentration

Z*e is the effective charge

ρ is the material resistivity

j is the current density

k is the Boltzmann's constant

T is the operating temperature(^{0}K)

The first term represents the concentration gradient-driven backflux diffusion and the second term the current-driven (drift) or the electromigration flux. Combining this with the continuity equation, the drift-diffusion equation can be transformed to the so-called 'electromigration equation' of the form:-

$$\frac{\partial c}{\partial t} = D\left(\frac{\partial^2 c}{\partial x^2} - \frac{Z*e\rho j}{kT}\frac{\partial c}{\partial x}\right)$$

1.3

The failure time of an interconnect is determined by employing some boundary conditions to the above equation and it is based on the time to reach a critical vacancy supersaturation.

An alternative physical model was proposed by [Korhonen et al.,1993(1)] to describe the mechanical stress σ arising under electromigration. A one-dimensional equation which describes this model is given below:-

$$\frac{\partial \sigma}{\partial t} = \frac{\partial}{\partial x}\left[\frac{DB\Omega}{kT}\left(\frac{\partial \sigma}{\partial x} + \frac{Z^*e\rho j}{\Omega}\right)\right]$$

1.4

where σ = stress

B = coefficient depends on the elastic properties

Ω = atomic volume

9

The equation describes the evolution of the stress and was derived in the case of vacancy equilibrium with the stress. Interconnect failure was associated with the build-up of the critical level of stress[Korhonen et al.,1993]. At present Korhonen's model is widely used to analyse the electromigration-induced failures in near-bamboo lines[Sarychev et al.,1999] .The models differ only in the treatment of the continuity equation. A detail comparison between the two model will be discussed chapter 2 .

1.2.5 The study of structural effects on the Mean Time to Failure

It is clear that the structural characteristics of the interconnect (macro and microstructure) are related to the mean time to failure t_{50}. These may be split between microstructural effects and macrostructural.

i) Microstructure

A number of early studies were carried out to investigate the effects of the microstructure of thin films or interconnect on the electromigration mean time to failure t_{50}. The increase of electromigration t_{50} with increasing grain size has been reported for aluminium conductors with a width exceeding several microns[Learn,1971]. In particular [Attardo and Rosenberg,1970], showed a linear relationship between grain size and the mean time to failure t_{50}.The number of grain boundaries that are found in a given width of interconnect is inversely related to the average size of its grains. The bigger the size of grain ,the smaller the number of grain boundaries available for atomic migration, therefore t_{50} will increase. Non-uniformity in the grain size causes a different number of atoms migrating from the fine-grained side to the coarse-grained side. With a mixture of grain sizes, there are bound to be some regions where the number of grain boundaries is different from the number in adjoining regions. The transitional zone between each region is similar to a grain boundary triple junctions, therefore damage will tend to occur at this points. The mean time to failure t_{50} is found to decrease with an increase in the standard deviation of the grain size[Agarwala et al.,1972].

When an interconnect is patterned from a film whose grain size is larger than the intended interconnect width, the result will likely look similar to a chain of single-grained segments. Such an arrangement is called a 'bamboo' structure. In a perfect bamboo structure there are no triple junctions and there is no continuous pathway provided down the interconnect by the few grain boundaries. The angle at which they transverse this span is important.

If the transversing boundary is inclined at any angle other than 90° with respect to the downwind direction, then there will likely be some migration at the boundary. A void may form on the edge of the interconnect at the upwind end of that grain boundary segment. In any case, the absence or near absence of triple junctions and the lack of continuous network pathways should lead to a larger t_{50}. This observation has been confirmed by experiment. [Pierce and Thomas,1981],[Gangulee and d'Heurle,1973].

ii) Macrostructure

The macrostructure of an interconnect includes such factors as size and shape, as well as the composite structure and composition of the entire metallization scheme. The grain boundary network that happens to be captured when an interconnect is patterned depends on the length and width of the pattern taken. A large number of unfavourable structural features, such as triple junctions, is captured along the length of a patterned interconnect as the length is increased.

It has been found that t_{50} decreases with increasing interconnect line length [Agarwala et al.,1970],[English et al.,1974]. Experiment conducted by Agarwala et al. has also shown that t_{50} increases with linewidth, where lifetime is observed to increase linearly with an increase in the stripe width. An empirical relationship was constructed for t_{50} versus line length and line width [Agarwala et al.,1970].

$$t_{50} = A.w.\exp\left(\frac{\alpha(w)}{\ell}\right) \qquad\qquad 1.5$$

where

A is a constant

w is the line width

α is a constant that depends on w

ℓ is the line length

However, there are also studies that show that t_{50} increases due to decreasing linewidth.[Kinsbron,1980],[Iyer and Ting,1984],Vaidya et al.,1980]. They found out that t_{50} start to increases below 2 microns. This relates to a bamboo structure where the linewidth is smaller than the average grain size.

1.2.6 Techniques for extending the Mean Time to Failure

It is a standard procedure to 'passivate' chips, that is to encapsulate them with a protective coating. Coating of aluminium interconnects has been reported to improve its electromigration lifetime. The effect of coating of aluminium film of large grains with SiO_2 glass has shown an increased activation energy from $E_A = 0.84eV$ to $E_A = 1.2eV$ i.e the activation energy for self-diffusion of aluminium in bulk or lattice (higher lifetime) [Black,1969].Other experiment involving coating with alumina-silicate glass also shows an improvement in lifetime[Spitzer,1969]. Both of these references conclude that the coating will inhibit surface diffusion.

However there is another theory by [Ainslie et al.,1971] which proposes that the coating actually impedes the growth of hillocks and whiskers, which reduces the formation of cracks. It was also proposed that the coating will be effective only for very thin films applied with relatively thick coating.

Another material which is also used as coating of aluminium film is silicon nitride[Blech,1976] which appears to slow down the surface diffusion. Overcoating of SiO_2 glass and silicon nitride are at present commonly used as passivation layers. In addition to retarding electromigration through surface transport, these overcoat layers enhance electromigration resistance of aluminium by causing grain size growth during the overcoat deposition and reflow process .[Sabnis,1990].Interconnect cladding layers of Ti,TiN,W,and TiW are also used to prevent interdiffusion [Malone,1997]. Another way of extending the interconnect lifetime is by adding small amounts of metallic impurities into the aluminium. Common impurities include copper, chromium, nickel,magnesium , and titanium.[Sabnis,1990]. Copper is the most widely used element for alloying with aluminium producing higher activation energy and larger t_{50} than pure aluminium.[Sabnis,1990]. At present, many studies are also geared towards the research on the effect of Cu on the microstructure of Al and the electromigration lifetime of interconnect[Domenicucci, et al., 1996]

1.3   Lifetime Reliability Issues of Electromigration

The reduction in scale has driven interconnects into the 'bamboo' region, where interconnect widths are the order of a single grain diameter. In such structures one expects that the median-time-to-failure or t_{50} for electromigration will be greatly increased due to the lack of grain boundaries available to carry metal atoms and there is now plenty of experimental data [Agarwala et al.,1970],[Attardo et al.,1971],[Kinsbron,1980],[Cho and Thompson,1989] to support this. However, the t_{50} is not the most important feature from a reliabilty point of view, and ,importantly, the same experiments show that in bamboo structures, the standard deviation or the shape factor σ_{sd} is also greatly increased as shown in Fig 1.1.
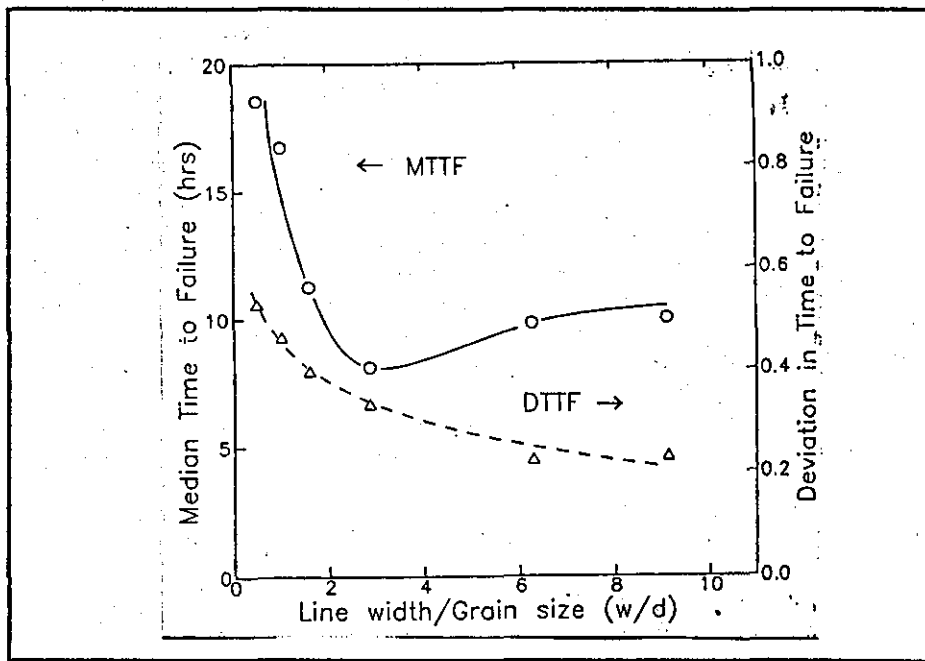
Fig1.1 Median time to Failure (MTTF) and Deviation time to Failure(DTTF) vs linewidth/grain size ratio. Figure taken from [Cho and Thompson,1989]

Based on the assumption of log-normal statistics, extrapolation of data regarding the time-to-failure (TTF) at say 0.01% cumulative failure is strongly dependent on the shape factor, as a result σ_{sd} is much more important from the point of view of reliabilty analysis where early failures occurs (an IC might have 10^6 interconnects, so 0.01% would mean 100 failures). Indeed, since for lognormal $t_{50} = \exp(\sigma)t_{16}$, a small increase in σ_{sd} will be enough to nullify, or even reverse, any increase in MTF gain from the bamboo grain structure. Therefore greater knowledge of the full statistics of TTF is needed before we can sure of the validity of standard reliability analysis.

Another aspect of reliability concern regards the actual probability distribution of the interconnect lifetime due to electromigration -induced failure. Electromigration failure is traditionally believed to follow a lognormal distribution as mentioned in section.1.2.4. However, the lognormal distribution cannot be scaled with length. The failure of a full interconnect is usually described by the well-known weakest link model[Agarwala et al.,1970],[Cho and Thompson,1989],[Vaidya et al.,1980]. If F(t) is the probability that the lifetime of a failure unit is smaller than t, then the

14

corresponding probability for the entire interconnect line, assuming n identical independent failure units is,

$$F_n(t) = 1 - (1 - F(t))^n \qquad\qquad 1.6$$

In general the form of distribution $F_n(t)$ should also exhibit the lognormal distribution, but it does not (if the lognormal distribution is used for $F(t)$). Therefore the assumption that the failure distribution lognormal is questionable[Lloyd and Kitchin,1991].

1.4   Aims of the Study

1.4.1   Study Objectives

1. To develop an equivalent electrical model by replacing the stress evolution equation (eqn 2.33) with a time development of a pseudo-voltage on an equivalent lumped CR network.

2. To develop the electromigration failure statistics for a realistic representation of complex grain boundary networks of near bamboo interconnects.

3. To investigate and analyse the statistics that been developed specifically whether it exhibits the lognormality and is if so what is the standard deviation(or the shape factor) σ_{sd}.

4. To develop the 'Elmore delay' method of approximating the TTF and then make a comparison analysis to the model under study. This will verify the validity of the model and allow rapid estimates of TTF for a given structure enabling statistics to be obtained rapidly.

5. To investigate the factors that affect the TTF and its distribution.

1.4.2 Study Methodology

In order to achieve the objectives specified above, the study will be organised as follows:-

1. First it is needed to develop a lumped CR network which will replace the drift-diffusion model for describing the stress build-up in a single grain. Later on the model will be analysed and verified by comparing the simulation results with other existing work found in the literature.

2. It is then necessary to calculate the statistics and the distribution for the time to failure (TTF) (including σ_{sd} and lognormality) for the equivalent lumped CR network of an example of a complex grain boundary network. The work will involve:-

    i) Establishing a CR circuit network which models the complex grain boundary structures in terms of the grain boundary lengths, their orientations and vacancy diffusion coefficients. The statistics of these parameters are presumed to be known from existing literature.

    ii) The equivalent network is then simulated to obtained the long-time stress build-up.

    iii) The TTF and its statistics are created by assuming a failure threshold for each network.

3. The equivalent CR network is always made from parallel capacitors to ground and series resistors. The electromigration problem becomes identical to calculating the signal delay in a general CR networks with stored charge. Such networks have been studied in detail for digital CMOS timing problems. The 'Elmore delay' gives a very good approximation to the delay time. An analysis will be made using

16

this method to obtain the TTF which will then be compared to the 'exact solution' for both a single grain boundary and complex grain boundary structures.

4. A single interconnect may be considered to be made from a number of grain-boundary networks connected in series. If each of these acts as an independent link, failure should occur at the weakest link model. Using the model above the effect of the links may also be investigated. To achieve this , a Voronoi network which represents the realistic grain structure of an interconnect will be created and the statistics of the TTF will be developed .

1.5   Thesis Outline

In Chapter 1, a brief overview of the technological importance of Electromigration studies on the VLSI and ULSI are discussed. Also the term electromigration is defined and its historical background, and an overview of the studies based on experimental and theoretical models, are briefly described. Further brief descriptions of important factors (such as the microstructure and macrostructure) on Electromigration behaviour and lifetime are given. Techniques for extending the lifetime under Electromigration and reliability issues affecting the interconnection technology are also discussed. Finally the objectives of the current study and its methodology are outlined.

A detailed literature survey on the research development on Electromigration are discussed in Chapter 2. These includes the overview of the 'state-of the art' specifications of the interconnect technology. The literature on the experimental aspects and their results are reviewed in detail. Next the development of the physical model of electromigration, which relate to the lifetime, are discussed. These range from the first electromigration model by James R. Black , the classical theory of Huntington and Grone, to the continuum models which includes the drift-diffusion model and the current and most accepted stress evolution model. The main differences, advantages and disadvantages between the drift-diffusion model and

17

stress evolution model are also discussed.

Chapter 3 discusses the development of the lumped element model and the signal delay method for producing the Time to Failure. A detailed description of both methods is presented. The Chapter also includes some of the initial results to demonstrate the validity of the lumped element model and that of the signal delay method.

Chapter 4 discusses in detailed the development of the program codes to perform the various task of the lumped element model. These are basically to i) demonstrate the validity of the model (as in the single grain boundary case),ii) simulate the stress/vacancy concentration profile and iii) simulate a realistic representation of interconnects by employing the Voronoi technique and most importantly iv) to simulate the Time to Failure of the interconnect so as to produce its statistical distribution pattern.

Chapter 5 discusses the various simulations undertaken , their results, analysis and meaning. There are three main categories of experiment simulated i) single grain boundary interconnect , ii) a more complex grain boundary network and iii) the more realistic representation of the complex grain boundaries.

Chapter 6 summarises all the important observations results and analysis and the conclusions. Some recommendations for improvement and further work are also included. Chapter 7 provides the list of all references used in the thesis.

CHAPTER 2

A REVIEW OF LITERATURE ON ELECTROMIGRATION

2.0   Introduction

Recent technological developments and advancement in computer-aided circuit design have ushered in an era of very-large scale integrated circuit (VLSI) with a million or more devices integrated on a single chip. However advanced or complicated the technology is, metal film stripes or interconnections are used to connect this large number of devices to form a complete VLSI circuit. The interconnect technology was initiated by the independent work of Jack S. Kilby, an engineer at Texas Instruments and Robert N. Noyce, a scientist at Fairchild, who then patented their ideas on how to interconnect transistors, capacitors and other active and passive components on a single piece of silicon.[Ghate,1986]. At present, the connections required to integrate a large number of components on a chip consume a large area of the chip, and to minimise signal delays, multilevel interconnections separated from each other by insulating layers are employed.

The present trend of interconnection technology employs a few hundred meters of 0.35 microns wide interconnects per chip distributed among 4-5 metallization levels (CMOS technology of 1995), and it is projected that by 2010 there will be 7-8 metallization levels containing 10,000 meters of interconnects that are only 0.07 microns wide[Ohring,1998]. The patterned interconnects will exhibit a strong bamboo morphology with grain boundaries approximately perpendicular to the stripe axis.

As the technology advances, the research activities on electromigration are also active today because electromigration itself remains a complex phenomenon involving many variables [Sabnis,1990][Ohring,1998]. Therefore, despite many years or

research, there is still a lot to be understood. Modern demands such as the miniaturisation of IC require continuous research work on various platforms such as the experimental and the theoretical and also in the development of new methods of testing electromigration. At present the links between the experiment and the theory are rather weak and are sometime based on speculation.[Kircheim,1991].The knowledge of failure modes or the physics of failure is extremely important in interpreting the data gathered under accelerated test conditions.

In this chapter, a review of the present or latest study on electromigration is presented. The review will cover the present interconnect technology, electromigration experiments on pulsed current, methods of testing and the development of models relating to the electromigration-induced failure of IC interconnects. The existing models will be of particular interest where comparison can be made, based on the results it offers, the assumptions it makes and the ability to be used in accelerated testing. Existing research shows that the study of electromigration-induced failure in IC interconnects is at present focused on:-

a) Experiments on electromigration under pulsed currents
b) Improvements in testing methods
c) The development of the physics of failure or the failure model

2.1   Overview of the Interconnect Technology

The IC's interconnects serves a variety of functions on an IC. These are:

i.   Contacts between the first layer of metallization and the substrate electrodes,
ii. Gate interconnects,
iii. Interconnects of the metallization layers,
iv. Vias contacts between the levels of the multi-level metallization.

Metallization is the term that refers to the total sum of all applications of metal films in the formation of silicon metal contacts and multilevel interconnections. [Ghate,1982]. The characteristics and materials for interconnects vary to satisfy the appropriate electrical requirements. A low ohmic resistance is a dominant criterion, which arises from the nature of the interconnect lengths. The interconnect resistance should be as small as possible to avoid I^2R losses, and to minimise the interconnect RC time constant (per unit length) in order to obtain the fastest possible performance.

For FET ICs ,vacuum-deposited aluminium films are widely used for connections within integrated circuits because it has low resistivity of around 3 $\mu\Omega$/cm[Herbst,1996], they are compatible with the fabrication process and are cost effective. Aluminium-alloy films have replaced pure aluminium films to enhance the reliability of ICs interconnections. Examples include the use of aluminium-silicon alloy to minimise contact pitting, aluminium-copper alloy to improve resistance to electromigration and aluminium-copper-silicon to resist both.

Bilayer and trilayer films with gold as the principal conductor are also used for interconnections where considerations of reliability outweigh cost and ease of processing. As gold films adhere poorly to silicon dioxide, refractory metals such as Mo,Ti:W and Ti/Pt provide the necessary adhesion to the silicon dioxide and act as a barrier layer between the silicon contact and the gold films.

Early MOS ICs used aluminium as the gate and interconnection material, but it is observed that this is not compatible with high-temperature processing. Later with the discovery that polysilicon films produced by the chemical decomposition of silane gas, is compatible with MOS silicon processing, was a breakthrough for producing large-scale-integrated MOS circuit using single and double polysilicon layers as multilevel interconnections[Ghate,1986].

As IC technology developed , it became necessary to use two or more levels of connections to achieve higher packing densities, shorter propagation delays and smaller chips. The basic elements of a two-level interconnection scheme are

21

'crossovers' and 'vias'. A crossover is a second level lead that crosses a first-level lead and is separated from it by an insulator layer. A via is a location for a level-to-level contact. Examples of metal-insulator combination are Al/SiO$_2$/Al, Al/polymide/Al, Ti:W/Al-Cu/ SiO$_2$/ Ti:W/Al, and Ti:W/Au/Ti:W/SiO$_2$/ Ti:W/Au.[Ghate,1986]. Aluminium and gold provide the desired low-resistance interconnections, and SiO$_2$ or polymide(an organic material applied like a paint) provides the necessary insulation between the layers.

The state-of -the art for Al interconnects in ICs are summarised below[Malone, 1997],:-

1. Metal Composition : alloy of aluminium (1-4% Cu). Claddings may be included.
2. Local operating temperature: approaching 100^{0}C.
3. Current density: 1x 10^6 A/cm^2.
4. Linewidth: 0.35 microns.
5. Thickness: < 1 microns.
6. Grain structure: near-bamboo or bamboo.
7. Interconnect architecture: multileveled, with tungsten plug interlevel splices.

With this specification in relation to the grain structure, interconnects should be resistant to electromigration, but in reality the advantage of this is reduced by the increase in current density and operating temperature. The absence or near absence of grain boundaries does not prevent the migration of Cu and Al along other paths. Recent studies have revealed that erosion voids and slitlike voids were observed in single-crystal lines[Joo and Thompson, 1997]. In the current study, Al is considered and not Cu because to set up a theory, we need to compare with experiments and many more results exist for Al than for Cu.

2.2 Electromigration study under pulsed currents

At present, research is also geared towards the understanding of how electromigration occurs under pulsed current conditions. In the past, the vast majority of both

experimental and theoretical work on electromigration in Al and Al-alloy films, and its effect on conductor lifetime in ICs, has concentrated on dc constant-current (reference to Chapter 1). However, many integrated circuit interconnects carry pulsed signals or current , therefore it is important to have an understanding about the nature of the problem so as to assess adequately the enhancement of the electromigration lifetime which have been reported in the literature.[English, et al.,1972], [Schoen,1980].[Gui, et al.,1998][English and Kinsbron,1982],[Liew, et al.,1990].

It is not the intention of the present research to discussed in detail all the literature concerning the electromigration behaviour under pulsed current, but to give some highlights on few results and the present focus of study. The basic difference between the dc and pulse testing is that in dc testing the atoms are under a constant influence of electron wind, whereas in the pulse testing the damage that may occur during pulse-on time has an opportunity to relax during the subsequent off-time.

The first study of electromigration behaviour under pulse current was an experiment conducted by [English et al.,1972] on thin film of titanium-gold alloy. The study was to compare the effects of several different sets of pulse conditions, ranging in frequency from 10^{-4} to 10^4 Hz, and in the duty cycle from 10% to 70 % of a square pulse train. Each pulse treatment was applied for 100 on-time hours for every test. The final analysis was conducted through a scanning electron microscope (SEM) where it was observed that the samples exhibited a range of results i.e. heavy damage, moderate damage and no damage. The main conclusion from the experiment was that the electromigration damage is a complex phenomenon depending on the pulse frequency and the duty cycle.

The damage pattern observed was explained by the authors under the assumption that electromigration damage is the result of a local build-up of vacancy concentration at some point of flux divergence. The build-up of vacancy concentration takes place rapidly at first, but eventually slows down when approaching some maximum level of supersaturation. During powering, the level of supersaturation will be reached during the time span of a sufficiently long pulse, but will decay during the off-time between

pulses. A study by [Rosenberg and Ohring,1971], estimates that the time to reach maximum supersaturation is 100 seconds for the case of aluminium. The authors suggested that some critical level of supersaturation had to be maintained or exceeded for a sufficient length of time, the ' incubation time', in order for damage to nucleate in the form of voids. They also suggested that voids were stable against any relaxation effects associated with the time between pulses. Heavy damage in the sample was found.

Another analysis was done [Rosenberg and Ohring,1971],in which the on-pulse length is shorter than the 'incubation time', but long enough to produce a large supersaturation of vacancies on one pulse. In this condition, no damage or void nucleation occurs. The reason being that the unpowered intervals are long enough to allow annealing reduction of local vacancy supersaturation or in other words it produces a considerable driving force for recovery before the next powered interval begins. For very short on- times and off- times, each pulse produce a relatively small increase in the vacancy supersaturation, and each following off- time allows little recovery, the supersaturation will then increase in small increments eventually reaching the critical level after many cycles when void nucleation will occur.

However another study to relate the lifetimes in very small aluminium conductor elements, under pulsed current at low duty cycle, and stressed with current density above 1×10^7 A/cm^2, shows that the time to failure decreases rapidly with increased current density above 2×10^7 A/cm^2. Failure appeared to be accelerated by the temperature increase by Joule heating during each pulse , and it was concluded that the failure mechanism was complex, involving temperature-accelerated electromigration, temperature cycling and chemical interactions with the film's substrate.[Kinsbron, et al.,1979]

A model was developed by [Schoen,1979], to take account of the effect of temperature cycling and damage relaxation upon electromigration lifetime. It is based on the fractional lifetime consumed per pulse interval which is a function of film temperature. The fractional lifetime consumed per pulse is computed assuming

the temperature in the film is an exponentially increasing function of time while the pulse is on. Damage relaxation during the pulse off- time is given by a time constant exhibiting the same activation energy as the dc electromigration lifetime i.e. self-diffusion in grain boundaries. Film temperature during the pulsed off-time is assumed to decrease exponentially with time. The assumptions are valid only when pulse on and pulse off- time exceeds the thermal time constant. The author claimed that the model has been applied to the experimental conditions used by Miller ,and the results shows a good agreement between the predicted and the measured lifetime as a function of pulse duty cycles for a frequency of 250kHz.

A numerical simulation model was recently developed to investigate the effect of temperature cycling on electromigration behaviour under pulsed current stresses.[Gui, et al.,1998]. The model is based on solving two partial differential equations which governs the physical processes. The temperature fluctuations has been given as a function of the pulse repetition frequency. They found that the temperature of the metallization remains at an average constant value at an operating frequency above 10 MHz and temperature oscillations reaches a maximum amplitude when the frequency is lower than 250 Hz.

Another explanation[English and Kinsbron, 1983] was given for the enhancement of lifetimes due to pulse current. They maintain that the enhancement of lifetime is not due to the relaxation or recovery of damage during the pulse off time but is due to a decrease in the mass transport rate, which decreases by a factor equal to the duty cycle. They argue that past studies have been conducted using current density at and above $4x \, 10^6 A / cm^2$ and were difficult to interpret due to the presence of thermal transients as well as the general elevation of temperature above ambient. They observed that the rate of mass transport per unit of on time is essentially constant, regardless of duty cycle, so long as the current density is not so high as to produce significant Joule heating on each pulse. The frequency range used was $0.01-10^5$ Hz with a current density range of $1x10^4$ to $2x10^6 \, A/cm^2$.

From the few studies indicated above, it is clear that the assumptions that the damage can be recovered during the off-times between pulses, thus causing the enhancement of lifetimes, is not universally accepted. Some of the literature published to discussed this issue include [Lloyd and Koch,1988],[Li, et al.,1992],[Ohfuji and Tsukada.,1995].

In an experiment using an ac bridge technique, the resistance of the line is found to increase linearly in time during current stressing and, when the current was interrupted, the resistance was seen to decrease. The decay is not purely exponential, but a combination of decay modes, each with its own characteristic decay time constant[Lloyd and Koch,1988]. This behaviour is also observed in another experiment using also an ac bridge but employing different testing method i.e. by using an early resistance change measurement(ECRM)[Niehof et al.,1993]. Lloyd and Koch offered an explanation for this behaviour , in which the resistance increase was due to the supersaturation of vacancies produced through structurally induced mass flux divergence. The decrease in resistance is more complex, where the small time constant refers to the decay of vacancy supersaturation, and the longer time constant due to relaxation of tensile and compressive stresses. This mechanism is also supported by [Li et al.,1992].Meanwhile Niehof and co-worker give the same explanation for the increase of resistance, but for the decay of resistance they assumed that the unstable microvoids will evaporate causing the resistance to recover.

In another study, it was suggested that the resistance decay was the result of several processes such as the decay of vacancy supersaturation, the concentration relief of mechanical stress, the motion of dislocations and the dissociation of vacancy-hydrogen complexes[Ohfuji and Tsukada,1995]. A study of the effect of duty cycle of pulsed dc currents on the critical length-current density product was performed [Frankovic et al., 1996]. In this study, it was shown that for a pulse frequency of 100 kHz, the jl_c product increases as the pulse duty cycle is decreased, meaning that for a given current density, the Blech (l_c) length becomes larger with decreasing duty cycle. The duty cycle dependence of the Blech length (l_c) means that electromigration resistance could be increased with small duty cycle. With small duty cycle would decrease the atomic flux but also increases the number of

interconnections that become sub-Blech-length (less than l_c) which are resistant to electromigration damage.

The effect of duty cycle on lifetime of aluminium interconnect is also of interest to researchers. The literature concentrates on the duty cycle dependence on the mean time to failure t_{50}. [Harrison,1988],[Liew, et al.,1990],[Clement,1992],[Dwyer,1996], [Gui, et al.,1998]. Their work are basically to find the suitable exponential number m to the modified Black's Equation for pulsed current i.e.

$$t_{50} = \frac{A}{d^m.j^n}.\exp\left(\frac{Q}{kT}\right)$$
2.1

A value of m=1 is produced by the on-time model in which it is assumed that damage only occurs during the period in which the current flows, whereas m=n=2 is called the average current density model. Among the researchers who develop theoretical predictions m=2 [Gui,et el.,1998],[Dwyer,1996],],[Liew, et al.,1990][Clement,1992]. A larger value of m indicates a larger t_{50} , and in such a case the lifetime is said to be enhanced. The average current density model predicts enhanced lifetimes. A range of value for m has been reported from other researchers (m=1-7.5) in the literature by [Malone and Hummel,1997] .

At present, the main issues of interest in the study of electromigration under the pulsed current can be summarise as below:-

1. The effect of the duty cycle on electromigration lifetime is not clear.
2. The interpretation of the enhancement of lifetimes due to the effects of damage recovery and the temperature cycling are not convincing yet and are complicated.
3. There is a large variation of values for 'm' of the duty cycle dependence in the equation of the mean time to failure.

4. Limitation of the pulse frequency, no higher than 1 MHz in most studies.

2.3   Electromigration Failure Models under constant dc current

Electromigration lifetime experiments are usually conducted in accelerated test conditions where test samples are subjected to higher than usual levels of accelerating variables such as temperature and current density. The results are then used to make predictions about the lifetime during actual use conditions using the acceleration factor derived from the parameters used. The validity of the whole procedure depends on the usage of correct failure or physical models. If other failure modes are present but not recognised in the data analysis, seriously incorrect conclusions will be derived[Meeker and Escobar, 1998]. In view of this problem, several models to describe the electromigration failure in thin -metal conductor stripes have been proposed over the years which vary from empirical and the semi-empirical to the physical models. In this section, a review of these models will be made and compared based on their advantages and disadvantages and their ability to produce the statistics of the failure times and the characteristics of its distributions.

2.3.1   The first electromigration failure model

The first electromigration failure model was the empirical model of James R. Black[Black, 1969(a)] which is the first to express a formulation of the mean time to failure, t_{50} and this model was mostly accepted. The equation of the mean time to failure introduced by Black is:-

$$t_{50} = \frac{A}{j^a} \exp\left(-\frac{Q}{kT}\right)$$ 2.2

where

t_{50} = mean time to failure

A = a constant which contains a factor involving the cross-sectional area of the film

j = current density

Q = an activation energy

k = Boltzman's constant (8.62×10^{-5} eV / K)

T = film temperature (Kelvin)

The paper by Lloyd [Lloyd, 1994], discussed the drawbacks of Black's model based on the j^{-2} dependence and the disadvantage of purely empirical models. Lloyd pointed out that although the model is fairly well accepted, it is in disagreement with solid state physics which indicate that the driving force for electromigration should have a current exponent of -1. He also referred to other arguments which relates the j^{-2} dependence to Joule heating. He argued that Joule heating can produce different and unbounded values of n (the exponent value of j). For failure to occur, flux divergence must occur which may be caused by temperature gradient produce by Joule heating. As the current density is increased not only will the temperature and the flux increase exponentially but also the flux divergence will increase. Therefore , he argued that the n would rise without bound and would be very sensitive to applied current . Therefore it would be very difficult, if not impossible, to make extrapolations to other conditions such as a flux divergence caused by structural defects. The disadvantage of this model as Lloyd pointed out is that when there are changes in the failure mechanism between the stress conditions and the use conditions, the extrapolations will be invalid because of the incorrect fitting parameters. In addition Black's model does not describe the statistics of the Time to Failure which are very important in analysing the failure behaviour due to electromigration.

2.3.2 The Electromigration Failure Model Based on Classical theory

In this model [Attardo, et al.,1971], the authors attempt to relate the time to failure t_f to various structural divergences which may be present in the conductor. The structural divergences considered in this model are due to the differences in grain size, grain-boundary mobility, and grain-boundary orientation with respect to the

electric field. The statistical distributions of divergences due to these attributes are empirically determined. A computer is used to simulate both the structure of a thin-film conductor and its time to failure. The model is then used to predict the dependence of the conductor reliability on the microscopic design features such as grain size distribution, conductor length and width. However the model that is used in the simulations is not 'realistic' (where a simple and fixed structure of grain boundaries is used) if compared to the 'Voronoi' technique which are one of the method used in producing realistic interconnects.

The model employs the diffusion mechanism of vacancies along the grain boundaries. The derivation of the model starts by employing the vacancy flux equation use by [Ghate, 1967], which actually originated from the classical theory by Huntington and Grone[Ho and Kwok,1989] i.e.:

$$J_v = \left(\frac{N_v}{kT}\right).D_v Z^* ej\rho \qquad\qquad 2.3$$

where

J_v = Vacancy flux

N_v = density of diffusing vacancies

k = Boltzmann's constant

T = absolute temperature

D_v = vacancy diffusion coefficient

Z^* = effective charge of ion

e = charge of electron

ρ = film resistivity

j = current density

The magnitude of the vacancy flux divergence, $\partial J_v / \partial x$ which is equal to the rate of vacancy accumulation at the divergent site is related to the failure time by :-

$$\frac{\partial J_v}{\partial x} = -\frac{\partial N_v}{\partial t} \qquad\qquad 2.4$$

The failure is defined as the time it takes to accumulate a critical number of vacancies N_v^c, so that the Time to Failure t_f is given by the equation below:-

$$t_f = \frac{N_v^c}{\left(\dfrac{\partial N_v}{\partial t}\right)} \qquad\qquad 2.5$$

and since the number of vacancies necessary to cause an open circuit is dependent on the width of the conductor, they derived the general equation:-

$$t_f = CW\left(\frac{\partial N_v}{\partial t}\right)^{-1} \qquad\qquad 2.6$$

where C is a constant of proportionality and W is the uniform width of the conductor. Therefore , failure time is directly related to the width of the conductor and inversely related to the magnitude of the flux divergence within it.

Next Attardo and co-workers worked on the distribution of the parameters that cause flux divergences. For the grain boundary mobility or diffusivity they used the results of [Hoffman and Turnbull,1954] and also from [Li,1961] to get the value of a critical angle θ of misorientation between two adjacent grains. For the triple point divergences they assume the distribution function of the angle ψ which the grain boundary makes with the electric field is uniform between 0^0 and 90^0. The grain size distribution was obtained experimentally and found to follow a lognormal distribution, while the mean grain diameter was obtained by assuming a square shape for each grain. The time to failure distribution was established by assuming that each grain boundary has a unique mobility associated with it(a random angle θ) , oriented at some random angle ψ with respect to the electric field and the magnitude of flux divergence at each location is calculated by taking the difference in the sum of the mobilities into and out of a given section of the conductor. The equation that does that is:-

$$t_f = CW(\sum_{\substack{paths \\ out}} A\sin\frac{1}{2}\theta_i \cos\psi_i - \sum_{\substack{paths \\ in}} A\sin\frac{1}{2}\theta_j \cos\psi_j)$$ 2.7

where A is a mobility constant

The simulation of the time to failure was performed on a IBM 360 model 50 computer and the results obtained are summarise below:-

1. mean time to failure t_{50} decreases with increasing conductor length.
2. standard deviation σ of the failure distribution decreases with increasing length
3. mean time to failure t_{50} increases linearly with increasing width in the range from 0.2 to 1 mm.
4. mean time to failure t_{50} increases with mean grain size if the variance of the grain size is kept constant.
5. mean time to failure t_{50} decreases with increasing variance of grain size distribution if the mean grain size is kept constant.
6. life distribution for electromigration failure approximates a lognormal distribution.

Another study[Schoen,1979], employed the same model as Attardo and co-workers and used the Monte Carlo method to simulate the dependence of electromigration lifetime on the parameters of linewidth, line length, and film grain size. In their work, a computer is used to create hypothetical lines having the same grain size distribution as real films. Each line is broken into sections and the grain boundary structure of each section is simulated statistically. The grain boundary orientation and diffusivity are simulated and the time to failure of the section is computed. The time to failure of the entire line is determined by the minimum failure time of a critical section which is defined as the section having the greatest imbalance of vacancy flux. This procedure is repeated on many hypothetical lines to build up the failure time distribution for the real lines.

The Monte Carlo simulation results shows similar results to those obtained by Attardo when analysing the effect on mean time to failure t_{50} of the various parameters. The time to failure distribution was found to follow the logarithmic extreme value statistics when the grain size is comparable or exceeds the linewidth (near bamboo structure). In this situation, surface electromigration was assumed to play a dominant role in determining electromigration lifetime. For linewidth that exceeds the grain size, the time to failure followed a lognormal distribution.

In another study [Marcoux, et al.,1989] , a 2D simulation model is developed by using a Hewlett-Packard computer. The model employed a Monte Carlo technique to generate two-dimensional geometrical patterns that simulates the grain structure of thin metal films by Voronoi tessellations. A Voronoi tessellation is a partitioning of the plane into cells bounded by polygons. These cell represents a carpet of metal grains from which a section is cut to produce the interconnect line. The software calculates the statistical characteristics of the grain structure and simulate the distribution of the parameters below:-

- the area distribution of grain size
- the diameter distribution of the grains
- the distribution of lengths of grain boundary segment
- the number of triple points
- the number of vertices

The common feature of Marcoux et al. model with the current work(lumped element model), is the ability to demonstrate the distribution of the length of grain boundary cluster. Extra features of the current work which are not in Marcoux et al. simulation results are i) number of grain boundary in a cluster and ii) number of cluster in an interconnect which are analysed to find their effect on Time to failure.

The Marcoux et al. model   uses Fortran program to approximate the steady state behaviour of the temperature and current density j distribution. For the grain boundary mobility or diffusivity D, eqn(2.8) is used:-

$$D = D_0 \exp(E_A / kT) \sin\left(\frac{\theta}{2}\right) \qquad\qquad 2.8$$

where θ is the misorientation (tilt angle) of adjacent grains grain

E_A is the activation energy

D_0 is the mobility constant

When these parameters have been worked out, they are substituted into the atomic flux equation:-

$$J_a = \left(\frac{N_b}{kT}\right).D \; Z_b * e\rho(j - j_c) \qquad\qquad 2.9$$

where

$\rho = \rho_0(1 + \alpha(T - T_0))$ is the resistivity at temperature T, α is temperature coefficient of resistance

$Z_b^* e = $ is the effective charge

$N_b = $ is the atom density in the grain boundary

$j_c = $ is the stress-induced counter current density term which is temperature dependent.

In this model, the parameters that are analysed which affect electromigration life time are i) current density ii) temperature and iii) linewidth

The results of the study are summarise below.

1. The mean time to failure t_{50} decreases linearly with increasing current density for a fixed line temperature, with Joule heating the decrease is non-linear.

2. The mean time to failure decreases linearly with decreasing linewidh (grain size > linewidth),however with further decrease in linewidth, the Mean Time to Failure and also the standard deviation increases.

3. The time to failure exhibits a lognormal distribution

An improvement to the classical model of Huntington and Grone which includes the 'backflux' force in the equation for electromigration atomic flux of eqn(2.3) was introduced by[Trattles, et al., 1994] . In this model, the electromigration damage is reduced to some extent by a 'backflux' force which is related to the build-up of a stress gradient and a concentration gradient along the conductor caused by the accumulation and depletion of metal. Therefore , the model solves the transport equation for atomic flux along a grain boundary in the presence of an electric filed, stress gradient and concentration gradient.

In the model it is assumed that the main cause of the flux divergence is the grain structure of the conductor and that these divergences occur at the triple-point junctions of the grain boundaries. Also in the model, the angle of mismatch θ between neighbouring grain lattices and the orientation angle ψ of the grain boundary with respect to the current flow are similar to that of [Attardo, et al., 1971]. When the electric field is applied to the conductor the divergence in the ion flux at the triple points results in the creation of a non-uniform ion concentration and a change in the stresses at these locations. It is assumed that the change in ion concentration between the two triple points is linear along the boundary and that there is no migration into or out of the grains. It is also assumed that the changes in stress at the triple points are a result of the material accumulation or depletion. An increase in ion concentration will result in a compressive stress at the triple point while a decrease in ion concentration will result in a tensile stress. It is also assumed that a linear change in stress exists along the grain boundary. The void is formed only after a critical tensile stress has been reached. There is also a critical compressive stress that the conductor can withstand before deformation takes place and hillocks grow. These critical stresses

are the cause of the incubation period where there is no observable degradation of the conductor.

Lifetime tests and resistance measuring technique are performed on a set of five conductors with different grain structures. The time to failure analysis of the conductor stressed with varying conditions (variation of current density and temperature) found the current density exponent of the Black Equation to be approximately 2.3. When stress and diffusion are not included in the model n=1 is found. This indicates the value n≈ 2 has been contributed by the localised stress and diffusion acting against the elctromigration force. The results from the simulations suggest that the resistance measuring technique provide a more accurate estimation of the activation energy Q than lifetime tests and the current-density exponent n was determined to be 2. A direct correlation between the time to failure and the rate of resistance changes was found when all conductors and stress conditions are considered together gives a relationship of the form:-

$$t_f = 0.223 R_{rc}^{-1.11}$$
2.10

where R_{rc} = the rate of relative resistance changes

2.3.3 The Continuum Models of Electromigration Failure

At present, a number of continuum models of electromigration failure are used to solve electromigration problems[Liu, et al.,1998]. The popular continuum models referred to are the vacancy drift and back diffusion model [Shazkes and Lloyd,1986] and the stress evolution model [Korhonen et al., 1993]. The latter model is now being widely used and has gained wide acceptance[Clement and Thompson, 1995], and has been used to analyse electromigration-induced failure in near-bamboo lines.[Sarychev, et al.,1999]. In this section, the literature that apply the drift diffusion

model will be reviewed first and then followed by a review on the stress evolution model .

2.3.3.1 The Drift Diffusion Models

The vacancy drift and back diffusion model popularly known as the drift diffusion model, gained early acceptance since the model developed by [Shazkes and Lloyd,1986], successfully was able to derive the j^{-2} dependence of Black's model for the mean time to failure t_{50}. The model was developed by treating both the Fickian diffusion (due to a vacancy concentration gradient) and mass transport due to the elecromigration driving force concurrently. Under an applied stress current, momentum transfer from the conduction electrons causes matter migration. As the concentration of the metal atoms increase there is an associated back-diffusion.. The general drift-diffusion equation derived by [Shazkes and Lloyd,1986] is :-

$$J_v = D\frac{\partial c}{\partial x} - \frac{DZ^* e\rho jc}{kT}$$ 2.11

where

   J_v = is the vacancy flux

   D = is the diffusivity

   Z^*e = is the effective charge

   ρ = line resistivity

   j = the current density

   k = Boltzman's constant

   T = temperature

   c = is the vacancy concentration

The first term arises from the vacancy concentration gradient -driven backflux diffusion and the second term represents the current-driven (drift) or electromigration flux. Note that, eqn(2.11) is in fact eqn(2.3) with vacancy concentration c replacing the density of diffusing vacancies N_v, but now with a back-diffusion term. In the one-dimension drift-diffusion model, the failure time is considered as the time to

reach a critical vacancy level at divergent sites i.e. the lifetime is believed to be determined mainly by void nucleation. In the study, the equation (2.11) and the continuity equation (2.12) is applied to a boundary conditions representing a semi-infinite solid with a perfectly blocking boundary. The combination of these two equation gives rise to an equation which is normally known as the 'electromigration equation' [Korhonen et al., 1993].

The continuity equation :-

$$\frac{\partial J}{\partial x} + \frac{\partial c}{\partial t} = 0$$
2.12

Combining eqn(2.11) and eqn(2.12), we obtained the electromigration equation :-

$$\frac{\partial c}{\partial t} = D\left(\frac{\partial^2 c}{\partial x^2} - \frac{Z^* e\rho j}{kT}\frac{\partial c}{\partial x}\right)$$
2.13

By taking the solution at the blocking boundary and assuming that the failure would occur when the vacancy concentration reached a critical level, c_{cr} , a new equation for time to failure can be derived. The boundary conditions use in Shazkes and Lloyd model are :-

$$c(-\infty, t) = c_{0'} ,$$

$$J_v(0, t) = 0, .$$

where c_0 = vacancy concentration at equilibrium for zero stress

This boundary condition represents a perfectly blocking boundary at x=0 .

Eqn(2.13) is solved by using the Laplace transform method and the solution is given by eqn(2.14)

$$c(x,t) = c_0 \, erfc\left(\frac{Z^* e\rho jD}{2kT.}\right)\left(\sqrt{\frac{t}{D}}\right)$$
2.14

giving a time to failure of :-

$$t_f = \left(\frac{2c_{cr}}{D}\right)\left(\frac{k}{Z^*e\rho}\right)^2\left(\frac{T}{j}\right)^2 \qquad\qquad 2.15$$

This model can be characterised as a nucleation dominated failure [Lloyd1994], where the failure is determined by the build-up of a critical vacancy concentration (usually at a terminal or blocking grain boundary) which then quickly leads to failure.[Tammaro and Setlik, 1999].

The model has been analysed for a range of boundary conditions in particular for the case of a finite aluminium stripe with blocking contacts at both ends.[Shatzkes and Lloyd,1986],[Clement, 1992]. The model has also been applied to the case where a blocking contact at one end and a constant vacancy supply at the other[Dwyer, et al., 1994]. These boundary conditions could represents the experimental situations in which electromigration is occurring along a stripe joining a large contact pad to an on-chip device. This model has also been applied to a finite line to compare the nonstationary period (nucleation model) and the stationary period(void growth model) to explain the j^{-2} dependence[Kircheim and Kaeber, 1991]. They found that void growth model also exhibits the j^{-2}. Recently [Tammaro and Setlik, 1999] claim that n=2 is the limiting behaviour of the nucleation models. The first two of these studies will be discussed here because of their significance towards the present work where their vacancy concentration time dependent equations will be used for comparison.

The study by [Clement,1992], involves the assumption that the boundaries at x=0 and x=ℓ are completely blocked such that no vacancies are allowed to pass (x indicates the distance along the interconnect, x=0 and x= ℓ corresponds to the blocking boundaries), that is

J(0,t)=0 and J(ℓ,t)=0

This corresponds to a situation that vacancies are conserved which could be maintained in a system where a thick strong passivation would preclude changes in the volume of the conductor. The other assumption made is that the

initial/background vacancy concentration is to be uniform at the equilibrium value, that is:-

$$c(x,0)=c_0$$

Here we define the direction of the electric field to be in the negative x direction. The vacancy flux is described by the drift - diffusion equation :-

$$J = -D\frac{\partial c}{\partial x} - \frac{Dc}{kT}Z^* e\rho j \qquad \text{2.16}$$

The vacancy concentration c as a function of space and time c(x,t) can be obtained by combining with the continuity equation below:-

$$\frac{\partial J}{\partial x} + \frac{\partial c}{\partial t} = 0 \qquad \text{2.17}$$

to give a drift-diffusion model of the Fokker-Planck type equation :-

$$\frac{\partial c(x,t)}{\partial t} = \frac{D\partial^2 c(x,t)}{\partial x^2} - \alpha D \frac{\partial c(x,t)}{\partial x} \qquad \text{2.18}$$

where

c is the vacancy concentration

D is the diffusion coefficient or diffusivity

$\alpha = \dfrac{Z^*.e.\rho.j}{k.T}$ is the drift coefficient

(the equation above and others from the literature have been altered to be compatible with the present study in order results may be compared)

The general equation for the vacancy concentration as a function of length and time is given as:-

$$\frac{c(x,t)}{c_0} = \frac{\alpha.\ell.\exp(-\alpha.x)}{1-\exp(-\alpha.\ell)} + \sum_{k=1}^{\infty}\left[\frac{16k\pi\alpha^2\ell^2\left[1-(-\ell)^k\exp\left(\frac{\alpha.\ell}{2}\right)\right]}{\left(\alpha^2\ell^2 + 4k^\pi\pi^2\right)^2}\right]x$$

40

$$\left[\left(\sin\frac{k\pi.x}{\ell}-\frac{2k\pi}{\alpha.\ell}\cos\frac{k\pi.x}{\ell}\right)x\exp\left(-\frac{\alpha.x}{2}-\left(k^2\pi^2+\frac{\alpha^2\ell^2}{4}\right)\frac{Dt}{\ell^2}\right)\right] \qquad 2.19$$

In steady state,

$$\frac{c(x,\infty)}{c_0}=\frac{\alpha.\ell.\exp(-\alpha.x)}{1-\exp(-\alpha.\ell)} \qquad\qquad 2.20$$

and

$$c_{max}=\frac{\alpha\ell}{1-\exp(-\alpha\ell)} \qquad\qquad 2.21$$

The summary of the results of the study are :-

i) Under dc stress conditions,the electromigration-induced vacancy concentration build-up at a blocking boundary saturates with time for finite length ℓ. The level at which vacancy concentration build-up saturates, decreases with decreasing j and ℓ.

ii) A threshold value of $j\ell$ is required to cause failure base on the assumption that the vacancy concentration at the blocking boundary must reach a critical value to initiate void formation. The maximum vacancy concentration c_{max} (Eqn(2.21) is dependent on $\alpha\ell$ or $j\ell\left(\frac{Z^*e\rho}{kT}\right)$.This results agrees with the result obtained by experiment [Blech,1976].

iii) The vacancy build-up as a function of time has a j^{-2} current density dependence below saturation.

Another study employing the drift-diffusion model was [Dwyer, et al.,1994].The study involve the assumption that vacancies are being collected at $x=\ell$ to form a void, making a blocking boundary. The condition on the vacancy flux J at $x=\ell$ is:

$J(\ell,t)=0$

At the other end of the stripe, vacancies are supplied from the contact pad in such a way to maintain a constant vacancy concentration c_0 at x=0. The boundary condition at x=0 is

$$c(0,t)=c_0$$

The drift-diffusion model of the Fokker-Planck type is again:-

$$\frac{1}{D}\frac{\partial c(x,t)}{\partial t}=\frac{\partial^2 c(x,t)}{\partial x^2}-\alpha\frac{\partial c(x,t)}{\partial x}$$ 2.22

The general solution to equation 2.22 is obtained by the method of Laplace transform, which yields the subsidiary equation of the form:-

$$\frac{c(x,s)}{c_0}=\frac{1}{s}+\frac{\frac{1}{s}\alpha\exp\left(-\frac{\alpha}{2}(\ell-x)\right)}{\sqrt{\frac{\alpha^2}{4}+\frac{s}{D}}\,x\cosh\sqrt{\frac{\alpha^2}{4}+\frac{s}{D}}\ell-\frac{\alpha}{2}\sinh\sqrt{\frac{\alpha^2}{4}+\frac{s}{D}}\ell}\,x\sinh\sqrt{\frac{\alpha^2}{4}+\frac{s}{D}}x$$ 2.23

The residues are found at the roots of the denominator and it is found that for $\alpha\ell>2$ there is one real root and infinite series of imaginary roots and for $\alpha\ell<2$ it has an infinite series of imaginary roots. The vacancy concentration is normally interested at x= ℓ. The real roots occurs at

$$\frac{\tanh\eta}{\eta}=\frac{2}{\alpha.\ell}$$ 2.24

where $\eta=\sqrt{\frac{\alpha^2}{4}+\frac{s}{D}}\ell$

The imaginary roots occurs at

$$\frac{\tan\xi}{\xi}=\frac{2}{\alpha.\ell}$$ 2.25

where

$$\pm i\xi = \sqrt{\frac{\alpha^2}{4} + \frac{s}{D}\ell}$$

Both the roots can be found by graphical methods,

The complete solution for the vacancy concentration is rather cumbersome and it has been found that the error in neglecting all but the first transient term is very small. A simpler expression for the vacancy concentration is thus

For the case $\alpha l \leq 2$

$$\frac{c(x,t)}{c_0} \approx \exp(\alpha.x) - \frac{2\alpha.\ell\exp\left[-\frac{\alpha(\ell-x)}{2}\right].\xi\sin\left(\xi\frac{x}{\ell}\right).\exp-\left(\frac{\alpha^2\ell^2}{4}+\xi^2\right).\frac{Dt}{\ell^2}}{\sqrt{\frac{\alpha^2\ell^2}{4}+\xi^2.\left(\xi^2-\frac{\alpha.\ell}{4}(2-\alpha.\ell)\right)}} \qquad 2.26$$

and for the case $\alpha l \geq 2$

$$\frac{c(x,t)}{c_0} \approx \exp(\alpha.x) - \frac{2\alpha.\ell\exp\left[-\frac{\alpha(\ell-x)}{2}\right].\eta\sinh\left(\eta\frac{x}{\ell}\right).\exp-\left(\frac{\alpha^2\ell^2}{4}-\eta^2\right).\frac{Dt}{\ell^2}}{\sqrt{\frac{\alpha^2\ell^2}{4}-\eta^2.\left(\eta^2-\frac{\alpha.\ell}{4}(2-\alpha.\ell)\right)}} \qquad 2.27$$

In the steady-state

$$\frac{c(x,t\rightarrow\infty)}{c_0} = \exp(\alpha x) \qquad 2.28$$

so that the condition for supersaturation, $c(x,t) = c^*$ becomes

$$\frac{c_{max}}{c_0} = \frac{c(x=1,t\rightarrow\infty)}{c_0} = \exp(\alpha.1) = \frac{c^*}{c_0} \qquad 2.29$$

43

where c* or c_{cr} is the critical vacancy concentration

The summary of the results form the study are:-

1. The saturation time t_{sat} increases exponentially with current density j.

2. The time to reach a given critical vacancy concentration c* or failure time varies as j^{-2}.

3. The breakdown or failure time is proportional to the critical vacancy supersaturation concentration c* or c_{cr}

These two models described above are based on a single grain boundary structure of an interconnect or as treating the interconnect as a single homogenous segment-neglecting microstructure.

There are several other studies conducted by Lloyd and co-workers with the drift-diffusion model of electromigration failure[Lloyd and Kitchin,1991],[Lloyd,1991],[Clement and Lloyd,1992],[Lloyd and Koch, 1992]. In the study by Lloyd and Kitchin, a statistical model of electromigration is developed based on the extension of the failure model of Shatzkes and Lloyd which incorporates the statistics of microstructure and the variations in the activation energy for grain-boundary conditions. The boundary condition applied somewhat arbitrarily are a 'semi-perfect' blocking barrier boundary, which would not completely stop the flux but reduce to some background level. The barrier is also assumed to lower the diffusivity in the same manner. The failure time t_f is defined as the time to reach an arbitrarily defined critical vacancy concentration c_{cr} .Under these conditions, the model is valid for passivated interconnects, i.e. there is a boundary condition that would allow a vacancy supersaturation to take place. The models assumes a lognormal distribution for grain size and for the activation energy for the self-diffusion in grain boundary. The failure distribution function F(t), for an element (made up of two adjoining segments separated by a barrier) are found not to be lognormal. The cumulative density function or CDF of an interconnect which is

composed of a number of failure elements based on the 'links in a chain' or ' weakest link model' is found to be approximated by multilognormal distribution.

A mathematical model based on the drift-diffuison equation to predicts the damage morphologies are develop [Lloyd and Koch, 1992]. The study is based on the concept that an electromigration induced mass flux divergence will create a local vacancy supersaturation in the grain boundaries and a steady-state vacancy concentration profile will be established where the vacancy generation rate is balanced by the rate at which vacancies diffuse to the surface via the boundary or through the lattice. The damage is in the form of crack-like voids and the thinning of an area near the grain boundary. The model is use to predict the failure morphology, where the appearance of the failures should vary with temperature. At low temperature, failure should be look like a crack, whereas at higher temperature, thinning will be experienced.

In another study conducted by [Lloyd , 1991], the previous study of [Shatzkes and Lloyd,1986] are reviewed and commented. The author comments that although the model correctly deals with the kinetics of grain boundary diffusion and predicts the j^{-2} dependence of lifetime, the geometrical effects of the grain boundary structure are not considered. The author also argues that the earlier models can only be used to describe the process which leads to the generation of an initial void, but does not describe the whole failure process. Since there must be two distinct stages to electromigration-induced failure, the failure time can be expressed as the sum of the time required to nucleate a void, and the time it takes the void to grow and form an open circuit. Once a void is formed, the earlier model in reference of [Shatzkes and Lloyd,1986] will be no longer valid. The void will possesses a free surface which is not present in a passivated film. With this free surface acting as a sink, the high electromigration-induced vacancy concentration described in the earlier model of [Shatzkes and Lloyd,1986] cannot be supported. The flux divergence will still be present, but instead of building an excess vacancy concentration, the flux divergence will feed vacancies into the void leading to $c=c_0$ model at the void end.

2.3.3.2 The Stress Evolution Models

One of the first to study the mechanical stress arising due to electromigration was Blech and co-workers [Blech,1976],[Blech and Herring, 1976] who explained the origin of the stress gradients and introduced the concept of a threshold length-current density product ($j\ell$) for electromigration. The metal atoms transported (via electromigration) to a blocking boundary build up a compressive stress with the highest level at the boundary. The resulting stress gradient will contribute to the driving force for mass transport. In the presence of a blocking boundary, a stress gradient could form which would act against the electromigration force and eventually stop mass flow. The critical length-current density product ($j\ell$) is due to the limitations on the stress that the conductor metal can sustain. If a maximum or 'yield' stress is reached, no further transport of atoms is possible because the electrical driving force is balanced by a compressive stress gradient which causes an equal but opposing driving force. Above this maximum stress, the stress gradient required to stop the mass flow can no longer be maintained and electromigration will continue and the aluminium deforms plastically which is commonly manifested in hillock formation. For short lines, however, the stress gradient can be maintained without exceeding the maximum stress. The electromigration force equation in the presence of stress gradient is given below [Blech and Herring, 1976].

$$F = Z^* e\rho j - \Omega \frac{\partial \sigma}{\partial x} \qquad\qquad 2.30$$

Since the study by Blech, many more studies were carried out to produce a physical model for stress evolution in interconnects. These include the works by Kircheim[Kircheim, 1992& 1993],and also the work by Korhonen and co-workers.,[Li, et al.,1992],[Korhonen et al, 1993]. In the study [Kircheim,1992] , the author proposes a model of electromigration in which generation of tensile and compressive stresses in grain boundaries during electromigration is caused by the annihilation and production of vacancies. The model is based on the two coupled partial differential equations for vacancy concentration and stress. In the development of the stress model, Kirchheim assume that the vacancies C_v are in equilibrium with

the stress σ i.e. if σ changes then C_v also changes immediately by the following relation:-

$$C_v = C_{0v} \exp\left(\frac{\Omega\sigma}{kT}\right) \qquad\qquad 2.31$$

where

C_{0v} is the vacancy concentration at zero pressure(stress)

Ω is the atomic volume

σ is the hydrostatic stress.

The tensile stress ($\sigma > 0$) increases the vacancy equilibrium concentration and therefore the magnitude of the material flux, i.e. shorten the lifetime of an Al lines. When the vacancies are in equilibrium with the stress, the vacancy flux equation of the drift-diffusion model will be modified by the inclusion of equation (eqn.2.31) giving rise to:

$$J_v = \frac{D_v C_v}{kT} eZ^* \rho j - \frac{D_v C_v}{kT} \Omega \frac{\partial\sigma}{\partial x} \qquad\qquad 2.32$$

Note that by combining with eqn(2.32) and (eqn2.31), eqn(2.32) also reduces to eqn(2.11) of the drift-diffusion model.

The model also assumes that the Time to Failure is defined as the time necessary to reach a critical stress σ_{cr}. The important results from the work of [Kirchheim, 1992] is that the Time to Failure is proportional to the current density j^{-n} where the current exponent n varies from 1 at low critical stress (± 10 MPa) and 2 at high critical stress (300Mpa). However the statistical distribution of the Time to Failure is not performed and the model does not include the continuity equation with a source/sink term.

Early work of Korhonen and co-workers proposed a model to predict the variation of lifetimes due to temperature and current density [Li, et al.,1992]. According to the

47

model, the failure of interconnect lines occurs through the rapid nucleation of voids by thermal stress. Small voids are trapped and grow at grain boundaries. After reaching a critical size, voids then begin to migrate and coalesce until the line is severely damaged. Failure times are determined by the largest/fastest growing void in a line. For low current density j, an approximate j^{-2} dependence of the lifetime is expected, and for higher currents they predict a large current dependence because the voids are expected to start migrating immediately upon the application of higher currents. They also found that for grain sizes smaller than the linewidth, the temperature dependence is characteristic of grain boundary diffusion, and for near bamboo structure lines, it approaches that of the lattice diffusion. For thermal stress induced voids already large, the lifetime is determined by current-induced coalescence and is proportional to the surface diffusion coefficient and a j^{-1} dependence.

In a later work, Korhonen et. al., developed a model which describes the mechanical stress arising from electromigration in a confined metal line which is deposited on an oxidised silicon substrate and covered by a rigid dielectric passivation.[Korhonen, et al.,1993(1)]. The stress evolution model equation derived by Korhonen et al. is given below (a complete description will be presented in Chapter 3) :-

$$\frac{\partial \sigma}{\partial t} = \frac{\partial}{\partial x}\left[K\left(\frac{\partial \sigma}{\partial x} + G\right)\right]$$
2.33

where

$K = \dfrac{D_a B\Omega}{kT}$ is the effective diffusivity

$G = \dfrac{Z^* e\rho j}{\Omega}$ is the electromigration driving force

Eqn (2.33) is an extension of eqn(2.32) which accommodates the continuity equation with a source/sink term. The model shows the evolution of the stress assuming vacancy equilibrium with the stresses and that failure was determined by the build-up of a critical level of stress. In the model, the stress state is purely hydrostatic and constant across the line cross section. It is a one-dimensional model which depicts a

thin interconnect having a columnar grain structure where all grain boundaries are perpendicular to the substrate. The material transport along the interconnect line is assumed to be affected by grain boundary diffusion only. The model has been applied for a semi-infinite and finite line with blocking boundaries and with constant diffusion coefficient. It assume that the line is finite and initially has thermal-induced voids and a diffusion coefficient dependent on vacancy concentration.

The stress evolution model has also been applied to an interconnect line consisting of several clusters of grains,(with at least one grain boundary along the line) and several bamboo grains.[Korhonen, et al.,1993(2)]. On the application of current, flux divergences arise due to the different diffusivities in the bamboo and cluster grains. The bamboo grain effectively blocks the atomic flux at the ends of the cluster section. The electromigration flux depletes atoms from the cathode end of a cluster and accumulates them at the anode end, thus creates a stress σ which opposes the electromigration flux. As time increases, the electromigration flux creates an oscillating stress pattern. A schematic diagram of the interconnect line used in the study and the stress distribution due to electromigration are shown in Figs 2.1 and 2.2 respectively.
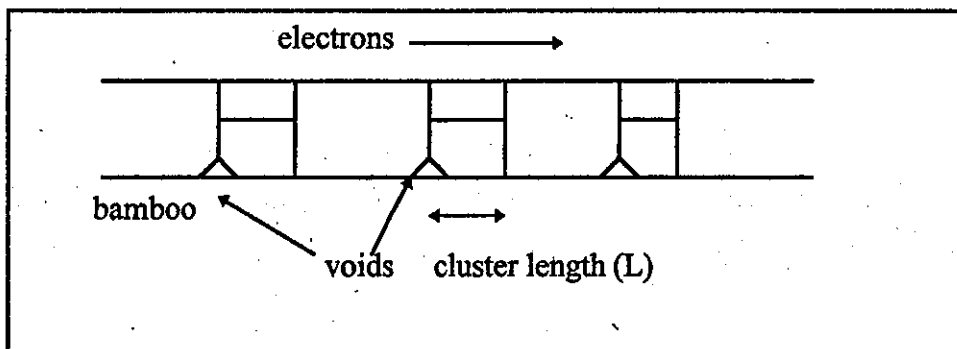
Fig.2.1 A schematic diagram of the cluster and bamboo sections of an interconnect line.
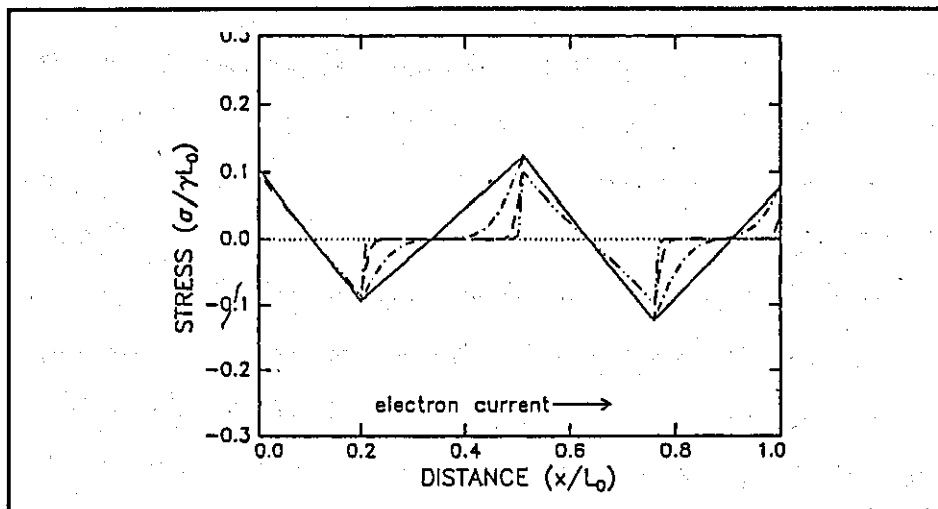
Fig2.2 The stress distribution during electromigration. Initial stress (small dots), final stress (solid line), stress at medium times(broken lines)

The failure distribution of the model in Fig 2.1 is found to be consist of :-

1. Early failures in interconnect line which contain clusters length L greater than the critical length ($L > L_{cr}$), because only grain boundary diffusion needs to be involve.

2. Long term failures where short clusters are distributed among long bamboo segments, because bulk or lattice diffusion dominates the lifetime.

3. Medium term failures where bamboo sections are short enough for the failure units to start interacting.

In another study [Knowlton,et al.,1997], the stress evolution model has been used to simulate the effects of grain structure on the time to failure. Realistic continuous film and line microstructures have been generated by a grain growth simulator with a large population of samples of lines in order to obtain meaningful failure time distributions for a variety of line characteristics and testing conditions. This enables the prediction of the occurrence of the failure mechanism as a function of linewidth, line length, critical stress, postpattern annealing time and current density. A log-normal distribution of grain sizes with a value of 0.28 for the standard deviation σ_{sd} has been used for the simulation of the film. Interconnect lines of widths and lengths (relative to the median grain size d_{50}) are then etched from this film. The failure

50

criterion for a line was taken to be the time at which the maximum stress in the line reached a predefined critical or failure stress σ_{cr}. It was also assumed that the critical stress σ_{cr} is uniform along the line length, although there is evidence lines are more likely to fail at locations where contamination is present (such that σ_{cr} varies with position). The model has been applied to the boundary conditions such that $\sigma(0,t) = \sigma(L,t) = \sigma_0$ or $J_a(0,t) = J_a(L,t) = 0$ which represents a line ending in two large contact pads(constant stress) or two studs(zero atomic flux).

The results of the simulation shows that the time to failure, as well as the failure mechanism, is strongly dependent upon the critical stress. Polygranular mechanisms will dominate if σ_{cr} is 100Mpa or less since the line contains clusters long enough to support stresses due to grain-boundary diffusion. If σ_{cr} is 400Mpa , the line will survive much longer, failure will require significant diffusion through the bamboo grains, and transgranular failure mechanisms will dominate.

The simulations have been carried out for 10 samples of lines with zero-stress boundary conditions and a linewidth-to-grain-size ratio of 0.5. When σ_{cr} is small, the lines fail due to polygranular mechanism since the clusters can easily support a stress large enough for failure. If the critical stress is large, the failure is due to transgranular mechanism. In both cases, the failure distribution is monomodal since only one failure mechanism is active. The failure distribution for the case of an intermediate critical stress is bimodal since both failure mechanisms are active, accounting for the large deviation in failure time. The standard deviation σ_{sd} for large critical stress is also quite large , the authors reason that the large variation arises from the fact that the maximum line steady-state stress achieved is sensitive to the spatial distribution of polygranular clusters along the line. A line in which the clusters are distributed relatively evenly along its length will survive longer than a line in which the clusters are distributed unevenly along its length. For the effect of length and linewidth, shows MTTF rises dramatically as does the standard deviation DTTF with decreasing linewidth/median grain size. The line length also affects the number of clusters. Since shorter lines are less likely to contain long cluster, the MTTF is higher than the longer lines. The standard deviation DTTF is also found to increase.The results from

the model is consistent with experimental on near-bamboo AL-Cu lines such as [Cho and Thompson,1989]. The study also includes the effect of postpattern annealing of interconnect and the results shows an improvement of lifetime for narrow lines. Postpattern annealing will results in the reduction of the number and lengths of clusters . Not only the cluster shrink , but long clusters may also split into two smaller clusters as large grains within a polygranular cluster can grow to span the width of the line. As a result the number of clusters which are longer than the critical length is reduced.

The study on the effect of the stress dependence of the atomic diffusivity on the stress evolution due to electromigration was conducted by [Park and Thompson, 1997]. They modelled the time evolution of the stress along interconnects through the use of a one-dimensional simulation as a function of current density. As a source for atomic flux divergence sites, a polygranular cluster region was introduced into the bamboo interconnect as a region of finite length with higher diffusion coefficient. The model assumes that the ends of the interconnects were at zero stress. The stress becomes tensile at the cathode end of the polygranular cluster and compressive at the anode end. The results of the simulation shows that the peak tensile stress first increased to a maximum of about 200 MPa and then decreased to a very small value, while the peak compressive stress continuously increased to maximum of about 400 MPa. The behaviour was explained by the effect of the stress on atomic diffusivity. The atomic diffusivity is larger in the tensile region that in the compressive region, therefore faster kinetics are applied in the tensile region and the peak tensile grows faster than the peak compressive stress during the initial time period. Such fast kinetics in the tensile region quickly leads to a quasi-steady state. At longer times, diffusion in the bamboo regions dominates the evolution of the stress. The peak tensile stress continues to decrease and the peak compressive stress continues to increase until a true steady state is reached, in which a minimum flux through the interconnect results in a small maximum compressive stress in the true steady state. The simulation results shows that the peak tensile and the compressive stresses in the steady state are dependent on the length and location of the polygranular and the current density.

A stress-evolution model was used to find the steady-state of the mechanical stress in interconnect lines was developed by [Gleixner and Nix, 1998]. The model is based in two dimensions, to take account of the effects of bamboo boundaries on the maximum stress which may develop, which the earlier stress-evolution model of Korhonen et.al, ignored. The model assumes that the mass transport is along the sidewalls and the grain boundaries, where diffusion along these paths is much faster than the line bulk. The results of the simulation reveals that the presence of bamboo grain boundaries may substantially increase the maximum electromigration stress, and the simulations on bounded interconnect segments show that variations in grain size may lead to large standard deviation in the maximum stress as line length decreases.

Despite the very different underlying physics, where under the stress evolution model, the current-induced flux creates a stress-directed counterflux, which retards electromigration damage, while the drift-diffusion or the 'electromigration equation' the counterflux arises due to the vacancy concentration gradient, both models have a similar mathematical formalism. In fact a number of papers[Clement and Thompson, 1995],[Clement, 1997],[Liu, et al, 1998] has showed it is possible to transform the Stress Evolution model into a drift-diffusion equation with an effective diffusion coefficient which is proportional to the vacancy concentration.

The other main difference between the two models is that in the drift-diffusion model used by researchers mention in earlier sections does not include the effect of sources or sinks of vacancies. The study of [Clement and Thompson,1995],[Clement,1997] include the recombination/generation effect and use the Stress Evolution model in terms of the drift-diffusion equation. The electromigration-induced transport of vacancies will change the local vacancy concentration and the stress. Korhonen et al. also assumes the vacancies are in equilibrium with the stress. They pointed out that dislocation climb is a mechanism by which the equilibrium between the stress and the vacancy concentration can be maintained.

The largest portion of the transported vacancies will be taken up in recombination/generation by climbing dislocations either in the grain boundary or at lattice dislocation, thereby changing the local stress. A very small number of vacancies will go into changing the local vacancy concentration to maintain local equilibrium with the stress. Since the concentration of vacancies is very small in comparison to the concentration of atoms, dislocations must climb only infinitesimal distances to restore the local vacancy concentration. With the inclusion of the recombination/generation effect, a drift-diffusion equation is derived once again but with the critical difference that the diffusion term D_v which is replace by $D_a B\Omega/kT$ which leads to an important differences in the time scale. [Korhonen,et al.,1993] pointed out that the vacancy concentration gradients can be created in a matter of seconds because of the almost negligible small mass transport and the other hand, stress evolution in interconnect lines during electromigration can last hundreds of hours. With the result obtained from these studies, it is shown that the analysis of the drift-diffusion equation in the interconnect network will cover both the current continuum models of electromigration failures.

Finally [Duan & Shen,2000] proposed an alternative failure criterion, that of a critical accumulation of flux divergence instead of the critical stress. He argue that the divergence of atomic flux , rather than the stress, are more appropriate in characterising the electromigration damage using the one-dimensional stress evolution model. This is based on the numerical analysis of the nanoindented single-crystal aluminium which shows that i) during electromigration, the maximum tensile stress and the maximum atomic flux divergence do not generally appear at the same location in a metal line and ii) the location of voiding predicted by the maximum flux divergence criterion is more in line with experimental observations [Joo et al., 1998 and 1999] than the predicted by the maximum stress criterion. Using the critical stress failure criterion, voiding should occur at the cathode end of the fast-diffusion segment. However analysis shows that the maximum flux divergence does not occur at the exact cathode end of the fast diffusion segment , but instead it appears near the cathode end but outside the fast diffusion segment.

However, the suggestion of [Duan and Shen,2000] that the voiding criterion is based on a critical accumulated flux divergence is shown to be equivalent to the widely accepted critical stress criterion of Korhonen based on the study by [Dwyer and Wan Ismail, 2001]. Solving the stress equation (eqn(2.33)), Duan and Shen find that the two criteria give different voiding points. However , it is clear that by integrating eqn(2.33), these two criteria are in fact identical where the stress and the atomic flux are related by the equation below:-

$$\sigma(x,t) = B\Omega \int_0^t \frac{\partial J_A}{\partial x} dt \qquad\qquad 2.34$$

In the study, the Dwyer and Wan Ismail (Appendix C)are able to reproduce the figures of [Duan and Shen,2000] for stress evolution and for the atomic flux , but are not able to reproduce the figure for the accumulated flux divergence, which in the study is found to be proportional to the tensile stress and thus is in line with eqn(2.31) Also for nanoindented single crystal aluminium line , the theoretical position of maximum stress lies outside the indented region if standard Electromigration models are to be assumed.

2.4 Summary

A survey of the literature, related to the electromigration problems in the interconnect of Integrated Circuit has been presented in Chapter 1 and 2. The past and present study of electromigration is reviewed with a focus on the physical and experimental nature of electromigration- induced failures.

The literature review have given an overview of electromigration which includes a review of the history and some salient features regarding electromigration. The failure mechanism of an interconnect is presented where the main cause is due to the presence of a flux divergence. The effects of the microstructure and macrostructure on the lifetime are also discussed. A brief description of the models of electromigration-induced failure are also presented. Various techniques of extending

the lifetime of interconnects due to electromigration are also being discussed where Al interconnects are being switched to Cu interconnect for next three generations of IC designs. The remainder of the thesis concentrates on Al for which most results are known.

Electromigration Time to Failure statistics are normally assumed to follow a lognormal distribution both from data produced by experimental observation and from models simulation. However this distribution cannot be scaled with length when considering the 'weakest link' model. Also from experimental data, it is also shown that the Median Time to Failure (MTTF) , which is used as the standard measurement for electromigration, increases in the near-bamboo type of interconnect, however the standard deviation (DTTF) are also increases giving rise to reliability concern where early failures occur minimising the advantage of the increase in the MTTF.

A complete review of the various models of electromigration-induced failure are made where focus is made to compare the different underlying physics of failure and the assumptions made in deriving the models and also the results they produce. The continuum models which comprise of the drift-diffusion and the stress evolution model are discussed in detail to establish their main differences , advantages and disadvantages. The past and the current work on the stress evolution model is reviewed extensively.

The main points to note for the remainder of this thesis are that:-

(i) Currently, the most widely accepted model of Electromigration is Korhonen's stress evolution model.

(ii) Studies using this model are generally one dimensional. Thus microstructure has been averaged across the linewidth so that interconnects are treated as having cluster sections with fast diffusion D_{fast} and bamboo sections with slow diffusion D_{slow}. Aside from this the microstructure detail is washed out.

(iii) The stress in the calculations have been assumed to be hydrostatic and uniform across the linewidth   which assumes passivation and substrate do not fix the metallisation position . This is unrealistic.

CHAPTER 3

THE DEVELOPMENT OF THE LUMPED ELEMENT MODEL

3.0   Introduction

A number of physical models now exist to describe the electromigration problem
which range from the empirical, such as Black's original equation[Black, 1969],and
the semi-empirical, such as that reference of Hu and co-workers[Liew,et al.,1990], to
the more quantitative continuum descriptions which includes the drift-diffusion
model   [Shatzkes   and   Lloyd,1986],[[Lloyd   and   Kitchin,1991   and
1994],[Clement,1992],[Dwyer, et al.,1994],[Kirchheim and Kaeber,1991] and the
Stress Evolution model [Korhonen et al.,1993].   Korhonen's model has received a
great deal of interest in the literature and must now be considered to be the currently
accepted model for Electromigration. The continuum models are more attractive as
they do not use arbitrary fitting parameters . However , these models have been
largely applied to the very simplest case of an interconnect whose properties, at
position x along the line, are averaged over its width and thus do not include the
microstructure in a realistic manner. Although the results for this special case are
encouraging (a j^{-2} dependence is found for the lifetime defined here as the time to
reach a critical stress σ_{cr}) it does not really provide a sufficient test for the validity of
the models. Beyond producing an inverse-square dependence on dc current, a second
and vital test for any model is that of its ability to predict the correct statistical
distribution of observed lifetimes, traditionally believed to be lognormal[Cho and
Thompson,1989][Thompson ,1990][Liew, et al., 1992],[Joo and Thompson ,1994].

The present work largely considers the theoretical aspects of the electromigration
problem where a new approach is developed to investigate microstructural effects
(lengths of grain boundaries, diffusivities, and angle of orientation) on the failure
time. The development of the lumped element model will be based on the Stress
Evolution model which is now the most accepted model in describing
electromigration. Within the Stress Evolution model, the current work will attempt to

demonstrate that the equation which describes the evolution of stress within the interconnect is equivalent to a slow (compared to original drift diffusion model) non-linear drift-diffusion equation description of the vacancy build-up. In the current model , it is assumed that the electromigration failure is caused when the stress reaches some critical yielding value of critical stress σ_{cr} or equivalently a vacancy concentration c_{cr} (eqn(2.31). The current model attempts to demonstrate that a good approximate description of the stress evolution in a grain boundary network can be obtained by considering, instead, an equivalent electrical problem on a lumped CR network. Using this approximation it is then possible to calculate the interconnect lifetimes or Time to Failure using commonly available software packages such as PSpice or Matlab.

The CR network obtained can also be utilised to predict an approximation to the failure time by involving Elmore's delay time[Elmore,1948]. This method is used by CMOS circuit designers to obtain rapid estimates of the time-delays in complex circuits. Just as with the supersaturation threshold for the electromigration lifetime, the CMOS time-delay is the time for some variable(a voltage in this case) to reach a given threshold.

3.1   Some background of the stress evolution models

The microstructure of a modern interconnect is characterised by a series of polygranular cluster regions separated by a number of single grains spanning the linewidth as shown in Fig 3.1. Such interconnects are said to possess a ' near-bamboo' microstructure.
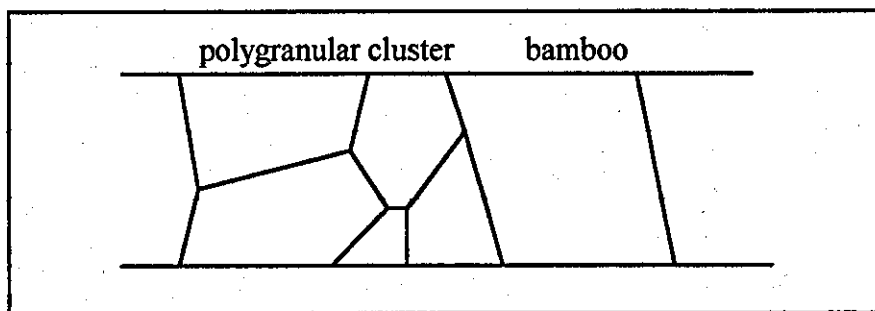
Fig 3.1 Schematic of typical near bamboo grain structure interconnect

Atomic diffusion is much greater along the grain boundaries than it is along the sidewall or through the grain bulk, so that matter migrates, at least at first, along the grain boundary networks that make up the cluster regions. The result is a mass accumulation downwind of the electron current where it is deposited in the grain boundaries at climbing dislocations producing a local compressive stress. Likewise, mass is depleted upwind producing a local tensile stress[Blech and Herring , 1976]. The resulting stress gradient causes a driving force that opposes the electromigration force, eventually leading to a non-equilibrium steady state[Gleixner and Nix, 1998]. It is generally argued that interconnect failure will occur if the stress reaches some critical value σ_{cr}. This cannot occur if the grain boundary cluster length is too short , as insufficient stress will arise, a pheomenon known as the Blech length effect[Blech and Herring,1976],[Knowlton et al.,1997]

In a typical interconnect, the evolution of the stress can be seen to pass through three distinct regions[Blech,1976]. First a quasi-steady state is reached in the cluster sections due to matter transport along the grain boundary. Second, the stress fields within these sections then stay roughly constant as significant stress develops in the single-grain bamboo sections. Finally stress coupling between the cluster sections occurs.

The distribution of cluster and bamboo sections results from some stochastic process (possibly described by the Voronoi network of Thompson and co-workers[Cho and Thompson,1989]. Likewise the diameter of an individual grain is generally taken to have a lognormal distribution, grain orientation possess a roughly uniform distribution $(0-90^{0})$[Kircheim and Kaeber,1991], while the atomic diffusion coefficient for a given grain boundary depends upon the crystalline faces of the two grains from which it is made. Fig 3.2(a) shows a dislocation model of a small-angle grain boundary. The line between points a and b corresponds to a boundary. Fig 3.2(b) shows the relationship between the tilt angle (θ) , Burgers vector of dislocation(b), and the spacing between the dislocations (d).
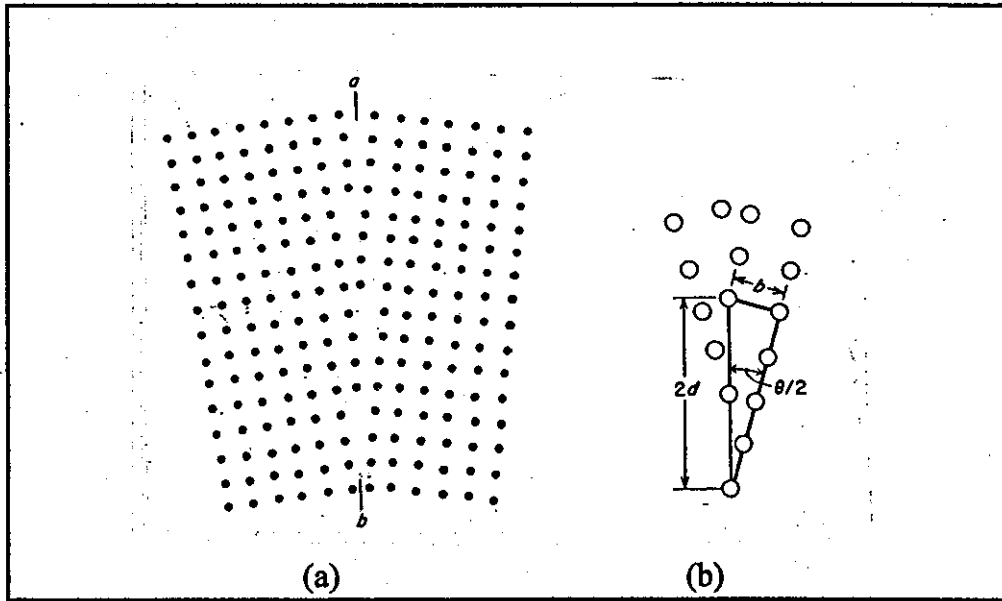
Fig 3.2(a) The dislocation model of a small-angle grain boundary

(b) The geometrical relationship between θ,the angle of tilt,

b, the Burger vector and d, the spacing between dislocations

The distribution of the diffusion coefficient for low angle tilt grain boundary is given by the equation derived by Turnbull and Hoffman [Kirchheim and Kaeber,1991] :-

$$D_{gb} = \begin{cases} D.\sin\dfrac{\theta}{2}\dots\dots\dots\dots\dots 0^0 \langle \theta \langle 36^0 \\[2em] D.\sin 18^0 \dots\dots\dots\dots\dots 36^0 \leq \theta \leq 120^0. \end{cases} \qquad 3.1$$

where D is constant and θ is the tilt angle of the grain boundary. In addition the effective charge $Z^* e$ may vary between grain boundaries. As a result the Time to Failure (TTF) for a particular metalisation process is itself a stochastic variable.

Most models for the evolution of stress are one-dimensional(most notably reference [Korhonen ,et al., 1993]). In this model, the microstructural effects and the electromigration current are averaged over the linewidth. This leads to an effective diffusion coefficient of :-

$$D_{eff} = \frac{\delta}{W} D_a^{GB}$$ 3.2

where D_a^{GB} is the atomic diffusion coefficient for migration along the grain boundary network, δ is the width of the grain boundary and W is the linewidth. Essentially Korhonen et al. argue that matter inclusion in the grain boundaries may be treated as a simple, uniform increase in the thickness of the grain boundary. The rigid passivation and substrate layers provide a simple volume constraint, which produces a hydrostatic pressure on the aluminium. Ignoring the traction between the grains and substrate and the grains and the rigid passivation layers leads to a homogenous hydrostatic stress again rendering the problem of one-dimensional. A more plausible constraint was considered by Gleixner and Nix , who included the traction at the surface, effectively treating the grain boundary as a Mode 1 crack stretching from the passivation to the substrate. The constraint on free energy minimisation, in this case, being a uniform pressure at the grain boundary interface rather than the uniform interface displacement assumed by Korhonen. Finite Element calculations then show that the stress field is not homogenous within a cross-section of the interconnect, but rather is localised around the grain boundary. The one-dimensional model can thus only really be considered as an approximation, as it cannot model, for example, the effects of a non-uniform distribution of bamboo-grains [Gleixner and Nix ,1998].

Gleixner and Nix consider the steady-state of a typical interconnect, by evaluating the stress field on a stick-network of grain boundaries. The aim of the current work is to look at a means of modelling the stress evolution ,on an interconnect of an arbitrary microstructure, by considering the matter transport on the cluster networks. For early failures, stress evolution is confined to the individual cluster sections [Blech ,1976] and thus the present model seeks only to study the stress evolution in an arbitrary single polycrystalline cluster, represented by a stick-network.

3.2   Stages of the development of the present model

The development stages of the lumped element model shall be as follows:-

i. The description of the stress evolution model under electromigration on a network of one-dimensional grain boundaries

ii. The development of the exact steady-state solution for a single polygranular section of columnar grains

iii. The development of the distributed CR network in a single grain boundary

iv. The development of the lumped C-R-C Π network in a single grain boundary.

v. The analysis of the accuracy of the C-R-C Π network-

vi. The development of the Matrix representation of the C – R – C Π networks

vii. The development of the signal or Elmore delay in estimating the Time to Failure

viii. The non-linear solution for concentration dependent $D(\sigma)$

In the development of the model, the assumptions of the pseudo-one-dimensional network and of modelling the exact distributed CR transmission line by the lumped elements are the only approximations made

3.3   The description of the stress evolution model

In electromigration , the total atomic flux density is generally taken to be

$$J_A = \frac{D_A C_A}{kT} \left(\Omega \nabla \sigma + Z^* e \rho j \underline{i} \right) \qquad 3.3$$

where σ is the normal tensile stress on the grain boundary, C_A is the atomic concentration, D_A is the atomic diffusion coefficient, Z^* is the effective electromigration charge, e is the electron charge, ρ is the resistivity of the film, j is the applied current and Ω is the atomic volume, k is the Boltzman's constant, T is the operating temperature and $\underline{i}$ is the unit vector along the interconnect [Korhonen, et al.1993]. Electromigration occurs largely as a result of electron scattering from the metal atoms, biasing the hopping probability in the downwind direction. This probability is mainly limited by the concentration of vacancies C_v and consequently varies with the stress. Equivalently one may view the matter transport as

a vacancy flux in the opposite direction. With this equivalence, the relation $\mu_v C_V = \mu_A C_A$ must hold for the atom and vacancy mobilities μ_A and μ_V, and then, provided that the mobilities satisfy the Einstein relation $D_{A,V} = \dfrac{kT}{Z^*e}\mu_{A,V}$, we obtain

$$D_V C_V(\sigma) = D_A(\sigma)C_A \qquad\qquad 3.4$$

The limiting factor for vacancy diffusion is then the atomic concentration C_A, which can be taken to be constant $\left(C_A = \dfrac{1}{\Omega}\right)$, thus the vacancy diffusion coefficient D_V is also constant and independent on stress σ. The electromigration vacancy flux may be written as [Korhonen ,et al.,1993]

$$J_V = -\frac{D_V \Omega C_V(\sigma)}{kT}\left(\nabla\sigma + \frac{Z^*e\rho j}{\Omega}\underline{i}\right) \qquad\qquad 3.5$$

Vacancy continuity [Korhonen,M.A.,1993] implies that

$$\nabla.J_V + \frac{\partial C_V}{\partial t} + \gamma = 0 \qquad\qquad 3.6$$

The final term on the left-hand side of eqn(3.6) describes the dynamics of the vacancy sources and sinks.

The current model is developed by using the model of Korhonen et al. and taking into account the decoupling of the stresses between grain boundaries [Gleixner and Nix ,1998] and also including the effects of the microstructure on the stress evolution. The model is developed by considering the stress evolution on the grain boundaries (where all variables are indicated by a superscript GB). In this case the vacancy current along a columnar grain boundary in the direction $\underline{r}$ is given by

$$J_V^{GB} = -\frac{D_V^{GB}\Omega C_V^{GB}(\sigma)}{kT}\left(\nabla\sigma_N^{GB} + \frac{Z^*e\rho j}{\Omega}\underline{i}\right).\underline{r} \qquad\qquad 3.7$$

and the vacancy continuity yields

$$\nabla . J_V^{GB} + \frac{\partial C_V^{GB}}{\partial t} + \gamma^{GB} = 0 \qquad 3.8$$

The term γ^{GB} describes the vacancy recombination at the grain boundary. In order to proceed the expression for this recombination rate and also a relationship between the normal stress on the grain boundary and the local vacancy concentration must be obtained. It is assumed that the vacancy concentration is kept roughly in thermal equilibrium with the normal stress[Korhonen ,et al.,1993] and is given by

$$C_V^{GB} \approx c_0 \exp\left(\frac{\Omega \sigma_N^{GB}}{kT}\right) \equiv c(r,t) \qquad 3.9$$

where c_0 is the vacancy concentration in stress free material

It is also assumed that the recombination of the vacancies occurs through dislocation climb, creating a local tensile stress field σ_N^{GB}, normal to the grain boundary.[Korhonen , et al.,1993]. Thus

$$\partial \sigma_N^{GB} = -B \frac{\partial C_A^{GB}}{C_A^{GB}} \quad = -\frac{B}{C_A^{GB}} \gamma^{GB} \partial t \qquad 3.10$$

$$\text{where } \gamma^{GB} = -\frac{\partial C_A^{GB}}{\partial t},$$

C_A^{GB} is the atom concentration in the grain boundary ($\approx \Omega^{-1}$) and B is a coefficient which depends upon the elastic properties of the metal (ranges from 0.5 to 0.75 times the Young's modulus for Al.)[Korhonen et al.,1993(1)]).Note the model assumes a linear and elastic relationship between stress and strain. The vacancy dynamics is described by the following cycle. First, deposited atoms are overwhelmingly incorporated at climbing dislocations which leads to a very slow increase in the local compressive stress, or equivalently , a slow decrease in the local tensile stress, at downwind sites. Second, the vacancy concentration is assumed to change quickly

65

with the tensile stress and thus $C_V^{GB}(r, t)$ decreases typically at downwind sites and typically increases at upwind sites with the stress.

From eqn.(3.9)

$$C_V^{GB} \approx c_0 \exp\left(\frac{\Omega \sigma_N^{GB}}{kT}\right)$$

$$\frac{\partial C_V^{GB}}{\partial \sigma_N^{GB}} = \frac{c_0 \Omega}{kT} \exp\left(\frac{\Omega \sigma_N^{GB}}{kT}\right) = \frac{\Omega}{kT} C_V^{GB}$$

$$\partial \sigma_N^{GB} = \frac{kT}{\Omega C_V^{GB}} \partial C_V^{GB} \qquad\qquad 3.11$$

The equation of the recombination is given by:-

$$\gamma^{GB} = -\frac{C_A^{GB}}{B} \cdot \frac{\partial \sigma_N^{GB}}{\partial t} \qquad\qquad 3.12$$

substituting eqn(3.11) into eqn (3.12) gives

$$\gamma^{GB} = -\frac{kT}{B\Omega} \frac{C_A^{GB}}{C_V^{GB}} \cdot \frac{\partial C_V^{GB}}{\partial t} \qquad\qquad 3.13$$

By using the values of the parameters used by Korhonen et.al,
where,

k= Botlzman's constant= 1.38×10^{-23} JK^{-1}

T= operating temperature in Kelvin = 500K

B= 50 Gpa= 50×10^9 Nm

Ω = atomic volume =1×10^{-29} m^3

$$\frac{C_A^{GB}}{C_V^{GB}} = 10^7$$

$$\gamma^{GB} = 1.38 \times 10^5 . \frac{\partial C_V^{GB}}{\partial t} >> \frac{\partial C_V^{GB}}{\partial t}$$

The inequality above means that the middle term in the continuity equation of eqn(3.8) can be ignored. The new continuity equation is given below

$$\nabla.J_V^{GB} + \gamma^{GB} = 0 \qquad\qquad 3.14$$

The stress evolution for a single columnar grain boundary in the direction of the interconnect (x) is derived below :-

If the stress is hydrostatic ($\sigma_{(r)}^{GB} = \sigma_{(x)}$) at all points in a plane perpendicular to the stripe length, then averaging over the width of grain boundary, gives

The average recombination

$$\bar{\gamma} = \frac{\delta}{W} . \gamma^{GB}$$

where δ = width of grain boundary,

W= average grain size

from eqn(3.12) gives the average recombination by the equation below

$$\gamma^{GB} = -\left(\frac{W}{\delta}\right).\left(\frac{C_A^{GB}}{B}\right).\left(\frac{\partial \sigma_N^{GB}}{\partial t}\right) \qquad\qquad 3.15$$

and subtituting γ^{GB} in the continuity equation (3.14)

$$\nabla.J_V^{GB} + \gamma^{GB} = 0$$

$$= \nabla \cdot \left(\frac{D_V^{GB} \cdot C_V^{GB}(\sigma)}{kT} \left(\Omega \nabla \sigma^{GB} + G \right) \right) - \left(\frac{W}{\delta} \right) \cdot \left(\frac{C_A^{GB}}{B} \right) \cdot \left(\frac{\partial \sigma^{GB}}{\partial t} \right) = 0$$

where $G = \dfrac{Z * e\rho j}{\Omega}$

Then

$$= \frac{\partial}{\partial x} \left(\frac{D_V^{GB} \cdot C_V^{GB}(\sigma)}{kT} \left(\Omega \frac{\partial}{\partial x} \sigma^{GB} + G \right) \right) - \left(\frac{W}{\delta} \right) \cdot \left(\frac{C_A^{GB}}{B} \right) \cdot \left(\frac{\partial \sigma^{GB}}{\partial t} \right) = 0$$

rearranging gives

$$\left(\frac{W}{\delta} \right) \cdot \left(\frac{C_A^{GB}}{B} \right) \cdot \left(\frac{\partial \sigma^{GB}}{\partial t} \right) = \frac{\partial}{\partial x} \left(\frac{D_V^{GB} \cdot C_V^{GB}(\sigma) \Omega}{kT} \left(\frac{\partial}{\partial x} \sigma^{GB} + G \right) \right)$$

Then

$$\frac{\partial \sigma^{GB}}{\partial t} = \left(\frac{\delta}{W} \right) \left(\frac{B}{C_A^{GB}} \right) \left(\frac{D_V^{GB} \Omega}{kT} \right) \left[C_V^{GB}(\sigma) \frac{\Omega}{kT} \frac{\partial \sigma^{GB}}{\partial x} \left(\frac{\partial \sigma^{GB}}{\partial x} + G \right) + C_V^{GB}(\sigma) \frac{\partial^2 \sigma^{GB}}{\partial x^2} \right]$$

$$\frac{\partial \sigma^{GB}}{\partial t} = \left(\frac{\delta}{W} \right) \left(\frac{B}{C_A^{GB}} \right) \left(\frac{D_V^{GB} C_V^{GB}(\sigma) \Omega}{kT} \right) \left[\frac{\partial^2 \sigma^{GB}}{\partial x^2} + \frac{\Omega G}{kT} \frac{\partial \sigma^{GB}}{\partial x} + \frac{\Omega}{kT} \left(\frac{\partial \sigma^{GB}}{\partial x} \right)^2 \right] \quad 3.16$$

Ignoring the dependence of $C_V^{GB}(\sigma)$ on σ and if $\dfrac{\Omega \sigma}{kT} \ll 1$, the first term on the right hand side is a diffusion term with diffusivity

$$D_V^{eff} = \left(\frac{\delta}{W} \right) \cdot \left(D_V^{GB} \right) \left(\frac{B\Omega}{kT} \right) \left(\frac{C_V^{GB}}{C_A^{GB}} \right) \qquad 3.17$$

which is equivalent to the equation of [Korhonen et al.,1993]

$$D_A^{eff} = \left(\frac{\delta}{W} \right) \cdot \left(D_A^{GB} \right) \left(\frac{B\Omega}{kT} \right) \qquad 3.18$$

where $D_A^{GB} = \dfrac{D_V^{GB} C_V^{GB}}{C_A^{GB}}$ from eqn(3.4)

Therefore the complete stress evolution equation over time is given below:-

$$\left(\frac{\partial \sigma^{GB}}{\partial t}\right) = = D_V^{eff}\left(\frac{\partial^2 \sigma_N^{GB}}{\partial x^2} + Z^* e\rho j \frac{\partial \sigma_N^{GB}}{\partial x}\right) \qquad 3.19$$

The difference between the effective grain boundary diffusion coefficient D_V^{eff} of eqn(3.18) and the diffusion coefficient for the bulk D_B using the values of [Korhonen,et al.,1993] and [Knowlton ,et al.,1997] are calculated below:-

$D_a = 3\times10^{-16}\,m^2\,/\,s$ = effective diffusion coefficient for the entire cross section
$\delta D_A^{GB} = 3\times10^{-22}\,m^3\,/\,s$
δ = grain boundary width = $1 \times 10^{-9}\,m$
$\dfrac{C_V}{C_A} = 10^{-7}$

and assume the grain size $W = 10^{-6}\,m$

from eqn(3.2),

$$D_a = \frac{\delta D_A^{GB}}{W}, \text{ therefore}$$

The atomic grain boundary diffusion coefficient

$$D_A^{GB} = \frac{D_a.W}{\delta} = \frac{3\times10^{-16} \times 1\times10^{-6}}{1\times10^{-9}} = 3\times10^{-13}\,m^2 s^{-1}$$

from the relationship eqn(3.4)

$$\delta D_V^{GB} = \delta D_A^{GB} \frac{C_A}{C_V}$$

$$D_V^{GB} = D_A^{GB} \frac{C_A}{C_V}$$

The vacancy diffusion coefficient at grain boundary
$$D_V^{GB} = 3\times10^{-13}\,m^2 s^{-1}.10^7 = 3\times10^{-6}\,m^2 s^{-1}$$

$$\frac{B\Omega}{kT} = \frac{50\times10^9.10^{-29}}{1.38\times10^{-23}.500} = 100/1.38 = 72$$

Therefore, the effective vacancy diffusion coefficient

$$D_V^{eff} = \left(\frac{\delta}{W}\right).\left(D_V^{GB}\right)\left(\frac{B\Omega}{kT}\right)\left(\frac{C_V^{GB}}{C_A^{GB}}\right)$$

$$D_V^{eff} = \frac{1x10^{-9}}{1x10^{-6}}.3x10^{-6}.72.1x10^{-7}$$

$$D_V^{eff} = 2.16\,x10^{-14}\,m^2s^{-1}$$

The Bulk diffusivity $= D_B = \dfrac{D_a}{200} = \dfrac{3x10^{-16}}{200} = 1.5x10^{-18}\,m^2s^{-1}$

where 200 is the ratio of D_a to D_B [Knowlton, et al.,1997]

which means that $D_V^{eff} > D_B$. Thus the effective diffusion along grain boundary is much faster than actual diffusion through bulk.

With the early failures occuring in cluster sections acting independently,equation (3.16) must be solved on the grain boundary network in each cluster section. Note that a ($J_V = 0$) quasi steady-state is reached on the grain boundary network long before it is reached through diffusion via the bulk because the true bulk vacancy diffusion is much smaller than the effective grain boundary diffusion coefficient as shown above. Early failure, though, will occur through vacancy transport along grain boundaries within a cluster section, as the maximum stress that arises is obtained first on the grain boundary network. Thus, the analysis of earlier failures in a single cluster, needs only to consider the transport along the grain boundary network and not the later bulk diffusion[Blech,1976]. Stresses in the grain bulk, and hence vacancy concentrations, arise as a result of grain boundary stresses and not bulk vacancy diffusion..

The equation describing the stress evolution at a grain boundary may equally be expressed in terms of the derived variable c(r,t), defined in eqn(3.9), which is closely related to the vacancy concentration in the grain boundary $C_V(r,t)$. Therefore, in terms of this variable , the vacancy concentration c(r,t) build-up for a single columnar grain boundary in the direction of the interconnect (x) are derived below :-

From the Korhonen et al. equation

$$J_V^{GB} = -\frac{D_V^{GB}\Omega c}{kT}\left(\frac{\partial \sigma_N^{GB}}{\partial x} + \frac{Z^* e\rho j}{\Omega} i\right)$$

but (in terms of variable c(r,t))

$$\sigma_N^{GB} = \frac{kT}{\Omega c}\partial c \qquad \text{from eqn(3.11)}$$

$$J_V^{GB} = -\frac{D_V^{GB}\Omega c}{kT}\left(\frac{kT}{\Omega c}\frac{\partial c}{\partial x} + \frac{Z^* e\rho j}{\Omega} i\right) \qquad\qquad 3.20$$

the vacancy recombination rate is given by:-

$$\gamma^{GB} = \left(\frac{W}{\delta}\right)\cdot\left(\frac{C_A^{GB}}{B}\right)\cdot\left(\frac{kT}{\Omega c}\frac{\partial c}{\partial t}\right) \qquad\qquad 3.21$$

and from the continuity equation eqn(3.14)

$$\nabla.J_V^{GB} + \gamma^{GB} = 0$$

substituting into the continuity equation above

$$= -\frac{\partial}{\partial x}\left(\frac{D_V^{GB}\Omega c}{kT}\left(\frac{kT}{\Omega c}\frac{\partial c}{\partial x} + \frac{Z^* e\rho j}{\Omega}\right)\right) + \left(\frac{W}{\delta}\right)\cdot\left(\frac{C_A^{GB}}{B}\right)\cdot\left(\frac{kT}{\Omega c}\cdot\frac{\partial c}{\partial t}\right) = 0$$

rearranging

$$\left(\frac{W}{\delta}\right)\cdot\left(\frac{C_A^{GB}}{B}\right)\cdot\left(\frac{kT}{\Omega c}\cdot\frac{\partial c}{\partial t}\right) = \frac{\partial}{\partial x}\left(D_V^{GB}\left(\frac{\partial c}{\partial x} + \frac{Z^* e\rho j c}{kT}\right)\right)$$

$$\left(\frac{\partial c}{\partial t}\right) = \left(\left(\frac{\delta}{W}\right)\cdot\left(\frac{B}{C_A^{GB}}\right)\left(\frac{\Omega c}{kT}\right)D_V^{GB}\cdot\left(\frac{\partial^2 c}{\partial x^2} + \frac{Z^* e\rho j}{kT}\frac{\partial c}{\partial x}\right)\right)$$

$$\left(\frac{\partial c}{\partial t}\right) = \left(\left(\frac{\delta}{W}\right)\cdot\left(\frac{B}{C_A^{GB}}\right)\left(\frac{\Omega c}{kT}\right)D_V^{GB}\cdot\left(\frac{\partial^2 c}{\partial x^2} + \frac{Z^* q.\rho.j}{kT}\frac{\partial c}{\partial x}\right)\right)$$

Therefore, the vacancy build-up equation is given below:-

$$\frac{\partial c}{\partial t} = D_V^{eff}\left(\frac{\partial^2 c}{\partial x^2} + \frac{Z^* e \rho j}{kT}\frac{\partial c}{\partial x}\right) \qquad 3.22$$

and eqn (3.20) can be replaced by

$$J_V^{GB} = -\frac{D_V^{GB}\Omega c}{kT}\left(\frac{kT}{\Omega c}\frac{\partial c}{\partial x} + \frac{Z^* e \rho j}{\Omega}i\right) = -D_V^{GB}\left(\frac{\partial c}{\partial x} + \alpha c\right) \qquad 3.23$$

eqn(3.22) is then replaced by

$$\frac{\partial c}{\partial t} = D_V^{eff}\left(\frac{\partial^2 c}{\partial x^2} + \frac{Z^* e \rho j}{kT}\frac{\partial c}{\partial x}\right) = D_V^{eff}\left(\frac{\partial^2 c}{\partial x^2} + \alpha \frac{\partial c}{\partial x}\right) \qquad 3.24$$

where α is $\dfrac{Z^* e \rho j}{kT}$ (this variable will be used in the later section in the development of the lumped element model)

Both equation(3.22) and equation(3.19) of Korhonen et.al's stress evolution model are non-linear Partial Differential Equation's(PDE). Therefore significant progress can only be made by linearisation. In both cases linearisation , relies on the fact that the ratio $c/c_0 = \exp(\Omega \sigma_N^{GB}/kT)$ does not change appreciably from unity. Setting $D \approx D_V^{eff}$ in eqn(3.22) reduces it to a linear drift-diffusion type, exactly equivalent to the Electromigration Equation model of Lloyd and co-workers, except that now $c(r,t)(=C_v(r,t))$ varies much more slowly as a result of the recombination affecting the diffusion coefficient as in eqn(3.17). The difference between eqn(3.22) and the Electromigration Equation (eqn(2.12) is one of time scale. A suitable analogy is the eventual flooding of a region despite possessing a very good drainage system. The Electromigration Equation model does not allow 'drainage'(recombination), so vacancy levels change very rapidly.

Eqn(3.22) must be solved on each grain boundary of a polygranular section of the interconnection, which are represented as a stick-network of one-dimensional columnar grain boundaries. The conditions on $c(r,t)$ at the intersection of two or more

grain boundaries are those of continuity. Integrating eqn(3.14) at an intersection of grain boundaries i,j,.... etc. yields

$$c_i(n,t) = c_j(n,t) \qquad \sum_i \delta_i J_i(n,t) = 0 \qquad\qquad 3.25$$

where i is the grain boundaries which join at node n and the current densities $(|J_v(n,t)| = J_i(n,t)$ on grain i) here are defined out of the node n, δ_i is the width of the i-th grain boundary, $c_i(n,t)$ is the 'vacancy concentration' at the intersect on grain boundary i at time t and the sum is over all the grains boundaries making the intersection.

3.4   The development of the exact 'steady-state' solution

In the development of the present model, the steady-state solution for a single polygranular section of columnar grains represented by a one-dimensional stick-network is considered first. This will be useful, as it is indicative of those nodes at which failure is likely and also leads to the well-known length effect for electromigration failure. But more importantly, the solution suggests a means of investigating the approach to the quasi-steady state and which will lead to an estimation of the failure time.

In the steady state both $J_v(r)$ and $D_v(r)$ are constant along grain boundary i, and are equal to J_i and D_i respectively. An auxiliary function $v(r)$ is introduced and is defined according to

$$c(r) = \exp(\alpha.r).v(r) \qquad\qquad 3.26$$

where $\alpha = Z^* e\rho j / kT$

From eqn(3.23)

$$J_i(r) = -D_i\left(\frac{\partial c(r)}{\partial r} + \alpha c(r)\right)$$

and after rearranged becomes

73

$$\frac{\partial c(r)}{\partial r} + \alpha c = -\frac{J_i}{D_i} \qquad\qquad 3.27$$

and this takes in the form of a linear equation of the first order and can be solved by

the integrating factor method where the Integrating factor $(I.F) = e^{\int -\alpha \partial r} = -e^{-\alpha r}$

Eqn(3.27) are now in the form of

$$\frac{\partial c(r)}{\partial r} \cdot e^{\int -\alpha \partial r} = -\frac{J_i}{D_i} \cdot e^{\int -\alpha . dr}$$

$$\frac{\partial}{\partial r}\left(c(r)e^{-\alpha r}\right) = -\frac{J_i}{D_i} \cdot e^{-\alpha r}$$

but from eqn(3.26), $c(r) = e^{\alpha r} . v(r)$

therefore

$$\frac{\partial}{\partial r}\left(v(r)\right) = -\exp(-\alpha . r)\frac{J_i}{D_i} \qquad\qquad 3.28$$

Note that continuity of c(r,t) at a grain boundary intersection (eqn(3.25)) also implies continuity of v(r,t) at those points. Integrating eqn(3.28) along the one-dimensional grain boundary (r_i, r_{i+1}) yields

$$v(r_{i+1}) - v(r_i) = -\frac{J_i}{D_i}\int_{r_i}^{r_{i+1}}\exp(-\alpha . r)dr$$

$$= J_i \frac{\left[\exp(-\alpha . r_i) - \exp(-\alpha . r_{i+1})\right]}{\alpha . D_i} \qquad\qquad 3.29$$

Eqn(3.29) has the appearance of a random resistor network with $v(r_i)$ as a (quasi) voltage at the node at r_i and J_i that of current. The resistor values are distributed according to

$$R_i = \frac{1}{D_i \delta_i d} \int_{r_i}^{r_{i+1}} \exp(-\alpha . r) dr \qquad 3.30$$

where δ_i is the width of the grain boundary i, d is the thickness of the grain boundary assumed to be thickness of metallisation. The topology of the electrical network is identical to the topology of the grain boundary network. An equivalent electrical circuit is obtained by placing a node at each edge or triple point and replacing the grain boundary between the connected nodes by the appropriate resistor R_i. The diffusion coefficient D_i is constant along a grain boundary, eqn(3.30) allows for extra nodes to be introduced, this divides the grain boundary into two (or more) resistors leaving the total sum unchanged. The extra resistor values can be calculated by using the same equation (3.30). To simplify the model, all the grain boundaries have been assumed to have the same average width $\delta_i = \delta$ and shall take the units of the area such that $\delta d = 1$.

3.5 The development of the distributed CR network for a single grain boundary

As described in the last section, the steady-state of the stress /vacancy build-up result mimicked exactly a random resistor network. It is common in previous (one-dimensional) models [Korhonen M.A.et.al,1993] to ignore the dependence of D_{eff} on stress, then the time development of the system mimics exactly a distributed inhomogeneous CR transmission line as derived below. At this point it is useful to introduce the following equivalent electrical circuit identification

i.) $\quad v(r,t) = c(r,t) \exp(-\alpha . r)$

ii) $\quad R(r) = \dfrac{\exp(-\alpha . r)}{D(r)}$

iii) $C(r) = \exp(\alpha.r)$

      where v= pseudo voltage,

            c= charge/vacancy concentration,

            R=resistance per unit length,

            C= capacitance per unit length.

Along a single grain boundary, the vacancy flux of equation (3.23) can be write in Laplace- space as the pair

$$J = -D\left[\frac{\partial c}{\partial x} - \alpha c\right] \qquad\qquad 3.31$$

$$\frac{\partial J}{\partial x} + sc - c_0 = 0 \qquad\qquad 3.32$$

and from eqn(3.28)

$$\frac{\partial}{\partial r}(v(r,t)) = -\exp(-\alpha.r)\frac{J_i(r)}{D_i(r)} \qquad\qquad 3.33$$

Equations 3.32 and 3.33 may be written for an arbitrary grain boundary, in terms of the pseudo-voltage (v(r,s)) and current (J(r,s)) in the Laplace domain as

$$\nabla.J_i(r,s) = -sc(r,s) + c_0 \qquad\qquad 3.34$$

$$\nabla.v(r,s) = -\exp(-\alpha.r)\frac{J_i(r,s)}{D_i(r)} \qquad\qquad 3.35$$

After substituting the equivalent electrical circuit identification (i)-(iii) ,the equations (3.34) and (3.35) becomes the transmission line pair

$$\nabla.J_i(r,s) = -sC(r)v(r,s) + c_0 \qquad\qquad 3.36$$

$$-\nabla.v(r,s) = R(r).J_i(r,s) \qquad\qquad 3.37$$

Eqns(3.36) & (3.37) represents a linear but inhomogenous transmission line system where the ' line capacitance' increases exponentially while the line resistance decreases exponentially with x, the distance down the line. Both these eqns (3.36 and 3.37) expresses an important point, i.e. the vacancy concentration equations can be transformed exactly into transmission line equations. This means that it is possible to model the line exactly with a distributed CR network of series resistance and parallel capacitance. The only approximation made in solving the problem will be to replace the distributed transmission line with a finite number of lumped capacitors and resistors which will be described in the next section.

3.6   The development of the lumped CR network for a single grain boundary

By using the same approach as in section 3.5, the vacancy build-up equation along a single grain boundary in Laplace space is given by the eqn(3.31) and (3.32)

$$J = -D\left[\frac{\partial c}{\partial x} - \alpha c\right] \hspace{4cm} 3.31$$

$$\frac{\partial J}{\partial x} + sc - c_0 = 0 \hspace{4cm} 3.32$$

In the literature, analytical solutions to the above problem exist in the analysis of a single one-dimensional grain boundary of length ℓ.[Shatzkes and Lloyd ,1986],[Lloyd and Kitchin ,1994],[Clement, 1991],[Lloyd,and Kitchin,1994] and [Dwyer.,et al.,1994] . Two typical cases are considered corresponding to a blocking boundary ($J(\ell,t) = 0$) at the downwind end and, at the upwind end , either Case(A); where $\sigma(0,t) = 0$ (equivalent to $c(0,t)=c_0$); or Case (B) where $J(0,t)=0$.

The vacancy concentration $c(x,s)$ and the vacancy current $J(x,s)$ at the boundaries x=0 and x=ℓ can be related by a transfer matrix T and a U vector with appropriate boundary conditions. Thus, integrating eqn(3.31) and eqn(3.32)

$$\begin{bmatrix} c(\ell,s) \\ J(\ell,s) \end{bmatrix} = T \begin{bmatrix} c(0,s) \\ J(0,s) \end{bmatrix} + U \qquad 3.38$$

The T and U matrices are given by

$$T = \frac{1}{\beta_+ - \beta_-} \begin{bmatrix} \beta_+ \exp(\beta_+ \ell) - \beta_- \exp(\beta_- \ell) & \exp(\beta_- \ell) - \exp(\beta_+ \ell) \\ s(\exp(\beta_- \ell) - \exp(\beta_+ \ell)) & \beta_+ \exp(\beta_- \ell) - \beta_-(\beta_+ \ell) \end{bmatrix} \qquad 3.39$$

and

$$U = \frac{c_0}{s}(I - T) \begin{bmatrix} 1 \\ \alpha D \end{bmatrix} \qquad 3.40$$

where $\beta_{\pm}(s) = \dfrac{\alpha}{2} \pm \sqrt{\dfrac{\alpha^2}{4} + \dfrac{s}{D}}$ and I is the identity matrix $= \begin{bmatrix} 1 & 0 \\ 0 & 1 \end{bmatrix}$. The value of $\beta_{\pm}$

is derived by [Dwyer, et al. 1994] and is reproduced as shown below.

From eqn(3.24), the vacancy build-up equation

$$\frac{\partial c}{\partial t} = D\left(\frac{\partial^2 c}{\partial x^2} + \alpha \frac{\partial c}{\partial x} \right)$$

Taking the Laplace Transform of the left hand side gives

$$sc - c_0 = D\left(\frac{d^2 c}{dx^2} + \alpha \frac{dc}{dx} \right) \qquad 3.41$$

$$\frac{sc - c_0}{D} = \frac{d^2 c}{dx^2} + \alpha \frac{dc}{dx} \qquad 3.42$$

let $u = c - \dfrac{c_0}{s}$ therefore $su = sc - c_0$

and $\dfrac{du}{dx} = \dfrac{dc}{dx}$

substitute into eqn(3.42) becomes

$$\frac{su}{D} = \frac{d^2u}{dx^2} + \alpha\frac{du}{dx} \qquad\qquad 3.43$$

This is an ODE which has solution of the form

$u = e^{\beta x}$

therefore eqn(3.43) becomes

$$\frac{se^{\beta x}}{D} = \beta^2 e^{\beta x} - \alpha\beta e^{\beta x} \qquad\qquad 3.44$$

cancelling the common term, eqn(3.44) becomes

$$\frac{s}{D} = \beta^2 - \alpha\beta$$

and after rearranging

$$\beta^2 - \alpha\beta - \frac{s}{D} = 0 \qquad\qquad 3.45$$

Solving the eqn(3.45) by the usual method $= \dfrac{-b \pm \sqrt{b^2 - 4.a.c}}{2.a}$ gives

$$\beta_+^- = \frac{\alpha \pm \sqrt{\alpha^2 + 4\dfrac{s}{D}}}{2} = \frac{\alpha}{2} \pm \sqrt{\frac{\alpha^2}{4} + \frac{s}{D}} \qquad\qquad 3.46$$

The two special cases as mentioned earlier are analysed. For case A (i.e. $c(0)=c_0$ and $J(\ell)=0$), the input and output matrix are shown below

$$\begin{bmatrix} c(\ell,s) \\ J(\ell,s) \end{bmatrix} = \begin{bmatrix} T_{11} & T_{12} \\ T_{21} & T_{22} \end{bmatrix} \cdot \begin{bmatrix} c(0,s) \\ J(0,s) \end{bmatrix} + \begin{bmatrix} U_1 \\ U_2 \end{bmatrix} \qquad\qquad 3.47$$

with the boundary condition, eqn(3.43) becomes

$$\begin{bmatrix} c(\ell,s) \\ 0 \end{bmatrix} = \begin{bmatrix} T_{11} & T_{12} \\ T_{21} & T_{22} \end{bmatrix} \cdot \begin{bmatrix} \dfrac{c_0}{s} \\ J(0,s) \end{bmatrix} + \begin{bmatrix} U_1 \\ U_2 \end{bmatrix} \qquad \text{3.48}$$

By expanding the matrix eqn(3.48)

$$c(\ell,s) = \frac{T_{11}c_0}{s} + T_{12}J(0,s) + U_1 \qquad \text{3.49}$$

$$0 \quad = \frac{T_{21}c_0}{s} + T_{22}J(0,s) + U_2 \qquad \text{3.50}$$

and solving for J(0,s) gives

$$J(0,s) = -\frac{\left(\dfrac{T_{21}c_0}{s} + U_2\right)}{T_{22}} \qquad \text{3.51}$$

substituting eqn(3.51) into eqn(3.49), gives

$$c(\ell,s) = \frac{T_{11}c_0}{s} + T_{12}\left(-\frac{\left(\dfrac{T_{21}c_0}{s} + U_2\right)}{T_{22}}\right) + U_1$$

$$= \frac{T_{11}c_0}{s} - \frac{T_{12}\cdot T_{21}\cdot c_0}{s\,T_{22}} - \frac{T_{12}\cdot U_2}{T_{22}} + U_1$$

$$= \frac{T_{22}\cdot T_{11}c_0}{s\,T_{22}} - \frac{T_{12}\cdot T_{21}\cdot c_0}{s\,T_{22}} - \frac{T_{12}\cdot U_2}{T_{22}} + \frac{T_{22}\cdot U_1}{T_{22}}$$

$$= \frac{T_{22}\cdot U_1 - T_{12}\cdot U_2}{T_{22}} + \left(T_{22}T_{11} - T_{12}T_{21}\right)\frac{c_0}{s\,T_{22}}$$

$$c(\ell,s) = \frac{T_{22}\cdot U_1 - T_{12}\cdot U_2}{T_{22}} + \frac{c_0\cdot \det T}{s\,T_{22}} \qquad \text{3.52}$$

In this case, the time constants depend upon the zeros of T_{22} and these occur when

$$\beta_+ \exp(\beta_-\ell) - \beta_- \exp(\beta_+\ell) = 0 \qquad \text{3.53}$$

In case B (i.e. $J(0)=J(\ell)=0$), the matrix equation is shown below

$$\begin{bmatrix} c(\ell,s) \\ 0 \end{bmatrix} = \begin{bmatrix} T_{11} & T_{12} \\ T_{21} & T_{22} \end{bmatrix} \cdot \begin{bmatrix} c(0,s) \\ 0 \end{bmatrix} + \begin{bmatrix} U_1 \\ U_2 \end{bmatrix}$$

3.54

By expanding the matrix eqn(3.54)

$$c(\ell,s) = T_{11}.c(0,s)+0+U_1$$

3.55

$$0 \quad = T_{21}.c(0,s)+0+U_2$$

3.56

therefore

$$c(0,s) = -\frac{U_2}{T_{21}} \text{ and } c(\ell,s) = -\frac{U_2.T_{11}}{T_{21}}+U_1$$

3.57

and the time constant depend upon zeros of T_{21}. These occur when

$$\exp(\beta_-\ell) = \exp(\beta_+\ell)$$

3.58

The above matrix equations are in terms of the input variables [$c(0,s),J(0,s)$] and output variables [$c(\ell,s),J(\ell,s)$]. For the equivalent electrical circuit in terms of the pseudo-voltage (v)and current (J), a transfer matrix t , connecting the input variables [$v(0,s),J(0,s)$] to the output variables [$v(\ell,s),J(\ell,s)$], can be obtained by manipulating the transfer matrix T which connects [$c(0,s),J(0,s)$] and [$c(\ell,s),J(\ell,s)$]. Thus

$$t = \begin{bmatrix} T_{11}\exp(-\alpha\ell) & T_{12}\exp(-\alpha\ell) \\ T_{21} & T_{22} \end{bmatrix} = \begin{bmatrix} \exp(-\alpha l) & 0 \\ 0 & 1 \end{bmatrix} \begin{bmatrix} T_{11} & T_{12} \\ T_{21} & T_{22} \end{bmatrix} = e.T$$

3.59

Referring to the earlier cases of A and B, and provided that the matrix elements $t_{22} = T_{22}$ and $t_{21}= T_{21}$ have dominant poles near s=0, the long time behaviour of $v(x,t)$ is determined by the small s behaviour of $v(x,s)$.

The t matrix (eqn 3.59) is approximated by expanding the transfer matrix T (eqn3.39) in small s, and the final equation is shown below :-

$$t \cong \begin{bmatrix} 1 + \dfrac{s}{\alpha^2 D}\big(\exp(-\alpha\ell) + \alpha\ell - 1\big) & -\left[\dfrac{1-\exp(-\alpha\ell)}{\alpha D}\right] - bs \\[3mm] -s\left[\dfrac{1}{\alpha}\big(\exp(\alpha\ell) - 1\big) + bs\exp(\alpha\ell)\right] & 1 + \dfrac{s}{\alpha^2 D}\big(\exp(\alpha\ell) - \alpha\ell - 1\big) \end{bmatrix}$$ 3.60

where

$$b = \frac{1}{\alpha^2 D^2}\left(\ell - \frac{2}{\alpha} + \left(\frac{2}{\alpha} + \ell\right)\exp(-\alpha l)\right)$$ 3.61

The t matrix in eqn(3.60) has the identical form as that of a single Π - section (t_Π) with capacitors C_1 and C_2 and resistor R as shown in Fig3.3, except for the two terms containing b .
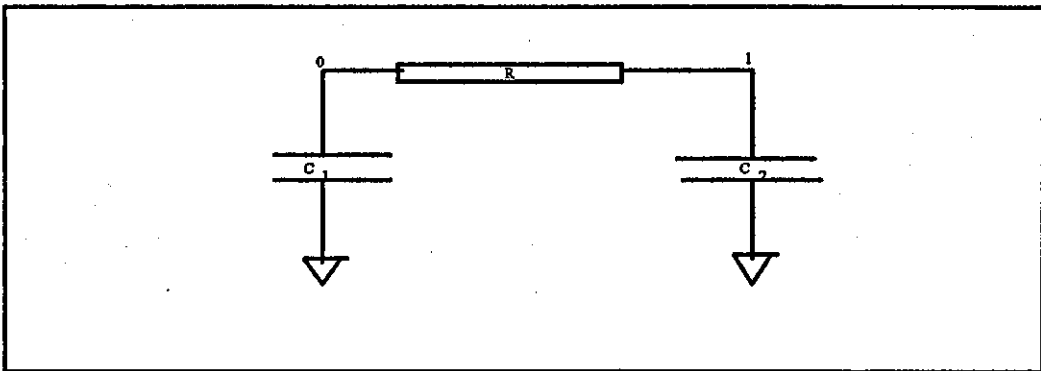
Fig 3.3   The equivalent C-R-C circuit (Π) with node 0 at x=0 and node 1 at

x=ℓ

The transfer function of the C-R-C is derived below :-

i)   **For resistor circuit in series**

$$I_1 \underline{\hspace{2cm}} \boxed{R} \underline{\hspace{2cm}} I_2$$
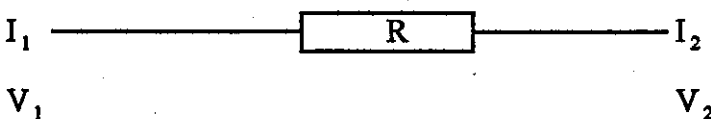
$$V_1 \qquad\qquad\qquad\qquad V_2$$

$V_2 = V_1 - I_1 R$

$I_2 = I_1$

In terms of matrix equation

$$\begin{bmatrix} V_2 \\ I_2 \end{bmatrix} = \begin{bmatrix} 1 & -R \\ 0 & 1 \end{bmatrix} \cdot \begin{bmatrix} V_1 \\ I_1 \end{bmatrix}$$

3.62

ii) For capacitor circuit in parallel
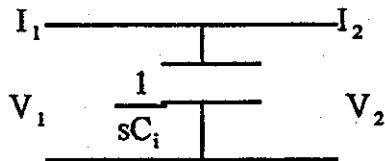
$V_1 = V_2$

$I_2 = I_1 - sC_i V_1$ where i= 1, 2

In terms of matrix equation

$$\begin{bmatrix} V_2 \\ I_2 \end{bmatrix} = \begin{bmatrix} 1 & 0 \\ -sC_i & 1 \end{bmatrix} \cdot \begin{bmatrix} V_1 \\ I_1 \end{bmatrix}$$

3.63

The final transfer function of the whole circuit is obtained by multiplying the 3 individual transfer function i.e.

$$t_\Pi = \begin{bmatrix} 1 & 0 \\ -sC_2 & 1 \end{bmatrix} \cdot \begin{bmatrix} 1 & -R \\ 0 & 1 \end{bmatrix} \cdot \begin{bmatrix} 1 & 0 \\ -sC_1 & 1 \end{bmatrix}$$

$$t_\Pi = \begin{bmatrix} 1 & 0 \\ -sC_2 & 1 \end{bmatrix} \cdot \begin{bmatrix} 1+sC_1R & -R \\ -sC_1 & 1 \end{bmatrix}$$

$$t_\Pi = \begin{bmatrix} 1+sC_1R & -R \\ -s(C_1+C_2+sC_1C_2R) & 1+sC_2R \end{bmatrix}$$

3.64

Equating eqn(3.64) and eqn(3.60), the capacitor and resistor values are derived as shown below

$$R = \frac{1-\exp(-\alpha\ell)}{\alpha D}$$

3.65

$$C_1 = \frac{\exp(-\alpha\ell)+\alpha.\ell-1}{\alpha(1-\exp(-\alpha.\ell))}$$

3.66

$$C_2 = \frac{\exp(\alpha \ell) - \alpha.\ell - 1}{\alpha(1 - \exp(-\alpha.\ell))}$$

3.67

The results obtained above has justified two important points. For the first point, the component values derived in equation 3.65-3.67 have satisfied the equation used in the development of the transmission line consisting of distributed CR network of series resistance and parallel capacitance i.e.

$$C_1 + C_2 = \int_{r_i}^{r_{i+1}} \exp(\alpha.r)dr \quad \text{and} \quad R = \frac{1}{D}\int_{r_i}^{r_{i+1}} \exp(-\alpha.r)dr$$

3.68

with $r_i = 0$ and $r_{i+1} = \ell$. The approximation used was to divide the total capacitance of that part of the network between the nodes $0 \; (r_i)$ and $\ell(r_{i+1})$ into two lumped capacitors C_1 and C_2 and to lump the resistance into a single component R.

The second point is that, a single Π-network used to model the medium-to-long time behaviour of the vacancy in a single grain boundary for case A is the best choice possible. However a single Π-network are unable to model case B accurately since the matrix element $T_{21} = t_{21}$ (eqn (3.48) & eqn(3.61)) is poorly approximated by the occurrence of the b term.

Let us refer back to the existing literature where two typical cases were considered. A single grain is considered to be parallel to the interconnect and thus the co-ordinate along the grain boundary to be x. For case A , where a single grain boundary with a constant vacancy supply at x=0 and a blocking boundary at x=ℓ, the vacancy build-up has been obtained [Dwyer,et al.,1994]. In the approach to the steady state, the vacancy concentration at x=ℓ was approximated by (see Chapter 2):-

$$\frac{c(\ell,t)}{c_0} \approx \exp(\alpha\ell) - \frac{2\alpha\ell\xi_\ell^2 \exp\left[-\left(\frac{\alpha^2\ell^2}{4} \pm \xi_\ell^2\right)\frac{Dt}{\ell^2}\right]}{\frac{\alpha^2\ell^2}{4} \pm \xi_\ell^2\left[\xi_\ell^2 \pm \frac{\alpha\ell}{4}(2-\alpha\ell)\right]}$$

3.69

The +(-) is taken in the case $\alpha\ell < 2(\alpha\ell > 2)$ and ξ_ℓ is the roots, respectively, of the imaginary(real) solution to $\tanh\xi = \dfrac{2\xi}{\alpha\ell}$ with the smallest roots. The time constant in eqn (3.53) may be approximated by

$$\tau \approx \frac{\exp(\alpha\ell) - \alpha\ell - 1}{\alpha^2 D} \qquad\qquad 3.70$$

as proven by the ratio of the time constant between the approximation and the exact value shown in Fig 3.4.
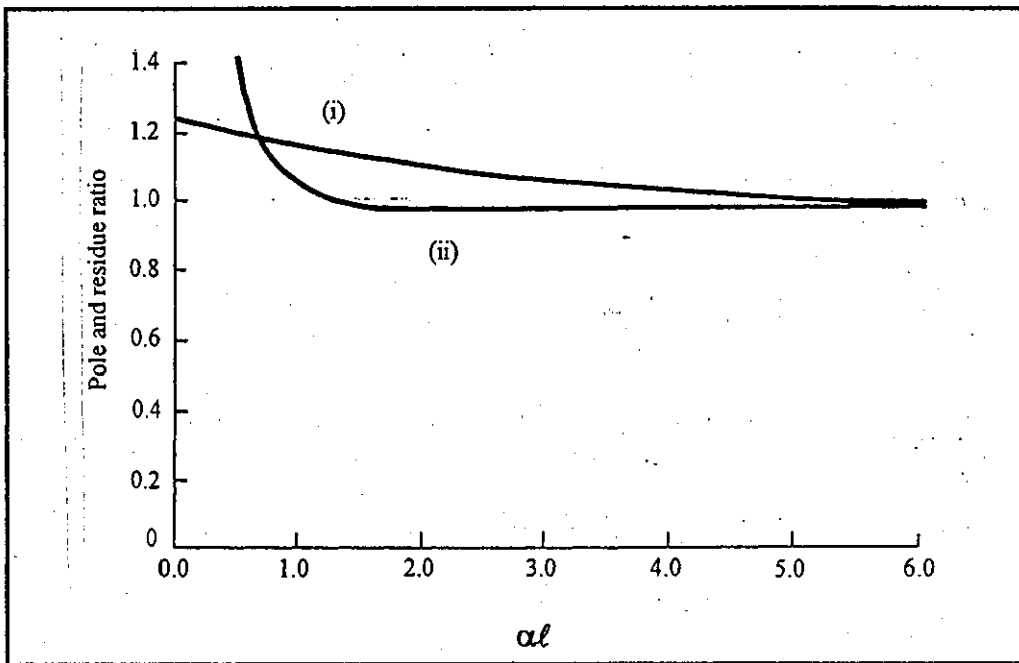
Fig 3.4 (i)Pole values-the variation of the ratio of $(\exp(\alpha\ell) - \alpha\ell - 1)/\alpha^2\ell^2$ to the exact time constant as a function of $\alpha\ell$. (ii) Residue values-the ratio of the coefficient of the dominat time exponential to $(\exp(\alpha\ell) - 1)$

It is also interesting to note from Fig3.4 that the coefficient of the exponential term in eqn(3.69) is approximately $\exp(\alpha\ell) - 1$ for a very wide range of values of $\alpha\ell$. As a result eqn(3.69) can be recast by

$$\frac{c(\ell, t)}{c_0} = \exp(\alpha\ell) - \left(-1 + \exp(\alpha\ell)\right).\exp\left[-\frac{\alpha^2 Dt}{\exp(\alpha\ell) - \alpha\ell - 1}\right] \qquad\qquad 3.71$$

$$c(\ell, t) = c_0 \exp(\alpha\ell) - \left(-c_0 + c_0 \exp(\alpha\ell)\right).\exp\left[-\frac{\alpha^2 Dt}{\exp(\alpha\ell) - \alpha\ell - 1}\right]$$

multiplying both side by $\exp(-\alpha\ell)$ gives

$$c(\ell, t)\exp(-\alpha\ell) = c_0 - \left(c_0 - c_0 \exp(-\alpha\ell)\right).\exp\left[-\frac{\alpha^2 Dt}{\exp(\alpha\ell) - \alpha\ell - 1}\right]$$

$$c(\ell, t)\exp(-\alpha\ell) = c_0.\exp(-\alpha\ell).\exp\left[-\frac{\alpha^2 Dt}{\exp(\alpha\ell) - \alpha\ell - 1}\right] \qquad 3.72$$

As introduced earlier where $v(x,t) = c(x,t).\exp(-\alpha x)$, eqn(3.72) represents the response of the series CR circuit with the initial condition $c(x,t=0)=c_0$ i.e. $v(x,t=0)=c_0\exp(-\alpha x)$. With the approximate time constant obtained, and with the resistor value chosen to be the 'steady state' value calculated as in eqn(3.65), the component values can be calculated

from eqn(3.70)

$$\tau = RC \approx \frac{\exp(\alpha\ell) - \alpha\ell - 1}{\alpha^2 D}$$

and eqn(3.65)

$$R = \frac{1 - \exp(-\alpha\ell)}{\alpha D}$$

therefore

$$C_2 = \frac{\tau}{R} = \frac{\exp(\alpha\ell) - \alpha\ell - 1}{\alpha^2 D} \times \frac{\alpha D}{1 - \exp(\alpha\ell)}$$

gives $\qquad C_2 = \dfrac{\exp(\alpha\ell) - \alpha.\ell - 1}{\alpha(1 - \exp(-\alpha.\ell))}$

Looking at the grain boundary from the opposite end one sees the same problem, but with $\alpha \rightarrow -\alpha$. This symmetry implies a second capacitor at $x=0$ given by

$$C_1 = \frac{\exp(-\alpha\ell) + \alpha.\ell - 1}{\alpha(1 - \exp(-\alpha.\ell))}$$

It should be note here, from Fig3.4 that the fit to the time constant is significantly less good for the case $\underline{\alpha}.\underline{r} < 0$ i.e. when the electrical current is from the blocking boundary to a vacancy sink.

In the case of a grain boundary blocked at both ends, case B, the approach to the steady state is again dominated by a single (although different) time exponential [Lloyd and Kitchin , 1991]. The vacancy concentration build-up are given by the equation below:-

$$\frac{c(x,t)}{c_0} \approx \frac{\alpha\ell.\exp(\alpha x)}{\exp(\alpha\ell) - 1} + \frac{\pi\alpha^2\ell^2[1 + \exp(-\frac{\alpha\ell}{2})]}{\left(\frac{\alpha^2\ell^2}{4} + \pi^2\right)^2} x$$

$$\left[\sin\left(\frac{\pi x}{\ell}\right) + \frac{2\pi}{\alpha\ell}\cos\left(\frac{\pi x}{\ell}\right)\right] x \exp\left(\frac{\alpha x}{2}\right) x \exp\left[-\left(\pi^2 + \frac{\alpha^2\ell^2}{4}\frac{Dt}{\ell^2}\right)\right] \qquad 3.73$$

The time constant in eqn(3.73) is unfortunately not well approximated by the source free response of the Π-equivalent circuit. This arises for the same reason as for case A when $\underline{\alpha}.\underline{r} < 0$. Nevertheless, these results for the single grain structure suggest the use of the equivalent CR network as a possible means of approximating the approach to the steady state in complex grain boundary networks, and consequently a means of estimating interconnect failure times.

As another example to illustrate the results of the lumped circuit method, we model the stress build-up in a line consisting of a pair of fast diffusing regions separated by a bamboo grain as in reference[Korhonen, et al., 1993(2)]. The three regions are each modelled as a single C-R-C Π section with the bamboo allowing a small amount of diffusion either through the grain bulk or along the stripe sidewall as in Fig3.5 below
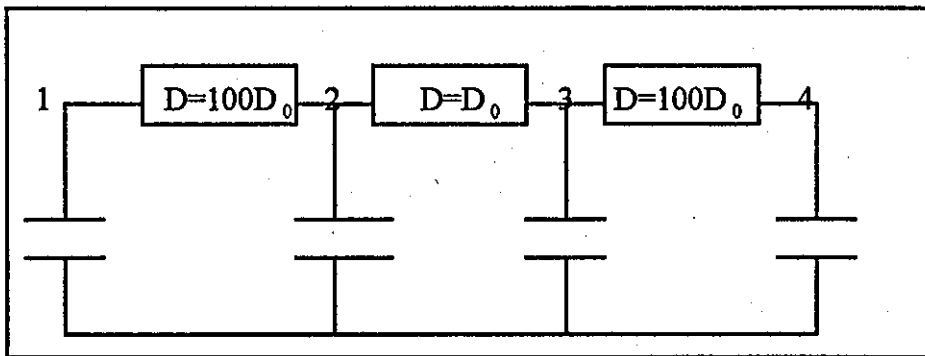
Fig3.5 The physical structure and a rather crude equivalent electrical network

The components values for each Π- section are given by eqn(3.49-3.51) and for simplicity, it is assumed that all regions have the same length. The values of $\alpha\ell$ are thus the same for all sections, the only difference being the resistor and capacitor values. The single-grain section has a much smaller diffusion coefficient($D=D_0$), and thus a much larger resistance(eqn(3.49), than the polygranular sections($D=100\,D_0$) .

The equivalent circuit has two time scales; a short time scale over which the fast diffusing sections reach a (quasi)-steady state and a longer time scale over which the whole system reaches a steady state. The build-up to the quasi-steady state is shown in Fig 3.6 Note that, at node 2, the stress is not a monotonic function of time, this reflects the fact that the grain boundaries between the node pairs(1,2) and (3,4) quickly, and independently, reach a quasi-steady state before moving towards the final non-equilibrium steady-state. At node 2 and 4 it is noticed that the stress is positive(due to tension where vacancy are building-up which leads to void formation) and at node 1 and 3 the stresses are negative (due to compressive stress arising from the accumulation of atoms).
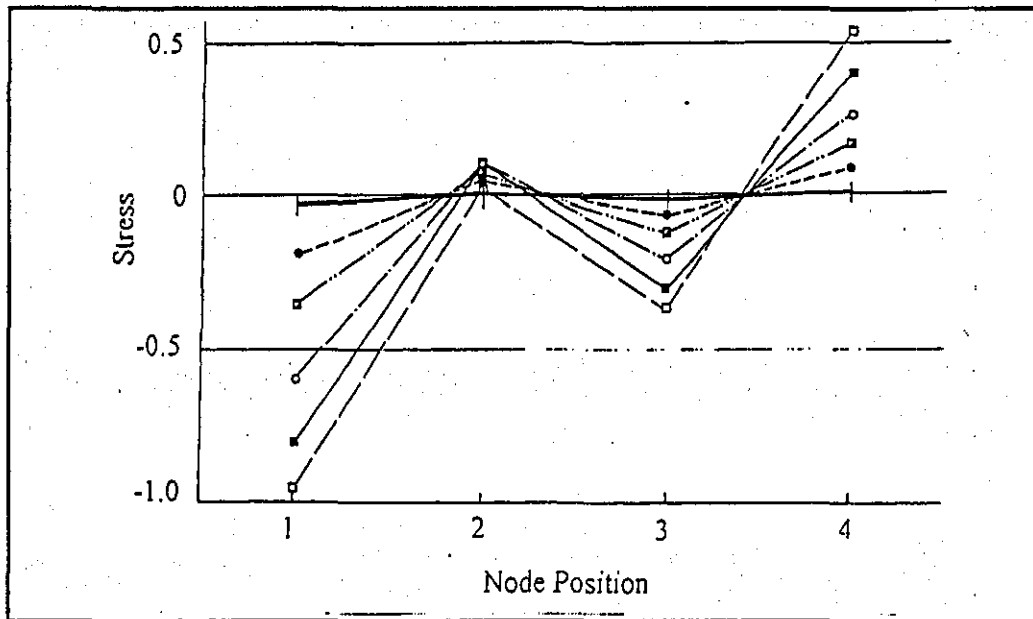
Fig 3.6 The stress build-up (profile) at nodes 1,2,3and 4. The different lines indicates the stress distribution at various time. Initial stress ,t=0(thick line),stress at t=0.2(broken line) , t=0.4(dash double dot),t=0.6(dash dot),t=0.8(thin line), and t=1.0(dash line)

3.7   Analysis on the accuracy of the $C-R-C$ Π elements

The accuracy of the t_Π matrix can be increased by including more sections in the transmission line. This corresponding to adding more nodes and thus more capacitor and resistor Π-sections. It is clear that a large number of C-R-C Π elements will lead to a very accurate solution while two capacitors and a single resistor leads to a sufficiently accurate solution for a single grain boundary in case A. Cascading two Π-sections of length $\frac{\ell}{2}$ produces a transmission matrix of the correct form leaving $t_{\Pi(11)}$ and $t_{\Pi(22)}$ unaltered to first order in s. However the accuracy of both $t_{\Pi(12)}$ and $t_{\Pi(21)}$ are increased. This is particularly important for the case B grain boundary where it is the roots of $t_{\Pi(21)}$ are important.

Introducing n-1 equally spaced nodes on a grain boundary divides it into n equal segments. The total transfer matrix for the n cascaded Π- sections from x=0 to $x=n\ell = L$ is the product of the n individual matrices i.e.

89

$$T_\Pi(L = n\ell) = [et_\Pi(\ell)]^n \qquad\qquad 3.74$$

$T_\Pi(n\ell)$ may then be obtained by first diagonalising the matrix $et_\Pi(\ell)$. If the eigenvalues of this matrix are $\lambda_+ \text{and} \lambda_-$, then by induction,

$$T_\Pi(n\ell) = \begin{bmatrix} \dfrac{\left(T_{\Pi,11} - \lambda_-\right)\lambda_+^n + \left(T_{\Pi,11} - \lambda_+\right)\lambda_-^n}{\lambda_+ - \lambda_-} & T_{\Pi,12}\dfrac{\lambda_+^n - \lambda_-^n}{\lambda_+ - \lambda_-} \\[4mm] T_{\Pi,21}\dfrac{\lambda_+^n - \lambda_-^n}{\lambda_+ - \lambda_-} & \dfrac{\left(T_{\Pi,11} - \lambda_-\right)\lambda_-^n - \left(T_{\Pi,11-} - \lambda_+\right)\lambda_+^n}{\lambda_+ - \lambda_-} \end{bmatrix} \quad 3.75$$

where the eigenvalues ($\lambda_+ \text{and} \lambda_-$) satisfy the characteristic equation

$$\lambda^2 - \left(\exp(\alpha\ell)t_{\Pi,11} + t_{\Pi,22}\right)\lambda + \exp(\alpha\ell) = 0 \qquad\qquad 3.76$$

Note that by setting $n\ell = L$, and taking the limit $\ell \to 0$ or $n \to \infty$, one obtain

$$\lambda_+(\ell)^n \to \exp(\beta_+ L) \quad \text{and} \quad \lambda_-(\ell)^n \to \exp(\beta_- L)$$

$$\frac{T_\Pi - \lambda_+}{T_\Pi - \lambda_-} \to \frac{\beta_+}{\beta_-} \qquad\qquad 3.77$$

so that as $n \to \infty$, $T_\Pi(L.s) \to T$ (the T matrix of eqn(3.39)). The question now is how few sections are needed to achieve an acceptable level of accuracy.

The improvement in accuracy obtained by including extra $\Pi-$ elements is apparent from observing the roots of $T_{\Pi,21}(n\ell,s) = 0.$ in eqn(3.75). These occur at $\lambda_+^n = \lambda_-^n$ which, according to eqns(3.64) and (3.76), corresponds to λ_+ and s values of

$$\lambda_+^m = \exp\left(\frac{\alpha\ell}{2}\right)\exp\left(\pm\frac{\pi mj}{n}\right) \quad , m=1,2,....n \qquad\qquad 3.78$$

90

or

$$\frac{\ell^2 s(m)}{D} = -\frac{1 + \exp(-\alpha\ell) - 2\exp\left(-\frac{\alpha\ell}{2}\right)\cos\left(\frac{m\pi}{n}\right)}{1 - \exp(-\alpha\ell)} \alpha\ell < 0 \qquad 3.79$$

where m=1,2,...n-1. The root closest to s=0, will dominate the approach to the steady state. This corresponds to m=1, which give maximum cancellation in the numerator, i.e.

$$s_{(1)} = -\frac{D}{L^2}\cdot\frac{1 + \exp\left(-\frac{\alpha L}{n}\right) - 2\exp\left(-\frac{\alpha L}{2n}\right)\cos\left(\frac{\pi}{n}\right)}{1 - \exp\left(-\frac{\alpha L}{n}\right)} n\alpha L = -\frac{D}{L^2}F^{(n)}(\alpha L) \quad 3.80$$

From eqn(3.80), as $n \to \infty$, $s_{(1)}$ tends to the correct limit of $-\frac{D}{L^2}\cdot\left(\frac{\alpha^2 L^2}{4} + \pi^2\right)$ to

which it is compared in Fig3.7 for various values of n. An accuracy of around 3% is obtained for n=5, i.e. five Π-sections, more or less independently of the projected grain length αL. Also it is noticed from Fig 3.7 that other poles ($s = s_m, m = 2,3...$, lying further from s=0) become less and less well represented as m increases, however this is not such a problem in the approach to the quasi-steady state provided that the residue at the first pole is correct. This residue can be calculated in the normal way, for example for case B, the blocked-locked case, at x=0

$$c(x = 0, s) = -\frac{U_2(L,s)}{T_{21}(L,s)} = \frac{c_0}{s}\left[1 + \frac{\alpha D(T_{22}(L,s) - 1)}{T_{21}(L,s)}\right]$$

$$= \frac{c(x = 0, t \to \infty)}{s} + \frac{A}{s - s_1} + ... \qquad 3.81$$

where s_1 is given in eqn(3.80). For a grain of length L made from nΠ- elements each

of length $\ell = \frac{L}{n}$, the residue A can be obtained by using d'Alembert's rule as

$$A = \lim_{s \to s_1} \frac{-(s - s_1)U_2(L,s)}{T_{21}(L,s)} = \frac{-U_2(L,s_1)}{\dfrac{\partial T_{21}(L,s_1)}{\partial s}} = G^{(n)'}(\alpha\ell) =$$

$$\frac{2c_0\alpha^3 L^3(1 + \exp(-\alpha L / 2))\sin^2(\pi / n)}{F^{(n)}(\alpha L)^2(\alpha C_1 + \alpha C_2 - F^{(n)}(\alpha L)(\alpha C_1)(\alpha C_2)(\alpha DR)/(\alpha^2 L^2))(1 - \exp(-\alpha L / n))} \quad 3.82$$

where $\dot{R}, C_1, C_2$ are given in eqns(3.65),(3.66)and (3.67). It is important to observe again that, as DR is independent of D, the residue A only depends upon n and the value of αL. Fig 3.8 again indicates that five Π - sections will give an accuracy for A better than 5% over the range αL between 0 and 5.
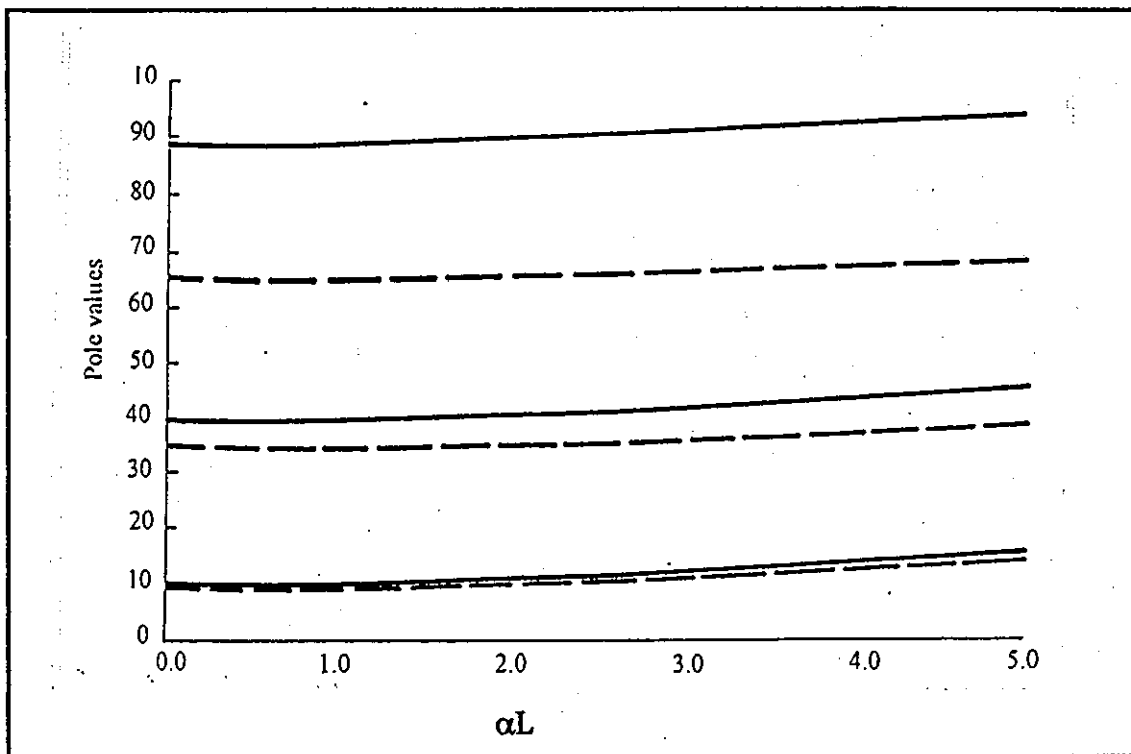
Fig 3.7 Exact(solid) and approximate(dotted) positions of the first three poles as a function of $\alpha\ell$ (n=5) in the blocked-blocked case.
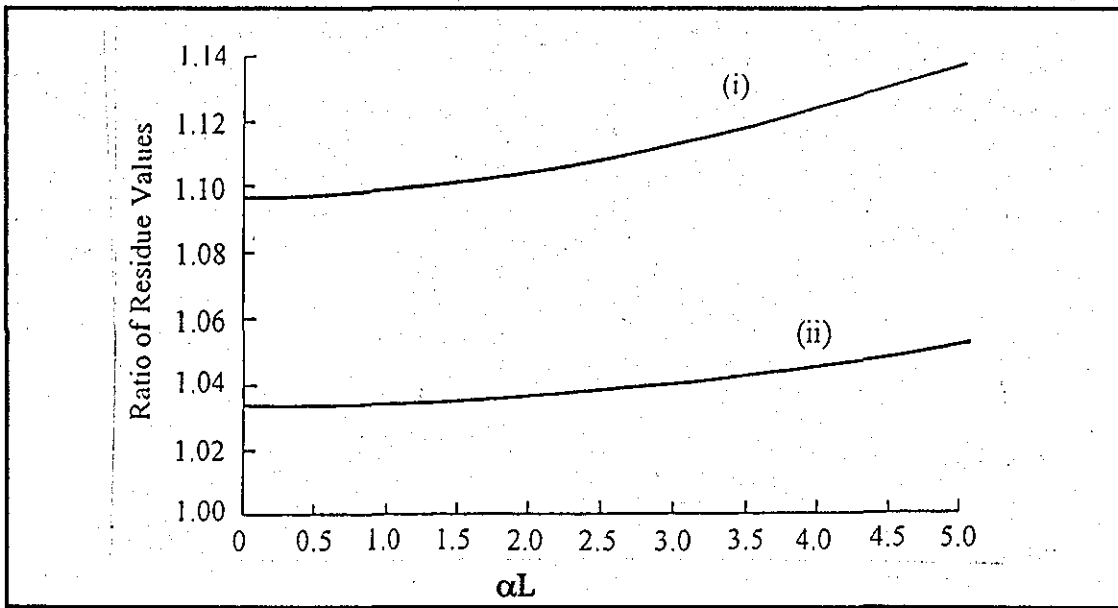
Fig 3.8 Exact and approximate value of residue (coefficient) at the lowest order pole
for (i) n=3 and (ii) n=5 in the blocked-blocked case

3.8 The development of the Matrix representation of the C – R – C Π
networks

In the last section, it has been mentioned that for better accuracy, a grain boundary
should be represented by more than 1 section of the C-R-C Π circuit (5 sections will
produce a satisfactory accurate representation of the vacancy concentration). This
corresponding to having more nodes and thus more capacitor and resistor Π-sections.
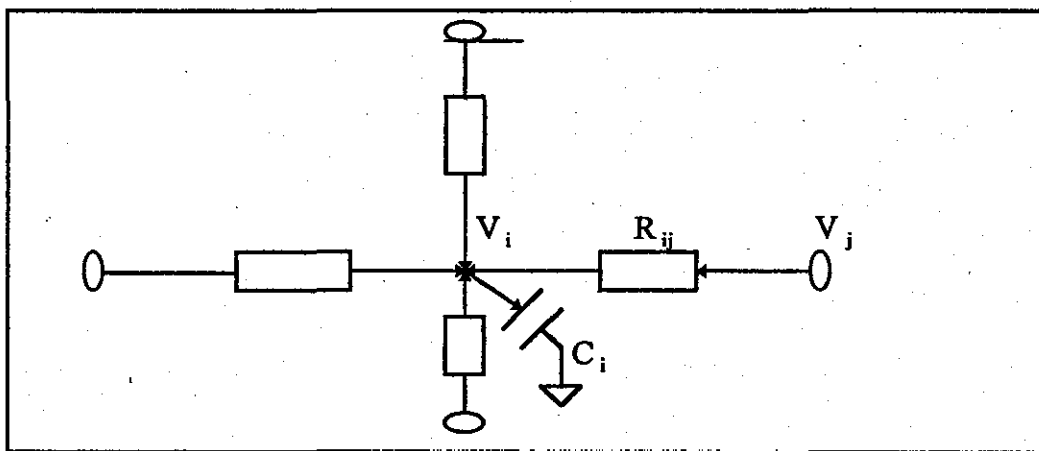
Fig 3.9 Example of Node i in a network

For a network of N+1 nodes(where N= total number of resistors in the network, the extra node is for the extra capacitors), will yields a set of simultaneous in the node voltages $\{V_i(t), i = 0,1,....N\}$ where the equation for the current flowing into node i (example for a node i in Fig 3.9) is given as

$$C_i \frac{dV_i}{dt} = \sum_{j=0}^{N} \frac{V_j - V_i}{R_{(i,j)}}$$ 3.83

Let us choose the source node to be node 0, i.e. $c(0,t)=V_0 = c_0$ and assume that the node 0 is only connected to node 1 so that $1/R_{(i,0)} = 0$ except for the case i=1. This merely means that the grain boundary connected to the void has at least one node between the void end and the next triple point. Eqn(3.83) may be rewritten as

$$C_i \frac{dV_i}{dt} = \sum_{j=1}^{N} \frac{V_j - V_i}{R_{(i,j)}} + \frac{V_1 - V_0}{R_{10}}$$ 3.84

where (i= 1,2,....N) and in matrix form as

$$\underline{\underline{C}} \frac{d\underline{V}}{dt}(t) = \underline{\underline{G}}\,\underline{V}(t) + \frac{c_0}{R_{10}}\underline{e} = \underline{\underline{G}}\,V(t) + \underline{U}$$ 3.85

where $\underline{\underline{C}}$ is the (NxN) diagonal matrix of node capacitances, $\underline{V}(t)$ is the (Nx1) vector of pseudo-voltages (excluding V_0), $\underline{e}$ is a vector in the direction (1,0,0,...0) and $\underline{\underline{G}}$ is the (NxN) conductance matrix with components

$$G_{ij} = \frac{1}{R_{(i,j)}}, \qquad G_{ii} = -\sum_{<i:j>} \frac{1}{R_{(i,j)}}$$ 3.86

where $< i:j > =$ set of nodes j connected to node i.

The voltage V(t) at each node (particularly the edge and triple point) and hence its equivalent vacancy concentration (given by the equation $c(t)=V(t)\exp(\alpha x)$) can be evaluated by integrating the eqn(3.85). The complete solution starting from the creation of the matrices and solving the matrix equation is discussed in Chapter 4. Finally the Time to Failure is determined once the vacancy concentration c(t) reaches some threshold value (failure criterion given by $c_{cr} = nc_0$ where n is the appropriate number).

3.9 The signal (Elmore) delay approximation of Time to Failure

One method to estimate the Time to Failure based on the vacancy build-up to some threshold value is to use the signal or Elmore delay technique. The signal (Elmore)delay technique is well known in modelling timings for CMOS circuits [Elmore,1948]. Delay in an RC network is manifestation of the inertia of a system. One way to quantify delay, as suggested by [Elmore,1948] , is to take the first order moment (essentially the mean value) of the Impulse Response.

Consider first a system with zero initial pseudo-charge(i.e. no vacancies at t=0). In this case considering V_0 as the input, $\dfrac{V_i(t)}{c_0}$ is the Unit-Step Response so that $\dfrac{1}{c_0}\dfrac{dV_i}{dt}$ is the Impulse Response. The Unit-Step Response tends to c_0 monotonically and consequently the Impulse Response is always positive [Lin and Mead ,1983]. In addition $V_i(t = 0) = 0$ guarantees that $\dfrac{dV_i}{dt}(t = 0) = 0$ through eqn(3.83). This leads to an Impulse Response at node i similar to that shown in Fig 3.10 and defines the delay (T_{Di}) as the time between the original impulse at node 0 and the mean value of the resulting Impulse Response at node i. The Impulse Response has a unity area so $\dfrac{1}{c_0}\dfrac{dV_i}{dt}$ may be considered a probability density function (pdf) and consequently the delay is simply its first-order moment. In the field

of CMOS design this is known as the signal delay at node i [Elmore , 1948],[Rubenstein, et al., 1983]
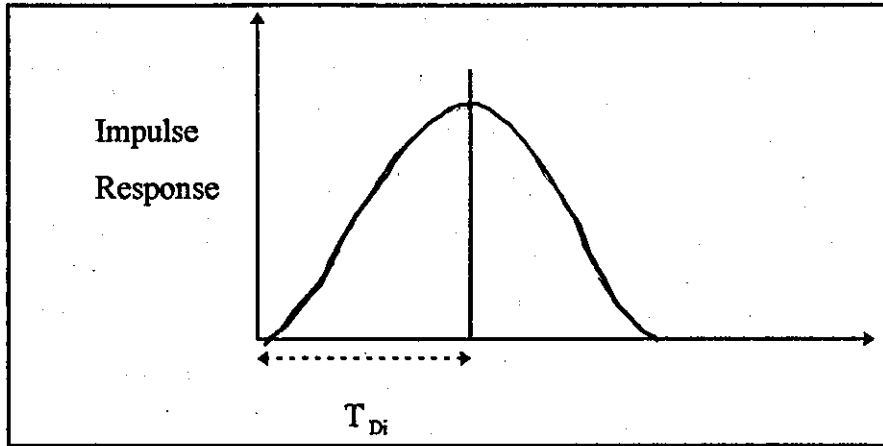
Fig 3.10 The definition of signal delay

The notion of delay can be extended to the case of non-zero initial 'charge' (i.e. vacancies present initially) required here by using a normalised impulse response as the total area is now $1 - \dfrac{V_i(0)}{c_0}$ rather than unity .The original definition of delay T_{Di} by [Elmore ,1948] with no initial charge is given by

$$T_{Di} = \int_0^\infty t \frac{dV_i}{dt} \frac{1}{c_0} dt \qquad\qquad 3.87$$

Thus the redefined delay T_{Di} with initial charge is given by

$$T_{Di} = \frac{\displaystyle\int_0^\infty t \frac{dV_i}{dt} \frac{1}{c_0} dt}{1 - \dfrac{V_i(0)}{c_0}} \qquad\qquad 3.88$$

Integrating eqn(3.88) by parts , an equivalent vector representation is obtained

$$T_{-D} = \frac{\int_0^\infty \left[1 - \frac{V(t)}{c_0} \right] dt}{\left[1 - \frac{V(0)}{c_0} \right]} = \frac{\lim_{s \to 0} \left[\frac{1}{s} - \frac{V(s)}{c_0} \right]}{\left[1 - \frac{V(0)}{c_0} \right]}$$ 3.89

where $V(s)$ is the Laplace transform of $V(t)$. Although eqns(3.88) and (3.89) are identical, eqn(3.89) are better for analysis purposes. This is because from eqn(3.89), the large time behaviour of each of the network pseudo-voltages, and hence the vacancy concentration at each node, may often be approximated by the steady-state term and the single decay term which is obtained through the first(smallest) s term. In the approach to the quasi steady state, the node voltages can be approximated by

$$\left[V(t) \right]_i \approx c_0 \left[1 - \left[1 - \frac{V_i(0)}{c_0} \right] \exp \left[-\frac{t}{T_{Di}} \right] \right]$$ 3.90

If the critical stress is σ_{cr} then $c^* = e^{\frac{\Omega \sigma_\alpha}{kT}}$ is the critical vacancy concentration, thus the critical voltage for failure at node i is $V^*_i = c^* \exp(-\alpha.r_i)$ and the time to failure at that node can be easily calculated from eqn(3.90)

The signal delay T_D for the C-R-C Π network is derived below.

From eqn(3.85) the matrix equation of the pseudo voltages at all nodes is given as

$$\underline{C} \frac{dV}{dt}(t) = \underline{G}V(t) + \frac{c_0 e}{R_{10}}$$

can be rewritten as

$$\frac{dV}{dt}(t) = \underline{C}^{-1} \underline{G}V(t) + \frac{c_0 e}{R_{10}}$$ 3.91

and applying Laplace transform equation 3.91 becomes

$$s.\underline{V}(s) - \underline{V}(0) = \underline{\underline{C}}^{-1}.\underline{\underline{G}}.\underline{V}(s) + \frac{c_0}{R_{10}}\frac{\underline{e}}{s}$$

$$s.\underline{V}(s) - \underline{\underline{C}}^{-1}.\underline{\underline{G}}.\underline{V}(s) = \underline{V}(0) + \frac{c_0}{R_{10}}\frac{\underline{e}}{s}$$

after rearranging

$$\underline{V}(s) = \left(s\underline{\underline{I}} - \underline{\underline{C}}^{-1}\underline{\underline{G}}\right)^{-1}\left(\underline{V}(0) + \frac{c_0}{R_{10}}\frac{\underline{e}}{s}\right) \qquad 3.92$$

where $\underline{\underline{I}}$ is the identity matrix, $\underline{V}(0)$ is the initial voltages.

Inserting eqn(3.92) into eqn(3.89) becomes

$$\left[1 - \frac{\underline{V}(0)}{c_0}\right]\underline{T}_D = \lim_{s\to 0}\left[\frac{1}{s} - \frac{1}{c_0}\left(\underline{\underline{G}}^{-1}\underline{\underline{C}} + s\left(\underline{\underline{G}}^{-1}\underline{\underline{C}}\right)^2 + s^2\left(\underline{\underline{G}}^{-1}\underline{\underline{C}}\right)^3 + ...\right).\left[\underline{V}(0) - \frac{c_0}{R_{10}}\frac{\underline{e}}{s}\right]\right] \quad 3.93$$

The terms in s^{-1} is cancel here , therefore with a slight abuse of standard vector notation,

$$\left[1 - \frac{\underline{V}(0)}{c_0}\right]\underline{T}_D = -\frac{1}{c_0}\underline{\underline{G}}^{-1}.\underline{\underline{C}}.\left(\underline{V}(0) - \frac{c_0}{R_{10}}.\underline{e}\right)$$

$$\left[1 - \frac{\underline{V}(0)}{c_0}\right]\underline{T}_D = -\frac{1}{c_0}\underline{\underline{G}}^{-1}.\underline{\underline{C}}.\underline{V}(0) + \frac{1}{c_0}\underline{\underline{G}}^{-1}.\underline{\underline{C}}\frac{c_0}{R_{10}}.\underline{e}$$

The initial condition of the network is represented by the voltages $\underline{V}(0)$ and the network is driven towards a final value of $c_0\underline{1}$. The fact that there is no dc path to ground and $v(\infty)=1$ means that

$$-\underline{\underline{G}}^{-1}\underline{e} = \underline{\underline{R}}\underline{e} = R_{10}\underline{1} \qquad 3.94$$

where $-\underline{\underline{G}}^{-1} = \underline{\underline{R}}$ (It turns out that the matrix $-\underline{\underline{G}}$ defined by eqn(3.86) is a Stieltjes or S-matrix so $\underline{\underline{G}}^{-1}$ always exists $= \underline{\underline{R}}$)

Therefore the equation above becomes

$$\left[1 - \frac{\underline{V}(0)}{c_0}\right]\underline{T}_D = -\underline{\underline{G}}^{-1}.\underline{\underline{C}}.\left(1 - \frac{\underline{V}(0)}{c_0}\right) \qquad 3.95$$

or

$$\left[1 - \frac{\underline{V}(0)}{c_0}\right]\underline{T}_D = \underline{\underline{R}}.\underline{\underline{C}}.\left(1 - \frac{\underline{V}(0)}{c_0}\right) \qquad 3.96$$

The signal delay at a particular node i is derived below.

Note that as defined in previous sections , $V(0) = c_0 \exp(-\alpha x)$, therefore

$$\left[1 - \frac{V(0)}{c_0}\right] = 1 - \frac{c_0 \exp(-\alpha x)}{c_0} = 1 - \exp(-\alpha x) \qquad 3.97$$

Substituting eqn (3.97) into eqn(3.96), and hence

the signal delay at node i is given by the equation below

$$T_{Di} = \frac{\sum_j R_{ij} C_j (1 - \exp(-\alpha x_j))}{(1 - \exp(-\alpha x_i))} \qquad 3.98$$

The calculation of the delay can be seen to derive from the inversion of the matrix G to obtain $\underline{\underline{R}} = -\underline{\underline{G}}^{-1}$. In some cases, such as tree structures with a single source, the matrix element R_{ij} may be simply read off. This is obvious by considering a general

tree structure with conductance matrix $\underline{\underline{G}}$ and a single source at node 0. The current flowing into the source node is the sum of the currents from each of the capacitors. The voltage drop between node 0 and node i due to the current from the capacitor at node j is $R_{ij}C_j\dfrac{dV_j}{dt}$ where R_{ij} is the resistance of the unique path between node i and the source node 0 that is common with the unique path between node j and the source. Thus the total voltage drop to node i is

$$c_0 - V_i = \sum_j R_{ij}C_j\frac{dV_j}{dt} \qquad\qquad 3.99$$

Many of the cluster networks making up a typical near-bamboo interconnect will have tree structures so that it will be possible to identify the (i,j) component of $\underline{\underline{R}} = -\underline{\underline{G}}^{-1}$. In general the calculation of delay will involve a special or more complex matrix of $\underline{\underline{R}}$. The creation of the special matrix $\underline{\underline{R}}$ is discussed in the development of the program code in Chapter 4. Finally the failure time t_f or Time to Failure (TTF) can be estimated as the first time that a node reaches its failure criterion of $\underline{V}_i^* = c^* \exp(-\alpha x_i)$. Thus from eqn(3.90)

$$\underline{V}^*_i = c_0 - (c_0 - \underline{V}(0)_i)\exp\left(-\frac{t}{T_{Di}}\right)$$

$$\left(c_0 - \underline{V}(0)_i\right)\exp\left(-\frac{t}{T_{Di}}\right) = c_0 - \underline{V}^*_i$$

$$\exp\left(-\frac{t}{T_{Di}}\right) = \frac{c_0 - \underline{V}^*_i}{c_0 - \underline{V}(0)_i}$$

taking logs on both sides gives

$$\left(-\frac{t}{T_{Di}}\right) = \ln\left[\frac{c_0 - \underline{V}^*_i}{c_0 - \underline{V}(0)_i}\right]$$

therefore

$$t_f = \min_{all\,i}\left\{-T_{Di}\,\ln\left(\frac{c_0 - \underline{V}^*_i}{c_0 - \underline{V}(0)_i}\right)\right\}$$

or

$$t_f = \min_{all\,i}\left\{T_{Di}\,\ln\left(\frac{c_0 - \underline{V}(0)_i}{c_0 - \underline{V}^*_i}\right)\right\} \qquad 3.100$$

As an example we compare the signal delay with an exact solution below. A single grain of length ℓ and supplied at x=0, with initial vacancy concentration $c(x,t=0)=c_0$, which has been divided into a number of segments is a special case of the tree network. In the limit of $N \to \infty$, the signal delay at x along the grain is

$$\left(1 - \exp(-\alpha x)\right)T_D(x) = \int_0^x R(y)\frac{dC}{Dy}(1 - \exp(-\alpha y))dy + R(x)\int_x^{\ell}(\exp(\alpha y) - 1)\frac{dC}{dy}dy$$

3.101

i.e

$$T_D(x) = \frac{\left(C_2(x) - C_1(x)\right)R(x)}{\left[1 - \exp(-\alpha x)\right]} + \left(C_2(\ell)R(\ell) - C_2(x)R(x)\right)$$

3.102

Thus the vacancy concentration along the grain is given as

$$c(x,t) = c_0\exp(\alpha x)\left(1 - (1 - \exp(-\alpha x))\exp\left[-\frac{t}{T_D(x)}\right]\right.$$

3.103

The time development of the vacancy concentration along the grain boundary, given in eqn(3.103) is compared to the exact solution of reference[Dwyer,et al,1994] in Fig 3.11 for $\alpha\ell = 2, D = 1$ and reduced times of $\frac{Dt}{\ell^2} = 0.1, 0.2, 0.4, 0.66, 10.0$. It is clear that eqn(3.103) gives a good approximation to the exact values for large times ($> \approx 0.2$) and that the failure time in this case is ≈ 0.66. This would correspond to a grain boundary length of around 8 μm giving a Time to Failure of around 7.2 hr.
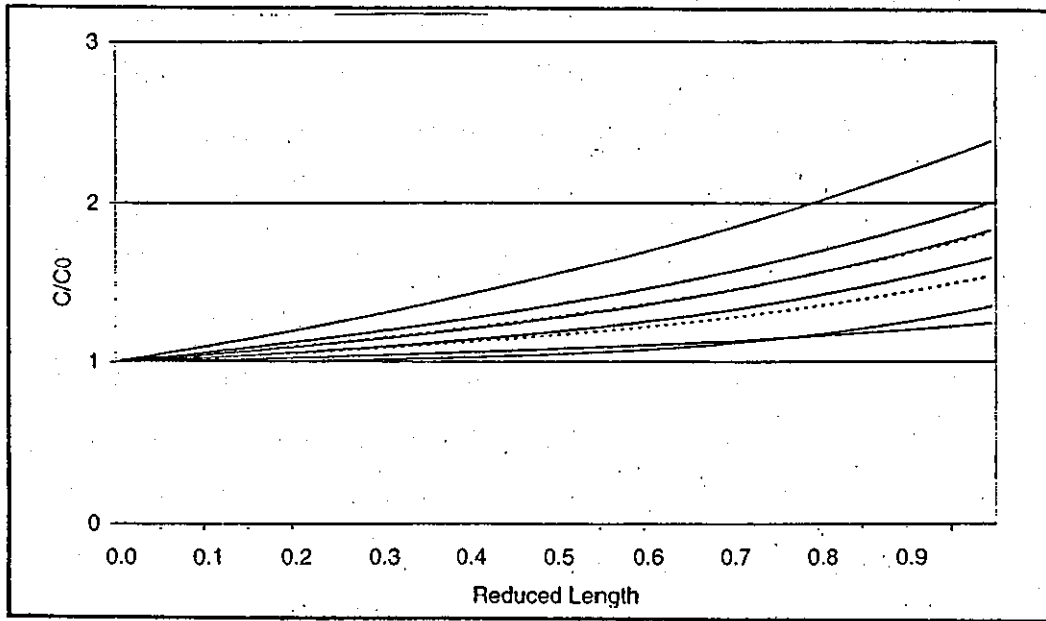
Fig 3.11 Signal delay approximation compared to the exact solution at all points along a single grain boundary blocked at x=ℓ and supplied at x=0, at reduced times Dt/ℓ^2 =0.1.0.2,0.4,0.66,10.0

3.10   The non-linear solution-concentration dependent D(σ)

In the previous sections, the effective diffusion coefficient has been set to a constant value as in most previous references as mentioned earlier. In actual fact, the effective diffusion coefficient depends upon the local stress/vacancy concentration, this arises from the more complicated form of the continuity equation. In this case, for the single, one dimensional grain boundary studied here, the equivalent transmission line equations become

$$\nabla v(x) = -\frac{\exp(\alpha x)J(x)}{D_v}$$ /   3.104

$$\frac{c_0}{v}\frac{\partial v}{\partial x} = -\frac{\partial J}{\partial x}$$ 3.105

102

The resistor values are identical to those of eqn(3.65). This is expected as the steady state is independent of D. On the other hand the capacitance per unit length depends upon the local pseudo-voltage, $C(x,t) = \dfrac{c_0}{v(x,t)}$. To get a reasonably accurate approach to the steady state , the capacitor values calculated from the steady state voltages obtained in section 3.5 can be used. In the steady state, the node voltages are often equal and the value of the capacitance per unit length is $\dfrac{c_0}{v_\infty}$. This leads to capacitor vales for a section of length ℓ given by

$$C_1 = C_2 = \frac{c_0 \ell}{2v_\infty} \qquad\qquad 3.106$$

where the appropriate v_∞ values has to be obtained first from the random resistor network in section 3.5. The network may be reasonably well approximated by lumped elements with voltage dependent capacitors.

3.11   Summary

In this chapter, the stress evolution model has been discussed in greater detailed and the equation based on the original model by [Korhonen, et al.,1993] has been re-derived. Under electromigration, the equation which describes the evolution of stress within an interconnect, is equivalent to a non-linear slow drift-diffusion equation description of the vacancy build-up which is the focus of the current work.

It has been shown that, provided that the vacancy flow through the grain boundary network can be reasonably mapped on to an underlying network of one -dimensional grain boundaries , two important points can be drawn. Firstly, the steady state solution for an arbitrary grain boundary network, with arbitrary conditions, behaves exactly as a similar network of random resistors. Secondly, by ignoring the dependence of the diffusivity D on stress σ (as also been considered in other references), the linearised drift-diffusion equation can be transformed exactly into a distributed CR transmission

line equivalent with inhomogeneous capacitance per unit length and resistance per unit length.

These two observations combine to demonstrate the possibility of treating vacancy build-up in a grain boundary network approximately by an equivalent electrical network of lumped elements. It has also discussed that vacancy build-up in a single grain may be approximated by a CR transmission line made from (typically five) cascaded C-R-C Π sections.

Once the C-R-C Π circuit is produced, a matrix representation approach is used for obtaining the voltages and hence the vacancy concentration (by the relationship $V = c.\exp(-\alpha x)$) of a particular node. By making use of some threshold or critical value of c^* the Time to Failure can be obtained. The signal or Elmore delay approximation method is also described as a alternative way of producing the Time to Failure.

In this chapter also, a few examples on the vacancy concentration build-up using the current model and the signal delay are compared to the available references so as to justify some of the assumptions and the approximations used and to validate the current model. More detailed experiments involving single grain, complex grain and realistic grain boundary will be discussed in Chapter 5.

CHAPTER 4

SOFTWARE DEVELOPMENT

4.0   Introduction

An important aspect of the study is to develop programming codes to   test and simulate the model that has been developed in Chapter 3. Choosing a suitable software package is very nearly as important in developing the model itself.   The criteria in choosing suitable software are basically   i) that it is able to solve and compute the mathematical equations of the model ii) it can work with matrices iii) it is able to handle graphics iv) it is a PC based software running on Microsoft Windows v) it is easy to access vi) and is user friendly i.e. easy to use and easy to check for errors.   With these criteria in mind, MATLAB® was thought to be the most rightful choice over the others, such as PSpice, for implementing the task.

MATLAB® is a technical computing software for high-performance numeric computation and visualisation. It integrates numerical analysis, matrix computation, signal processing, and graphics in an-easy-to-use environment where problems and solutions are expressed just as they are written mathematically. MATLAB stands for matrix laboratory.[MATLAB®, 1992].

Apart form the ability to work with matrices the extensive availability of built-in functions and toolboxes will help reduce the overall programming time. These built-in functions and toolboxes are programming codes that calculate, solve or simulate certain algorithms that may be time consuming if developed by the user. The program codes have been developed using a PC Pentium 1 with processor speed of 166 MHz and 32Mbyte RAM and also on a mini computer system in Computer Aided Engineering (CAE) laboratory of the Electronic & Electrical Engineering Department in Loughborough University.

4.1 Stages of developing the programming codes

The development of the software followed a systematic approach. Once a model is developed, the programming code will be developed soon afterwards to test the model functionality, the results obtained are then compared to relevant results in the literature. This is to ensure that the model developed behaved appropriately giving similar or better results than those in the literature, confirming that the model is valid. This will also provide a way forward to work on more complex and demanding models. Therefore, the development of the programming codes has been done through a number of stages which could be identified as follows

i) development of programming codes for an interconnect with a homogeneous microstructure .i.e. a single grain boundary or an interconnect with same kind of microstructure at all points.

ii) development of programming codes on example of cluster network with more complex grain boundaries microstructure.

iii) development of programming codes for realistic computer generated interconnect samples consisting of a number of clusters each with a complex grain boundary microstructure.

The programming structure for MATLAB® consists of main program files (script files) and subroutine files (function files). One of the main advantages in organising the codes in this way is for ease in detecting and correcting errors. The program codes that have been developed basically involve solving the relevant equations from the exact theoretical model, the Lumped element model and the Signal (Elmore) delay method. The program codes that have been developed and tested in successive stages are as follows :-

A. Program codes for simulating the vacancy concentration response and the Time to Failure of a **single grain boundary** sample of interconnect based on the lumped element model. The codes consist of creating files which comprise of :-

106

i) function files for calculating the resistors, capacitors and its initial voltages values

ii) function files for creating the G matrix of resistors and the C matrix(diagonal) of capacitors

iii) a function file for creating VIN vector of initial voltages of capacitors

iv) a function file for creating the U vector of the boundary/initial conditions

v) a script file for simulating the vacancy concentration.

B. Program codes for simulating the vacancy concentration response of a **single grain boundary** based on the exact solutions (relevant references from literature).

i) script file for simulating the vacancy concentration response of a single grain boundary with both ends blocked (reference from[Clement,1992]).

ii) script file for simulating the vacancy concentration response of a single grain boundary with one end supplying vacancies and the other blocked.[reference from [Dwyer, et al.,1994]).

C. Program codes to calculate the Time to failure of a single grain boundary interconnect based on the two cases (B(i) and B(ii)) using

i) the lumped element approximation.

ii) the exact theoretical model.

iii) the Signal(Elmore) delay approximation.

D. Program codes for simulating the vacancy concentration response of an example single cluster interconnect consisting of five grain boundaries using the Lumped element model. The codes consist of the following files.

i) function files for calculating the resistors, capacitors and initial voltages values

ii) function files for creating the G matrix of resistors and the C matrix(diagonal) of capacitors

iii) a function file for creating VIN vector of initial voltages of capacitors

iv) a function file for creating the U vector of the boundary/initial conditions

v) a script file for simulating the vacancy concentration, Time to Failure and other relevant data for analysis.

E. Program codes for simulating the vacancy concentration response of computer generated , realistic samples of interconnects which consist of a number of clusters with complex grain boundary structure based on lumped element model. The codes consist of the following files

i) function files for creating Voronoi network representing the metalisation film.

ii) function files for simulating the annealing processes.

iii) function files for creating the interconnect samples consisting of a number of clusters of complex grain boundaries structure.

iv) function files for calculating and storing geometrical properties of the grain boundaries.

v) function files for labelling the nodes and the grain boundaries.

vi) function files to calculate the Time to Failure of the interconnect sample based on the lumped element model and the signal delay and thus producing the data on the lifetime statistics.

4.2 Single grain boundary with one end blocked

A program code **simall1g.m** has been developed to simulate the vacancy concentration response for a single grain boundary with one end supplying the vacancy concentration and the other end being blocked. The program codes incorporate the exact theoretical solution based on the work by [Dwyer,et al.,1994].The main objective of the program code is to make a comparative study between the lumped element model with that of the exact solution. Fig. 4.1 shows the flow chart of the program code.

The program code consist of three main processes, these include i) the simulation of vacancy concentration based on the lumped element model ii) the simulation of the

vacancy concentration based on the exact solution iii) the determination of Time to failure using the Lumped element model, the exact solution and the signal delay.

The vacancy concentration response for the lumped element model is produced by computing the matrices of conductance G, capacitance C , pseudo voltages VIN and matrix U. Prior to producing these matrices, functions files were developed to calculate the component values of the resistors, capacitors and the pseudo voltages. Detailed explanation on the calculation involve will be given later. For the theoretical model , the vacancy concentration build-up is simulated using eqn(2.26) for the case $\alpha l \leq 2$ and eqn(2.27) for the case $\alpha l \geq 2$ as described in Chapter 2.

The purpose of **simall1g.m** is to simulate the vacancy concentration build-up for a single grain where one end is blocked and has a vacancy supply c_0 at the other. The program will compare the results of the work by [Dwyer, etal.,1994] , with the lumped element model.and the signal delay method

```
┌─────────────────────────────────────────┐
│              User input                  │
│   nosim= number of simulation required   │
└─────────────────────────────────────────┘
                    │
                    ▼
          ┌──────────────────┐
          │   simno = 1      │
          └──────────────────┘
                    │
                    ▼
            ◇ simno <= nosim ◇
                    │
                    ▼
┌─────────────────────────────────────────────────────┐
│                  user input                         │
│   x= length of grain boundary                       │
│   d= vacancy diffusion coefficient                  │
│   c_0 = initial vacancy concentration at zero stress│
│   cr = the critical vacancy concentration           │
│   theta = angle of orientation                      │
│   alpha = drift component                           │
│   alpha eff=alphax cos(theta) = the effective drift component │
└─────────────────────────────────────────────────────┘
                    │
                    ▼
┌─────────────────────────────────────────┐
│              gmatone.m                   │
│   m-file to create the resistor matrix G │
└─────────────────────────────────────────┘
                    │
                    ▼
┌─────────────────────────────────────────┐
│              cmatone.m                   │
│   m-file to create capacitor matix C     │
└─────────────────────────────────────────┘
┌─────────────────────────────────────────┐
│              vmatone.m.                  │
│   m-file to crate initial voltage matrix VIN │
└─────────────────────────────────────────┘
┌─────────────────────────────────────────┐
│              umatone.m                   │
│   m-file to create the U matrix          │
└─────────────────────────────────────────┘
                    │
                    ▼
```

The simulation of the voltage response is done by the following process:-
    i)   assignment of the duration of time = t

    ii)   diagonalising the matrix of $Q = C^{-1} G$.

    iii)   solving the voltage response by the equation :-

$$V = S^{-1}\left(S. VIN.\exp^{Dt}\right) + S^{-1}\left(D^{-1}S. U.\exp^{Dt}\right) - S^{-1}D^{-1}S. U$$

the conversion of the voltage response to vacancy concentration response is obtained by the equation :-

$$C_v = V \times exp^{alphaeff.x} \quad , C_v \text{ is the vacancy concentration}$$

the time to failure is determined by interpolating between the data points of the vacancy concentration C_v and the time t. The command of Matlab to do the this is :-

TTF = interp1(C_v , t, critical vacancy concentration)

continue

simulation of the exact solution

alpha x >2

yes

no

get the real roots
rroot.m

get the imaginary roots
iroot.m

solve equation 2.22 and simulate the vacancy concentration response

solve equation 2.23 simulate the vacancy concentration response

the time to failure is determine by interpolating between the data points of the vacancy concentration C_v and the time t. The command of Matlab to do the this is :-

TTF = interp1(C_v , t, critical vacancy concentration)

calculate the Time to failure by signal delay method

rmatone.m
m-file for the resistance matrix RG

calculate the signal delay by the equation

$$TD = RG.C. \left(\frac{(1 - \frac{VIN}{c_0})}{(1 - e^{(-alphaeff.x)})} \right) , TTF = TD.Ln \left(\frac{\left(1 - e^{(-alphaeff.x)}\right)}{c_0 . v_{cr}} \right) , V_{cr} = cr.e^{(-alphaeff.x)}$$

simno=simno +1

produce the vacancy concentration response graph and the results of Time to failure

Fig 4.1 The program flow chart of simall1g.m

4.2.1 Calculation of the component values (C, R and Vin) for the Lumped Element Model

In the lumped element model, the equation for calculating the components for a single section are:-

resistor value R(1) $= \dfrac{1 - \exp(-\text{alphaeff} * x)}{\text{alphaeff} * D}$ 4.1

first capacitor C(1) $= \dfrac{\exp(-\text{alphaeff}.x) + \text{alphaeff}.x - 1}{\text{alphaeff}(1 - \exp(-\text{alphaeff}.x))}$ 4.2

second capacitor C(2) $= \dfrac{\exp(\text{alphaeff}.x) - \text{alphaeff}.x - 1}{\text{alphaeff}(1 - \exp(-\text{alphaeff}.x))}$,   4.3

Vin(1) = 1 , Vin(2)=exp(-alphaeff.x)*Vin(1)

where

alphaeff = alpha.cos(θ) ,

D is the diffusion coefficient

θ is the grain boundary angle of orientation to the direction of electric field

x is the length of the grain boundary/number of sections used.

For example, if three sections are used to represent the grain boundary, there will be a total of 3 resistors with the values decreasing exponentially and 6 capacitors with the values increasing exponentially. The values of these components are calculated as follows:-

C(3) = exp(alphaeff. x) C(1) ,   C(4) = exp(alphaeff.x)C(2)

C(5) =exp(2.alphaeff.x).C(1),   C(6)=exp(2.alphaeff.x).C(2)

R(2)=exp(-alphaeff.x)R(1) ,   R(3)=exp(-2.alphaeff.x)R(2)

The values above represents values for each individual section, once connected the actual calculation for the capacitors will have to take account the parallel connections between the sections, and thus there will be a total of 3 resistors and 4 capacitors.

4.2.2 Creating matrices for solving voltage and vacancy concentration response.

Creating the matrices version of the problem is based on solving Kirchoff's voltage and current laws by the mesh analysis technique. To describe this, consider a single grain boundary sample of interconnect which is represented by the C-R-C Π circuit of 2 sections as shown in Fig 4.2 below.
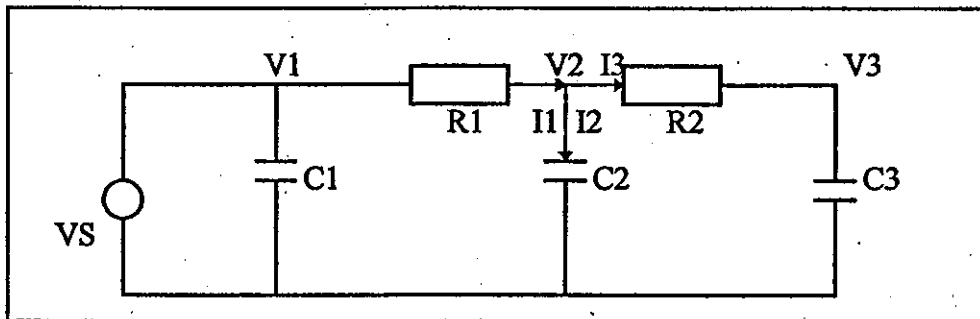
Fig 4.2 C-R-C circuit (2 sections)

Analysing the circuit above

$V1 = Vs$ therefore $\quad C1\dfrac{dV1}{dt} = 0$ $\hspace{4cm}$ 4.4

$I1 = I2 + I3$ $\hspace{6cm}$ 4.5

$$I1 = \frac{V1 - V2}{R1} \; , I2 = C2\frac{dV2}{dt} \; , I3 = \frac{V2 - V3}{R2} = C3\frac{dV3}{dt}$$

from equation 4.5,

$I2 = I1 - I3$

therefore by substitution

$$C2\frac{dV2}{dt} = \frac{V1 - V2}{R1} - \frac{V2 - V3}{R2} \hspace{3cm} 4.6$$

i.e. $\quad C2\dfrac{dV2}{dt} = \quad -\left(\dfrac{1}{R1} + \dfrac{1}{R2}\right)V2 + \left(\dfrac{1}{R2}\right)V3 + \left(\dfrac{1}{R1}\right)V1 \hspace{1cm} 4.7$

also $C3\dfrac{dV3}{dt} = \left(\dfrac{1}{R2}\right)V2 - \left(\dfrac{1}{R2}\right)V3 \hspace{3cm} 4.8$

112

These equations forms a set of simultaneous equations which may be expressed as a linear matrix equation :-

$$
\begin{bmatrix} C2 & 0 \\ 0 & C3 \end{bmatrix} \begin{bmatrix} \dfrac{dV2}{dt} \\ \dfrac{dV3}{dt} \end{bmatrix} = \begin{bmatrix} -\dfrac{1}{R1}-\dfrac{1}{R2} & \dfrac{1}{R2} \\ \dfrac{1}{R2} & -\dfrac{1}{R2} \end{bmatrix} \begin{bmatrix} V2 \\ V3 \end{bmatrix} + \begin{bmatrix} \dfrac{Vs}{R1} \\ 0 \end{bmatrix} \qquad 4.9
$$

The matrix is in the form of :-

$$
C.\frac{dV}{dt} = G\,\underline{V} + \underline{U} \qquad 4.10
$$

where C is a diagonal matrix of capacitance,(excluding the first capacitor C1), G is the conductance matrix , $\underline{V}$ is the vector of pseudo voltages of the nodes and $\underline{U}$ represents the vectors of the grain boundary conditions e.g. vacancy concentration held fixed at some vacancy supply point as in the example above.

Equation 4.10 can be rewritten as :-

$$
\frac{dV}{dt} = C^{-1}G\,\underline{V} + \underline{U} \qquad 4.11
$$

Replacing matrix $C^{-1}G$ by Q matrix, equation 4.11 becomes

$$
\frac{d}{dt}\underline{V} = Q\underline{V} + \underline{U} \qquad 4.12
$$

By diagonalizing the Q matrix , the above equation becomes

$$
\frac{d}{dt}\underline{V} = SDS^{-1}\,\underline{V} + \underline{U} \qquad 4.13
$$

$$
\frac{d}{dt}(S\underline{V}) = D(S\underline{V}) + S\underline{U} \qquad 4.14
$$

Integrating the above equation, yields

$$
S\underline{V} = A.e^{Dt} - D^{-1}S\underline{U} \qquad 4.15
$$

Solving for A by taking the initial condition at t=0, $\underline{V} = \underline{V}_0$,therefore gives

$$S\underline{V}_0 = A - D^{-1}S\underline{U}$$

therefore $A = S\underline{V}_0 + D^{-1}S\underline{U}$, hence

substituting A into equation 4.15 hence becomes

$$S\underline{V} = \left(S\underline{V}_0 + D^{-1}S.\underline{U}\right).exp^{Dt} - D^{-1}S\underline{U} \qquad 4.16$$

Therefore the voltage equation becomes

$$\underline{V} = S^{-1}(S.\underline{V}_0.exp^{Dt}) + S^{-1}(D^{-1}S.U.exp^{Dt}) - S^{-1}D^{-1}S\underline{U} \qquad 4.17$$

The vacancy concentration build-up C_v is obtained by the equation below:-

$$C_v = V.e^{(alphaaeff.x)} \qquad 4.18$$

This equation will be used in the simulation of the vacancy concentration response at any point along the interconnect line. In treating matrix problems, the arrangement of the terms in the equation above are very important as the matrices may not commute. This method of simulating the vacancy concentration response is applicable to single and complex grain boundary interconnects.

4.2.3   Program codes to simulate the exact solution

Two program codes are developed to find the real and imaginary roots for the case of $\alpha l \geq 2$ and $\alpha l \leq 2$ respectively. Two function files, **rroot.m** for finding the real root and **imroot.m** for imaginary roots will be fed into the script file **simall1g.m** to compute the vacancy concentration build-up of the exact solution. At first an approximate value for the roots are determined by a graphical method. Once obtained, this value can be improved further by applying the Newton-Raphson method. The Newton-Raphson method is used because it converges to a solution quickly. The Newton-Raphson formula is given by :-

$$x_{n+1} = x_n - \frac{f(x_n)}{f'(x_n)} \quad \text{where n is the number of iterations.} \qquad 4.19$$

These programs are used only to find the best possible values for the real and imaginary roots. The accuracy chosen for these roots is 4 decimal places. The vacancy concentrations are plotted on the same graph, so direct comparison can be made between the exact solution and the lumped element model. The flow charts of **rroot.m** and **imroot.m** are as shown in Fig4.3

4.2.4 The signal or Elmore delay method of approximating Time to Failure

The signal or Elmore delay provides a means of estimating the Time to Failure of interconnects. This method is incorporated into the script file **simal1lg.m** so that direct comparison of the Time to Failure can be made between the three solutions (lumped element model, exact solution and signal delay). The Program flow chart to create the matrix RG will be discussed later with the more realistic model of interconnect in section 4.7.

The signal delay (TD) equation is shown below :-

$$TD = RG.C. \left(\frac{(1 - \frac{VIN}{c_0})}{\left(1 - e^{(-alphaeff.x)}\right)} \right) \qquad 4.20$$

where TD = signal delay

RG = a special resistance matrix

C = diagonal matrix of capacitance

VIN = initial voltages of nodes

alphaeff = effective drift component of electromigration

x = length along the grain boundary

The program will compute this equation, and later will solve for the Time to Failure by using the equation :-

$$TTF = TD.Ln \left(\frac{\left(1 - e^{(-alphaeff.x)}\right)}{1 - \frac{V_{cr}}{c_0}} \right) \qquad 4.21$$

where

115

TTF = Time to Failure

Ln = natural logarithm

c_0 = initial vacancy concentration

cr = critical vacancy = $c_0 e^{\frac{\Omega \sigma_{cr}}{kT}}$

V_{cr} = cr.exp$(-$ alphaeff. x$)$

4.3 Single grain boundary interconnect sample with two ends blocked

A program code **sg2ball.m** has been developed to simulate the vacancy concentration response for a single grain boundary with both ends being blocked. The program codes incorporate the exact theoretical solution based on the work by [Clement,1992].Again , the main task or objective of the program code is to make the comparative study between the lumped element model with that of the exact solution. Fig. 4.4 shows the flow chart of the program code.

The program code consist of three main processes which include i) the simulation of vacancy concentration based on the lumped element model ii) the simulation of the vacancy concentration based on the exact solution iii) the determination of Time to Failure by the lumped element model, the exact solution and the signal delay.

As in the previous section, the vacancy concentration response for the lumped element model is produced by computing the matrices of conductance G, capacitance C , pseudo voltages VIN and matrix U. For the exact solution , the complete vacancy concentration build-up is based on eqn(2.19) as described in Chapter 2.

The purposes of the programs rroot.m and imroot.m are to find the real and imaginary roots from equation 2.20 and 2.21.

if roots are real   if roots are imaginary

| display graphical solution of the roots | display graphical solution of the roots |

| user inputs root= first approximation of root decpt = accuracy of root in | user inputs root = first approximation of root decpt = accuracy of root |

| solve equation 4.4 and store in variable a | solve equation 4.5 and store in variable a |

| solve the differential of equation 4.4 and store in variable b | solve the differential of equation 4.4 and store in variable b |

| divide a/b and store in variable y | divide a/b and store in variable y |

absolute (y) > decpt

iteration <15 → number of iterations has exceed limit

root1=root-y

iteration = iteration +1

root = root1

|abs(root)|< 0.0001 → first approximation not suitable

compute a,b,y

display exact root and number of iterations

root1 = root
the correct root value is fed to the script file simall1g.m

Fig4.3 The program flow charts for calculating the real roots and imaginary roots

117

The purpose of sg2ball.m is to simulate the vacancy concentration build-up for a single grain boundary where both ends are blocked. The program will compare the results of the work by [Clement,1992] , with the lumped element model. The Time to Failure will be compared between the 'exact solution'of Clement , signal delay and the lumped model solution.

```
┌─────────────────────────────────────────┐
│              User input                   │
│   nosim= number of simulation required    │
└─────────────────────────────────────────┘
                    │
                    ▼
            ┌─────────────────┐
            │   simno = 1     │
            └─────────────────┘
                    │
                    ▼
              ◇ simno <= nosim ◇
                    │
                    ▼
    ┌─────────────────────────────────────────────────┐
    │                  user input                       │
    │        x= length of grain boundary                │
    │        d= vacancy diffusion coefficient           │
    │        c₀ = initial vacancy concentration at zero  │
    │             stress                                 │
    │        cr = the critical vacancy concentration     │
    │        theta = angle of orientation                │
    │        alpha= drift component                      │
    │   alphaeff= alpha x cos(theta) the effective       │
    │             drift component                        │
    └─────────────────────────────────────────────────┘
                    │
                    ▼
    ┌─────────────────────────────────────────────────┐
    │                 CImatone.m                        │
    │  m-file to create the resistor and capacitor      │
    │  matrix G                                         │
    └─────────────────────────────────────────────────┘
                    │
                    ▼
    ┌─────────────────────────────────────────────────┐
    │                 cmatone.m                         │
    │      m-file to create capacitor matix C           │
    └─────────────────────────────────────────────────┘
    ┌─────────────────────────────────────────────────┐
    │                 vmatwo.m.                         │
    │    m-file to crate initial voltage matrix VIN     │
    └─────────────────────────────────────────────────┘
                    │
                    ▼
    ┌─────────────────────────────────────────────────┐
    │                  tcone.m                          │
    │        m-file to create the U matrix              │
    └─────────────────────────────────────────────────┘
```

The simulation of the voltage response is done by the following process:-

i) assignment of the duration of time $= t$

ii) diagonalising the matrix of $Q = C^{-1} G$.

iii) solving the voltage response by the equation :-

$$V = S^{-1}\left(S.VIN.exp^{Dt}\right) + S^{-1}\left(D^{-1}.S.U.exp^{Dt}\right) - S^{-1}D^{-1}S.U$$

the conversion of the voltage response to vacancy concentration response is solve by the equation :-

$$C_v = V \times exp^{alphaeff.x} \;,\; C_v \text{ is the vacancy concentration}$$

the time to failure is determine by interpolating between the data points of the vacancy concentration C_v and the time t. The command of Matlab to do the this is :-

TTF = interp1(C_v , t, critical vacancy concentration)

↓ continue

118

```
┌─────────────────────────────────────────┐
│     simulation of the exact solution     │
│        by solving equation 2.16          │
└─────────────────────────────────────────┘
                    ↓
┌─────────────────────────────────────────┐
│ the time to failure is determine by      │
│ interpolating between the data points of │
│ the vacancy concentration C_v and the    │
│ time t. The command of Matlab            │
│   to do the this is :-                    │
│   TTF = interp1(C_v , t, critical         │
│            vacancy concentration)         │
└─────────────────────────────────────────┘
                    ↓
┌─────────────────────────────────────────┐
│  calculate the Time to failure by signal  │
│           delay method                    │
└─────────────────────────────────────────┘
                    ↓
┌─────────────────────────────────────────┐
│               rmatone.m                   │
│   m-file for the resistance matrix RG     │
└─────────────────────────────────────────┘
                    ↓
┌─────────────────────────────────────────┐
│  calculate the signal delay by the        │
│            equation                       │
└─────────────────────────────────────────┘
                    ↓
┌─────────────────────────────────────────┐
│           simno=simno +1                  │
└─────────────────────────────────────────┘
                    ↓
┌─────────────────────────────────────────┐
│ produce the vacancy concentration         │
│ response graph and the results of         │
│ Time to failure                           │
└─────────────────────────────────────────┘
```

$$TD = RG.C. \left(\frac{(1-\frac{VIN}{c_0})}{(1-e^{(-alphaeff.x)})} \right) \ , \ TTF = TD.Ln\left(\frac{\left(1-e^{(-alphaeff.x)}\right)}{1-\frac{V_{cr}}{c_0}} \right) \ , \ V_{cr} = cr.e^{(-alphaeff.x)}$$

FIG 4.4 The program flow chart of sg2ball.m

4.3.1 Creating matrices for solving voltage and vacancy concentration response.

The approach of simulating the voltage and vacancy concentration response is identical to that in section 4.2.2 . The only difference is in the treatment of the matrices. In this case the total charge in the system will be conserved.

With reference to Fig 4.2

$$\text{Total Charge (TC)} = \sum_{i=1}^{3} C(i).V(i)\Big|_{t=0} \qquad\qquad 4.22$$

$$V1 = \frac{TC - \sum\limits_{i=2}^{3} C(i).V(i)}{C1} \qquad\qquad 4.23$$

$$V1 = \frac{TC}{C1} - \frac{C2.V2}{C1} - \frac{C3.V3}{C1} \qquad\qquad 4.24$$

Therefore the earlier equation 4.7 becomes

$$C2\frac{dV2}{dt} = -\left(\frac{1}{R1} + \frac{1}{R2}\right)V2 + \left(\frac{1}{R2}\right)V3 + \left(\frac{1}{R1}\right)\left(\frac{TC}{C1} - \frac{C2.V2}{C1} - \frac{C3.V3}{C1}\right) \qquad 4.25$$

After rearranging

$$C2\frac{dV2}{dt} = -\left(\frac{1}{R1} + \frac{1}{R2} + \frac{C2}{R1.C1}\right)V2 + \left(\frac{1}{R2} - \frac{C3}{R1.C1}\right)V3 + \left(\frac{TC}{R1.C1}\right) \qquad 4.26$$

Therefore the linear matrix equation for the whole circuit:-

$$\begin{bmatrix} C2 & 0 \\ 0 & C3 \end{bmatrix}\begin{bmatrix} \dfrac{dV2}{dt} \\ \dfrac{dV3}{dt} \end{bmatrix} = \begin{bmatrix} -\dfrac{1}{R1} - \dfrac{1}{R2} - \dfrac{C2}{R1.C1} & \dfrac{1}{R2} - \dfrac{C3}{R1.C1} \\ \dfrac{1}{R2} & -\dfrac{1}{R2} \end{bmatrix}\begin{bmatrix} V2 \\ V3 \end{bmatrix} + \begin{bmatrix} \dfrac{TC}{.R1.C1} \\ 0 \end{bmatrix} \quad 4.27$$

The difference between equation 4.9 and 4.27 is in the G matrix and the $\underline{U}$ vector.

4.3.2 The program codes to simulate the 'exact' solution

This program t1g2blk.m is to simulate the exact theoretical solution for a single grain boundary with double blocking ends. The program enables the theoretical response of the vacancy concentration at various points on the grain be monitored. The original equations of reference[Clement,1992] have been modified by replacing the positive sign of the α to negative sign because the original equation deals with negative electric field. Another important term in the original equation that has been modified is that the solution is in the form of infinite series of summation. It is time consuming to compute for large values of k, a reasonable value of k=20 is chosen which would give a sufficiently accurate answer. This new equation is included in the

main program of sg2ball.m so that direct comparison can be made between theoretical and the simulated approach.

4.4 The programs codes developed for single grain boundary

The programs that have been developed are shown in the Table 4.1, 4.2

No	Program title	Associate m-files	sub-m-files	Description
1	simall1g.m			main program involving simulation and combining with the theoretical solution and the elmore delay approximation.
		1. gmatone.m	1. oneres.m	to develop the matrix of the resistors derived from the sub-m-file which calculated the values.
		2. cmatone	1. onecap.m	to develop the diagonal matrix of capacitor derived from the sub-m-file which calculate the values of capacitors
		3. vmatone.m	1. onevolt.m	to develop the initial voltage vectors derived from the sub-m-file which calculated the values.
		4. umatone.m		to develop the U vectors of the initial boundary condition
		5. rroot.m		program to find the real roots using Newton-Raphson method for the case $\alpha x >= 2$
		6. imroot.m		program to find the imaginary roots using Newton-Raphson method for the case $\alpha x <= 2$

Table 4.1 Single grain boundary- Single blocking ends

No	Program title	Associate m-files	sub-m-files	Description
1	sg2ball.m			main program involving simulation and combining with the theoretical solution.
		1. crmatone.m	1. oneres.m 2. onecap.m	to develop the matrix of both the resistors and capacitors derived from the sub-m-files which calculated the values.
		2. cmatone	1. onecap.m	to develop the diagonal matrix of capacitor derived from the sub-m-file which calculate the values of capacitors
		3. vmatwo.m	1. onevolt.m	to develop the initial voltage vectors derived from the sub-m-file which calculated the values.
		4. tcone.m	1. onecap 2. onevolt	to calculate the total charge
		5. umatwo.m		to develop the U vectors of the initial boundary condition
	t1g2blk.m			main program involving simulation the theoretical solution of section 3.1.2

Table 4.2 Single grain boundary - Double blocking ends

4.5 A representative example of a complex grain boundary network

The next stage of program code development is to apply the lumped element model to complex grain boundaries. In reality, the metalisation film will undergo annealing and patterning processes during which the final interconnect samples are produced. Many clusters with complex grain boundary microstructures are formed which run along the interconnect line. The parameters of these networks (the vacancy diffusion coefficients, the lengths and orientation of the various grain boundaries) are statistically distributed making the lifetime also a stochastic parameter. It is the aim of these program codes to study the effect of these parameters on the electromigration lifetime behaviour and to produce an interim statistical analysis of Time to Failure.

The model under study is a simple single,though realistic, cluster made up of 5 grain boundaries as shown below. In fact a number of other references have also used more or less this kind of model [Gleixner and Nix,1999],[Trattles, et.al, 1994] to study electromigration behaviour.
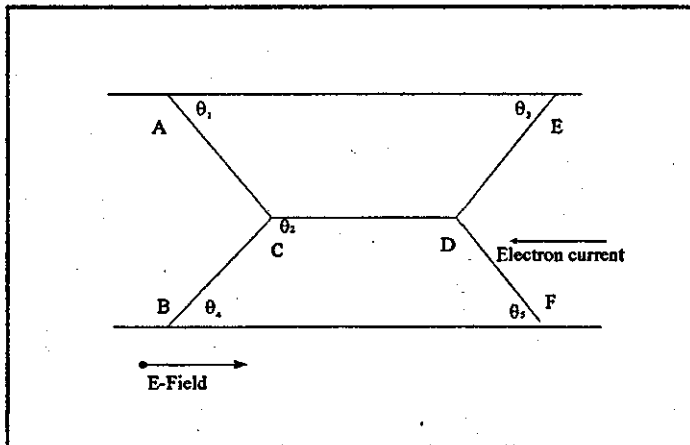
Fig 4.5 The complex grain boundary model

Two program codes **net1ball.m**(one end supplying vacancies with the others blocked) and **net2ball.m**(all ends being blocked) have been developed to simulate the vacancy concentration build-up at various nodes and to determine the Time to Failure. It also incorporates the signal delay for estimating Time to Failure. The program flow charts are as shown in Fig 4.6 (net1ball.m) . and Fig4.7 (net2ball.m)

In the simulation of the lumped element model,the cluster case has program flow which is identical to that of the single grain boundary interconnect.. The difference is merely in the number of grain boundaries, which will affect the various calculations of the components and their matrices and vectors. The flow charts describing these calculations will be shown later for a more realistic model of a complete interconnect.

The purpose of **net1ball.m** is to simulate the vacancy concentration build-up for a complex grain boundary network where one end has a supply of vacancies c_0 and the others are blocked. The program will also compare the Time to Failure between the lumped model solution with the signal delay approximation.

```
┌─────────────────────────────────────────┐
│              User input                  │
│   nosim= number of simulation required   │
└─────────────────────────────────────────┘
                    │
                    ▼
            ┌──────────────┐
            │  simno = 1   │
            └──────────────┘
                    │
                    ▼
            ◇ simno <= nosim ◇
                    │
                    ▼
```

user input
s= number of sections per grain boundary
c_0 = supplyvacancyconcentration
x1-x5 = length of 5 grain boundaries
d1-d5 = vacancy diffusion coefficient of 5 grain boundaries
cr = the critical vacancy concentration
theta1-theta2 = angle of orientation for 5 grain boundaries
alphaeff1-alphaeff5 = the effective drift component

resmat.m
m-file to create the resistor matrix G

cmat.m
m-file to create capacitor matrix C

matcrg.m.
m-file to crate initial voltage matrix VIN

umat2.m
m-file to create the U matrix

The simulation of the voltage response is done by the following process:-
i) assignment of the duration of time = t
ii) diagonalising the matrix of $Q=C^{-1}G$.
iii) solving the voltage response by the equation :-

$$V = S^{-1}\left(S \cdot VIN.exp^{Dt}\right) + S^{-1}\left(D^{-1}S.U.exp^{Dt}\right) - S^{-1}D^{-1}S.U$$

the conversion of the voltage response to vacancy concentration is obtained by the equation :-

$$C_v = V \times exp^{alphaeff.x} \quad , C_v \text{ is the vacancy concentration}$$

the Time to Failure is determined by interpolating between the data points of the vacancy concentration C_v and the time t. The command of Matlab to do the this is :-   TTF = interp1(C_v , t, critical vacancy concentration)

continue

124

```
                    ↓
┌─────────────────────────────────────────────────────────┐
│                                                         │
│        calculate the  Time to failure by signal delay method │
│                                                         │
└─────────────────────────────────────────────────────────┘
                    ↓
┌─────────────────────────────────────────────────────────┐
│                    rmatcg1.m                            │
│           m-file for the resistance  matrix  RG         │
└─────────────────────────────────────────────────────────┘
                    ↓
┌─────────────────────────────────────────────────────────┐
│          calculate the signal delay by the equation     │
│                                                         │
│                                                         │
└─────────────────────────────────────────────────────────┘
```

$$TD = RG.C. \left(\frac{(1 - \frac{VIN}{c_0})}{(1 - e^{(-alphaeff.x)})} \right) \ , \ TTF = TD.Ln \left(\frac{\left(1 - e^{(-alphaeff.x)}\right)}{1 - \frac{V_{cr}}{c_0}} \right) \ , \ V_{cr} = cr.e^{(-alphaeff.x)}$$

```
                    ↓
        ┌───────────────────────┐
        │   simno=simno +1      │
        └───────────────────────┘
                    ↓
┌─────────────────────────────────────────────────────────┐
│      produce the vacancy concentration response graph   │
│            and the data  of Time to failure             │
└─────────────────────────────────────────────────────────┘
```

FIG 4.6 The program flow chart of net1ball.m

125

The purpose of **net2ball.m is** to simulate the vacancy concentration build-up for a complex grain boundary where all ends are blocked.

```
┌─────────────────────────────────────────┐
│              User input                  │
│   nosim= number of simulation required   │
└─────────────────────────────────────────┘
                    │
          ┌──────────────────┐
          │     simno = 1    │
          └──────────────────┘
                    │
              ◇ simno <= nosim ◇
                    │
┌─────────────────────────────────────────────────┐
│                   user input                     │
│   s= number of sections per grain boundary       │
│   c_0 = supply vacancy concentration             │
│   x1-x5 = length of 5 grain boundaries           │
│   d1-d5 = vacancy diffusion coefficient of 5 grain boundaries │
│   cr = the critical vacancy concentration        │
│   theta1-theta2 = angle of orientation for 5 grain boundaries │
│   alphaeff1-alphaeff5 = the effective drift component │
└─────────────────────────────────────────────────┘
                    │
┌─────────────────────────────────────────────────┐
│                  crmat.m                         │
│   m-file to create the resistor and capacitor matrix G │
└─────────────────────────────────────────────────┘
                    │
┌─────────────────────────────────────────────────┐
│                  cmat.m                          │
│        m-file to create capacitor matrix C       │
└─────────────────────────────────────────────────┘
                    │
┌─────────────────────────────────────────────────┐
│                  vmat.m.                         │
│     m-file to crate initial voltage matrix VIN   │
└─────────────────────────────────────────────────┘
                    │
┌─────────────────────────────────────────────────┐
│                  tcgr.m                          │
│     m-file to create the total charge matrix TC  │
└─────────────────────────────────────────────────┘
                    │
┌─────────────────────────────────────────────────┐
│                  umat2.m                         │
│        m-file to create the U matrix             │
└─────────────────────────────────────────────────┘
```

The simulation of the voltage response is done by the following process:-
- i) assignment of the duration of time = t
- ii) diagonalising the matrix of $Q=C^{-1}G$.
- iii) solving the voltage response by the equation :-

$$V = S^{-1}\left(S.VIN.exp^{Dt}\right) + S^{-1}\left(D^{-1}S.U.exp^{Dt}\right) - S^{-1}D^{-1}S.U$$

the conversion of the voltage response to vacancy concentration response is solve by the equation :-

$$C_v = V \times exp^{alphaeff.x} , C_v \text{ is the vacancy concentration}$$

the time to failure is determine by interpolating between the data points of the vacancy concentration C_v and the time t. The command of Matlab to do the this is :-

$$TTF = interp1(C_v, t, \text{critical vacancy concentration})$$

┌──────────────────────┐
│   simno = simno +1   │
└──────────────────────┘

Fig 4.7 The program flow chart of net2ball.m

4.6 The programs codes developed for 'self generated' complex grain boundary

The programs that have been developed are shown in the Table 4.3, 4.4

No	Program title	Associate m-files	sub-m-files	Description
1	net1ball.m			main program · to simulate the vacancy concentration and calculate the TTF based on lumped element model and signal delay
		1. resmat.m	1. newres.m	to develop the matrix of the resistors derived from the sub-m-files which calculated the values of resistance.
		2. cmat.m	1. newcap.m	to develop the diagonal matrix of capacitors derived from the sub-m-file which calculate the values of capacitors
		3. matcrg.m	1. inicrg.m	to develop the initial voltage vectors derived from the sub-m-file which calculated the values of the initial voltages.
		4. umat2.m		to develop the U vectors of the initial boundary condition

Table 4.3 Complex grain boundary -one end has supply vacancy

No	Program title	Associate m-files	sub-m-files	Description
1	net2ball.m			main program to simulate the vacancy concentration and calculate the TTF based on lumped elemnt model
		1. crmat.m	1. newres.m 2. newcap.m	to develop the matrix of both the resistors and capacitors derived from the sub-m-files which calculated the values.
		2. cmat.m	1. newcap.m	to develop the diagonal matrix of capacitor derived from the sub-m-file which calculate the values of capacitors
		3. vmat.m	1. inicrg.m	to develop the initial voltage vectors derived from the sub-m-file which calculated the values.

		4. tcrg.m	1. inicrg.m	to calculate the total charge consumed in the circuit
			2. newcap.m	
		5. umatnew.m		to develop the U vectors of the initial boundary condition

Table 4.4 Complex grain boundary -all ends blocked

4.7 The development of program codes for realistic grain boundaries

To obtain meaningful statistical data on the electromigration Time to Failure a more realistic model representing the interconnect must be developed. Many studies involving computer simulations on electromigration lifetime employ Voronoi tec\hnique to generate a realistic representation of interconnect [Joo and Thompson,1994],[Knowlton, et al.,1989],[Marcoux, et al.,1989]

Voronoi techniques have also been employed in this part of the software development. MATLAB® provides a built-in function to generate a Voronoi network consisting of straight lines joining the nodes. With this facility , a program code **vrnoittf2.m** has been developed in an attempt to produce realistic statistical data of electromigration Time to Failure. The process of obtaining the required data can be understood better by referring to process flow chart of Fig4.8 below.

Production of Al /Cu Film by Voronoi method

Annealing treatment of Al/Cu film

Production of interconnect samples

Calculation of TTF of grain boundary clusters using lumped element model

Calculation of TTF of grain boundary clusters using signal delay method

Determine the TTF of the interconnect (the smallest time among the TTFs of grain boundary clusters)
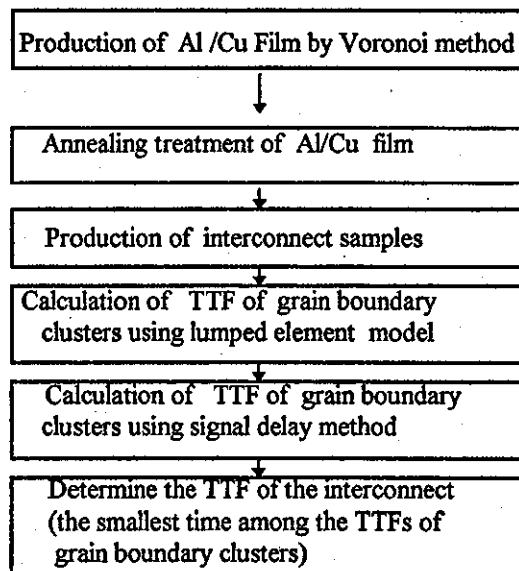
Figure 4.8   The program flow chart of the main processes
                  for producing the Time to Failure for realistic interconnects

With reference to Fig.4.8, to obtain the electromigration lifetime of interconnect samples, the program needs to undergo several processes. The development of the program codes starts with creating the Voronoi network which will represent a conductor film , which in this study is aluminium or copper*. Once the film been created, it will often undergo an annealing process during where the grain will grow in size. The program code which simulates this process is the function file **annealing.m**. The main processes that are involved in the annealing treatment are i) grain growth ii) the annihilation of unsustainable grain boundaries and iii) recombination of grain boundaries which allows for larger grains to grow at the expense of smaller ones. For the simulation of the annealing process, the algorithm for grain growth and the rules for annihilation and recombination, are based on the work by [Kawasaki, et.al, 1989].

After the annealing process, the Al film is patterned to form interconnect samples, and the program code to do this is **slice2.m**. The program will simulate the slicing of the Al film into various number of interconnect samples depending on the desired width. Once the interconnect samples have been generated, the simulation of their Time to Failure can be achieved, a function file **vrttf.m** will do the simulations based on the lumped element model and the signal delay method. First, the Time to Failure of each cluster of grain boundaries will be calculated and then the minimum Time to Failures among the cluster in the sample will be considered to give the Time to Failure of the interconnect sample.

For the whole simulation exercise, the only limitation of the program codes is in the calculation of the Time to Failure where the maximum number of grain boundaries per cluster is limited to eleven. A script file **vrnoittf2.m** has been developed to simulate the whole process and the program flow chart is shown in Fig. 4.9.

* To be specific we have looked at Al because parameter values for Al are better known than for Cu and more experimental results exist for Al.

```
┌────────────────────────────────────────────┐
│                annealing.m                  │
│  m-file for the simulation of the annealing process │
│   of the Voronoi network                    │
└────────────────────────────────────────────┘
                      ↓
┌────────────────────────────────────────────┐
│                figvrnoi.m                   │
│  m-file for the production of a hard copy of │
│  interconnect samples                       │
└────────────────────────────────────────────┘
                      ↓
┌────────────────────────────────────────────┐
│                geometry.m                   │
│  m-file for the calculation of the geometrical │
│  properties of the grain boundaries i.e. length │
│  of grain boundaries and the angle of orientation │
└────────────────────────────────────────────┘
                      ↓
┌────────────────────────────────────────────┐
│                lablenode.m                  │
│  m-file for the making of labels for the nodes │
│  (vertices) and the grain boundaries        │
└────────────────────────────────────────────┘
                      ↓
┌────────────────────────────────────────────┐
│                User input                   │
│  nosample =                                 │
│  sample= 1 ( start counter)                 │
└────────────────────────────────────────────┘
                      ↓
        no      ╱◇◇◇◇◇◇◇◇◇◇◇◇◇◇◇◇╲
    ←───────── ◇  sample<= nosample?  ◇
                ╲◇◇◇◇◇◇◇◇◇◇◇◇◇◇◇◇╱
                      ↓ yes
┌────────────────────────────────────────────┐
│                slice2.m                     │
│  m -file to produce the interconnect samples │
└────────────────────────────────────────────┘
                      ↓
┌────────────────────────────────────────────┐
│               newgeometry.m                 │
│  m -file to calculate the new values of the │
│  length and angle of grain boundaries       │
└────────────────────────────────────────────┘
                      ↓
┌────────────────────────────────────────────┐
│                newnode.m                    │
│  m-file for making the new labels for the new │
│  nodes and the grain boundaries             │
└────────────────────────────────────────────┘
                      ↓
┌────────────────────────────────────────────┐
│                User input                   │
│  nocluster =          , clusterno = 1(start counter) │
└────────────────────────────────────────────┘
                      ↓
      no       ╱◇◇◇◇◇◇◇◇◇◇◇◇◇◇◇◇╲
    ←───────── ◇  clusterno<= nocluster?  ◇
                ╲◇◇◇◇◇◇◇◇◇◇◇◇◇◇◇◇╱
                      ↓ yes
┌────────────────────────────────────────────┐
│                vrttf.m                      │
│  m-file to calculate the exact solution and │
│  Elmore delay of the Time to Failure of     │
│  the grain boundaries clusters and hence    │
│  the interconnect samples                   │
└────────────────────────────────────────────┘
                      ↓
┌────────────────────────────────────────────┐
│         clusterno=clusterno+1               │
└────────────────────────────────────────────┘
                      ↓
┌────────────────────────────────────────────┐
│            sample=sample+1                  │
└────────────────────────────────────────────┘
                      ↓
┌────────────────────────────────────────────┐
│                   end                       │
└────────────────────────────────────────────┘
```
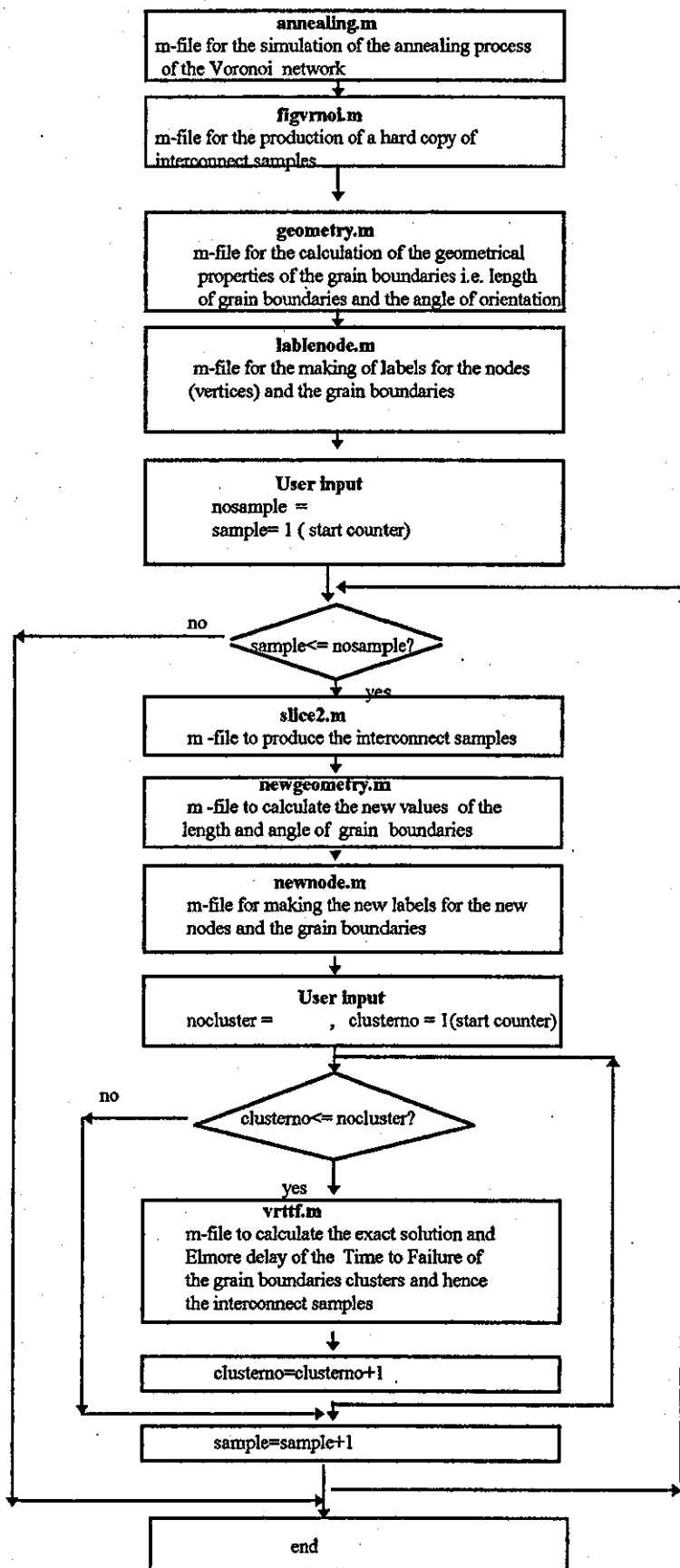
Fig4.9   The flow chart of the simulation of the Time to Failure
          for the script file **vrnoittf2.**

4.7.1 The simulation of producing samples of Al films

The samples of the Al films (consisting of the grain boundary clusters) are constructed by the Voronoi method as mentioned earlier. These grain boundaries are produced by using the available built-in function of the MATLAB® i.e. voronoi(vx,vy). The grain boundaries are all then straight lines connecting the vertices in the Voronoi diagram.

4.7.2 The simulation of annealing process

The annealing treatment of the Al films is simulated by increasing the size of the grains. A program code **annealing.m** has been developed to simulate this by using the rules developed in the Vertex model for 2D grain growth[Kawasaki et.al,1989] which is suitable since it involves the manipulation of the co-ordinates of the vertices. The annealing treatment simulation will improve the Voronoi diagrams which are initially produce by the built-in function of MATLAB®. The simulation will exhibit the growth and the collision of grain boundaries processes where grain boundaries recombine or are annihilated when a grain boundary length is forced below a critical value unsustainable. The program flow chart of the annealing process is as shown in Fig 4. 10

First a Voronoi network is generated and its geometrical data is compute and stored. This process is done through a function file **geometry.m.** The geometrical data computed are i) lengths of the grain boundaries and ii) angles of orientation. A flow chart showing the process is shown in Fig4.11.

The initial Voronoi network generated by the computer only provides information on the co-ordinates of the nodes in terms of vx and vy. It is vital to label the nodes and the lines (grain boundaries) connecting these nodes. This is needed for identification purposes for calculating the Time to Failure. A program code **labgrain1.m** has been developed to do this task and the flow chart describing the labelling process is shown in Fig.4.12. Although the nodes and their grain boundaries are labelled, there is not yet any information on how they are connected to each other. A program code

conmtrix.m is developed to solve this problem. All of the information on the Voronoi network can then be stored, such as i) the connectivity between each node, is stored in matrix NODMAT. ii) the grain boundary identification numbers are stored in matrix GBMAT. iii) the length of the grain boundaries are stored in LGTHMAT and iv) the angle of orientation of the grain boundaries are stored in matrix ANGLEMAT. These matrices will be called when computing later processes such in the annealing and calculation of Time to Failure. Fig 4.13 shows the program flow chart of **conmtrix.m.**

In the simulation of the annealing process itself, there are three main processes that are being simulated i.e. i) grain growth ii) grain boundary annihilation and iii) grain boundary recombination for every time step. To simulate this processes, three function files are developed i.e. i) **grwth1.m** for simulating the process of grain growth, ii) **lamda1.m** for classifying nodes which can form triangles (for annihilation) or switches(for recombination) and iii) **trisw1.m** for simulating the annihilation and recombination process. Program flow charts to describe this processes are as shown in Fig4.14 , Fig 4.15, and Fig 4.16 for the **grwth1.m** , **lamda1.m** and **trisw1.m** respectively. The equation use for simulating the grain growth is obtained from [Kawasaki,et.al,1989] and is given below :-

$$\frac{dr_i}{dt} = -\frac{1}{Z} \cdot \sum_{j}^{(i)} \frac{(r_j - r_i)}{|r_i - r_j|} \qquad 4.28$$

$$Z = \frac{1}{6} \cdot \sum_{j}^{(i)} |r_i - r_j| \qquad 4.29$$

(i) = number of nearest neighbours of node i

$\sum_{j}^{i}$ is the sum of all the nearest neighbours(node j's) of node i

$(r_j\_r_i)$ is the difference between the co-ordinates of the nearest neighbours(nodej's) and the co-ordinates of node i.

$|r_i\_r_j|$ is length of the line or grain boundary between node i and all the neighbouring nodes j.

$\dfrac{dr_i}{dt}$ is the rate of change of co-ordinate i with time t (this will give the

new co-ordinates after some time steps dt)

For the program code **lamda1.m,** the nodes to be identified are those nodes which can form triangles and switches. These are those which satisfy the following criteria

i)   the length between any two nodes(the length of grain boundary) has become shorter than the critical vertex size Δ.

ii) the test for a triangle in the connectivity matrix NODMAT has been passed.

The test for a node being part of a triangle is described below, based on an example from a Matlab book by [Biran.& Breiner, 1999]in a section on graph theory. With reference to the Fig4.17 there is only one triangle,.
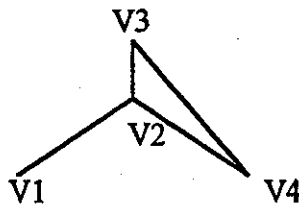
Fig 4.17

The connectivity matrix $A = \begin{vmatrix} 0 & 1 & 0 & 0 \\ 1 & 0 & 1 & 1 \\ 0 & 1 & 0 & 1 \\ 0 & 1 & 1 & 0 \end{vmatrix}$

Taking a cube $= A^3 = \begin{vmatrix} 0 & 3 & 1 & 1 \\ 3 & 2 & 4 & 4 \\ 1 & 4 & 2 & 3 \\ 1 & 4 & 3 & 2 \end{vmatrix}$

The triangle is one having the length of path equals to 2 on the diagonal i.e. node V2, V3 and V4. This algorithm, i.e. first take the cube of the connectivity matrix NODMAT and then search for all nodes having a value equals to 2 on the diagonal entries of the matrix NODMAT, this will provide all the possible nodes that can form a triangle. This algorithm is applied in function files **lamda1.m** and **trisw1.m**

The program code **trisw1.m** is developed to simulate the annihilation and the recombination process of the grain boundaries. The first step is to find all the nodes and their neighbouring nodes (those nodes that are connected to the identified grain boundaries). The annihilation simulation is described below:-

4.7.2.1 The recombination process

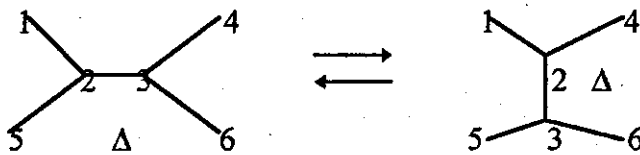An example of the recombination process is shown in Fig 4.18(a).

Fig 4.18(a) Recombination process . Here the length of grain boundary

connecting nodes 2 and 3 has become less than Δ, so the switch occurs

The algorithm to perform the recombination processes is:-

i) create a 90^0 rotational matrix ROTMAT

ii) calculate the original co-ordinates (vxo,vyo)which is half way between nodes 2 and 3

iii) calculate the new co-ordinates of node 2 and 3 = original co-ordinates -vxo, vyo and then multiply by the rotational matrix. This will rotate node 2 and node 3 (90^0 clockwise).

iv) select the appropriate neighbour nodes to node 2 and node 3 which needs to be recombined/switched (i.e node 5 and 4 only)

v) modify the connectivity matrix NODMAT so that node 4 is now connected to node 2 instead of node 3, and Node 5 connected to node 3 instead of node 2

4.7.2.2 The annihilation process

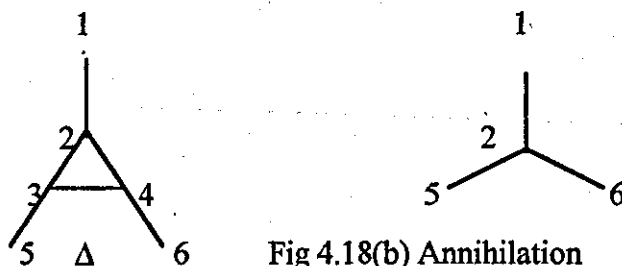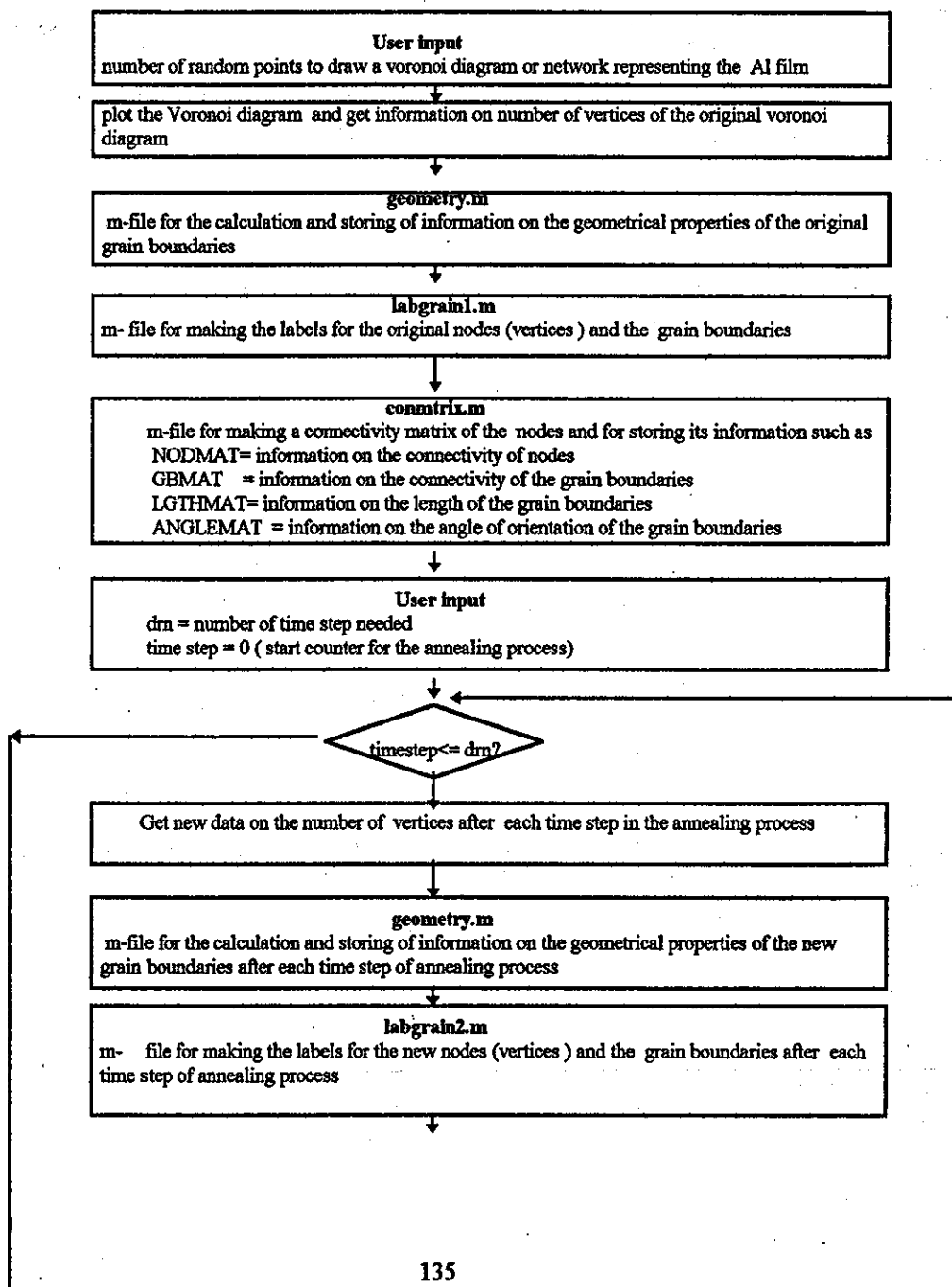An example of the annihilation process is shown in Fig 4.18(b).

Fig 4.18(b) Annihilation

134

Here the area of the triangle $\{r_2, r_3, r_4\}$ has become less than Δ^2. It is considered unstable and vanishes.

The algorithm to perform the annihilation processes is:-

i) find the centre point of node 2,3 and 4 and label the node as node 2

ii) select the neighbours of each node of the triangle node 2,3 and 4 which are not part of the triangle i.e. neighbour node 1, 5 and 6

iii) modify the connectivity matrix NODMAT so that node 1, 5 and 6 is connected to node 2.

User input
number of random points to draw a voronoi diagram or network representing the Al film

↓

plot the Voronoi diagram and get information on number of vertices of the original voronoi diagram

↓

geometry.m
m-file for the calculation and storing of information on the geometrical properties of the original grain boundaries

↓

labgrain1.m
m- file for making the labels for the original nodes (vertices) and the grain boundaries

↓

conmtrix.m
m-file for making a connectivity matrix of the nodes and for storing its information such as
NODMAT= information on the connectivity of nodes
GBMAT = information on the connectivity of the grain boundaries
LGTHMAT= information on the length of the grain boundaries
ANGLEMAT = information on the angle of orientation of the grain boundaries

↓

User input
drn = number of time step needed
time step = 0 (start counter for the annealing process)

↓

timestep<= drn?

↓

Get new data on the number of vertices after each time step in the annealing process

↓

geometry.m
m-file for the calculation and storing of information on the geometrical properties of the new grain boundaries after each time step of annealing process

↓

labgrain2.m
m- file for making the labels for the new nodes (vertices) and the grain boundaries after each time step of annealing process

↓

135

```
┌─────────────────────────────────────────────────────────────────────────┐
│                              conmtrix.m                                    │
│  m-file for making a connectivity matrix of the  new nodes and storing its information such as │
│  NODMAT= information on the connectivity of nodes                          │
│  GBMAT   = information on the connectivity of the grain boundaries         │
│  LGTHMAT= information on the length of the grain boundaries                │
│  ANGLEMAT = information on the angle of orientation of the grain boundaries │
└─────────────────────────────────────────────────────────────────────────┘
                                    ↓
┌─────────────────────────────────────────────────────────────────────────┐
│                              grwth1.m                                      │
│  m-file for the simulation of the growing of the grains                    │
└─────────────────────────────────────────────────────────────────────────┘
┌─────────────────────────────────────────────────────────────────────────┐
│                              lamda1.m                                      │
│  m-file for the detection of the grain boundaries which have the length less than the critical value │
│  for the grain boundaries to annihilate or to switch                       │
└─────────────────────────────────────────────────────────────────────────┘
                                    ↓
┌─────────────────────────────────────────────────────────────────────────┐
│                              trisw1.m                                      │
│  m-file for the simulation of the annihilation and the switching of the grain boundaries process │
└─────────────────────────────────────────────────────────────────────────┘
                                    ↓
┌─────────────────────────────────────────────────────────────────────────┐
│                              output.m                                      │
│  m-file for the plotting of new Voronoi network after each time step of the annealing process │
└─────────────────────────────────────────────────────────────────────────┘
                        ┌──────────────────────────┐
                        │   timestep=timestep +1   │
                        └──────────────────────────┘
```

Fig4.10. Program flow chart of annealing.m   [end]

```
                    ┌──────────────────────────────────┐
                    │           geometry.m              │
                    └──────────────────────────────────┘
                                   ↓
                    ┌──────────────────────────────────┐
                    │  n= number of  line ( grain boundaries) │
                    │       joining each vertices        │
                    │  k=1                               │
                    └──────────────────────────────────┘
                                   ↓
                                                      no
                              ◇ k <=n ◇ ──────────────→
                                   │ yes
                                   ↓
        ┌──────────────────────────────────────────────────┐
        │   calculate the length and angle of  the grain boundaries │
        │                                                    │
```
$$Lxy(k)= \sqrt{\left(vx2(k) - vx1(k)\right)^2 + (vy2(k) - vy1(k))^2}$$

$$thetarad(k)= \tan^{-1}\left(\frac{(vy2(k) - vy1(k))}{(vx2(k) - vx1(k))}\right)$$
```
        └──────────────────────────────────────────────────┘
                                   ↓
        ┌──────────────────────────────────────────────────┐
        │                    k=k+1                           │
        └──────────────────────────────────────────────────┘
                                   ↓
        ┌──────────────────────────────────────────────────┐
        │                    exit                            │
        └──────────────────────────────────────────────────┘
```
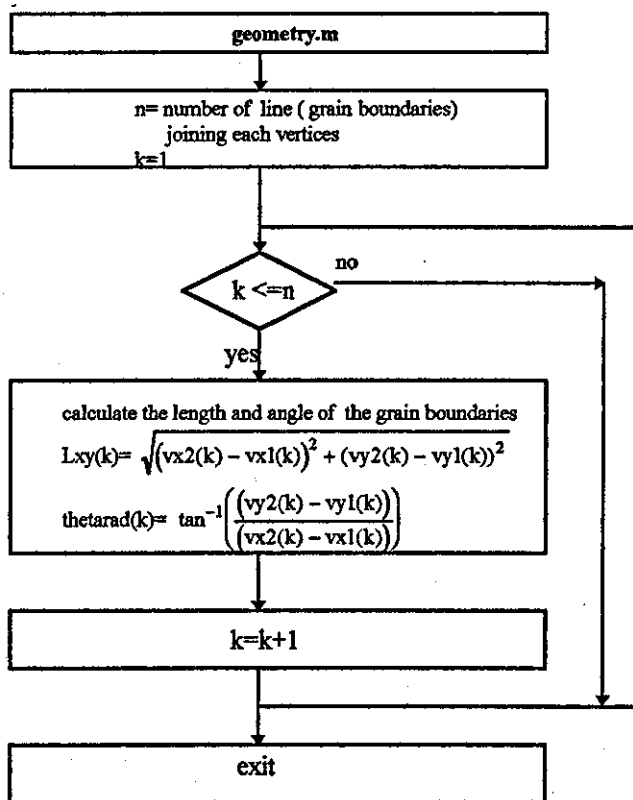
Fig 4.11   The program flow chart for calculating the length and angle of orientation of the grain boundaries of m-file geometry.m
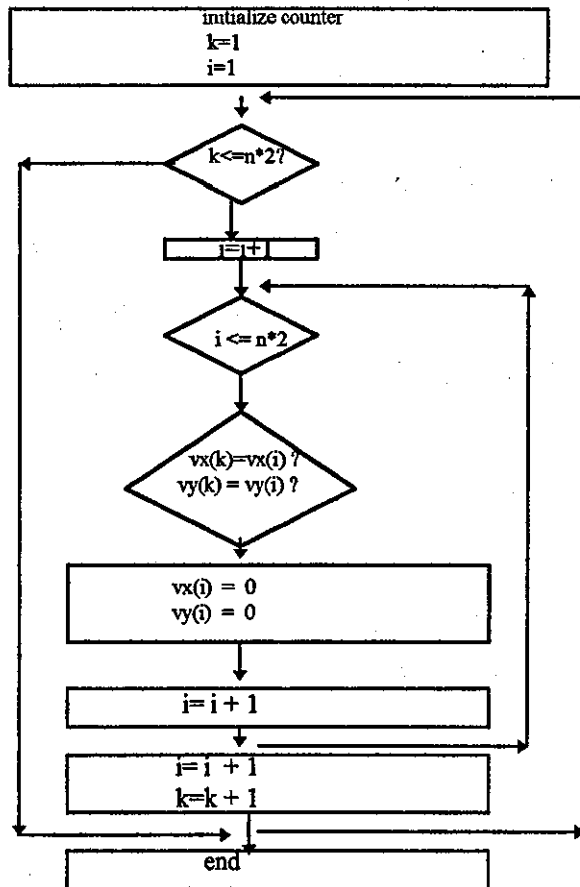
Fig 4.12(a)   The program flow chart for labelling of nodes and its grain boundaries in the **labgrain1.m**
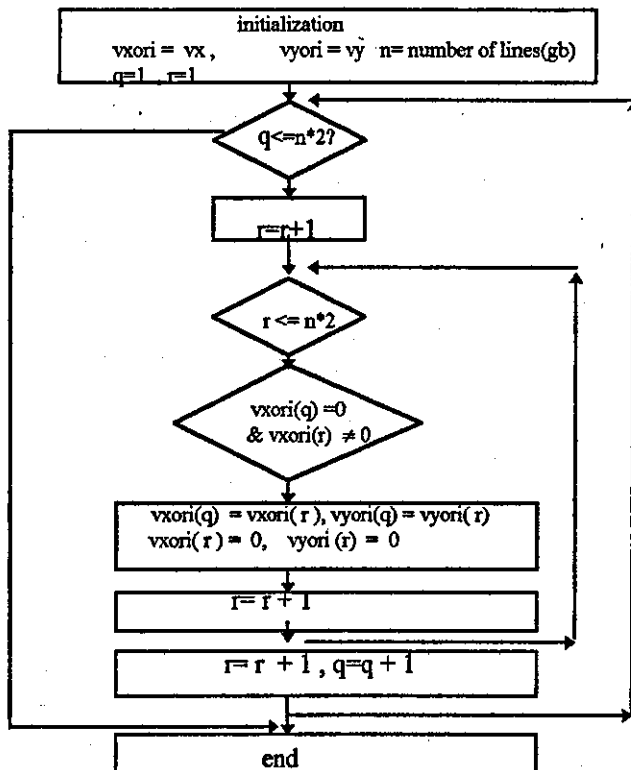This routine is for assigning a zero for redundancy vertices from the original array.

Fig 4.12(b) This routine is for eliminating the zeros. The final values of vxori and vyori are the
co-ordinates of the nodes. To label the nodes and the grain boundaries , text and int2str
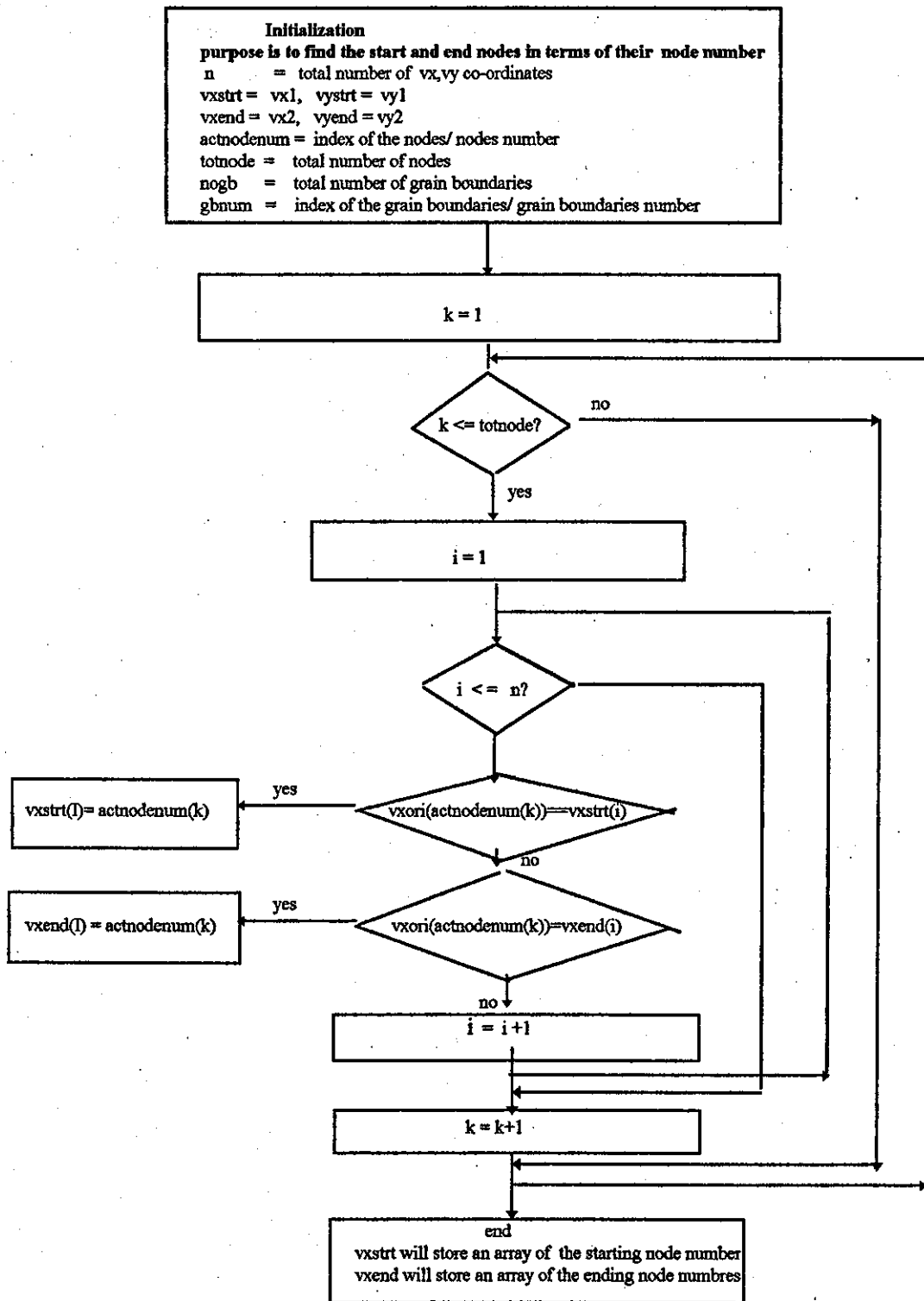commands are used.

Initialization
purpose is to find the start and end nodes in terms of their node number
n   = total number of vx,vy co-ordinates
vxstrt = vx1,   vystrt = vy1
vxend = vx2,   vyend = vy2
actnodenum = index of the nodes/ nodes number
totnode   =   total number of nodes
nogb   =   total number of grain boundaries
gbnum   =   index of the grain boundaries/ grain boundaries number

k = 1

k <= totnode?   no

yes

i = 1

i <= n?

yes   vxstrt(I)= actnodenum(k)   vxori(actnodenum(k))==vxstrt(i)

no

yes   vxend(I) = actnodenum(k)   vxori(actnodenum(k))=vxend(i)

no

i = i+1

k = k+1

end
vxstrt will store an array of the starting node number
vxend will store an array of the ending node numbres

Fig 4.13(a)   The flow chart for the creation of the connectivity matrix in conmtrix.m file. This is the first part of the program where the vx strt and vxend coordinates and hence the vy co-ordinates are converted into their respective starting and ending node numbers.

initialization
purpose to build the matrix which store information on i)connectivity ii)grain boundary number
iii) length of the grain boundaries iv) angle of the grain boundaries
nomember = total number of the starting nodes(vxstrt) which is equal
        to the number of connectivity path
connect   = 1 (if there is a connection between two nodes, assign a 1)
noconnect = 0 (if there is no connection between two nodes, assign a 0)

i = 1 (the rows of matrix)

i <= totnode   no

yes

j = 1 (the columns of matrix)

no   j <= totnode

yes

l = 1 (the index number for the connectivity path

l <= nomember   no

yes

i=j ?

yes

NODMAT (i,j)=noconnect
GBMAT(i,j)   =noconnect
LGTHMAT(i,j) =noconnect
ANGLEMAT(i,j)=noconnect

no

vxstrt(l) = i & vxend(l)=j

yes

NODMAT(i,j)= connect
GBMAT(i,j)   = gnnum(l)
LGTHMAT(i,j)= Lxy(l)
ANGLEMAT(i,j)= Thetadeg(l)

no

vxend(l)= i, & vxstrt(j)=j

yes

NODMAT(i,j)= connect
GBMAT (i,j) = gbnum(l)
LGTHMAT(i,j) = Lxy(l)
ANGLEMAT(i,j)= Thetadeg(l)

no

l = l+1

j = j+1

i = i + 1

end

Fig 4.13(b)   The second part of the program in which the matrices are built by comparing the contents
of the vxstrt and vxend with the contents of NODMAT(i,j). If equal , then connectivity
exist and a 1 is assigned to the matrix of NODMAT(i,j) and if not, a 0 is assigned.

Initialization
dt = 0.0001 the growing rate
i = 1

i <= totnode

yes

Store variables with data
a = find all nodes connected to node(i) using the NODMAT
z = the total number of nodes connected to node(i)

z <= 1 only 1 node connected

no

yes

$$D(i) = \frac{\sqrt{(vxori(i) - vxori(a(z)))^2 + (vyori(i) - vyori(a(z)))^2}}{6}$$

New co-ordinates of vx=vxnew(i)=vxori(i) + $\left(\left(-\frac{1}{D(i)}\right)dt\left(\frac{(vxori(i) - vxori(a(1)))}{\sqrt{(vxori(i) - vxori(a(1)))^2 + (vyori(i) - vyori(a(1)))^2}}\right)\right)$

A similar equation holds for new co-ordinates of vy by changing vxnew with vynew and vxori with vyori

z <=2 2 nodes connected

no

yes

$$D(i) = \frac{\sqrt{(vxori(i) - vxori(a(1)))^2 + (vyori(i) - vyori(a(1)))^2} + \sqrt{(vxori(i) - vxori(a(2)))^2 + (vyori(i) - vyori(a(2)))^2}}{6}$$

New co-ordinates for vx = vxnew(i)=vxori(i) +

$\left(\left(-\frac{1}{D(i)}\right)dt\left(\frac{(vxori(i) - vxori(a(1)))}{\sqrt{(vxori(i) - vxori(a(1)))^2 + (vyori(i) - vyori(a(1)))^2}}\right) + \left(\frac{(vxori(i) - vxori(a(2)))}{\sqrt{(vxori(i) - vxori(a(2)))^2 + vxori(i) - vxori(a(2)))^2}}\right)\right)$

A similar equation holds for new co-ordinates of vy by changing vxnew with vynew and vxori with vyori

z = 3

yes

$$D(i) = \frac{\sqrt{(vxori(i) - vxori(a(1)))^2 + (vyori(i) - vyori(a(1)))^2} + \sqrt{(vxori(i) - vxori(a(2)))^2 + (vyori(i) - vyori(a(2)))^2}}{6}$$

$$+ \frac{\sqrt{(vxori(i) - vxori(a(3)))^2 + (vyori(i) - vyori(a(3)))^2}}{6}$$

continue

140

New co-ordinates of vx =vxnew(i)=vxori(i) +

$$\left[\left(-\frac{1}{D(i)}\right)dt\left(\frac{(vxori(i)-vxori(a(1)))}{\sqrt{(vxori(i)-vxori(a(1)))^2+(vyori(i)-vyori(a(1)))^2}}\right)+\left(\frac{(vxori(i)-vxori(a92)))}{\sqrt{(vxori(i)-vxori(a(2)))^2+vxori(i)-vxori(a(2)))^2}}\right)\right]$$

$$+\left(\frac{(vxori(i)-vxori(a(3)))}{\sqrt{(vxori(i)-vxori(a(3)))^2+(vyori(i)-vyori(a(3)))^2}}\right)$$

equation is same for new co-ordinates of vy by changing vxnew with vynew and vxori with vyori

i = i +1

end

**Fig 4.14   The program flow chart for grain growth in the m-file
grwth1.m**
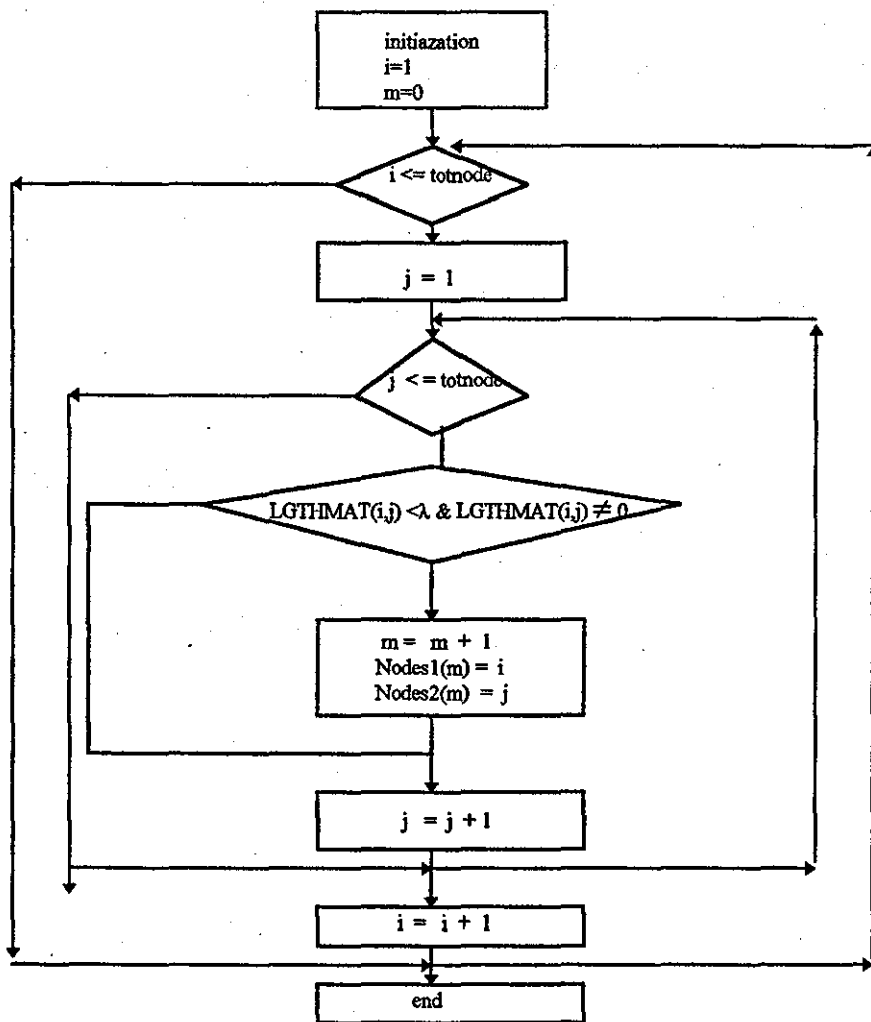
Fig 4.15(a) The flow chart of m-file lamda1.m. This first part of the program will list all nodes having the grain boundaries length less than the critical vertex size Δ

Fig4.15(b) Program flow chart of second part lamda1.m

The purpose of **trisw1.m** is to identify the nodes of the voronoi network which make up triangles and potentially swith. Once identified , the program will simulate the annihilation and recombination processes.

```
┌─────────────────────────────────────────┐
│              lamda1.m                    │
│ m-file for pre identification of the triangle and switch nodes │
└─────────────────────────────────────────┘
```

Left branch:

count the number of possible nodes that make up triangles and store in variable No_postrinodes

redundant nodes in the list are removed giving the actual nodes that can make up triangles and store in variable TRINODES1

find the other nodes that are attached to the existing nodes of TRINODES1 by making use of the connectivity matrix NODMAT and store in variable NEXTRI.

the nodes in NEXTRI are checked again for any additional nodes by making use of the connectivity matrix NODMAT and store in variable ADDTRINODES

the redundant nodes in ADDTRINODES are removed and new list of nodes is stored in variable TRIAN

the nodes in TRIAN are tested for being part of a triangle and the final list is stored in variable TRIANGLE

the nodes of the TRIANGLE are labelled
node1 = TRINODE1
node2= TRINODE2
node3=TRINODE3

count the number of triangles found in the voronoi diagram and store in variable No_TRIANGLE

calculate the centre of the triangle and store the new coordinates of the centre node in variable vxnew and vynew.

find the neighbours for each of the node of the triangle and select the nodes which are not part of the triangle. and store in variable selnb1, selnb2, selnb3

make a connection from the centre to the selnb1,selnb2 and selnb3 by using the connectivity matrix NODMAT

Right branch:

count the number of possible nodes that will switch and store in variable No_posswnodes

redundant nodes in the list are removed giving the actual nodes that will switch and store in variable SWINODES1

compare the list of nodes in SWINODES1 and that of TRINODES1, if same, remove the node from the list of SWINODES1.

assign a label for the nodes of SWINODES and store in variable **swnodei and swnodej**. Make swnodei always have a higher values of vy and store in new variable as **swnodi and swnodj**

remove a node if that node makes another switch to another node, so as not to simulate 2 grain boundaries at the same time.

find the neighbours of each nodes of swnodi and swnodj and store in variable NEI and NEJ respectively. Create a rotational matrix ROTMAT, which will rotate the nodes 90 ^{0} clockwise

modify the existing connectivity matrix NODMAT by selecting the nodes which to be connected to the new position . The selected nodes are stored in variable selnei, selnej

the new coordinates of swnodi and swnodj are calculated and are stored in variable vxnew and vynew. The process involves:-
1. calculating the centre point between swnodi and swodj and store in variable vxo and vyo
2. calculating the new points after making the 90 ^{0} rotation and store in variable NEWPT1 and NEWPT2 = the original vx, vy coordinates of swnodi and swnodj minus vxo and vyo respectively are multiplied by ROTMAT
3. the new coordinates are calculated by:-
vxnew(swnodi)= NEWPT1 (1:)+ vxo
vynew(swnodi)= NEWPT1 (2,:)+ vyo
vxnew(swnodj)= NEWPT2 (1,:) + vxo
vynew(swnodj)= NEWPT2(2, :) + vyo

Fig 4. 16 The program flow chart of trisw1.m

4.7.3 The simulation for creating samples of interconnects

Simulation is performed by the program code **slice2.m** where the Voronoi network is sliced into equal samples of interconnects. As the result of this slice, new points or nodes have to be recalculated and also the geometrical information such as the lengths and angles of orientation of the grain boundaries has to be updated. The interconnect samples will consist of a random distributed of grain boundary clusters each of which will have its own characteristics such as:

    i) The number of grain boundaries making up the cluster

    ii) The length of each grain boundaries in the cluster

    iii) the length of the cluster (the spanning of the grain boundaries in the x direction i.e. in the direction of the moving vacancies)

    iv) The angle of orientation of each of the grain boundaries.

The algorithm for developing the program codes is:-

    i) trim the Voronoi diagram into film samples by using the axis function

    ii) slice of film into the interconnect samples by using the axis function

    iii) identify grain boundaries inside the sliced off area

    iv) calculate the new co-ordinates of the nodes inside the sliced area

A program flow chart for the production of interconnect is as shown in Fig. 4.19.The critical stage of the simulation is in the calculation of the new co-ordinates for the nodes inside the sliced area i.e. the interconnect sample. The calculation is based on the equation of straight line y =mx+c

    where

$$\text{gradient } m = \frac{y2 - y1}{x2 - x1} \qquad\qquad 4.30$$

$$\text{intercept } c = \frac{(y2.x1) - (y1.x2)}{x1 - x2} \qquad\qquad 4.31$$

Example: to calculate new co-ordinates for node 1

144
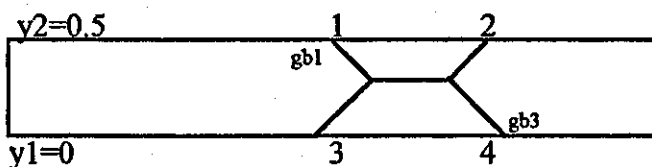
Node 1= x co-ordinate = $\dfrac{(y2 - c(gb1))}{m(gb1)}$, and y co-ordinate = y2

Node 4= x co-ordinate= $\left(\dfrac{y1 - c(gb3)}{m(gb3)}\right)$, and y co-ordinate = 0

i) production of Al film

First trim the Voronoi network to produce the sample film(1 x 1)
x1c1= 0 (the start point of slicing x axis of the original Voronoi diagram)
x2c1=1 (the end point of slicing axis of the original; Voronoi diagram)
y1c1= 0 (the start point of slicing y axis of the original Voronoi diagram)
y2c1=1 (the end point of slicing y axis of the original Voronoi diagram)
                    To execute the slicing process = axis([x1c1 x2c1 y1c1 y2c1])

ii) production of interconnect sample

Second slice the Voronoi network to produce the interconnect sample film(((y2c2-y1c2) x 1)
x1c2= 0 (the start point of slicing x axis of the original Voronoi diagram)
x2c2=1 (the end point of slicing axis of the original; Voronoi diagram)
y1c2= user input
y2c2= user input
to execute the slicing process = axis[(x1c2 x2c2 y1c2 y2c2])

initialise
vxstrt = vx1
vxend = vx2
vystrt = vy1
vyend = vy2
k = 1 (counter)

k <= nogb

yes

Compare start and end value of grain boundary co-ordinates
with the respective co-ordinates of the slice(box), at least
one co-ordinates must lie within the sliced box
(6 conditions)

iii   yes

produce the grain boundaries number

k = k +1

end

FIG 4.19(a) The flow chart for the production of films and the interconnect samples.
The first part of the program **slice2.m** produces the film and the
interconnect samples and identifies the grain boundaries that are inside
the sliced area.

145

```
┌─────────────────────────────────────────────────────┐
│                  Initialisation                      │
│                                                      │
│  gbinbox= all the grain boundaries in the slice area or box │
│  nogbinbox = the total number of grain boundaries found in the box │
└─────────────────────────────────────────────────────┘
                         │
                    ┌─────────┐
                    │  l = 1  │
                    └─────────┘
                         │
                    ╱─────────────╲
                   ╱  l <= nogbinbox ╲
                   ╲                 ╱
                    ╲───────────────╱
                         │
┌──────────────────────────────────────────────────────────┐
│  assign new variables to the co-ordinates of the grain boundaries │
│        x1(gbinbox(l))= vxstrt(gbinbox(l))                 │
│        x2(gbinbox(l))=vxend(gbinbox(l))                   │
│        y1(gbinbox(l))=vystrt(gbinbox(l))                  │
│        y2(gbinbox(l))= vystrt(gbinbox(l))                 │
└──────────────────────────────────────────────────────────┘
                         │
                    ┌─────────┐
                    │ l = l+1 │
                    └─────────┘
                         │
                    ┌─────────┐
                    │   end   │
                    └─────────┘
```
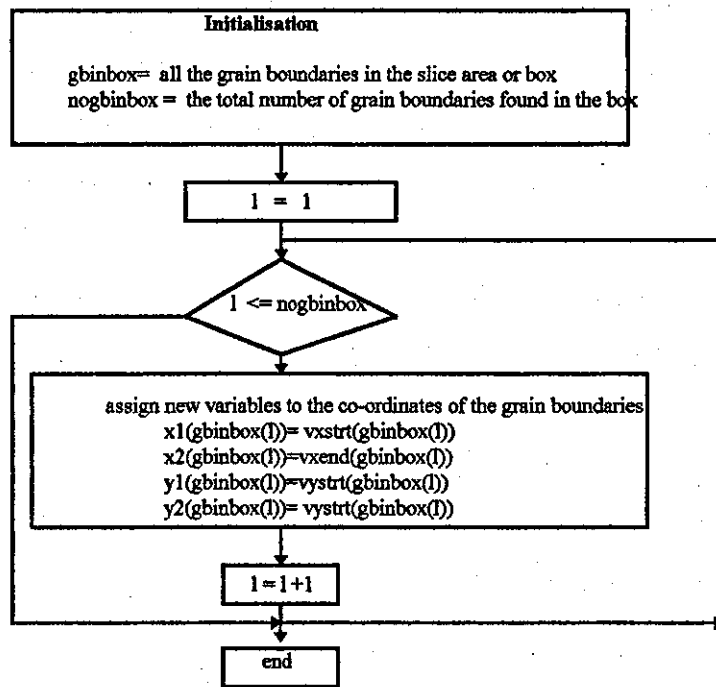
Fig4.19(b) The program flow chart from a part of **slice2.m** assigns new variables for the co-ordinates of the grain boundaries

```
                    ┌─────────┐
                    │  j = 1  │
                    └─────────┘
                         │
        no          ╱─────────────╲
                   ╱  j <= nogbinbox ╲
                   ╲                 ╱
                    ╲───────────────╱
                         │ yes
┌──────────────────────────────────────────────────────────┐
│  calculate the gradient m and the y intercept c of each grain │
│  boundaries in the box using the straight line equation of y=mx +c │
│                                                          │
│  gradient m  =  y2-y1   , c  =  (y2.x1) - (y1.x2)       │
│                 x2-x1              x1-x2                   │
└──────────────────────────────────────────────────────────┘
                         │
                    ┌─────────┐
                    │ j = j+1 │
                    └─────────┘
                         │
                    ┌─────────┐
                    │   end   │
                    └─────────┘
```
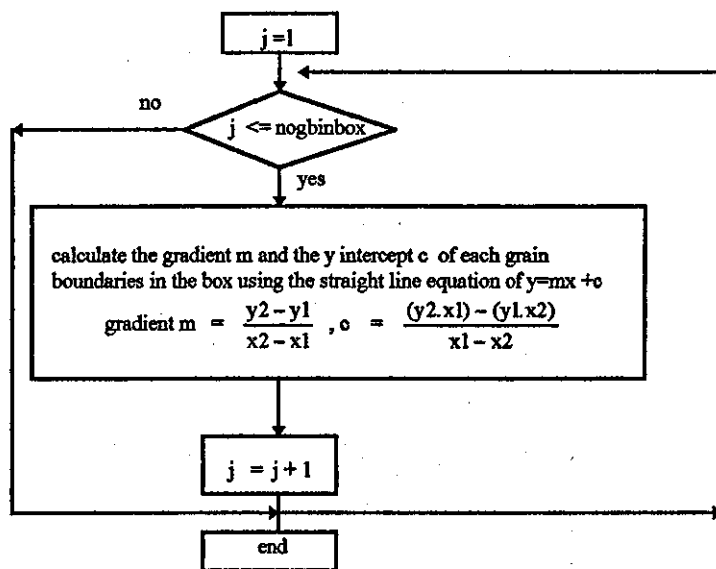
Fig 4.19(c) The program flow chart from a part of **slice2.m** which calculates the gradient and the intercept c for each of the grain boundaries in the sliced area

146
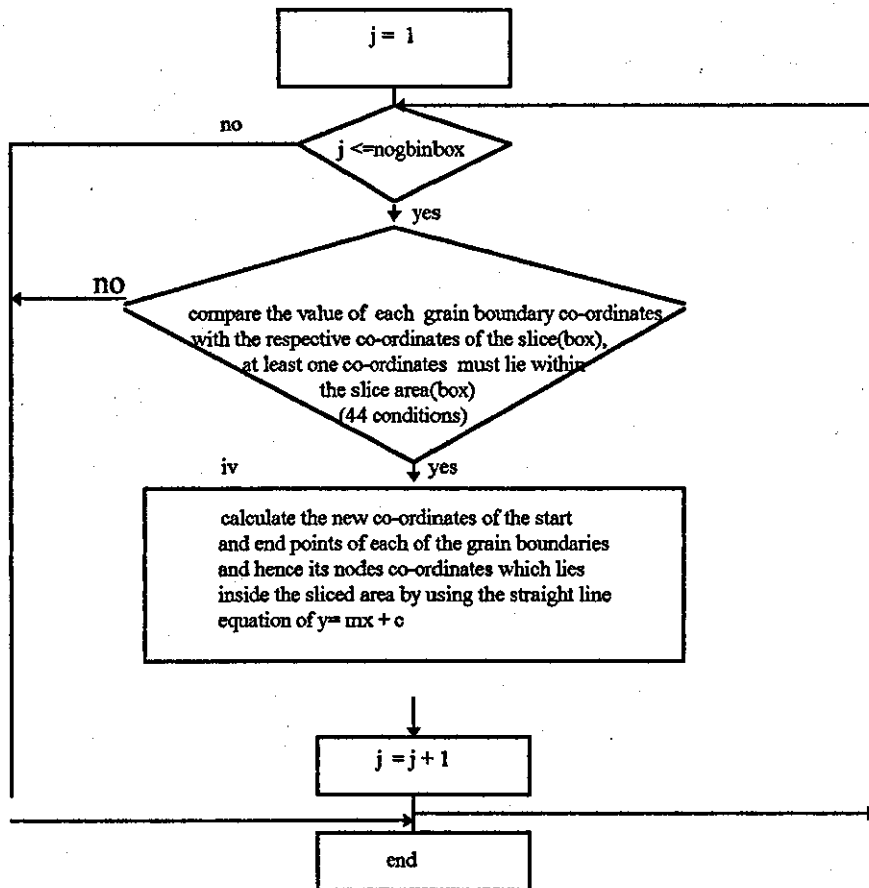
Fig 4.19(d)   The program flow chart from a part of **slice2.m** calculates
the new co-ordinates of the start and end of the grain
boundaries and hence the co-ordinates of the new nodes
in the sliced area or box

After the simulation of the production of interconnect samples, the new nodes in the
sliced area will undergo the several process i) calculation of the new geometrical
properties ii) labelling of the new nodes and iii) and creating the new connectivity
matrix.

4.7.4   Simulation of the Time to Failure

The interconnect samples are now ready for experiment in which the Time to Failure
are now calculated. The program code that simulate this is **vrttf.m** and the program
flow chart is shown in Fig 4.20

The purpose of the program is to calculate the Time to Failure of the interconnect samples.
The calculation is based on the lumped model equation and the signal or Elmore delay estimation.

```
┌─────────────────────────────────────────────────────┐
│             Assignment of variables                  │
│                                                       │
│   LG= length of grain boundaries after slicing process│
│   AG= angle of orientation of grain boundaries after  │
│        slicing process                                │
└─────────────────────────────────────────────────────┘
```

```
┌─────────────────────────────────────────────────────┐
│              common input parameters                  │
│   co= 1     the vacancy concentration ( stress σ = 0) │
│   cr = 2    the critical vacancy concentration        │
│   alpha=5   the electromigration force                │
│   Diff = 5  the effective vacancy diffusion           │
│                   user input                          │
│   GB =    total number of grain boundaries in a cluster│
│   LGB=    number of grain boundaries forming the longest path│
│   s   =   number of sections of  CR circuit per grain boundaries│
└─────────────────────────────────────────────────────┘
```

```
                  ◇ q = 1: GB ◇
```

```
┌─────────────────────────────────────────────────────┐
│   user input                                          │
│   x(q) = the length of each grain boundaries          │
│                                                       │
│   ang(q)= random generator  between 0 ⁰  and  120 ⁰   │
└─────────────────────────────────────────────────────┘
```

$$0 < ang(q) < 36^{0}$$

Diffusion coefficient
$$d(q)= Diff \times sin\left(\frac{ang(q)}{2}\right)$$

$$36^{0} < ang(q) < 120^{0}$$

$$d(q)= Diff \times sin\left(18^{0}\right)$$

```
┌─────────────────────────────────────────────────────┐
│                   user input                          │
│   theta(q)  = angle of orientation of each grain boundaries│
│   alphaeff(q)  = alpha  x  theta(q)                   │
└─────────────────────────────────────────────────────┘
```

```
┌─────────────────────────────────────────────────────┐
│                    vrmat4.m                           │
│          m-file to produce the resistor or G matrix   │
└─────────────────────────────────────────────────────┘
```

```
┌─────────────────────────────────────────────────────┐
│                    vcmat3.m                           │
│          m-file to produce the capacitor or C matrix  │
└─────────────────────────────────────────────────────┘
```

```
┌─────────────────────────────────────────────────────┐
│                    vcrgmat.m                          │
│       m-file to produce the initial charge or VIN matrix│
└─────────────────────────────────────────────────────┘
```

```
┌─────────────────────────────────────────────────────┐
│                    vumat3.m                           │
│          m-file to produce the U matrix               │
└─────────────────────────────────────────────────────┘
```

continue

148

continue

$\downarrow$

The simulation of the voltage response is done by the following process:-
i)   assignment of the duration of time $= t$

ii) diagonalising the matrix of $Q=C^{-1}G$.

iii) solving the voltage response by the equation :-

$$V = S^{-1}\left(S.VIN.exp^{Dt}\right) + S^{-1}\left(D^{-1}S.U.exp^{Dt}\right) - S^{-1}D^{-1}S.U$$

the conversion of the voltage response to vacancy concentration response is solve by the equation :-

$$C_v = V \times exp^{alphaeff.x} \quad , C_v \text{ is the vacancy concentration}$$

the time to failure is determine by interpolating between the data points of the vacancy concentration C_v and the time t. The command of Matlab to do the this is :-
TTF = interp1(C_v , t, critical vacancy concentration)

to calculate the Time to failure by signal or Elmore delay method

elmore3.m
create the resistor matrix RG

compute the signal or Elmore delay using the equation below:-
ED= Signal or Elmore delay, RG=resistor matrix, C=capacitor matrix
VIN= pseudo or initial voltage matrix,
  x= the length of the point along the grain boundary which is to be monitored
  Vcr= the critical voltage, TTFELMORE= Time to failure of signal delay

$$ED = \frac{RG.C^{-1}.\left(1 - \frac{VIN}{c_0}\right)}{1 - e^{(-alphaeff.x)}} \quad , \quad V_{cr} = cr.e^{(-alphaeff.x)}$$

$$TTFELMORE = \quad ED.LN\left(\frac{\left(1 - e^{(-alphaeff.x)}\right)}{1 - \frac{V_{cr}}{c_0}}\right)$$

end

FIG 4.20 The program flow chart of **vrttf.m** for the estimation of the Time to Failure of the grain boundary clusters/interconnect by using the lumped element model and the signal delay method.

The simulation of the Time to failure of the interconnect samples is done one sample at a time by inputting the information required below:-

i) Number of samples needed for the experiment

ii) Number of clusters present in the sample (by inspection)

iii) The length of the cluster(by inputting the start and end node of the cluster will automatically calculate the length)

iv) The number of grain boundaries found in the cluster(by inspection)

v) The number of grain boundaries forming the longest path (by inspection)

vi) The length of the grain boundary (by inputting the grain boundary number will generate the length of each grain boundaries in the cluster)

vii) The angle of orientation of the grain boundary (by inputting the grain boundary number will generate the angle of orientation)

viii) The number of section of component per grain boundaries

Once this information is fed into the system, the Time to Failure is calculated automatically using the lumped element model and the signal delay. Basically the process involved in the calculation of the Time to Failure is identical to that for the single and complex grain boundaries as mentioned earlier. The simulation of the Time to Failure using the Lumped element model is done by computing the matrix eqn(4.10) where the voltage response of a particular node is obtained through eqn(4.17) and the equivalent vacancy concentration response through eqn(4.18). Similarly, the Time to Failure for signal or Elmore delay method is by solving eqn(4.20) and eqn(4.21). The matrices that are required in the simulation of the Time to Failure of realistic interconnects by both methods are as follows:-

i) the conductance matrix G (created by function file **vrmat4.m**)

ii) the capacitance matrix C (**vcmat3.m,**)

iii) the initial charge matrix VIN (**vcrgmat3.m**)

iv) the U matrix (**vumat3.m**)

v) the signal delay or elmore resistance matrix RG - (**elmore3.m**)

4.7.5 Calculation of the lumped element components

The calculation for the lumped element components i.e. the resistances and capacitances and the initial voltages for complex grain boundaries is identical to that of the single grain boundaries case, the only difference is to take account the extra grains boundaries that makes the complete network. The algorithm of calculating the components are as follows:-

a) **calculation of resistors values**

   i) **The first resistor values for each grain boundary in the cluster**

$$r1(z) = \frac{\left(1 - e^{(-alphaeff(z))}.L(z)\right)}{alphaeff(z).d(z)}$$

   where z = counter for the number of grain boundaries in the cluster

   L = x/s , x = length of each grain boundaries, s = number of sections per grain boundary

   ii) **All the resistors values for each grain boundaries that make up the longest path (from the start node to the end node of the cluster)**

   example:_

   first grain boundary $= r(i) = e^{(-k.alphaeff(1).L(1))}.r1(1)$

   2nd grain boundary $= r(i) = e^{((-alphaeff(1).x(1))-(y.alphaeff(2).L(2)))}.r1(2)$

   3rd grain boundary $= r(i) = e^{((-alphaeff(1).x(1))-(alphaeff(2).x(2))-(p.alphaeff(3).L(3)))}.r1(3)$

   where k,y and p is a counter.

   iii) **All the resistor values for the wing grain boundaries**

   example :-

   first wing grain boundary $= r(i) = e^{(-w.alphaeff(LGB+1).L(LGB+1))}.r1(LGB+1)$

   where k,y,p,w = counter , LGB = number of grain boundaries in the longest path

b) Calculation of capacitors values

i) The first two capacitors value for each grain boundaries in the cluster

$$c1(z) = \frac{\left(e^{(-alphaeff(z).L(1))+alphaeff(z).L(z)-1}\right)}{\left(alphaeff(z).(1-e^{(-alphaeff(z).L(z))}\right)} \quad ,$$

$$c2(z) = \frac{\left(e^{(alphaeff(z).L(1))-alphaeff(z).L(z)-1}\right)}{\left(alphaeff(z).(1-e^{(-alphaeff(z).L(z))}\right)}$$

where z = counter for the number of grain boundaries in the cluster,

$L = x/s$, x = length of each grain boundaries, s = number of sections per grain boundary

ii) All the capacitors values for each grain boundaries that make up the longest path

first grain boundary $=$
$$c(i) = e^{(k.alphaeff(1).L(1))}.c1(1)$$
$$c(i+1) = e^{(k.alphaeff(1).L(1))}.c2(1)$$

2nd grain boundary $=$
$$c(i) = e^{(alphaeff(1).x(1)+(y.alphaeff(2).L(2))}.c1(2)$$
$$c(i+1) = e^{(alphaeff(1).x(1))+(y.alphaeff(2).L(2))}.c2(2)$$

3rd grain boundary $=$
$$c(i) = e^{(alphaeff(1).x(1)+(alphaeff(2).x(2)+(p.alphaeff(3).L(3)))}.c1(3)$$
$$c(i+1) = e^{(alphaeff(1).x(1))+(alphaeff(2).x(2)+(alphaeff(3).L(3))}.c2(3)$$

where k, y and p is a counter

iii) All the capacitors values for the wing grain boundaries

first wing grain boundary $=$
$$c(i) = e^{(w.alphaeff(LGB+1).L(LGB+1))}.c1(LGB+1)$$
$$c(i+1) = e^{(w.alphaeff(LGB+1).L(LGB+1))}.c2(LGB+1)$$

For the capacitance, after calculating all the values, it must be recalculated to take account the parallel connections throughout the network in the cluster.

4.7.6   The signal or Elmore delay resistance matrix (RG)

*The resistance matrix RG (R as used in section 3.9 of Chapter 3) for the signal delay is different from the G matrix of the Lumped Element model. The matrix depends on the   point where the output is going to be monitored. The resistance will be the sum of all the resistance of the unique path between the input and the output that is common with the unique path. To illustrate this , an example is given below
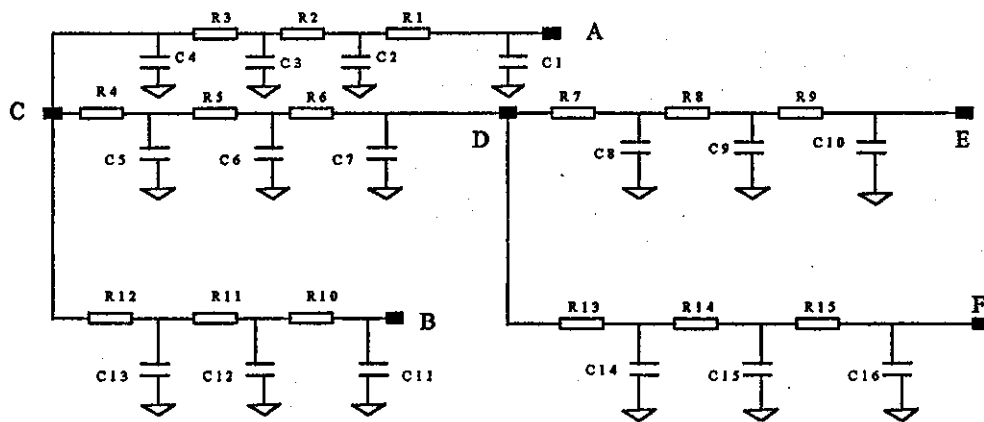
Fig 4.21   C -R network

With reference to Fig 4.21, a cluster made up of 5 grain boundaries which is modelled by a 3 section , lumped element component per grain boundary. The desired output is monitored at point E, hence the resistance of RG matrix is made up of :-

RG(1,1)=R(1)

RG(1,2)=R(1)+R(2).

$\vdots$

RG(1,9)= R(1)+R(2)+........R(9)

RG(1,10)=R(1)+R(2)+R(3)

$\vdots$

RG(1,12)=R(1)+R(2)+R(3)

RG(1,13)=R(1)+R(2)+R(3)+R(4)+R(5)+R(6)

$\vdots$

RG(1,15)=R(1)+R(2)+R(3)+R(4)+R(5)+R(6)

The program chart for creating RG matrix is shown in Fig 4.22

* For tree networks the G matrix may be inverted exactly to RG matrix

The purpose of elomore3.m is to create the RG matrix for calculating the Time to failure by signal or Elmore delay approximation method. The RG matrix created is for calculating signal delay at the end point of the cluster of grain boundary.
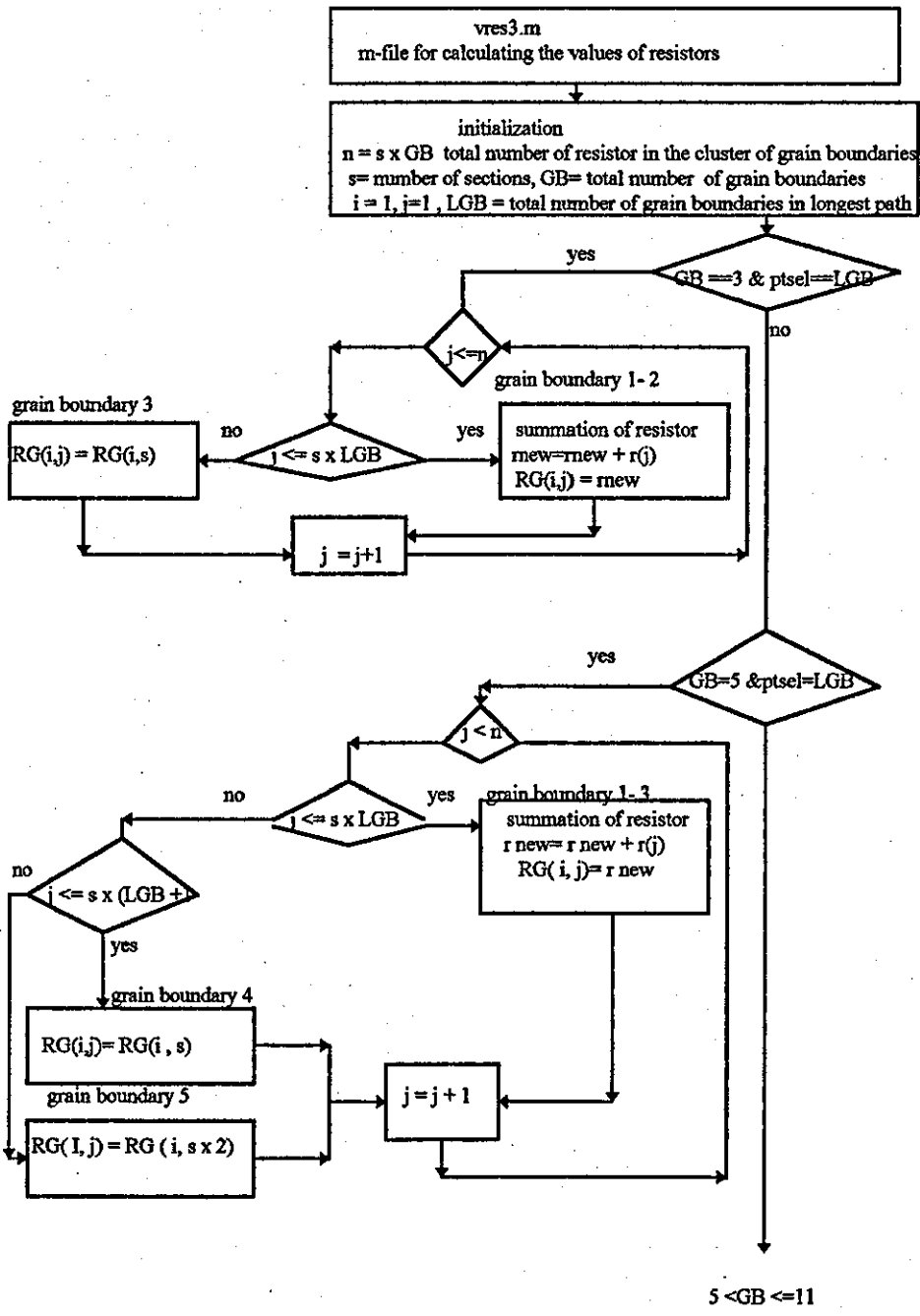
Fig 4.22 The program flow chart of a part of elmore3.m for creating the RG matrix . The flow chart shown is for 5 grain boundary cluster. The program can cater for a maximum of 11 grain boundaries.

4.8 The program codes developed for the simulation of realistic interconnect samples

No	Program title	Associate m-files	sub-m-files	Description
1	vrnoittf2.m			main program to simulate the TTF of realistic interconnect samples by the lumped element model and signal delay approximation.
		1. annealing.m	1. geometry..m	calculating and storing information on geometrical properties of grain boundaries.
			2. labgrain1.m	labelling of nodes and grain boundaries
			3. geometry.m	calculating and storing new information on geometrical properties after each time step of annealing process.
			4. labgrain2.m	labelling of new nodes and grain boundaries after each time step of annealing process
			5. conmtrix.m	connectivity matrix of the new nodes and new information after each time step of annealing process
			6.lamda1.m	to detect the grain boundaries having length less than the critical value for annihilation or recombination process.
			7.trisw1.m	simulation of the annihilation or recombination process growth of grain
			8. output.m	plotting new voronoi network after each time step of annealing process.

		2.figvrnoi.m		to produce a hard copy of the interconnect sample
		3.geometry.m		calculating and storing information on geometrical properties of grain boundaries.
		4. lablenode.m		labelling of nodes and grain boundaries
		5.slice2.m		simulation of production of the interconnect samples
		6.newgeometry.m		calculating and storing information on new geometrical properties of grain boundary after slicing process.
		7. newnode.m		labelling of nodes and grain boundaries
		8.vrttf.m		simulation of the calculation of the Time to Failure of the interconnect samples
			1. vrmat4 2. vres3.m	creating the resistance matrix G. The resistance are obtain from vres3.m
			3. vcmat3 4. vnoicap3.m	creating the capacitance matrix C. The capacitance are obtain from vnoicap3.m
			5. vcrgmat3.m 6. vcrg3.m	creating the initial voltages matrix VIN. The initial voltages are obtain from vcrg3.m
			7. vumat3.m	creating the U matrix
			8. elmore2.m	creating the signal delay resistance matrix RG

Table 4.5 The program codes for simulation of realistic interconnect.

CHAPTER 5

RESULTS AND DISCUSSION

5.0   Introduction

In this chapter, the results of all the simulation will be presented and discussed. The simulation results are divided into three main parts consisting of :-

1. Simulation results for a single grain boundary.
2. Simulation results for a ' self generated' complex grain boundary interconnect
3. Simulation results for a 'computer generated' realistic sample of interconnect .

The first simulation is vital to the whole study since the simulation results of the lumped element model first be proven valid before the study can proceed to estimate the statistics of Time to Failure (TTF). The second part of the simulation will apply the model to a complex structure of grain boundaries. Finally the third part will apply the model to realistic interconnect samples to obtain the actual Time to Failure and its statistics. The lumped element model developed will be verified if the simulation results are comparable to the results obtained by i) exact theoretical solution from the literature and ii) by the signal or Elmore delay approximation of the TTF.

5.1 Simulation results of a single grain boundary

As far as the literature is concerned, analytical solutions only exist in the form of a single one-dimensional grain boundary of length ℓ .[Shatzkes, and Lloyd,1986],[Lloyd,and Kitchin,1994],[Clement, 1992] and [Dwyer et.al,1994]. It was based on two typical boundary conditions which corresponds to a blocking boundary ,where vacancy flux $J(\ell,t)=0$ at the downwind end, and at the upwind end, either case (A); $J(0,t)=0$; or case

157

(B) where stress ,$\sigma(0,t)=0$ or (equivalent to vacancy concentration $(c(0,t)=c_0)$. The current work will investigate both of these boundary conditions

5.1.1 Case (A) -upwind end of conductor are blocked (J(0,t)=0)

In the present work, the reference of [Clement,1992] is used to compare the simulation results of the lumped element model. This boundary conditions corresponds to a situation that vacancies are conserved which could be maintained in a system where a thick passivation would preclude changes in the volume of the conductor. Eqn(2.19) may be solved exactly and the vacancy build-up equation (exact solution) is given below:-

$$\frac{c(x,t)}{c_0} = \frac{\alpha.\ell.\exp(-\alpha.x).}{1-\exp(-\alpha.\ell)} + \sum_{k=1}^{\infty}\left[\frac{16k\pi\alpha^2\ell^2\left[1-(-1)^k\exp\left(\frac{\alpha.\ell}{2}\right)\right]}{\left(\alpha^2\ell^2+4k^x\pi^2\right)^2}\right]x$$

$$\left[\left(\sin\frac{k\pi.x}{\ell}-\frac{2k\pi}{\alpha.\ell}\cos\frac{k\pi.x}{\ell}\right)x\exp\left(-\frac{\alpha.x}{2}-\left(k^2\pi^2+\frac{\alpha^2\ell^2}{4}\right)\frac{Dt}{\ell^2}\right)\right] \quad 5.1$$

where

$\alpha \quad = \quad \dfrac{Z^*e\rho j}{kT} \quad$ = electromigration drift component

$D \quad = \quad$ effective vacancy diffusion coefficient= $D_V^{GB}\dfrac{B\Omega}{kT}.\dfrac{\delta}{d}$

$c(x,t) = $ vacancy concentration at distance x and time t

$c_0 \quad = \quad$ equilibrium vacancy concentration in the absence of stress.

$\ell \quad = \quad$ the length of conductor

In the simulation of both the exact solution by Clement and the lumped element model, the Time to Failure(TTF) for the single grain boundary is assume to be the time taken for the vacancy concentration to reach some critical (threshold) value of (c_{cr}). The approach of the simulation is i) first to obtain the vacancy concentration build-up at a

chosen location of the conductor and ii) to calculate the Time to Failure. For the lumped element model, the steps involve in obtaining the vacancy build-up are i) to obtain the transient response of the voltages ($v(x,t)$) ii) to convert this into a vacancy concentration by the formula $c(x,t)=v(x,t) \cdot \exp(\alpha x)$ as described in Chapter 3. A reasonable value of c_{cr} is $\approx 2\,c_0$,as this corresponds to 500 Mpa which is $\dfrac{1}{2}$ of the yield stress of Al. The model can be seen to be accurate up to $c_{cr} \approx 100$. ($c_{cr} = c_0 e^{\frac{\sigma_{cr}\Omega}{kT}}$)

a) Comparison between lumped element model and exact solution

The vacancy concentration profile is shown in Fig 5.1 consisting of the exact solution and the lumped element model response for 1 section and 5 sections of the C-R-C $\prod$ circuits. In the simulation of the lumped element model, the values of the components and its initial voltages are calculated first as shown in Table 5.1a and 5.1.b. Once it is obtained, the vacancy concentration are computed by solving the relevant equations (eqn(4.17) and 4.18) described in Chapter 4. Note that the total value of the resistance and capacitance are equal for both the single and 5 sections i.e. to total resistance is 0.9502 Ω and total capacitance is 19.08 farad.

Resistors Values	Capacitors Values	Initial Voltages
R1=0.9502	C1=2.1571	1
	C2=16.9284	0.0498

Table 5.1a - Component values for 1 section

Resistors Values	Capacitors Values	Initial Voltages
R1=0.4512	C1=0.3298	1
R2=0.2476	C2=1.0933	0.5488
R3=0.1359	C3=1.9921	0.3012
R4=0.0748	C4=3.6298	0.1653
R5=0.0409	C5=6.6139	0.0907
	C6=5.4269	0.0498

Table 5.1b - Component values for 5 sections
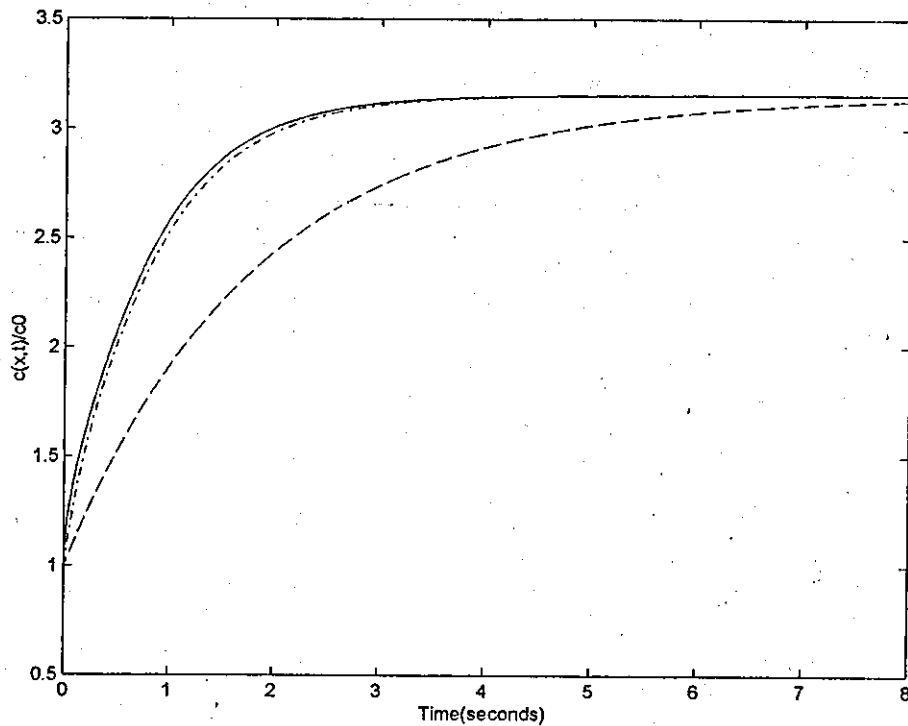
Fig 5.1 The vacancy concentration build-up at x=ℓ=3 for a single grain boundary (case

(A))with parameter α = 1, ℓ=3, D=1. Exact solution(solid line),1 section(dash

line),5 sections (dash dot line) for the lumped element model.

With reference to Fig.5.1 ,the vacancy build-up is monitored at the blocking end of the
conductor line (x=ℓ=3) and represented by three curves i.e. i) the exact solution (solid
black line) ,the lumped element model with 1 section (dotted blue line) and a 5
sections(dashed red line) . As evident from the Fig5.1, a single section does not give a
good approximation. The 5 sections is a much better approximation which correspond to
about 91% accuracy based on the TTF compared to the exact solution. The Time to
Failure obtained are determined by the critical vacancy concentration c_{cr} = $2c_0$, for the
exact solution is 0.4452 seconds while the lumped element model is 0.4895 seconds for a
5 sections C-R-C $\prod$ circuit and 1.1323 seconds for a 1 section C-R-C $\prod$ circuit.

160
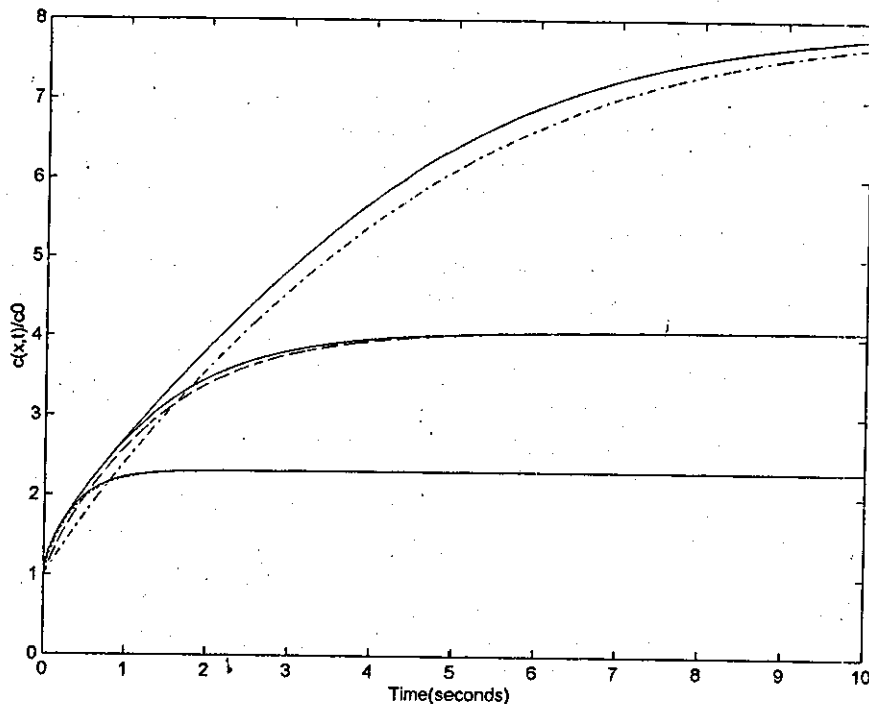
Fig 5.2 The vacancy concentration profile for different values of $\alpha\ell$ monitored at the blocking ends of the conductor. Exact solutions(solid line),lumped element model are represented by i) $\alpha\ell=2$ (dotted line), $\alpha\ell=4$ (dashed line) and $\alpha\ell=8$ (dash dot line)

b) The effect of $\alpha\ell$ on the build-up of vacancy concentration

The build-up in the vacancy concentration at the blocking boundary at $x=\ell$ for different values of $\alpha\ell$ is shown in Fig.5.2. For a finite conductor length ℓ the vacancy concentration build-up will saturate. The level at which this saturation occurs depends on $\alpha\ell$ i.e. the electromigration drift component and length ℓ. The saturation level decreases with decreasing α and length ℓ. This result agrees with that of the reference [Clement,1992],where it observed here that the vacancy concentration profile of the lumped element model fits exactly the vacancy concentration profile of the 'exact solution'. The characteristic of these effect of $\alpha\ell$ on the vacancy concentration is known as the Blech length effect.

161

c) The effect of angle of orientation of grain boundary on Time to Failure

It is well established in the literature that the electromigration Time to Failure is a statistical variable. It depends on the macroscopic design parameters, such as the length and width of the interconnect, and the micostructural features, such as the grain size distribution which is generally taken to have a lognormal distribution, grain orientation angles which possess a roughly uniform distribution(between 0^0-90^0) [Attardo et.al,1971], and the atomic diffusion coefficient for a given grain boundary. A simulation to study the effect of the angle of orientation of the grain boundary to the direction of electric field on the Time to Failure is carried out. This is done by varying α and the angle of orientation θ to give the effective drift component $\alpha_{effective} = \alpha \times \cos(\theta)$, (in this case $\theta=0$ is parallel to the interconnect length). The other parameters are kept unchanged where drift component $\alpha=1$, length $\ell=3$, diffusion coefficient $D=1$, critical vacancy concentration $c_{cr} = 2\,c_0$ and the number of section $s=5$.

no	θ	TTF(exact solution)	TTF(lumped element model)
1	0	0.4452 seconds	0.4895 seconds
2	20^0	0.5063 seconds	0.5525 seconds
3	50^0	1.2722 seconds	1.3486 seconds
4	89^0	do not fail	do not fail

Table 5.2 The Time to failure at different angle of orientation θ

As shown in Table5.2 , the Time to Failure for grain boundary oriented at an angle more than $\theta= 0^0$ records a larger time. Also it is shown in Fig5.3 that the grain boundary oriented at $\approx 90^0$ to the electric field, the vacancy concentration does not reach the critical vacancy concentration c_{cr} and this means that the conductor does not fail. As the angle of orientation gets larger or nearer to 90^0 the time to failure will also increases until there will be no vacancy flows along the boundary. At this angle it is completely

ineffective in diffusing/transporting the vacancies along the grain boundaries. There will be vacancy flow through the grains which will eventually lead to failure Note here that changes in D only affect the time to reach the saturation value of $c_0 e^{\alpha \ell}$ and not whether failure occurs. This results is in agreement with the literature[Attardo, et.al,1971] in which the TTF is dependent on the microstructure of the grain boundary i.e. in this case the angle of orientation of the grain boundary with respect to the electric field.
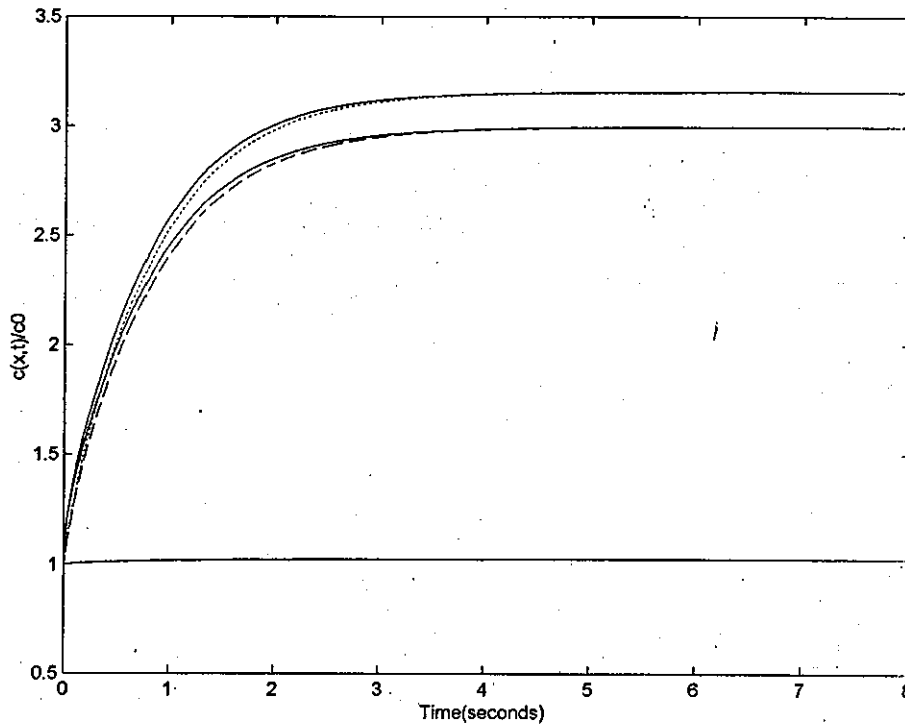
Fig 5.3 The vacancy concentration profile for a single grain boundary with both ends
blocked and with different angles of orientation with respect to the direction of
electric field. The exact solutions (solid line), lumped element model
are represented by i) $\theta=0^0$ (dotted line), $\theta=20^0$ (dashed line) and $\theta=89^0$ (dash
dot line(can't be seen since it overlap the exact solution))

5.1.2 Case (B) At upwind end of stress relief($\sigma(0,t) = 0$ or c(0,t)=c_0)

In this set of boundary conditions, vacancies are collecting at x=ℓ to form a void, thus making it a blocking boundary and at the other end of the conductor, vacancies are supplied, from for example a contact pad, in such a way as to maintain a stress free contact $\sigma = 0$ or equivalent a constant vacancy concentration c_0 at x=0. In the present work, the reference of [Dwyer et.al,1994] is used to compare with the simulation results of the lumped element model.   The simpler version (approximate) of vacancy concentration build-up equation is shown below.

for $\alpha\ell \leq 2$

$$\frac{c(x,t)}{c_0} \approx \exp(\alpha.x) - \frac{2\alpha.l \exp\left[-\frac{\alpha(l-x)}{2}\right].\xi \sin\left(\xi\frac{x}{l}\right).\exp-\left(\frac{\alpha^2 l^2}{4}+\xi^2\right).\frac{Dt}{l^2}}{\sqrt{\frac{\alpha^2 l^2}{4}+\xi^2.\left(\xi^2 -\frac{\alpha.l}{4}(2-\alpha.l)\right)}} \qquad 5.2$$

and for the case $\alpha\ell \geq 2$

$$\frac{c(x,t)}{c_0} \approx \exp(\alpha.x) - \frac{2\alpha.l \exp\left[-\frac{\alpha(l-x)}{2}\right].\eta \sinh\left(\eta\frac{x}{l}\right).\exp-\left(\frac{\alpha^2 l^2}{4}-\eta^2\right).\frac{Dt}{l^2}}{\sqrt{\frac{\alpha^2 l^2}{4}-\eta^2.\left(\eta^2 -\frac{\alpha.l}{4}(2-\alpha.l)\right)}} \qquad 5.3$$

where

$\alpha \quad = \quad \dfrac{Z^*e\rho j}{kT} \quad$ = electromigration drift component

$D \quad = \quad$ effective vacancy diffusion coefficient $=D_V^{GB}\dfrac{B\Omega}{kT}\cdot\dfrac{\delta}{d}$

$c(x,t) =$ vacancy concentration at distance x and time t

$c_0 \quad =$ equilibrium vacancy concentration in the absence of stress.

$\ell \quad =$ length of the conductor/strip

$\xi \quad =$ the imaginary roots

$\eta \quad =$ the real roots

a) Comparison between lumped element model and exact solution

The vacancy concentration profile is shown in Fig 5.5 consisting of the exact solution and the lumped element model response. Two sets of conditions, as in the literature, are considered i.e. $\alpha\ell > 2$ and $\alpha\ell < 2$ are simulated.

i) simulation results for $\alpha\ell > 2$

In the simulation of the lumped element model, the values of the components and the initial voltages are calculated and are shown in Table 5.3a and 5.3.b. As in the previous section, the vacancy concentration is obtained by computing the appropriate equations (eqn(4.17 and 4.18)). For this simulation, two sets of $\alpha\ell$ values are chosen as an example, i.e. $\alpha\ell$=4 **and** $\alpha\ell$=5. To solve eqn(5.3), the real root η are needed and the approximate values can be found by graphical method as shown in Fig 5.4(a) for $\alpha\ell$=4 and Fig.5.4(b) for $\alpha\ell$=5. A function file **rroot.m** is use to calculate the exact value of the roots and it is found to be 1.9150 for $\alpha\ell$=4 and 2.4641 for $\alpha\ell$=5.

No of Sections	Resistors Values	Capacitors Values	Initial Voltages
1	R1=0.9817	C1=3.0746	1
		C2=50.5235	0.1832
5	R1=0.5507	C1=0.4528	1
	R2=0.2472	C2=1.7804	0.4493
	R3=0.1112	C3=3.9624	0.2019
	R4=0.0500	C4=8.8185	0.0907
	R5=0.0224	C5=19.6260	0.0408
		C6=18.9580	0.0183

Table 5.3a - Component values for $\alpha\ell$=4

No of Sections	Resistors Values	Capacitors Values	Initial Voltages
1	R1=0..9933	C1=4.0339	1
		C2=143.3792	0.0067
5	R1=0.6321	C1=0.5820	1
	R2=0.2325	C2=2.7183	0.3679
	R3=0.0855	C3=7.3891	0.1353
	R4=0.0315	C4=20.0855	0.0498
	R5=0.0116	C5=54.5982	0.0183
		C6=62.0402	0.0067

Table 5.3(b) - Component values for $\alpha\ell=5$
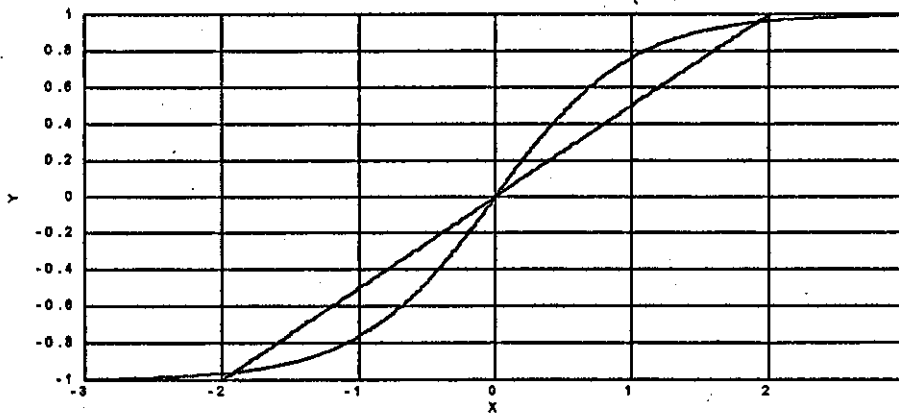
Fig 5.4(a) Graphical solution of $\tanh\eta = \dfrac{2\eta}{\alpha\ell}$ at $\alpha\ell = 4, \eta \approx 1.9$
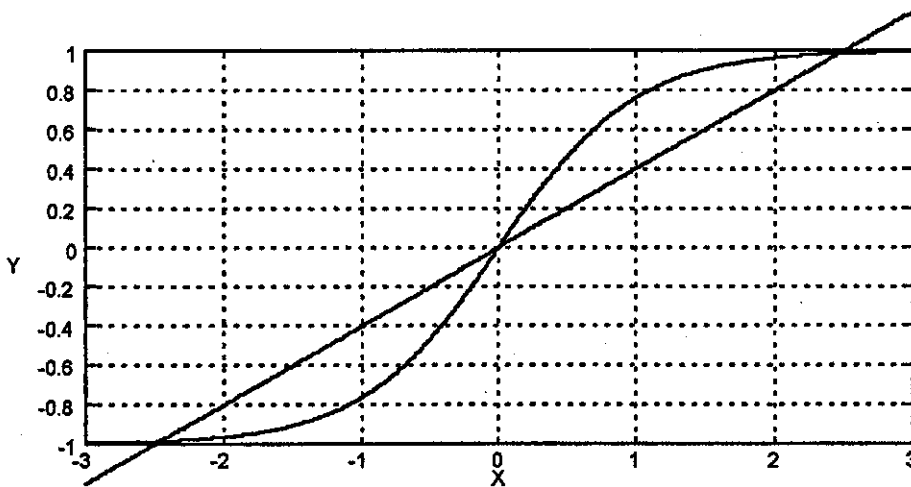
Fig 5.4(a) Graphical solution of $\tan\eta = \dfrac{2\eta}{\alpha\ell}$ at $\alpha\ell = 5, \eta \approx 2.4$
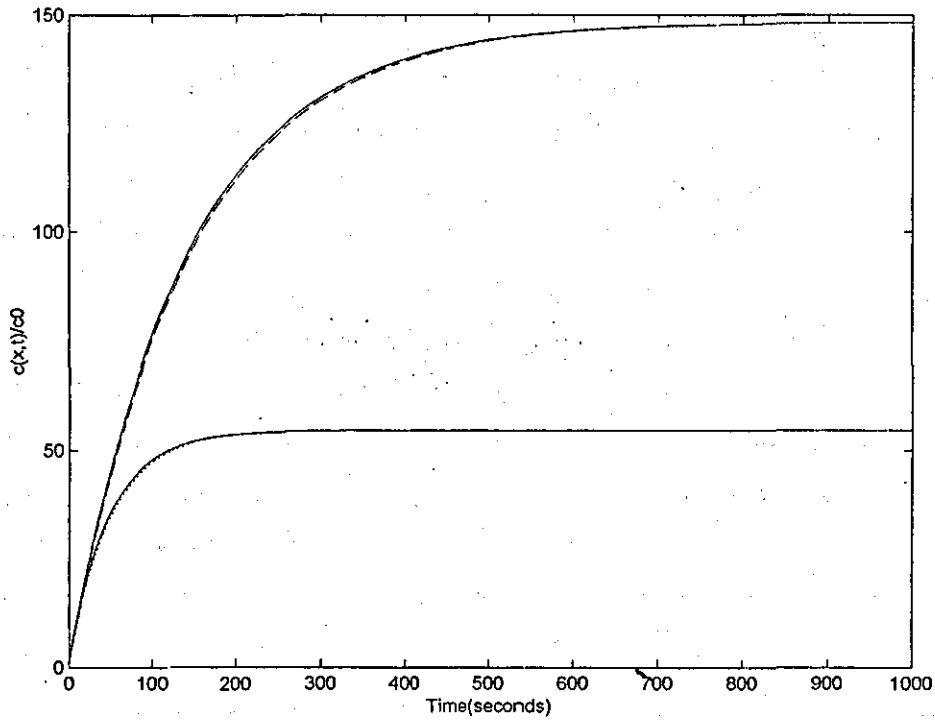
Fig 5.5 The vacancy concentration profile monitored at the blocking ends of the
conductor. The exact solutions (solid line), lumped element
model are represented by i) $\alpha\ell$=5 (dashed line), $\alpha\ell$=4 (dotted line)

With reference to Fig 5.5 above, the vacancy concentration for both the exact solutions
and the lumped element model does exhibit the same build-up profile. From the figure it
looks like that a single C-R-C circuit is sufficient to produce the same response which
fits exactly the exact solution response for both conditions of $\alpha\ell$. However, by analysing
the Time to Failure for each conditions, it is found that 5 sections of C-R-C circuit gives
a better results than a single section as shown in Table 5.4 below.

Simulation type	TTF($\alpha\ell$=4)	% error	TTF($\alpha\ell$=5)	% error
Exact solution	61.9374 secs	-	42.2738 secs	-
Lumped element(1 section)	64.5109 secs	4.1	43.7627 secs	3.5
Lumped element(5 sections)	62.0160 secs	0.9	42.3785 secs	0.25
Signal delay (1 section)	64.5083 secs	4.1	43.7621 secs	3.5
Signal delay (5 sections)	61.8502 secs	0.14	42.8698 secs	1.4

Table 5.4 The Time to Failure (TTF) for different type of simulation with critical
vacancy $c_{cr} = 40c_0$

ii) simulation results for $\alpha\ell < 2$

For this simulation, two sets of $\alpha\ell$ are chosen as an example, i.e. $\alpha\ell = 0.5$ and $\alpha\ell = 1$. To solve the equation 5.4 of the exact solution, the imaginary root ξ is needed and the approximate values can again be found by a graphical method as shown in Fig 5.6(a) for $\alpha\ell = 0.5$ and Fig.5.6(b) for $\alpha\ell = 1$. A function file **imroot.m** is used to calculate the exact value of the roots which are found to be 1.3933 for $\alpha\ell = 0.5$ and 1.1665 for $\alpha\ell = 1$. The values for the components are as shown in Table 5.5(a) and 5.5 (b) for $\alpha\ell = 0.5$ and $\alpha\ell = 1$ respectively.

No of Sections	Resistors Values	Capacitors Values	Initial Voltages
1	R1=0.3935	C1=0.2707	1
		C2=0.3780	0.6065
5	R1=00952	C1=0.0508	1
	R2=0.0861	C2=0.1105	0.9048
	R3=0.0779	C3=0.1221	0.8187
	R4=0.0705	C4=0.1350	0.7408
	R5=0.0638	C5=0.1492	0.6703
		C6=0.0811	0.6065

Table 5.5(a) - Component values for $\alpha\ell = 0.5$

No of Sections	Resistors Values	Capacitors Values	Initial Voltages
1	R1=0.6321	C1=0.5820	1
		C2=1.1363	0.3679
5	R1=0.1813	C1=0.1033	1
	R2=0.1484	C2=0.2443	0.8187
	R3=0.1215	C3=0.2984	0.6703
	R4=0.0995	C4=0.3644	0.5488
	R5=0.0814	C5=0.4451	0.4493
		C6=0.2628	0.3679

Table 5.5(b) - Component values for $\alpha\ell = 1$
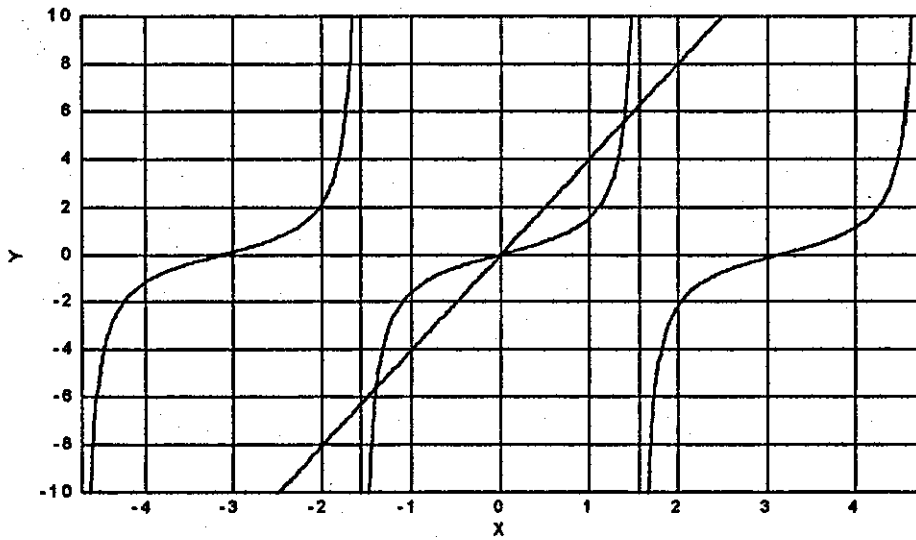
Fig 5.6(a) Graphical solution of $\tan\xi = \dfrac{2\xi}{\alpha\ell}$ at $\alpha\ell = 0.5$ where the root $\xi \approx 1.3$
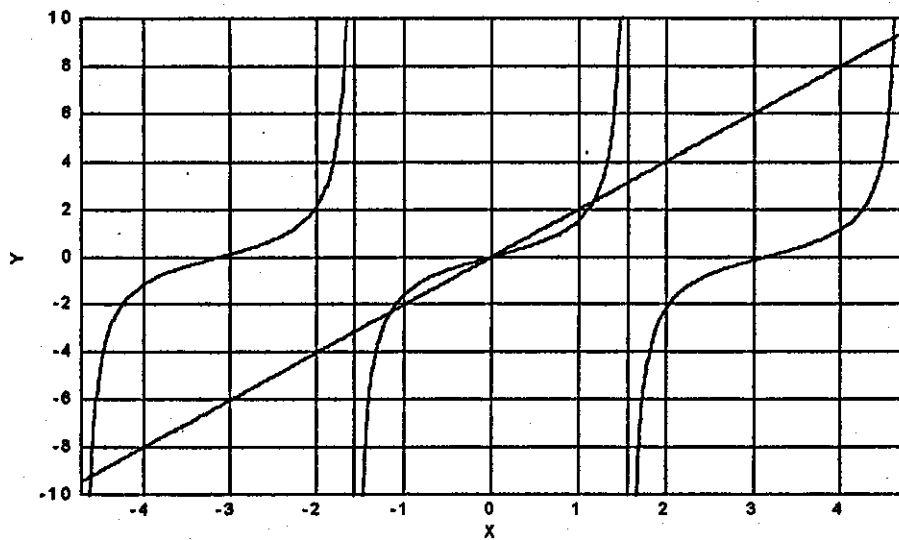
Fig 5.6(a) Graphical solution of $\tan\xi = \dfrac{2\xi}{\alpha\ell}$ at $\alpha\ell = 1$ where the root $\xi \approx 1.1$
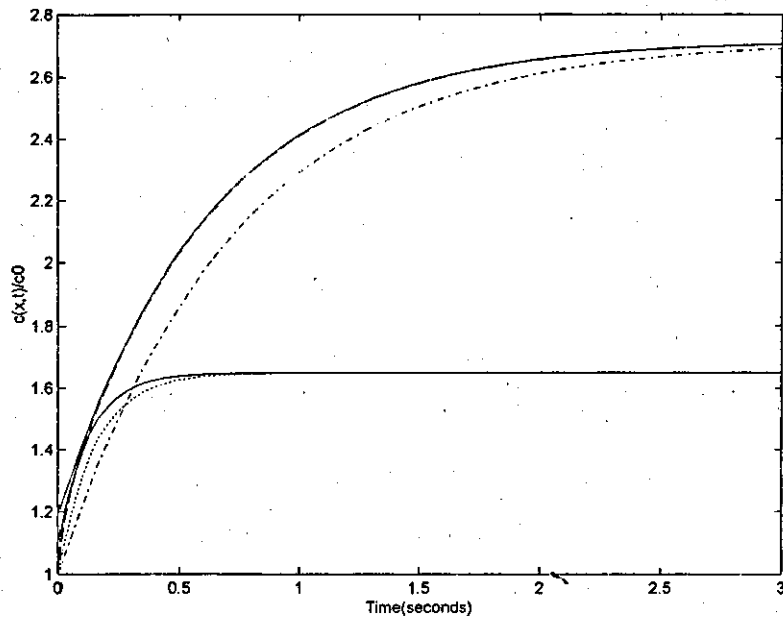
Fig 5.7 The vacancy concentration profile monitored at the blocking ends of the
conductor. The exact solutions (solid line), lumped element model using 1
section are represented by (i) $\alpha\ell$=0.5 (dotted line), (ii)$\alpha\ell$=1 (dash dot line)
For 5 sections (dashed lines),match exactly the exact solution.

From Fig 5.7 above, it is evident that for the lumped element model , a single section
does not give a good fit to the response of the vacancy concentration. 5 sections fit
exactly the vacancy concentration response of the exact solution. The results on the
analysis of the Time to Failure does show that 5 sections is better than one, but also that
5 sections is acceptably good when compared with the 'exact solution' and signal delay
as shown in Table 5.6

Simulation type	TTF($\alpha\ell$=0.5)	% error	TTF($\alpha\ell$=1)	% error
Exact solution	0.1637 secs	-	0.4676 secs	-
Lumped element(1 section)	0.2191 secs	33.8	0.6265 secs	33.9
Lumped element(5 sections)	0.1657 secs	1.2	0.4734 secs	1.2
Signal delay (1 section)	0.2191 secs	33.8	0.6265 secs	33.9
Signal delay (5 sections)	0.1604 secs	2.01	0.4893 secs	4.6

Table 5.6 The Time to Failure (TTF) for different type of simulation with critical
vacancy $c_{cr} = 1.5c_0(\alpha\ell = 0.5)$ and $c_{cr} = 2c_0(\alpha\ell = 1)$

5.1.3 Summary on the results of the simulation of a single grain boundary conductor

It has been demonstrated that the stress evolution in a single grain boundary does mimics the time development of the voltage on an equivalent, lumped electrical circuit.. This is apparent from the simulation results obtained by comparing the vacancy concentration response of the lumped element model and the two exact solutions found in the literature. Two sets of different boundary conditions are investigated and both produce similar results for the lumped element model and the exact solution.

It has also been demonstrated that five sections of CR network gives better results than a single section of CR network by observing the vacancy concentration profile and the results of the Time to Failure in particular for case (A) and for $\alpha\ell < 2$ for case(B). A single section of CR network is adequate for the condition when $\alpha\ell > 2$ for case(B) although from simulation results of Time to Failure does show that five sections is better than one section.

The signal or Elmore delay approximation of the Time to Failure has also been calculated for case(B) and result shows a small and acceptable level of error compared with the exact solution. With these results, it can be deduced that the signal or Elmore delay approximation method can be applied to get fast and efficient results on the electromigration Time to Failure.

Based on the simulation results obtained, it has proved that the lumped element model is valid and workable in investigating the electromigration behaviour as in the stress evolution model and able to predict the electromigration lifetime of a single grain boundary. The model will be tested on more complex grain boundary structures and hopefully on a realistic sample of interconnect where the statistics of the Time to Failure will be analysed. The other important parameter to validate the developed model is to prove that the distribution of the Time to Failure follows a lognormal distribution.

5.2 Simulation results on an example of a typical complex grain boundary

5.2.1 Introduction

A real interconnect consists of many grain boundary clusters made up of very complex grain boundary structures which run along the whole interconnect. For simulating realistic interconnect, computer programs are used to generate these grain boundaries structures in order to investigate the electromigration problem[Joo and Thompson,1994][Knowlton et al.,1997][Marcoux et al., 1989]. In the current work, realistic interconnect will be simulated using the Voronoi technique and this work will discussed in the following section. It is worthwhile to work on the lumped element model for an ' artificial' complex network first before pursuing the work on a 'realistic' interconnect.

The 'artificial or self generated' complex grain boundary interconnect is constructed from five grain boundaries of equal length L. For the centrepiece (CD) it has the value $\alpha_{eff}\ell = \alpha L = 1$, while the limbs, all at an angle θ of $\dfrac{\pi}{4}$ to the direction of current flow,

i.e. $\alpha_{eff}\ell = \alpha.\cos\left(\dfrac{\pi}{4}\right)L = \dfrac{1}{\sqrt{2}}$. The model with this set-up is as shown in Fig 5.8(a) with

its equivalent lumped element model of CR network in Fig 5.8(b).
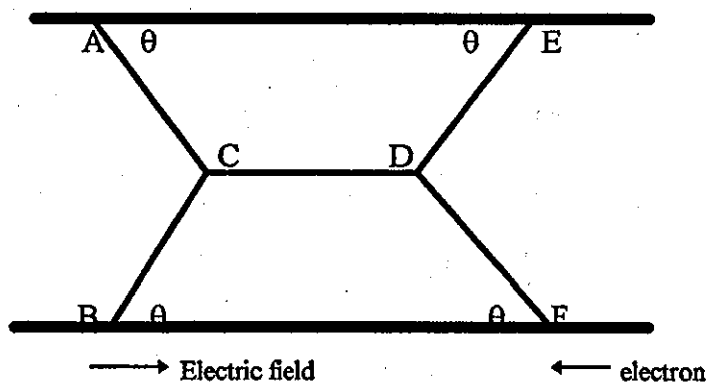
Fig 5.8(a) The schematic diagram of complex grain boundaries
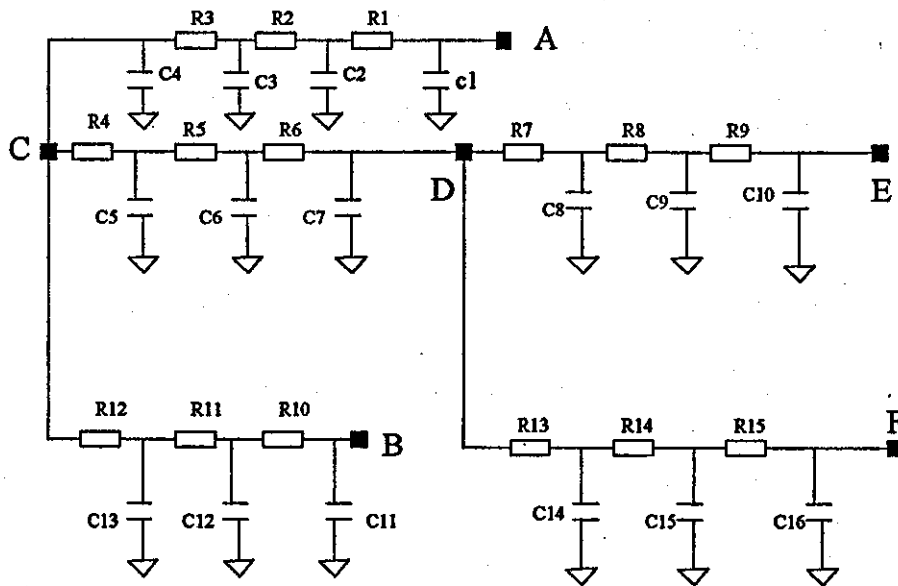
Fig 5.8(b) The equivalent CR network with 3 sections per grain boundary

The equivalent model of the lumped CR network will have a total of 16 capacitors and 15 resistors if modelled by a 3 sections per grain boundary or 26 capacitors and 25 resistors for 5 sections per grain boundary. The points of A,B,C,D,E and F are the nodes where vacancy concentration build-up will be monitored.

5.2.2 Simulation Objectives

The objectives of this simulation exercise are :-

i) To investigate the microstructural effects on electromigration in complex grain boundaries

ii) To calculate the Time to Failure of the interconnect

iii) To compare the results between the lumped element model and the signal delay approximation of Time to Failure.

As described in the literature review in Chapter 2, the grain boundary triple point junctions are the most likely sites for void formation. Failure at these sites is believe to depend on grain boundary parameters such as the effective grain boundary diffusion coefficients D_{eff} , the length of the grain boundary and the angle of orientation in the intersecting boundaries. These parameters will determine the Time to Failure and also the location or the sites where the vacancy concentration is accumulated (voids formation).

The structure of the complex grain boundary network (Fig5.8(a)) are simulated to obtain the vacancy build-up at certain nodes of interest such as nodes C,D and E. In this setup ,it is assumed that x=0 is taken at node A and the boundary conditions are (c(x=0,t)= c_0 or $\sigma = 0$ and all the other nodes J(x=L,t)=0. With this boundary conditions, the node A is the source/sink where vacancy concentration is being supplied and all the other nodes are being blocked. The critical vacancy concentration $c_{cr} = 2c_0$ is the failure criterion. All the grain boundaries are of equal length L= 1, the effective diffusion coefficient D =1, the electromigration drift component α=1.

5.2.3   The Vacancy concentration profile at nodes

The complex grain network is modelled by an equivalent CR network consisting of five sections for each grain boundaries. As in the case of single grain boundary , the network circuit is simulated by solving the relevant matrix equation and the program code developed for this purpose is **net1ball.m.** The vacancy build-up profiles at nodes C,D and E are as shown in Fig.5.9.

174
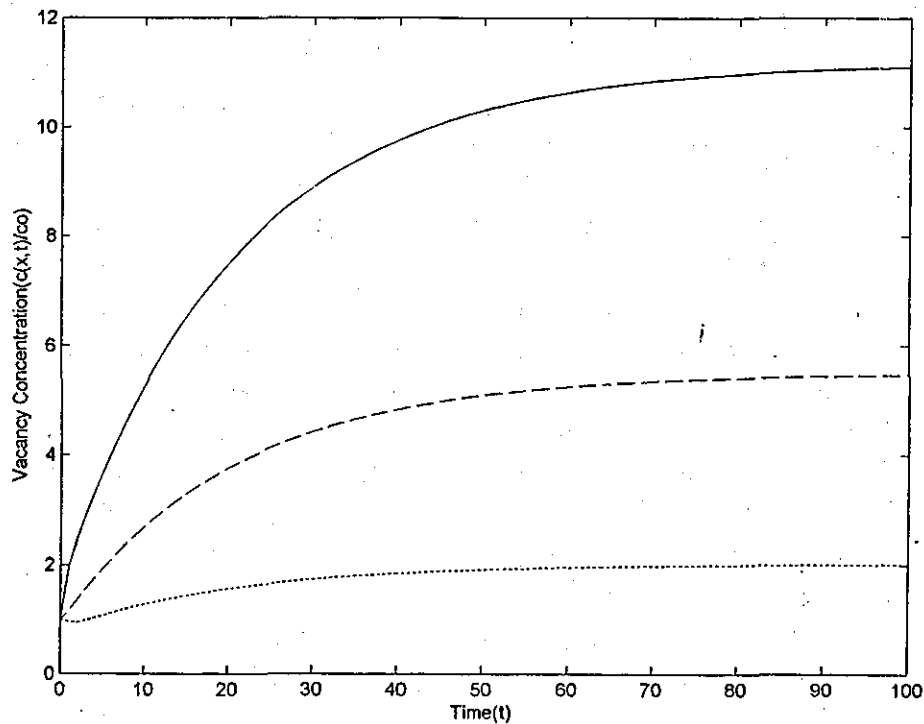
Fig5.9 The vacancy concentration build-up at node C (dotted line), node D (dashed
line) and node E(solid line)

As shown in Fig 5.9 ,failure will occur first at node E where the vacancy concentration
reaches the critical vacancy c_{cr} at Time to Failure of 1.064. At the triple junctions node
D the Time to Failure is 5.4679 and node C, the vacancy concentration does not reach the
critical value and therefore failure will not takes place.

5.2.4 The effect of angle θ (and the microstructure) on vacancy concentration at
nodes

The same model is now used but with a different angle of orientation for grain
boundaries DE and DF.(here an angle of 89^0 to the direction of electric field). The
vacancy concentration profile for nodes C,D and E are as shown in Fig 5.10. This time
failure will occur first at node D , the triple junction point. The Time to Failure recorded
is 4.1281 compared to 4.4632 for node E. Also it is noted that the vacancy build-up of
node E is almost the same as at node D. If the angle θ is 90^0 , the final concentration at

175

all points along grain boundary DE will be the same as at node D. The reason is that there

is no component of the drift along the grain boundary DE as $\alpha_{eff} x = \alpha . \cos\left(\dfrac{\pi}{2}\right) . x = 0$.

Also diffusion values on the different limbs will alter the Time to Failure.
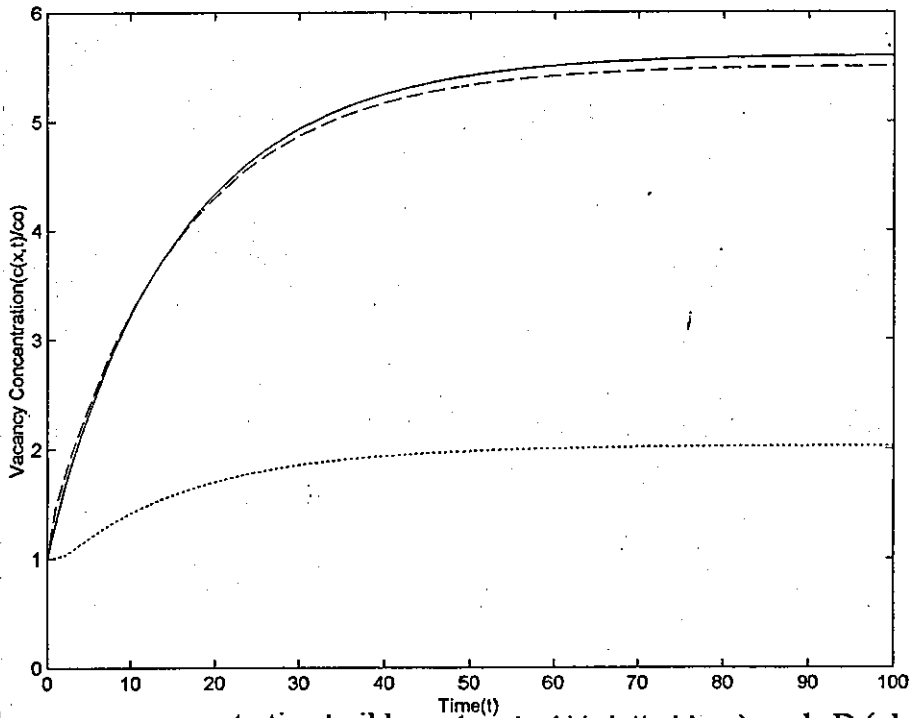
Fig5.10 The vacancy concentration build-up at node C (dotted line), node D (dashed

line) and node E (solid line)

5.2.5   The Time to Failure and changeover angle θ

The analysis of the structure shown in Fig5.8(a) are repeated to find the exact angle of
orientation which will cause the changeover of the failure nodes from E/F to nodes D.
The parameters used in the simulation are the same as before, where all the grain
boundary lengths L=1, diffusion coefficient D=1, the electromigration drift α=1 and the
failure criterion c_{cr} =2 c_0 , s= 5 (five sections per grain boundary) , but with varying

angle of orientation θ ranges from 70^0–90^0 . The results of the Time to Failure for node
E and D are shown in Table 5.7 and in Fig 5.11. The results shows that the changeover
from node E/F to node D occurs at about θ= 86.8^0 .

Angle (radians)	Angle (degrees)	TTF(node E)	TTF(nodeD)
1.2282	70.27	2.0292	4.082
1.2419	71.05	2.0781	4.0383
1.2833	73.42	2.2305	3.9128
1.3449	76.94	2.4741	3.7304
1.3633	78.00	2.5508	3.6763
1.3649	78.09	2.5575	3.6716
1.377	78.78	2.6086	3.6365
1.3811	79.02	2.6262	3.6245
1.3914	79.60	2.6708	3.5945
1.4336	82.02	2.8597	3.4724
1.4366	82.19	2.8735	3.4638
1.4794	84.64	3.0841	3.3415
1.4878	85.12	3.129	3.3179
1.4982	85.72	3.1857	3.2885
1.5085	86.30	3.2424	3.2596
1.5329	87.70	3.3797	3.1914
1.5337	87.75	3.3843	3.1891
1.5418	88.21	3.4309	3.1666
1.5435	88.31	3.4408	3.1618
1.5483	88.58	3.4684	3.1486

Table 5.7 The Time to Failure at node E and D as angle θ of DE

and DF are varied (simultaneously with same value)
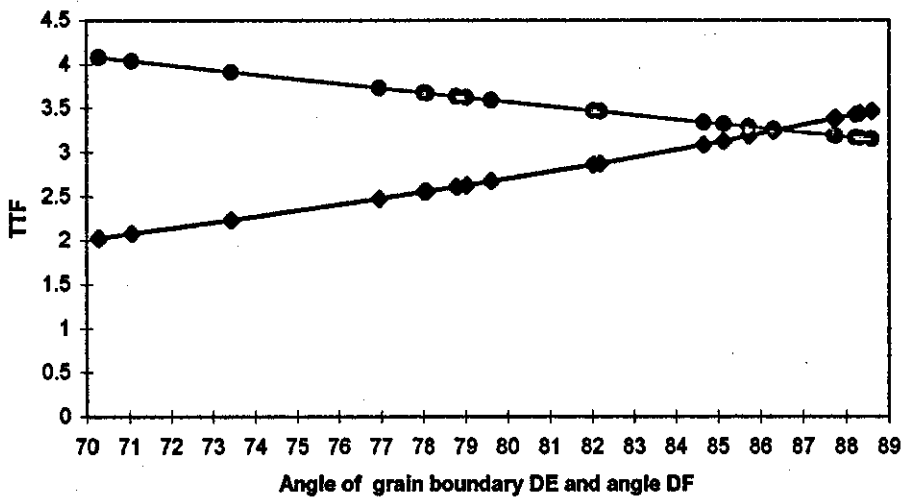
Fig 5.11 The Time to Failure at node D (red circle) and node E (blue triangle)
for a range of values of angle DE and DF (angle DE=DF) calculated
by the lumped element model with equal length L=1, D=1, α=1 and $c_{cr} = 2c_0$.

177

5.2.6 Signal delay versus lumped element model for changeover angle θ

The analysis of the structure shown in Fig5.8(a) are repeated to compare the results above (lumped element model) with the signal delay method. The parameters used in the simulation are the same where all the grain boundary lengths L=1, diffusion coefficients D=1, the electromigration drift α=1 and the failure criterion c_{cr} =2c_0, s=5 , (5 sections/grain boundary) but with varying angle of orientation θ ranges from 80^0–90^0. The results of the Time to Failure for node E and D for the lumped element model and the signal delay are shown in Table 5.8 and in Fig 5.12. The results shows that the changeover from node E/F to node D using the signal delay occurs at θ= 88.8^0 rather than the lumped element model of 86.8^0 (error of 2.3%).

θ	TTFm(node E)	TTFm(node D)	TTFs(node E)	TTFs(node D)
81.39	2.8097	3.504	3.2829	3.9948
82.1	2.9318	3.4278	3.3731	3.9449
83.66	2.994	3.3901	3.4197	3.9203
84.17	3.0399	3.365	3.4515	3.904
84.91	3.1089	3.3284	3.499	3.8803
85.30	3.1455	3.3092	3.5244	3.8679
85.82	3.195	3.2837	3.5589	3.8514
86.33	3.2444	3.2585	3.5936	3.8352
86.70	3.2807	3.2403	3.6192	3.8235
86.86	3.296	3.2326	3.63	3.8186
88.06	3.415	3.1742	3.7151	3.7812
88.10	3.4187	3.1725	3.7177	3.7801
88.42	3.4509	3.157	3.741	3.7702
88.48	3.4573	3.1539	3.7457	3.7682
88.87	3.4977	3.1347	3.775	3.756
89.00	3.5113	3.1283	3.7849	3.7519
89.29	3.5409	3.1145	3.8065	3.7431
89.427	3.5549	3.1079	3.8169	3.739
89.75	3.5882	3.0925	3.8413	3.7292
89.81	3.595	3.0893	3.8464	3.7272

Table 5.7 The Time to failure for at nodes E and D for the lumped element model (TTFm) and the signal delay (TTFs)
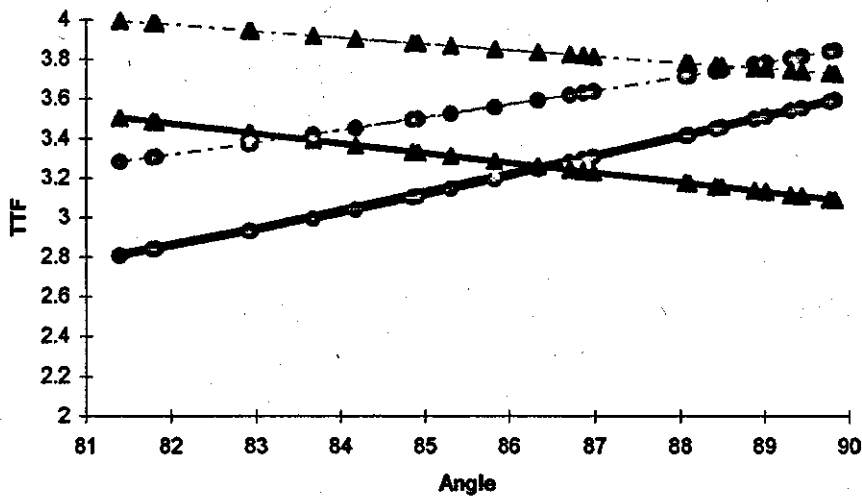
Fig 5.12. The Time to failure at different angle of orientation θ for node E and D.
TTF for lumped element model at node D(blue triangle with solid black
line) and node E (red circle with solid black line). TTF for signal delay is
represented by the dashed line.

5.2.7   Signal delay versus lumped element model on Time to Failure

The next simulation exercise is to compare the signal delay with the lumped element
model ' of a more complex interconnect cluster section consisting of eleven grain
boundaries as shown in Fig5.13. At this stage the network and its microstructure are
chosen to demonstrate the accuracy and reliability of the approximation rather to obtain
the detailed information on the Mean Time to Failure statistics. The distribution of
cluster lengths and sizes, of individual grain boundary lengths and orientations, and of
diffusivities are not yet known well enough for this to be meaningful. Thus the grain
boundaries are chosen from a uniform distribution centred on 45^{0} , the lengths of the
grain boundaries are chosen from a uniform distribution between 0.25 µm and 0.5 µm
while the effective vacancy diffusion coefficient is constant D=1. A program code
vnoigb.m is developed to simulate the Time to Failure for both method of the lumped

179

element model and signal delay of approximation where the network is modelled by s=3(three sections per grain boundary).
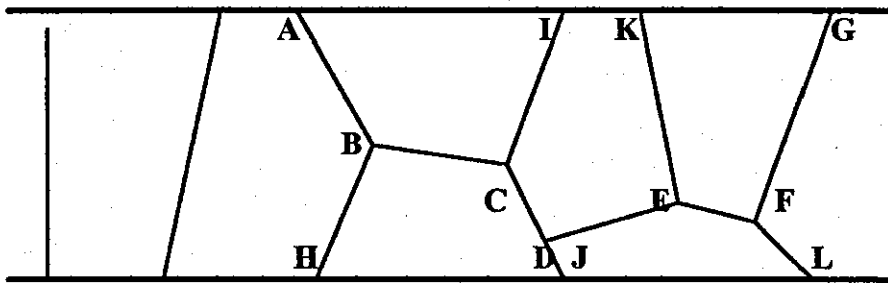
Fig 5.13 An example of near bamboo interconnect

The vacancy concentration profile at nodes B,C,D,E,F and G are shown in Fig 5.14.
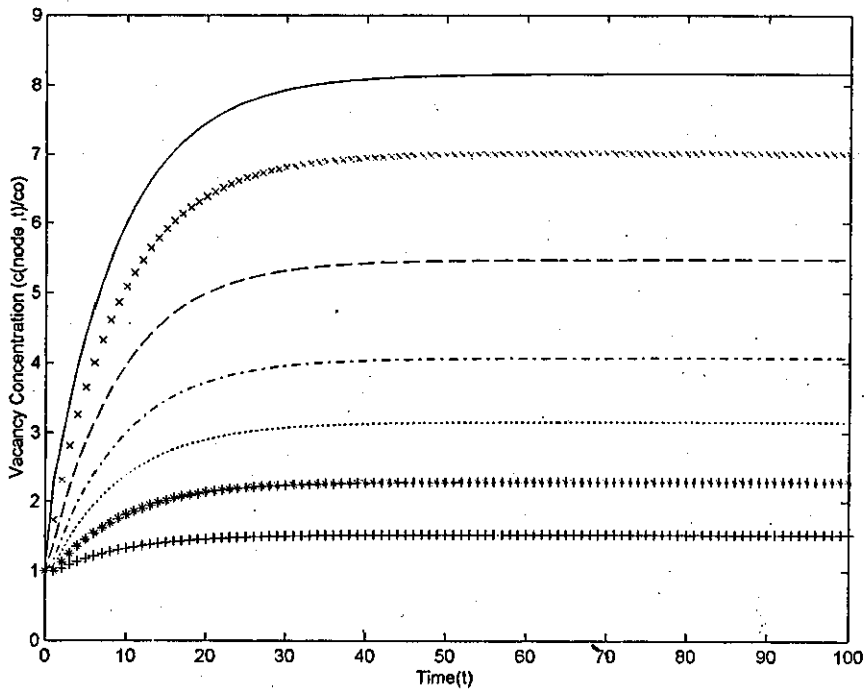
Fig 5.14 The vacancy concentration profile at node B(+), node C(*), node D(dotted line), node E(dash dot line), node K(dashed line) , node F(x) and node G(solid line)

The data on the Time to Failure of node G for both the lumped element model(TTFm) and the signal delay(TTFs) is shown in Table 5.8 and are also represented in graphical form in Fig. 5.15

L(AB)	L(BC)	L(CD)	L(DE)	L(EF)	L(FG)	TTFm	TTFs	%Error
0.4533	0.2847	0.2997	0.318	0.2538	0.3613	2.6133	2.4473	-6.35212
0.4579	0.4274	0.3262	0.2984	0.3257	0.2877	2.4475	2.3205	-5.18897
0.3355	0.3353	0.4318	0.4596	0.3426	0.3866	2.2893	2.2112	-3.41152
0.4689	0.2841	0.4735	0.3247	0.3211	0.2662	2.2701	2.2171	-2.3347
0.3023	0.4458	0.3653	0.4486	0.4007	0.3538	2.3974	2.298	-4.14616
0.33	0.4317	0.4361	0.36	0.4208	0.4598	2.5719	2.4728	-3.85318
0.2532	0.4208	0.2588	0.4021	0.2541	0.3967	2.3366	2.2203	-4.97732
0.4248	0.3696	0.2803	0.429	0.3183	0.4664	3.1714	2.9545	-6.83925
0.2927	0.3599	0.3286	0.3483	0.2799	0.3646	3.5544	3.2977	-7.22203
0.2843	0.3575	0.4337	0.3365	0.2889	0.3556	2.8927	2.753	-4.8294
0.4233	0.4957	0.35	0.4063	0.344	0.355	2.3177	2.2971	-0.88881
0.3086	0.4829	0.4139	0.4068	0.3493	0.4138	2.5905	2.4247	-6.40031
0.4957	0.4259	0.2787	0.3413	0.3917	0.4185	2.6924	2.6608	-1.17367
0.4376	0.358	0.4508	0.4864	0.4005	0.4684	3.2286	2.9349	-9.09682
0.3392	0.3586	0.4042	0.4746	0.4478	0.4175	2.812	2.5708	-8.57752
0.3322	0.3993	0.4574	0.3989	0.453	0.4254	3.1315	2.7883	-10.9596
0.361	0.4879	0.3118	0.297	0.3523	0.4027	2.573	2.4464	-4.92033
0.3354	0.3269	0.3215	0.3758	0.3266	0.3608	2.3386	2.2178	-5.16548
0.3628	0.4572	0.3485	0.4295	0.3652	0.2719	2.3675	2.303	-2.72439
0.3055	0.3805	0.4283	0.3624	0.4922	0.2623	2.1993	2.1599	-1.79148
0.2703	0.3905	0.3437	0.343	0.3	0.3917	2.8748	2.7481	-4.40726
0.2754	0.3086	0.2658	0.4999	0.3746	0.4182	2.2769	2.1907	-3.78585
0.4053	0.311	0.3158	0.4149	0.4005	0.4149	2.8402	2.66	-6.34462
0.3268	0.4197	0.2677	0.3068	0.3646	0.3956	2.7804	2.6543	-4.53532
0.457	0.2783	0.4771	0.2805	0.4305	0.4385	3.1289	2.9554	-5.54508
0.3071	0.4142	0.372	0.3433	0.2953	0.3555	2.5071	2.5182	0.442743
0.2981	0.3127	0.2843	0.4738	0.3338	0.3678	2.9028	2.7642	-4.7747
0.4101	0.4203	0.2837	0.3155	0.2673	0.2951	2.5919	2.4268	-6.36984
0.3986	0.4147	0.3919	0.448	0.4583	0.4097	2.3792	2.3318	-1.99227
0.2759	0.3519	0.2632	0.2875	0.3278	0.4742	3.2455	3.0263	-6.75397
0.4244	0.2707	0.2983	0.2532	0.4688	0.3333	2.468	2.3664	-4.11669
0.4917	0.3294	0.2826	0.4508	0.2534	0.3636	2.505	2.4708	-1.36527
0.3854	0.3628	0.4468	0.2539	0.4404	0.4396	2.7782	2.5599	-7.85761
0.4166	0.4856	0.4344	0.4977	0.4073	0.3622	2.5503	2.4364	-4.46614
0.2518	0.3855	0.3284	0.354	0.4181	0.3358	2.504	2.374	-5.19169
0.2983	0.4805	0.4419	0.4533	0.2997	0.4818	3.5295	3.2811	-7.03782
0.464	0.3229	0.3494	0.4861	0.3146	0.2515	2.3536	2.1884	-7.01903
0.3172	0.2908	0.3042	0.2632	0.4169	0.3267	2.164	2.1112	-2.43993
0.4282	0.4853	0.4261	0.3954	0.4374	0.4314	3.0216	2.824	-6.53958
0.4896	0.2637	0.3483	0.2956	0.2519	0.2544	1.8535	1.8928	2.120313

0.4998	0.4057	0.3275	0.3058	0.2838	0.4819	2.3812	2.3053	-3.18747
0.3699	0.3219	0.3156	0.4793	0.2534	0.4247	2.6419	2.4548	-7.08202
0.4287	0.3094	0.3158	0.4944	0.3865	0.4505	2.7835	2.6626	-4.34345
0.3719	0.4185	0.3054	0.2671	0.3019	0.4096	2.9305	2.7226	-7.09435
0.4322	0.4141	0.3362	0.3368	0.4296	0.2892	3.0795	2.9183	-5.23462
0.3675	0.2645	0.3639	0.4638	0.4467	0.25	2.559	2.3993	-6.24072
0.377	0.3314	0.4716	0.4709	0.4498	0.2663	2.1188	2.0086	-5.20106
0.4608	0.4644	0.3914	0.2757	0.3534	0.3172	2.5189	2.4369	-3.25539
0.4015	0.274	0.3607	0.3436	0.4812	0.4696	2.4413	2.3349	-4.35833
0.4591	0.2929	0.456	0.4712	0.4909	0.2621	2.1729	1.9914	-8.35289

Table 5.8 The data of 50 simulations of Time to Failure at node G for lumped element

model (TTFm) and signal delay approximation (TTFs) for $c_{cr} = 2c_0$, L=length

of grain boundary.
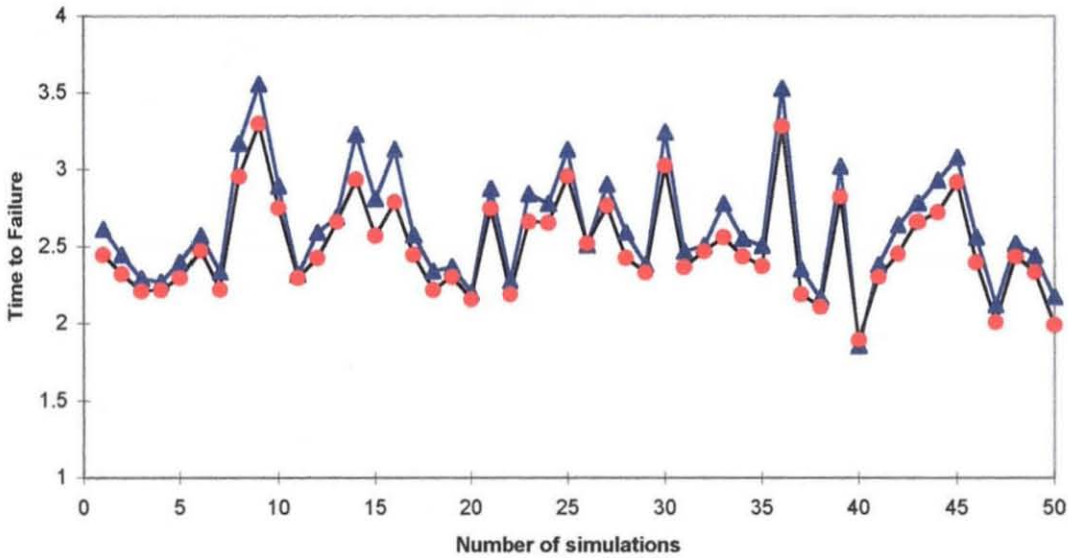
Fig5.15 The Time to Failure at node G for lumped element model(blue triangle) and

signal delay(red dot). The failure criterion used is $c_{cr} = 2c_0$

The failure criterion was chosen as $c_{cr} = 2c_0$, corresponding to a critical yielding stress of

$\sigma_{cr} = 478$ MPa. The simulation are repeated for different failure criterion of $c_{cr} = 4c_0$,

which corresponds to 956 MPa and the results are shown in Table 5.9 and Fig 5.16.

L(AB)	L(BC)	L(CD)	L(DE)	L(EF)	L(FG)	TTFm	TTFs	Error
0.2735	0.4881	0.3842	0.3735	0.3231	0.4385	4.6024	4.7924	4.128281
0.4534	0.4306	0.3406	0.4124	0.2519	0.4863	5.003	5.2129	4.560664
0.354	0.266	0.3275	0.4952	0.4971	0.3104	6.6125	6.6035	-0.19555
0.3692	0.4265	0.4293	0.3527	0.4886	0.4246	4.6322	4.8319	4.339041
0.2989	0.3415	0.2537	0.4344	0.2755	0.441	5.2883	5.3521	1.386233
0.4164	0.2621	0.45	0.4238	0.4283	0.4333	4.3636	4.5702	4.488962
0.3767	0.4039	0.488	0.4567	0.4618	0.4123	4.0777	4.3767	6.49661
0.3462	0.3938	0.2989	0.4283	0.4355	0.4667	5.4538	5.5875	2.905006
0.372	0.4406	0.4929	0.284	0.3283	0.3349	5.802	5.9744	3.745872
0.3932	0.4345	0.3459	0.4643	0.3114	0.401	4.5852	4.7187	2.900661
0.3744	0.4416	0.2913	0.3021	0.3491	0.3773	4.9685	5.0742	2.296628
0.3611	0.499	0.486	0.4537	0.3272	0.4092	5.601	5.7161	2.500869
0.3325	0.3411	0.4292	0.4456	0.3081	0.4472	4.8137	4.9745	3.493829
0.4055	0.4909	0.2777	0.2743	0.4197	0.3499	5.5563	5.6463	1.955501
0.3579	0.4958	0.4871	0.3329	0.2915	0.4109	4.7616	4.9541	4.1826
0.3255	0.3273	0.3594	0.4557	0.2907	0.3813	6.6054	6.6136	0.178168
0.363	0.4042	0.3411	0.4571	0.399	0.2584	6.3434	6.3686	0.54754
0.3749	0.4573	0.3997	0.3497	0.4084	0.2515	5.2451	5.341	2.083695
0.4688	0.4352	0.3609	0.4091	0.3022	0.3105	5.035	5.1585	2.683383
0.4384	0.452	0.3713	0.4066	0.386	0.3175	4.5992	4.8789	6.077264
0.3355	0.287	0.4098	0.4822	0.2908	0.2827	5.2597	5.3428	1.80558
0.2992	0.376	0.3444	0.4539	0.3472	0.3262	5.5634	5.613	1.077699
0.2667	0.2817	0.2911	0.383	0.3544	0.4512	4.8725	4.9248	1.136364
0.3372	0.3849	0.3593	0.4246	0.4592	0.2549	5.2063	5.2926	1.875109
0.4006	0.4333	0.289	0.3005	0.4223	0.3449	5.2363	5.3142	1.692595
0.4307	0.4239	0.4063	0.3939	0.4732	0.3231	5.1179	5.2609	3.107075
0.3332	0.3506	0.3219	0.3915	0.3137	0.3807	5.5478	5.5884	0.882148
0.4302	0.4657	0.3415	0.3337	0.4539	0.3561	4.1022	4.3587	5.573179
0.4265	0.3027	0.4593	0.4714	0.4424	0.267	5.3329	5.4692	2.961498
0.4821	0.3467	0.4527	0.4488	0.4892	0.4966	3.4986	3.8351	7.311403
0.3151	0.3813	0.4565	0.3132	0.3879	0.4164	4.1524	4.3321	3.904485
0.2954	0.4222	0.4808	0.3503	0.3501	0.2661	4.9462	5.0441	2.127151
0.3025	0.4948	0.4505	0.3103	0.3418	0.3255	6.1163	6.2195	2.242308
0.2821	0.4474	0.4346	0.3897	0.2852	0.3014	6.7978	6.8466	1.060316
0.4504	0.4432	0.4518	0.4762	0.4146	0.4955	4.1234	4.4678	7.483052
0.4337	0.3742	0.329	0.4476	0.35	0.273	5.8004	5.8543	1.171128
0.4252	0.3792	0.4387	0.4858	0.3858	0.4653	5.3434	5.5827	5.199461
0.3512	0.3464	0.3817	0.3484	0.2575	0.4286	7.9589	7.9474	-0.24987
0.2509	0.4946	0.2536	0.3541	0.372	0.4455	5.1266	5.2199	2.027203
0.4881	0.4448	0.4123	0.287	0.4747	0.4547	4.3719	4.7443	8.091431
0.468	0.4174	0.4554	0.41	0.4458	0.3912	5.7461	5.9473	4.371632
0.4978	0.3705	0.3402	0.4871	0.4039	0.2531	6.8851	7.0285	3.115766
0.4401	0.3285	0.3736	0.4862	0.3744	0.3886	4.6775	4.8949	4.723622
0.386	0.4182	0.4951	0.2549	0.4957	0.3447	5.4935	5.5687	1.63393
0.4456	0.4762	0.3029	0.4357	0.3263	0.2862	5.7929	5.9261	2.894142
0.268	0.4691	0.4271	0.2548	0.4674	0.4498	4.3942	4.5926	4.310794
0.3269	0.4574	0.4274	0.4376	0.4862	0.2635	4.9188	5.0572	3.007127

183

0.459	0.4439	0.359	0.2533	0.4596	0.321	4.9305	5.172	5.247262
0.2585	0.3896	0.396	0.4415	0.4917	0.2946	8.5266	8.509	-0.38241
0.4054	0.3201	0.3281	0.4448	0.4308	0.4033	5.1641	5.3288	3.578568

Table 5.9 The data of 50 simulations of Time to Failure at node G for lumped element

model (TTFm) and signal delay approximation (TTFs) for $c_{cr} = 4c_0$, L=length

of grain boundary.
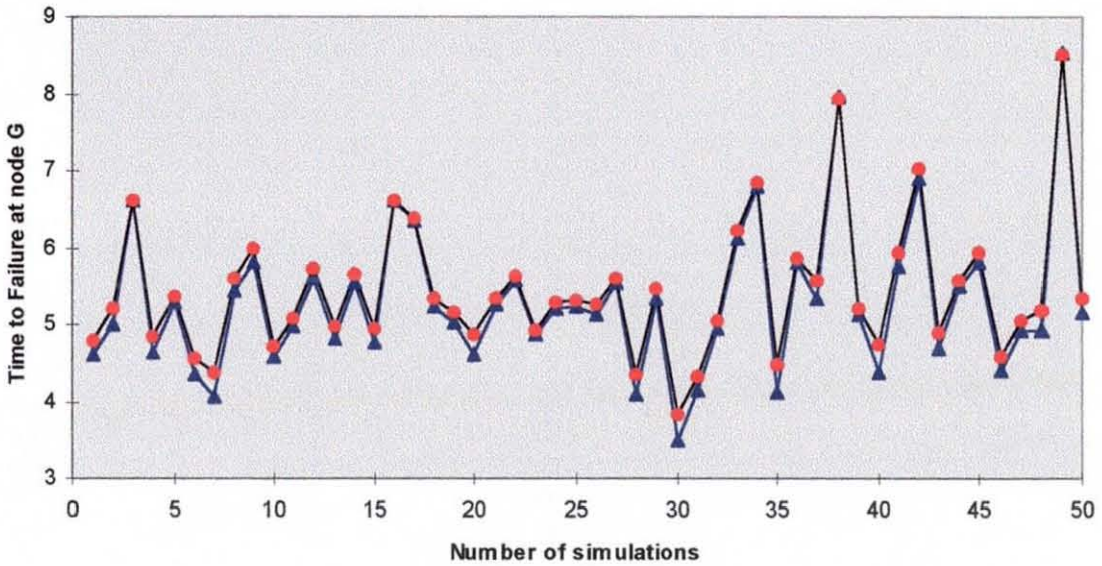
Fig5.16 The Time to Failure at node G for lumped element model(blue triangle) and

signal delay(red dot). The failure criterion used is $c_{cr} = 4c_0$

From these results it shows that the Time to Failure obtained from the signal delay gives

a very good approximation to Time to Failure obtained by the lumped element model for

both failure criterion where the maximum percentage error is about 10% and 8% for

$c_{cr=} 2c_0$ and $c_{cr=} 4c_0$.

5.2.8   Summary of simulation results of complex grain boundary

The current two- dimensional lumped element model of the complex grain boundary cluster includes some of the details of the microstructure(the various grain boundary lengths, orientation and diffusivities) in obtaining the estimation of interconnect life times. Previous one-dimensional studies[Korhonen et.al,1993] have treated the cluster sections as having no internal structure, having been washed out in the simplification. For early failures, occurring as a result of stress build-up in the cluster sections, it is the micro-structural detail that determines the Time to Failure distribution as been described in the literature review in Chapter 2 . This has been successfully demonstrated in the simulation examples where the length of grain boundaries, angle of orientation and diffusivities produce an effect on the Time to Failure.

In the single grain boundary simulation examples, it was demonstrated that the build-up of vacancies at particular points or nodes is equivalent to the development of a pseudo-voltage on a related lumped element, electrical network made up from cascading a relatively small number of CR-II elements. The simulation results shows that it is also applicable to complex grain boundaries where vacancy concentration profiles has been obtained and the Time to Failure can be estimated by assuming failure occurs when the vacancy concentration reaches a fixed level (critical vacancy concentration) as also been used in the stress evolution model of Korhonen et.al and drift diffusion models of Lloyds at al.

Another important result from the simulation exercises is the demonstration of the signal delay estimation of Time to Failure which gives a very good accuracy, within an expected range, to the failure time obtained by the detailed lumped element model calculations. With this , rapid estimates of the Time to Failure TTF can be performed to allow for its statistics to be assessed more readily.

At this stage, the data obtained on the Time to Failure is not of particular significance since the structure of the grain boundaries in the examples do not represent realistic interconnects. The next stage of work is to apply this method (the lumped element model and signal delay) to more realistic interconnects, with structures determined from the Voronoi method of reference[Joo Y.C and Thompson C.V,1994], as a means to determine the Time-to Failure (TTF) distribution . In this way it is hoped to be able to estimate the deviation of TTF (DTTF) and perhaps, the distribution of time-to first failures(TTTF).

5.3 Simulation of realistic interconnects

5.3.1 Introduction

In order to evaluate the reliability of the IC interconnects, it is important to determine the Median Time to Failure (MTTF) and the Deviation in the time to failure (DTTF) or σ_{sd}. Only with the reliable values for both the MTTF and DTTF, plus with the knowledge of the distribution of the Time to Failure (TTF), may the time for early failures be predicted. The lumped element model developed is not completely tested for its validity unless the data on the TTF, MTTF and DTTF is obtained and does exhibit the characteristics found by others. The previous sections have already dealt with rather a simple structure starting with single grain boundary and it is shown to be in agreement with other authors. This is followed by an analysis of a 5 grain boundaries cluster and one of 11 grain boundaries.

In the present work, an attempt is made to obtain a realistic structure of the grain boundary networks and to obtain the associated Time to Failure values and finally to analyse its MTTF and its DTTF so as to prove the validity of the model developed. As commonly used by others , the Voronoi method is also used in the present work to obtain a realistic presentation of Al or Cu films to produce the interconnect samples for the experiment. The construction of the Voronoi network is done through the built-in

function of the MATLAB software package and attempts are also made to simulate the annealing processes.

5.3.2 The objectives of the experiment are basically :-

1. To produce the Time to Failure (TTF) for :-
    i) Each grain boundary cluster in the interconnect
    ii) Interconnect samples (by taking the shortest time among the grain boundary clusters)

2. To convert the arbitrary data into meaningful statistical data such as the Time to Failure, cluster length etc. based on actual experimental parameters.

3. To analyse the data gathered so as to show that the cumulative distribution of the Time to Failure follows the Lognormal distribution.

4. To analyse the effect of scaling of the interconnect.

5. To analyse the effect of the microstructure properties such as the length, the angle of orientation of the grain boundaries on the Time to Failure.

6. To analyse the effect of the cluster length and the number of grain boundaries on the Time to Failure of the interconnects

7. To analyse the effect of annealing on the Time to Failure.

8. To analyse the effect of the variation of the interconnect linewidth on the mean Time to Failure and its standard deviation.

9. To compare the results between the lumped element model and the signal delay approximation of Time to Failure

5.3.3   An example of the detailed simulation processes based on the Matlab® program codes developed.

Basically the complete simulation processes in producing the Time to Failure (TTF) of interconnects is as follows:

(a)   The production of Al films samples

(b)   The annealing of the Al films samples

(c)   The production of the IC interconnects samples

(d)   The calculation of Time to Failure

(a)   The production of a sample of Al film

(i)   Creating Voronoi vertices

The production of the Al film samples was done by making use of the built-in voronoi function in Maltab®. The vertices of the Voronoi are created by using a random number generator to generate the random points of x and y.

(clipping from the Matlab® program codes)

```
fprintf('\n Draw a realistic interconnect using Voronoi technique \n' )

no=input('Enter the no of points needed = ');

for p=1:no;
    xpt(p)=rand;
    ypt(p)=rand;
end
% to produce the reference voronoi diagram or network
[vx_original,vy_original]=voronoi(xpt,ypt)
```

(clipping from Matlab workspace)

Draw a realistic interconnect using Voronoi technique
Enter the no of points needed = *30*
note: the bold and italic number/letter are the required input to the program code)

vx_original =
  Columns 1 through 7

   0.7850   0.9487   0.7301   0.4397   0.3730   0.4284   0.7657
   0.8871   0.7657   0.8992   0.3187   0.3835   0.4146   0.7608

  Columns 8 through 14

   0.7223   0.6025   0.5088   0.6240   0.4397   0.6703   0.3187
   0.7657   0.6222   0.6240   0.4397   0.4624   0.6240   0.5088

vy_original =
  Columns 1 through 7

   0.6443   0.6325   0.4614   0.7973   0.6154   0.4539   0.5924
   0.6686   0.5924   0.3886   0.8747   0.6136   0.4220   0.6185
  Columns 8 through 14

   0.4751 0.5482   1.6438   1.0417   0.7973   0.8772   0.8747
   0.4752 0.5317   1.0417   0.7973   0.7778   1.0417   1.6438

The above data (vxoriginal and vyoriginal) are part of the vertices produce by Matlab®
from a 30 random points to create the Voronoi network

ii)   The production of the Voronoi diagram

The Voronoi diagram is plotted by the following Matlab code
(clipping from Matlab® program codes)

```
plot(vx_original,vy_original,'-');
axis([0 1 0 1]);
```

This will produce the graphical presentation of the Voronoi diagram in (1 x 1) scale
(clipping from Matlab® Figure file)
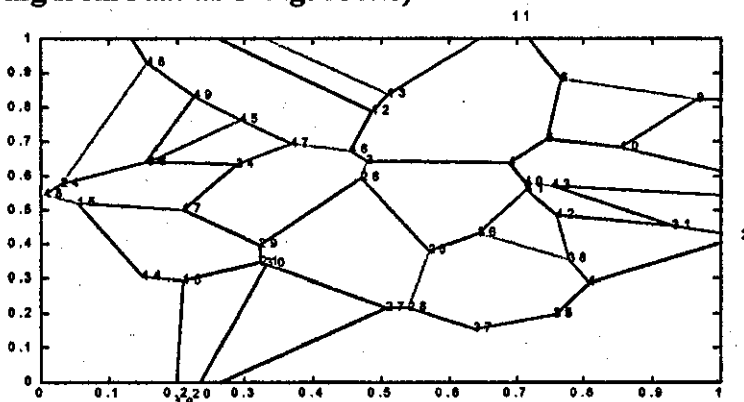
Fig 5.18 An example of a Voronoi network from 30 random points. The nodes have
been labelled by a program code **lablenode.m**

189

(clipping from Matlab® work space)

The node number and its coordinate

NODE(o)	vx(o)	vy(o)
1	0.8078	0.2909
2	1.03	0.4246
3	0.4784	0.6427
4	0.688	0.6368
5	0.7457	0.7061
6	0.7647	0.8819
7	1.249	0.5022
8	3.524	0.6292
9	0.965	0.8248
10	0.8533	0.6821
11	0.6945	1.062
12	0.4864	0.7895

GB#	vxstrt(o)	vxend(o)	vystrt(o)	vyend(o)	gblength(o)	gbangle(o)
1	0.8078	1.03	0.2909	0.4246	0.2589	31.08
2	0.4784	0.688	0.6427	0.6368	0.2096	-1.608
3	0.7457	0.7647	0.7061	0.8819	0.1768	83.83
4	1.249	3.524	0.5022	0.6292	2.279	3.196
5	0.965	0.8533	0.8248	0.6821	0.1812	51.94
6	0.7647	0.965	0.8819	0.8248	0.2083	-15.92
7	0.6945	0.7647	1.062	0.8819	0.1931	-68.67
8	0.965	3.524	0.8248	0.6292	2.567	-4.37
9	0.4864	0.5102	0.7895	0.8374	0.05351	63.63
10	0.15	0.05434	0.3056	0.5198	0.2346	-65.95

(A part of the output of function file **lablenode.m** listing down the nodes number , grain boundary number and its geometrical properties)

NODMAT =
 Columns 1 through 12

```
0   1   0   0   0   0   0   0   0   0   0   0
1   0   0   0   0   0   1   0   0   0   0   0
0   0   0   1   0   0   0   0   0   0   0   0
0   0   1   0   1   0   0   0   0   0   0   0
0   0   0   1   0   1   0   0   0   1   0   0
0   0   0   0   1   0   0   0   1   0   1   0
0   1   0   0   0   0   0   1   0   0   0   0
0   0   0   0   0   0   1   0   1   0   0   0
```

(A part of the output from function file **conmtrix.m** which forms a connectivity matrix **NODMAT** which contains the connectivity information of all the nodes in the Voronoi diagram (for this example, reference to fig 5.18, node 1 is connected to node 2, therefore NODMAT (1,2)s = 1, also node 3 is connected to node 4,i.e. NODMAT(3,4)=1)etc.)

GBMAT =
 Columns 1 through 12

```
0   1   0   0   0   0   0   0   0   0   0   0
1   0   0   0   0   0   25  0   0   0   0   0
0   0   0   2   0   0   0   0   0   0   0   0
0   0   2   0   66  0   0   0   0   0   0   0
0   0   0   66  0   3   0   0   0   65  0   0
0   0   0   0   3   0   0   0   6   0   7   0
0   25  0   0   0   0   0   4   0   0   0   0
0   0   0   0   0   0   4   0   8   0   0   0
0   0   0   0   0   6   0   8   0   5   0   0
```

(A part of the output from function file **conmtrix.m** which forms a grain boundary matrix **GBMAT** which contains the information of all the grain boundary number in the Voronoi diagram (for this example, reference to fig 5.18, node 1 is connected to node 2, therefore GBMAT(1,2) = 1(grain boundary number 1), also node 3 is connected to node 4 i.e GBMAT(3,4)=2(grain boundary number 2), etc.)

LGTHMAT
Columns 29 through 35

```
0   0   0        0       0   0   0.1059
0   0   0.1042   0       0   0   0
0   0   0        0       0   0   0
0   0   0        0       0   0   0
0   0   0        0       0   0   0
0   0   0        0       0   0   0
0   0   0        0.0596  0   0   0
0   0   0        0       0   0   0
0   0   0        0       0   0   0
0   0   0        0.3754  0   0   0
```

(A part of the output from function file **conmtrix.m** which forms a length of grain boundary matrix **LGTHMAT** which contains the information of all the length of the grain boundary in the Voronoi diagram (for this example, reference to fig 5.18, node 1 is connected to node 35, therefore LGTHMAT(1,35) = 0.1059(the length of grain boundary connecting node 1 and node 35), also node 2 is connected to node 31 i.e LGTHMAT(2,31)=0.1042(length of grain boundary connecting node 2 and node 31), etc.)

ANGLEMAT

Columns 29 through 35

```
0   0   0          0   0   0   61.1117
0   0   -17.1422   0   0   0   0
0   0   0          0   0   0   0
0   0   0          0   0   0   0
0   0   0          0   0   0   0
0   0   0          0   0   0   0
0   0   0   -19.5346   0   0   0
0   0   0          0   0   0   0
```

```
0    0    0     0      0    0    0
0    0    0  -25.2303   0    0    0
```

(A part of the output from function file **conmtrix.m** which forms the angle of orientation of grain boundary matrix ANGLEMAT which contains the information of all the orientation of the grain boundary in the Voronoi diagram (for this example, reference to fig 5.18, node 1 is connected to node 35, therefore ANGLEMAT(1,35) = 61.1117(the orientation angle of grain boundary connecting node 1 and node 35), also node 2 is connected to node 31 i.e ANGLEMAT(2,31)=-17.1422(the orientation angle of grain boundary connecting node 2 and node 31), etc.)

These matrices are important to provide information or use as test condition for executing statement in the program when performing the annealing processes. The data of these matrices will be updated for every time step in the annealing process.

b)   The annealing process of the film

In this simulation example, the Al film will undergo the annealing process during which the grain will grow in sizes. The time duration for the process is set to be unlimited i.e. it depends how many time steps needed. A program code **annealing.m** is used to do the simulation.
(clipping from Matlab® work space)

the number of annealing timestep needed: *5*
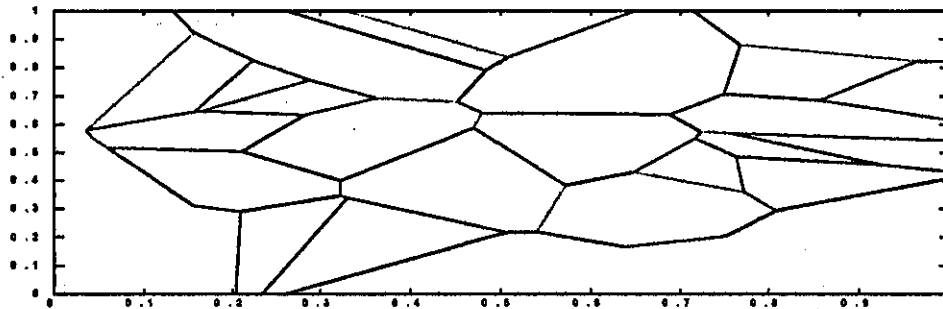
Fig 5.19 An example of the final picture of an annealed sample of Al film after going the annealing processes for a duration of 5 time steps.

c)   The production of the interconnect samples

In this simulation , 10 equal sized of samples from the non-annealed/annealed Al films are produced. The process involved in slicing the Al films into various samples depend on the width of the samples required.
(clipping from Matlab® program codes)

192

Run the clipping process to obtain a realistic interconnect
Number of samples of interconnect lines required: *10*
(clipping from Matlab® Figure file)
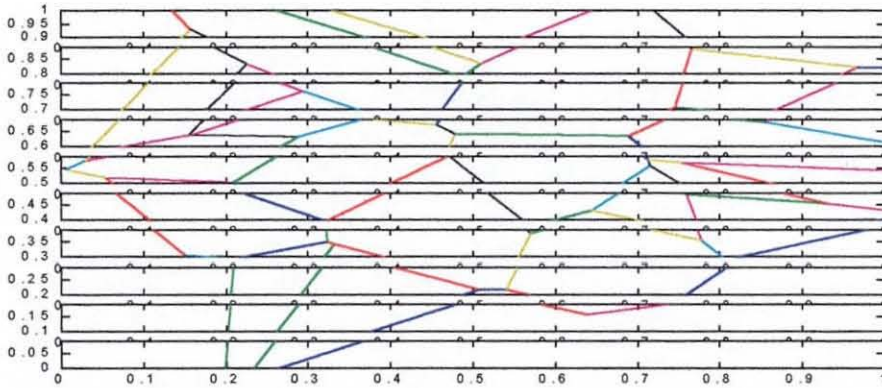
Fig 5.20 An example of 10 samples of interconnect (clipping from Matlab Figure file)

d)   The calculation of the Time to Failure of interconnect sample

i)   The slicing process to form a patterned interconnect sample

In this simulation, the interconnect samples are patterned according to the required size
by a slicing process. A program code **slice2.m** is used for this purpose.

(clipping from Matlab® workspace)

sampleno =

1

the y clip start point axis= *0.3*
the y clip end point axis= *0.4*

(Cliping from Matlab® Figure File)
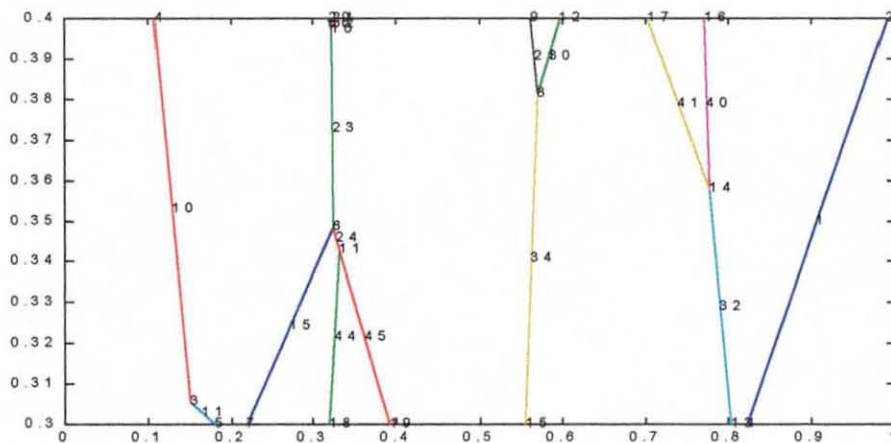
FIG 5.21 An example of interconnect sample after the slicing process

193

In the slicing process, the grain boundaries inside the box are detected and the nodes and the grain boundaries are re-labelled with new points and the information on the geometry is calculated as indicated below. The (o) indicates old value and (n) indicates new value.

(clipping from Matlab® work space)
gbinbox =

Columns 1 through 12

　1　10　11　15　21　23　24　30　32　34　40　41
Columns 13 through 16
　44　45　50　52
(these number represents the grain boundaries identification number that are found inside the sliced area or box)

nogbinbox = (total of grain boundaries inside the box)

16

(The number represents the total number of grain boundaries found in the sliced area or box)

ii)　**The re-labelling of the new nodes and the calculation of new geometrical properties**

GB	vxs(o)	vxs(n)	vxe(o)	vxe(n)	vys(o)	vys(n)	vye(o)	vye(n)
1	0.8078	0.8229	1.03	0.9888	0.2909	0.3	0.4246	0.4
10	0.15	0.15	0.05434	0.1078	0.3056	0.3056	0.5198	0.4
11	0.2083	0.1806	0.15	0.15	0.2949	0.3	0.3056	0.3056
15	0.324	0.324	0.2083	0.2194	0.3485	0.3485	0.2949	0.3
21	0.5704	0.5704	0.4693	0.5614	0.3812	0.3812	0.5928	0.4
23	0.3218	0.3218	0.324	0.324	0.3971	0.3971	0.3485	0.3485
24	0.324	0.324	0.3304	0.3304	0.3485	0.3485	0.3429	0.3429
30	0.6446	0.5972	0.5704	0.5704	0.4331	0.4	0.3812	0.3812
32	0.8078	0.8035	0.7766	0.7766	0.2909	0.3	0.3578	0.3578
34	0.5704	0.5704	0.5405	0.5556	0.3812	0.3812	0.2167	0.3
40	0.7766	0.7766	0.7585	0.7706	0.3578	0.3578	0.4859	0.4
41	0.6446	0.7027	0.7766	0.7766	0.4331	0.4	0.3578	0.3578

(The above data represents the grain boundary geometry information where)

GB　　　　　　　grain boundary number

vxs(o)	the old value of vx start coordinates for the grain boundary	
vxe(o)	the old value of vx end coordinates for the grain boundary	
vys(o)	the old value of vy start coordinates for the grain boundary	
vye(o)	the old value of vy end coordinates for the grain boundary	
vxs(n)	the vx end coordinates for the grain boundary	
vxe(n)	the old value of vx end coordinates for the grain boundary	
vys(n)	the vy start coordinates for the grain boundary	
vye(n)	the vy end coordinates for the grain boundary	

NODE(n)	vx(n)	vy(n)
1	0.8229	0.3
2	0.9888	0.4
3	0.15	0.3056
4	0.1078	0.4
5	0.1806	0.3
6	0.324	0.3485
7	0.2194	0.3
8	0.5704	0.3812
9	0.5614	0.4
10	0.3218	0.3971
11	0.3304	0.3429
12	0.5972	0.4
13	0.8035	0.3
14	0.7766	0.3578
15	0.5556	0.3
16	0.7706	0.4
17	0.7027	0.4
18	0.3183	0.3
19	0.3912	0.3
20	0.3187	0.4
21	0.324	0.4

(The new nodes identification number and its new x and y coordinates)

GB#	vxstrt(n)	vxend(n)	vystrt(n)	vyend(n)	gblength(n)	gbangle(n)
1	0.8229	0.9888	0.3	0.4	0.1937	31.08
10	0.15	0.1078	0.3056	0.4	0.1033	-65.95
11	0.1806	0.15	0.3	0.3056	0.03114	-10.44
15	0.324	0.2194	0.3485	0.3	0.1153	24.87
21	0.5704	0.5614	0.3812	0.4	0.02079	-64.45
23	0.3218	0.324	0.3971	0.3485	0.04868	-87.44
24	0.324	0.3304	0.3485	0.3429	0.008545	-41.4
30	0.5972	0.5704	0.4	0.3812	0.03274	34.95
32	0.8035	0.7766	0.3	0.3578	0.0638	-65.04
34	0.5704	0.5556	0.3812	0.3	0.08258	79.69
40	0.7766	0.7706	0.3578	0.4	0.04257	81.96

(The above data represents the grain boundary geometry information where)

GB#	grain boundary number
vxstrt(n)	the vx start coordinates for the grain boundary
vxend(n)	the vx end coordinates for the grain boundary
vystrt(n)	the vy start coordinates for the grain boundary
vyend(n)	the vy end coordinates for the grain boundary

These new data are calculated by program codes i) **newnode.m**(to label the new nodes and its grain boundaries after the slicing process), ii) **newgeometry.m** (to calculate the new geometrical properties of the grain boundaries)

iii)   The calculation of the Time to Failure

In this particular example, the Time to Failure is calculated for grain boundary cluster with the start node at Node 7 and the end node at Node 19 (Fig 5.21). The program code will automatically calculate the cluster lengths. After this point, data which are required to calculate the Time to Failure have to be keyed-in into the program code.

(clipping from Matlab® work space)

Enter the total number of clusters of grain boundaries found in sample no:1 = *3*

To calculate the length of the cluster of grain boundaries
Enter the start point of the cluster no:1 :Keyin "N(X)" X=node number= *N(7)*

Enter the end point of the cluster no:1:keyin "N(X)" X=node number= *N(19)*

clustlgh =   0.1718

The common input parameters defining the grain structure
The total number of grain boundaries in the cluster: *5*
The number of grain boundaries forming the longest path: *3*

ptsel =   3
(this number represent Node 19 is use to calculate TTF by signal delay approximation method)

The length of Grain Boundary(LG) NO 1 =*LG(15)*
x =   0.1153
Angle of Grain Boundary(Ag) NO 1 =*AG(15)*
theta =   0.4341(in radians)
The length of Grain Boundary(LG) NO 2 =*LG(24)*
x =   0.1153   0.0085
Angle of Grain Boundary(AG) NO 2 =*AG(24)*
theta =   0.4341 -0.7226

The length of Grain Boundary(LG) NO 3 =*LG(45)*
x =   0.1153   0.0085   0.0744

Angle of Grain Boundary(AG) NO 3 =*AG(45)*
theta =   0.4341   -0.7226   -0.6139

The length of Grain Boundary(LG) NO 4 =*LG(23)*
x =   0.1153   0.0085   0.0744   0.0487

Angle of Grain Boundary(AG) NO 4 =*AG(23)*
theta =   0.4341   -0.7226   -0.6139   -1.5262

The length of Grain Boundary(LG) NO 5 =*LG(44)*
x =   0.1153   0.0085   0.0744   0.0487   0.0445

Angle of Grain Boundary(AG) NO 5 =*AG(44)*
theta =-0.7226   -0.6139   -1.5262   1.2955

The letters LG and AG stands for length of grain boundary and angle of orientation respectively. All the information is stored in their respective matrices LGTHMAT and ANGLEMAT. The data are obtained by simply keying the correct grain boundary numbers. In this example , the cluster is characterised by i) the longest path consisting of grain boundaries number **15,24and 45** and ii) the wings consisting of grain boundaries number **23 and 24**. Once the data are keyed-in, the program codes will calculate automatically the Time to Failure by the lumped element model (solving the matrix equation) and the signal delay approximation method.

(Clipping from Matlab® work space)
TTFS =   0.0229

TTFELMORE =   0.0219

TTFS is the result of simulation of Time to Failure for the lumped element model and TTFELMORE is the for the Elmore delay approximation.

5.3.4 The production Al film samples for the current experiment

The samples of the Al films consisting of the grain boundaries are constructed by the Voronoi method which are also developed by others[Kirchheim& Kaeber,1991],[Joo,and Thompson,1994][Marcoux et.al,1989],[Knowlton,et.al. 1997]. In the current work, each samples of Al films is constructed from 50 random points to create the Voronoi network. The Voronoi network is scaled up to make a 1 by 1 area so as to make a presentable sample of Al films. 10 samples of non-annealed Al films are produce randomly for the experiment as shown in Figures 5.22(a)-5.22(j)
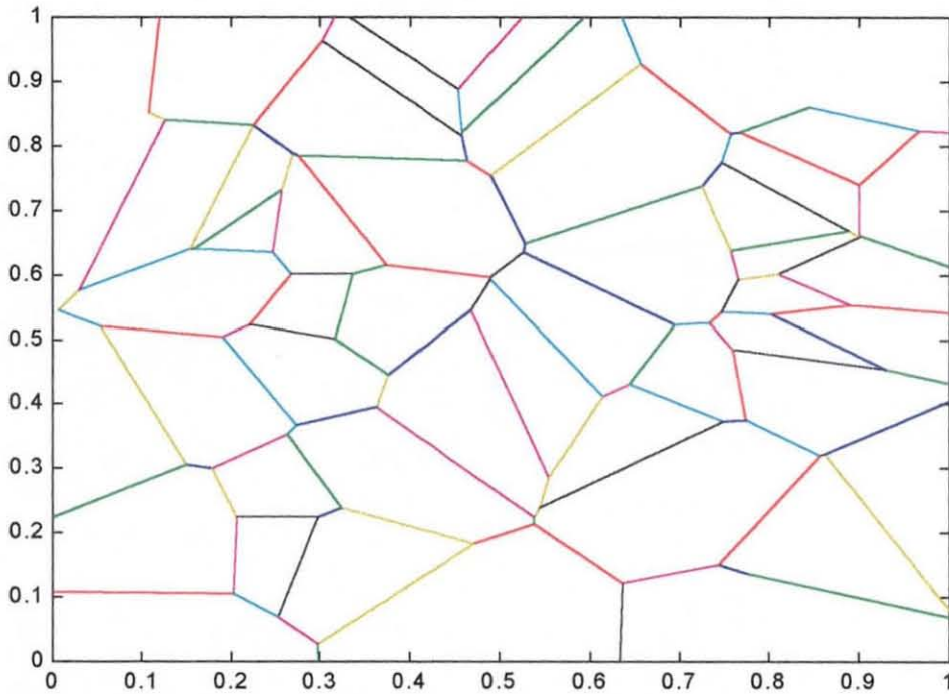
Fig 5.22(a) Voronoi network representing Al film sample no: 1
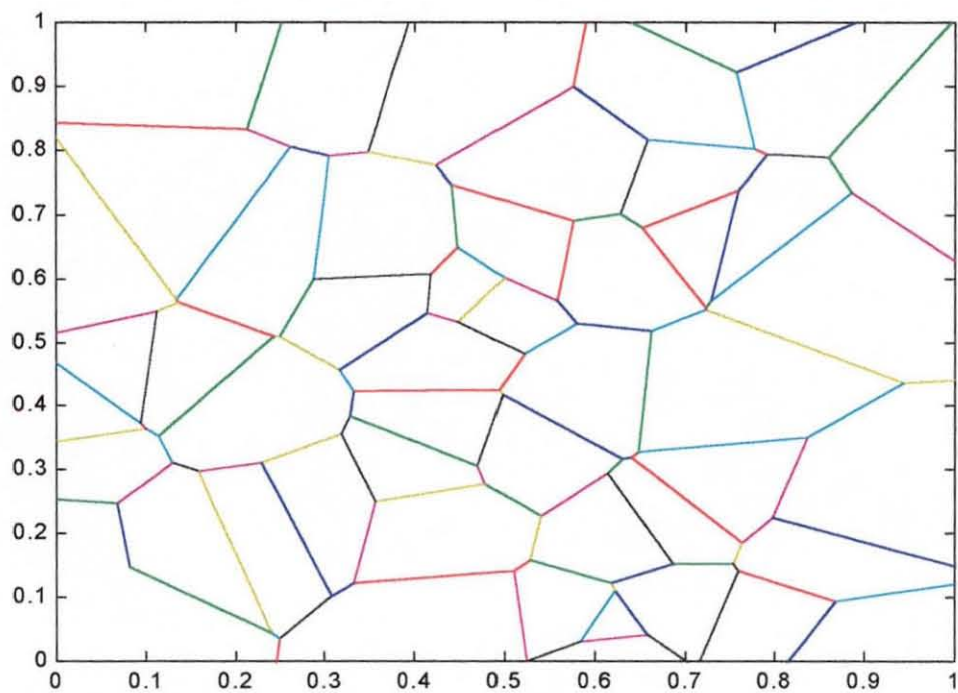
Fig 5.22(b) Voronoi network representing Al film sample no: 2
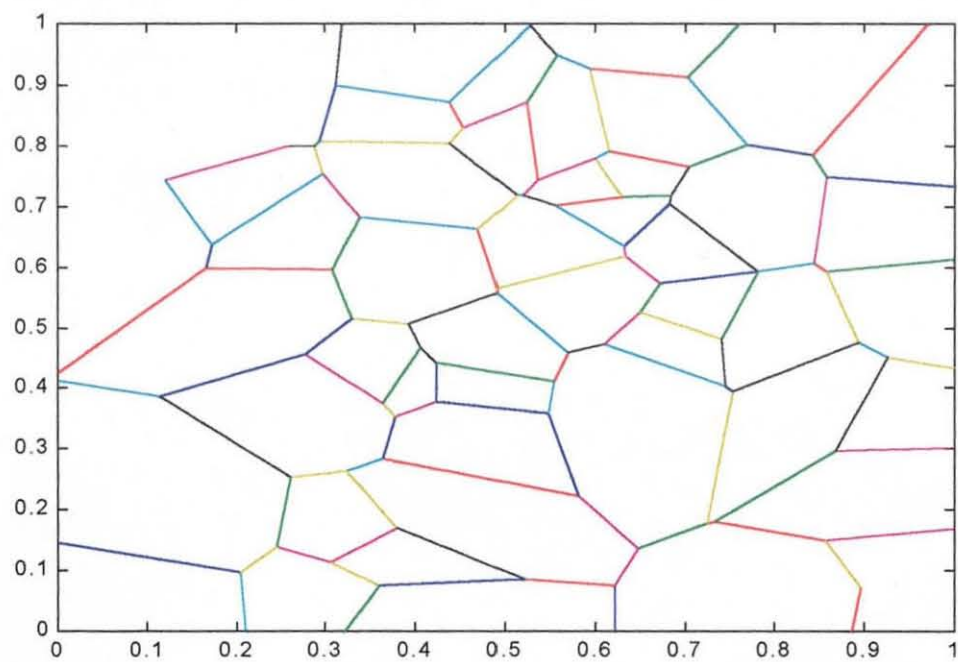
Fig 5.22(c) Voronoi network representing Al film sample no: 3
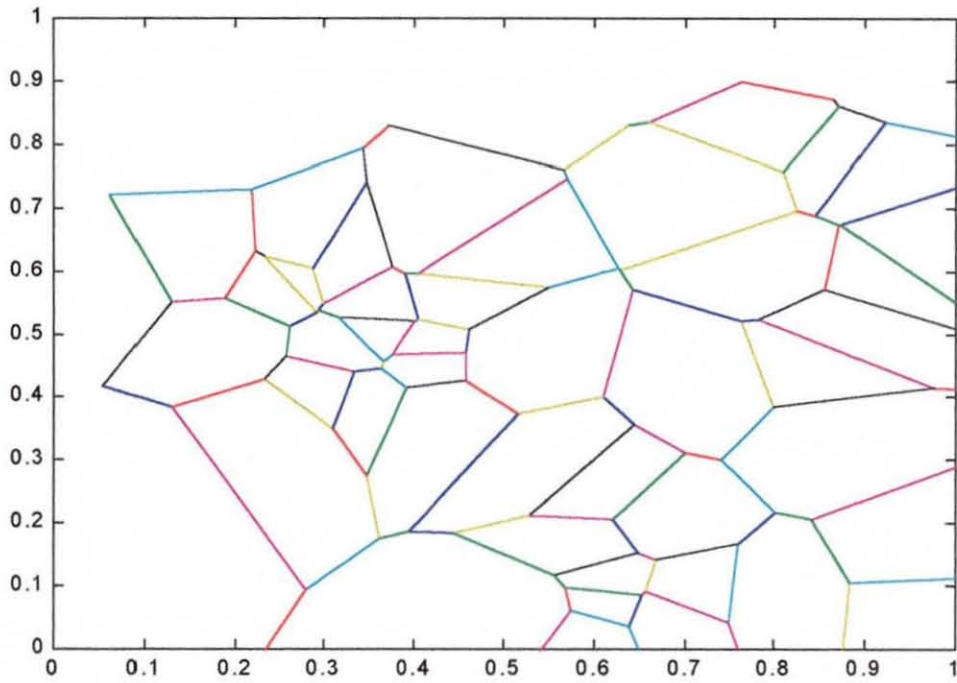
Fig 5.22(d) Voronoi network representing Al film sample no: 4
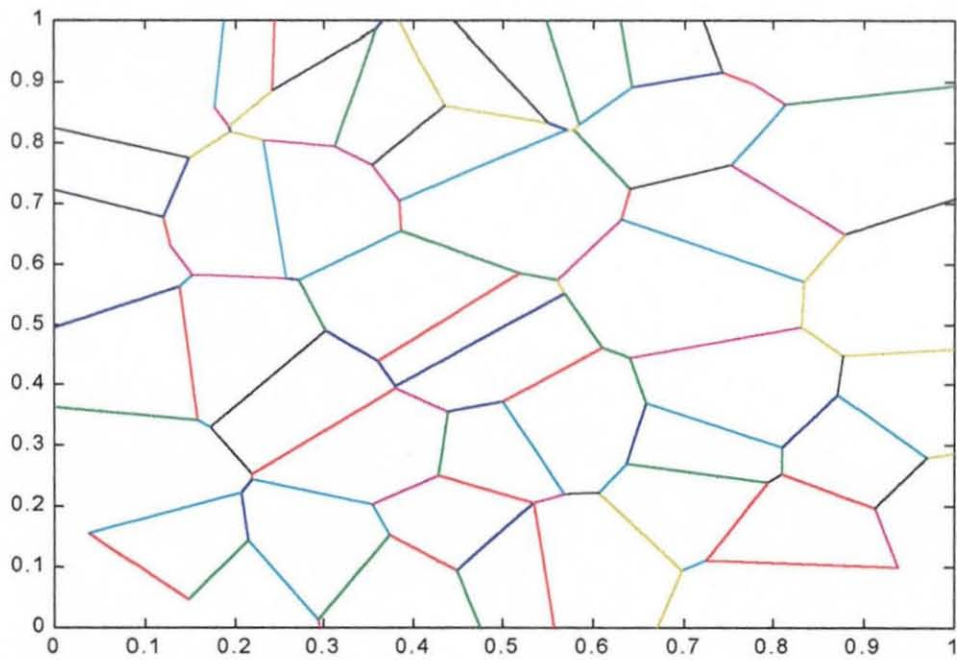
Fig 5.22(e) Voronoi network representing Al film sample no: 5
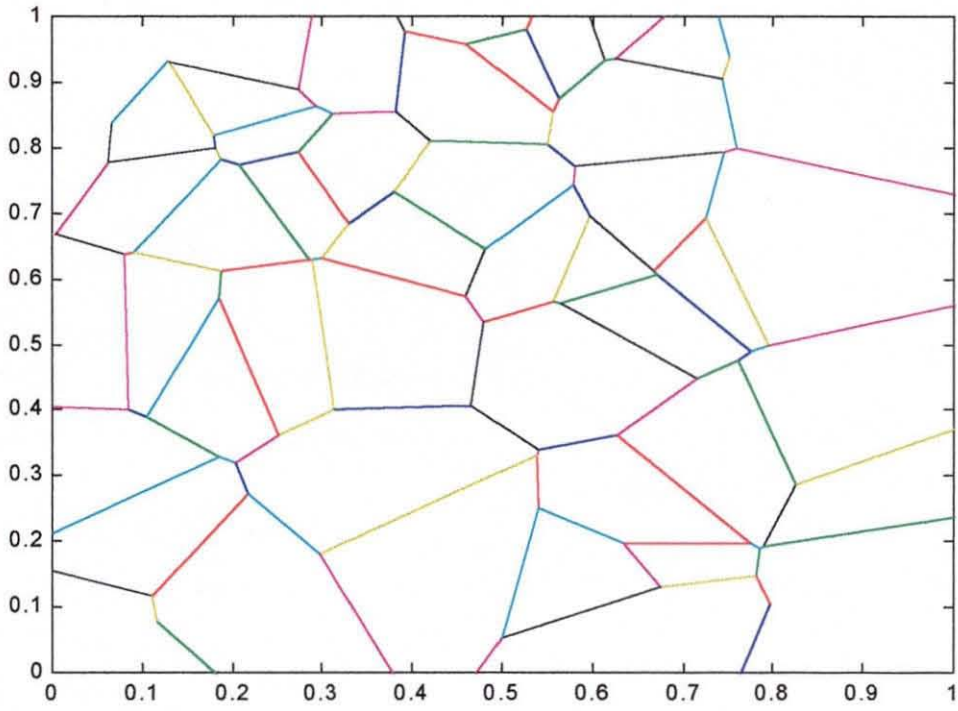
Fig 5.22(f) Voronoi network representing Al film sample no: 6
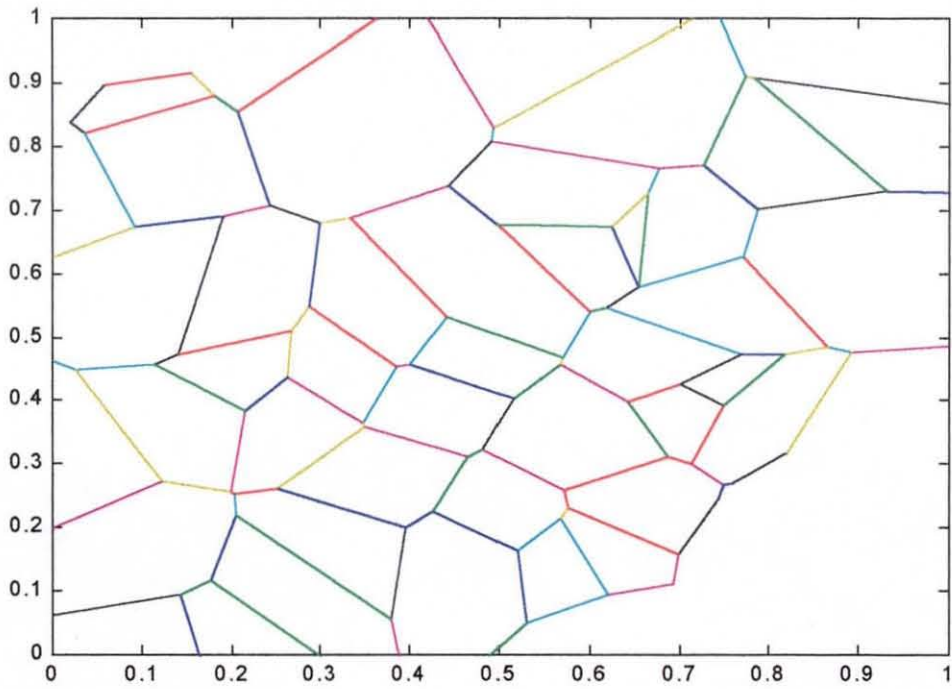
Fig 5.22(g) Voronoi network representing Al film sample no: 7
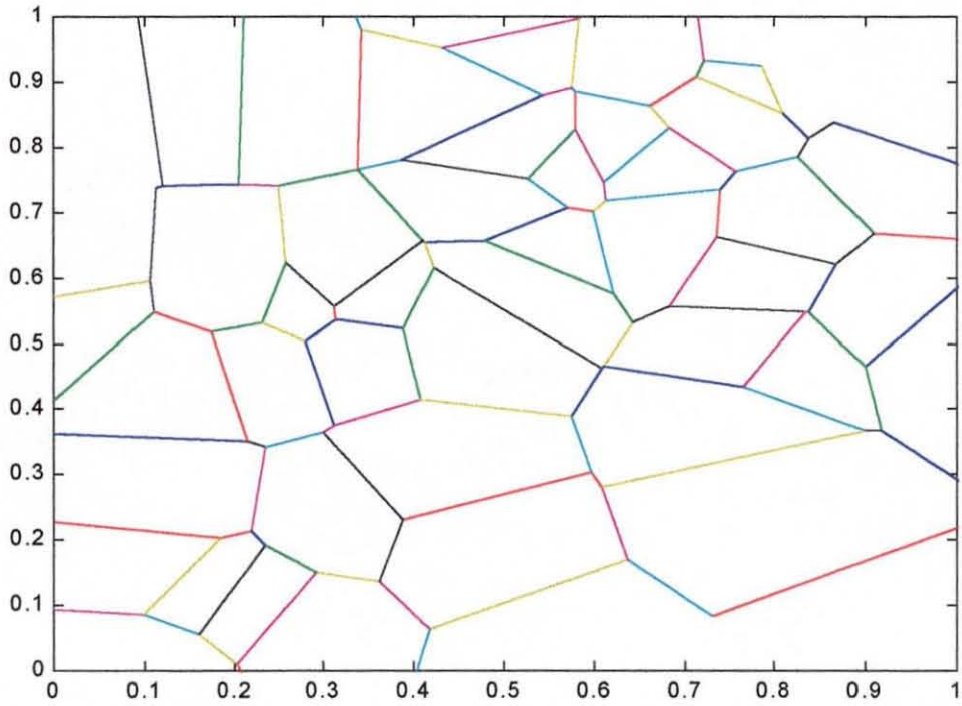
Fig 5.22(h) Voronoi network representing Al film sample no: 8
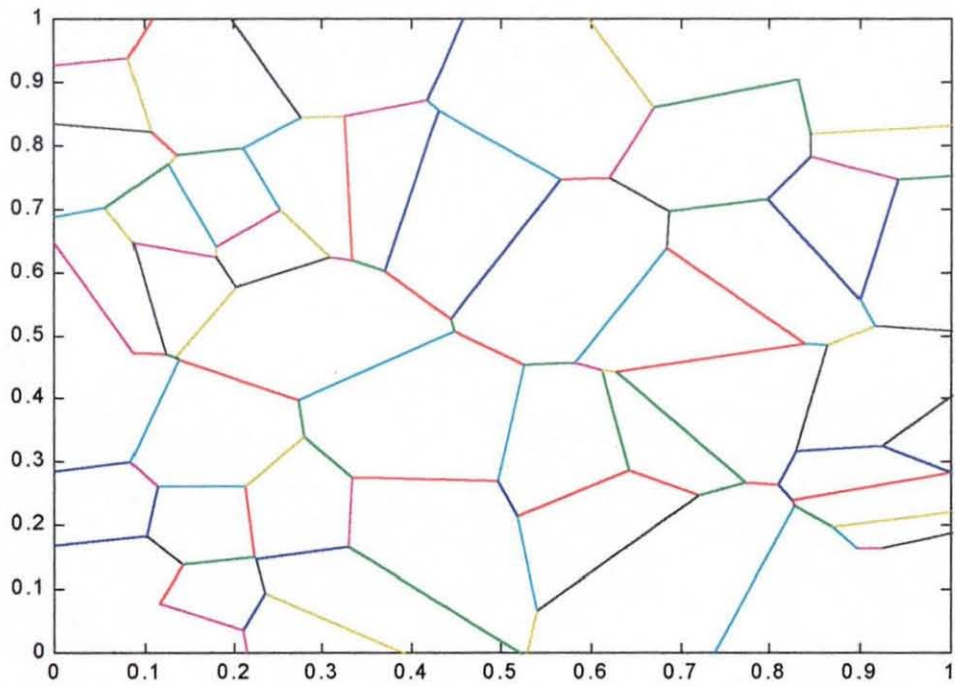
Fig 5.22(i) Voronoi network representing Al film sample no: 9
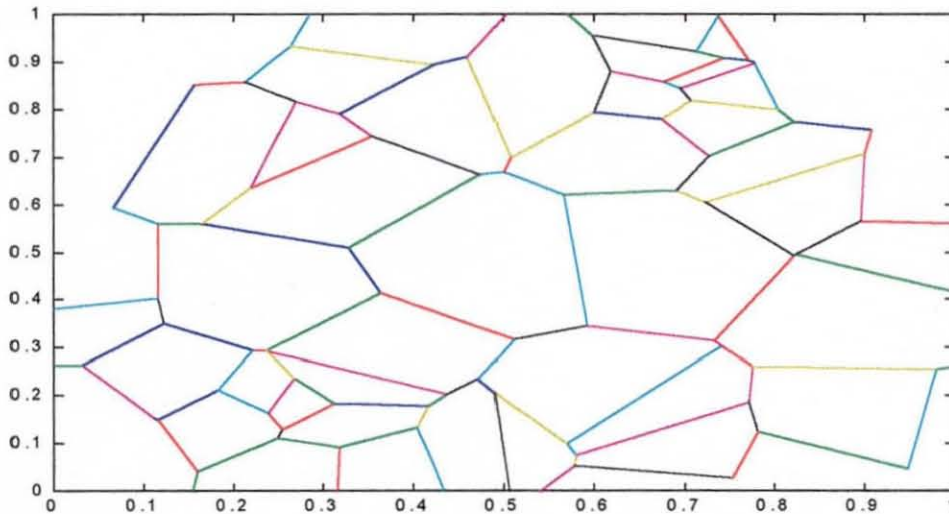
Fig 5.22(j) Voronoi network representing Al film sample no: 10

5.3.5 The simulation of the annealing process for the Al film samples

The annealing treatment of the Al films is simulated by increasing the size of the grains. A Matlab® program code (annealing.m) is developed to simulate this by using the rules developed in the Vertex model for 2D grain growth[Kawasaki et.al,1989].Other references which produces the simulation of grain growth/annealing includes [Weaire and Kermode,1983] who work on the 2-dimensional soap froth, [Mulheran,1992] who work on the statistical properties of 2-dimensional random Voronoi network, [Anderson et.al,1984] who simulate the grain growth using Monte Carlo method, [Frost, et al.,1990] who work on the effect of grain boundary grooving at the free surface of a film by introducing the stagnation condition on grain boundary. The Kawasaki reference is important here because it is the only reference available which provides an algorithm in simulating the annealing processes which is thought to be suitable in the current work as it involves the manipulation of the coordinates of the vertices in the Voronoi network.

In the current work, simulation of the annealing process does not include the groove-induced stagnation condition , where after the film is annealed for a time τ_{stag}, total stagnation occurs. Also the simulation does not include the post-patterning of the

203

interconnect where the interconnect is subjected to another annealing process[Knowlton,et.al]. In the current work, the simulation of the annealing process is based on the work of [Joo and Thompson,1994] and [Kircheim and Kaeber,1991] and does not include those extra annealing processes.

The annealing simulation will improve the Voronoi network which are initially produced by the built-in function of MATLAB. The simulation of the annealing process will produce a different layout of the grain boundaries through stretching or compressing effect/force on the grain boundaries. The simulation will exhibit the growth and the collision of grain boundaries, and processes where grain boundaries can recombine or be annihilated when a grain boundary length shrink below critical value. Essentially during the annealing process large grains grow at the expense of small grains, and grains become more spherical. An example of the annealed Al film, produced by Kircheim & Kaeber is shown in Fig 5.23 below.
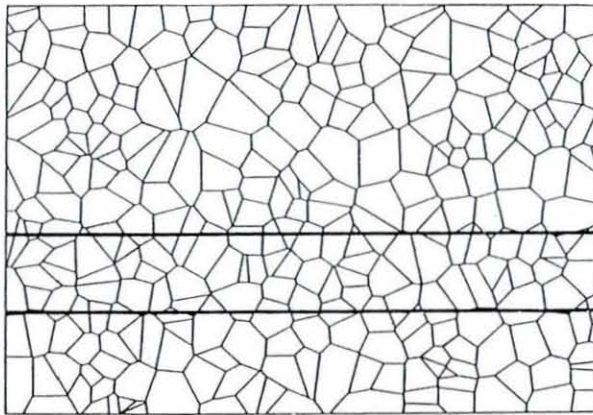
Fig 5.23 Al film sample from [Kirchheim.R and Kaeber.U,.1991]

An example of the simulation results using the program code **annealing.m** is shown in Fig. 5.24 to show the growth, annihilation and recombination processes. The Voronoi network is created from 20 random points
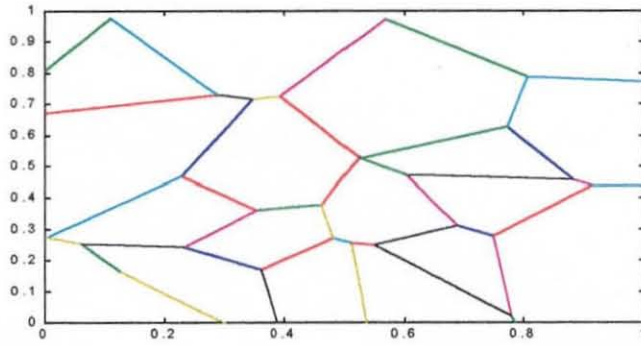
Fig 5.24(a) Voronoi network before annealing
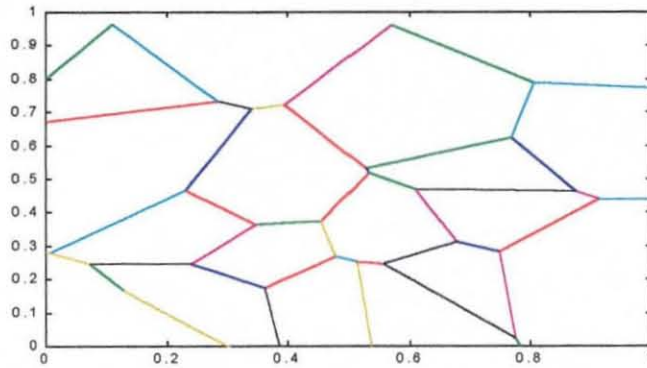
Fig 5.24(b) After annealing 1 time step (growing and recombination of grain)
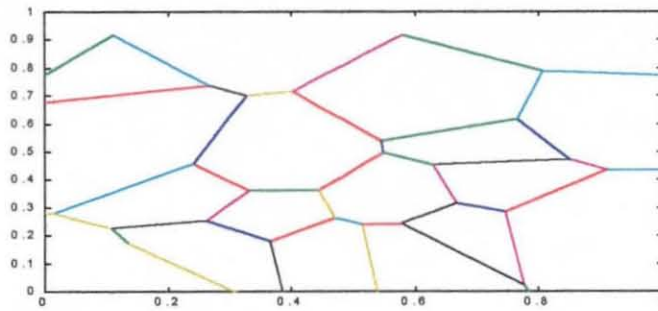
Fig 5.24(b) After annealing 5 time step (growing and recombination of grain)
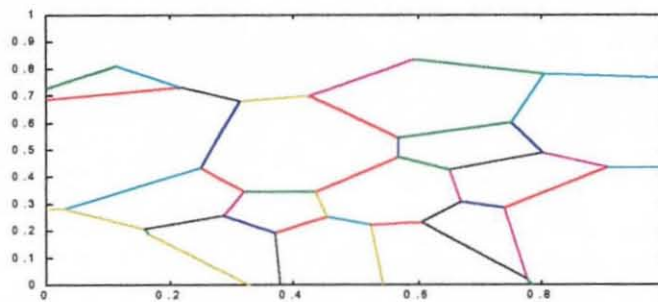
Fig 5.24(c) After annealing 10 time step (growing of grain)

205
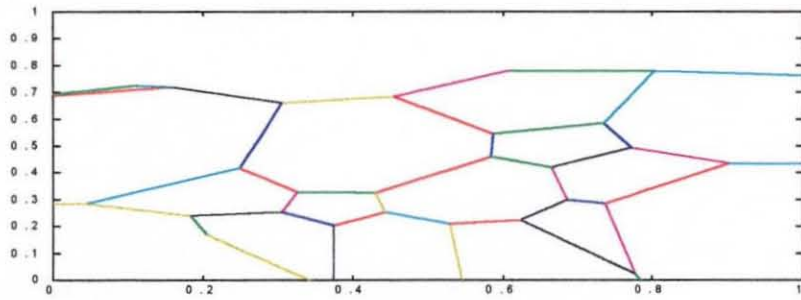
Fig 5.24(c) After annealing 15 time step (growing of grain)
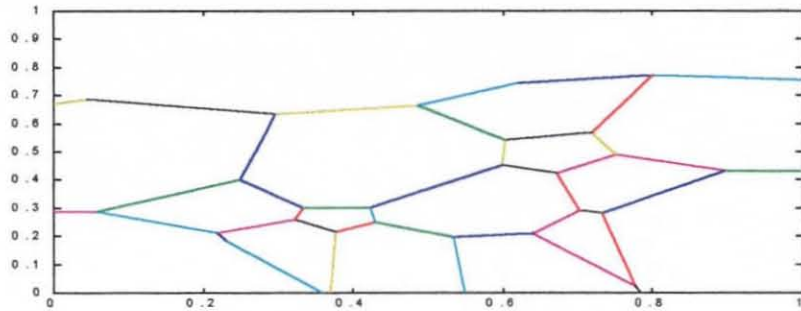
Fig 5.24(d) After annealing 20 time steps (growing and annihilation of grain)

Another example of the simulation results using the program code **annealing.m** is shown in Fig. 5.25 from larger Voronoi network created from 100 random points
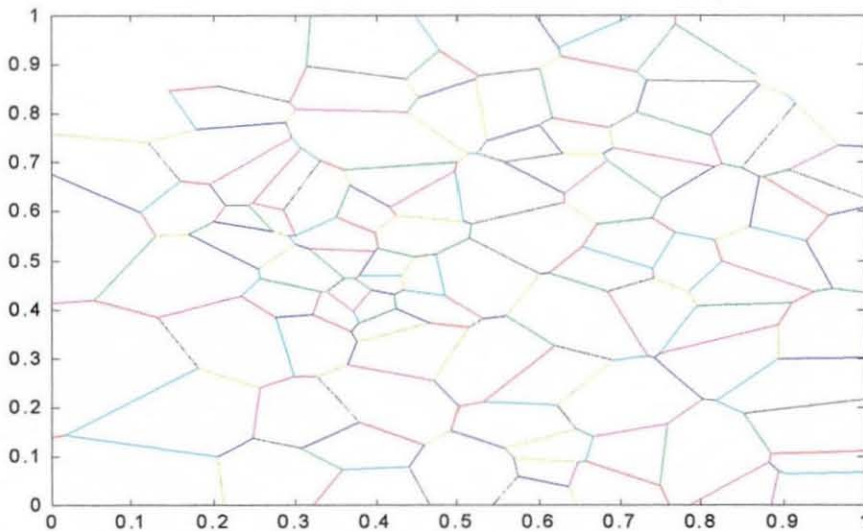
Fig 5.25(a) Before annealing
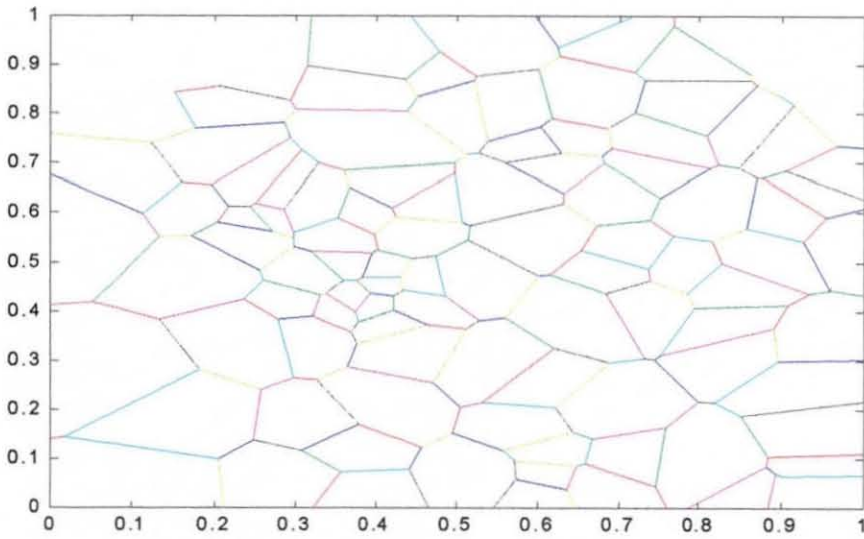
Fig 5.25(b)   After annealing 2 time steps
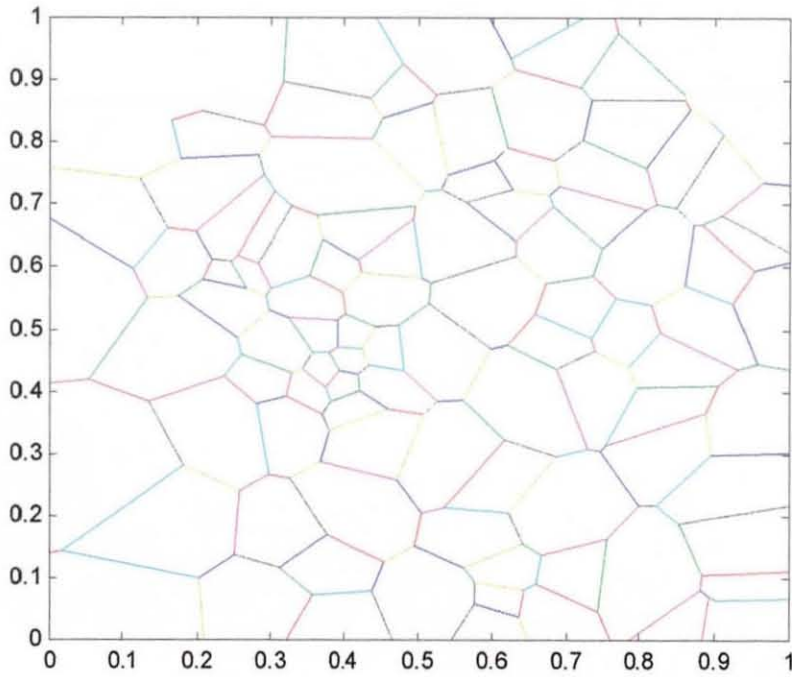
Fig 5.25(c) After annealing 4 time steps
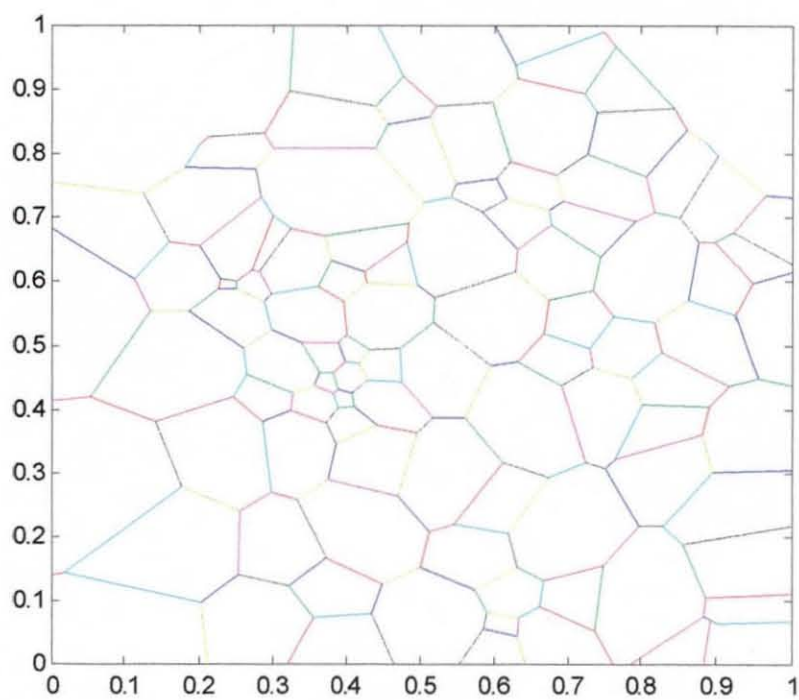
Fig 5.25(d) After annealing 6 time steps
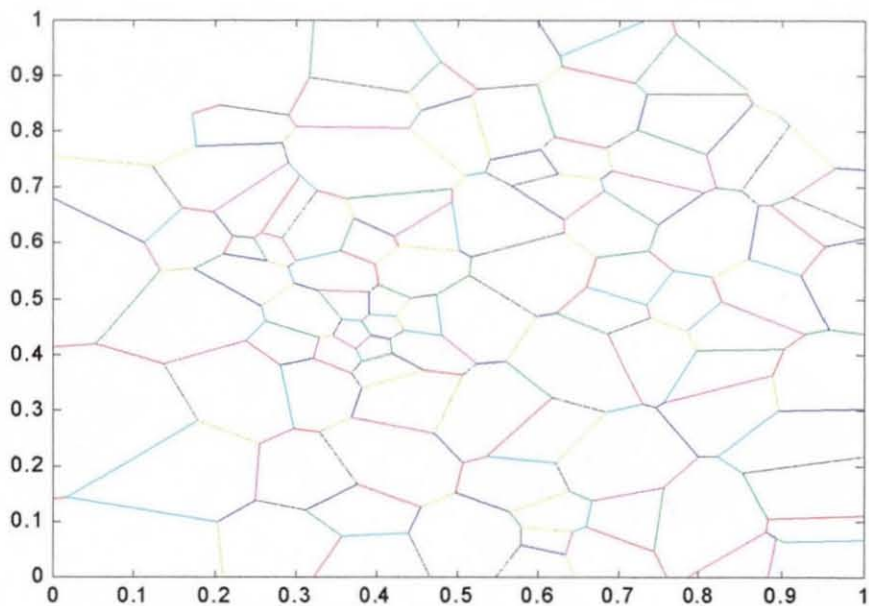
Fig 5.25(e) After annealing 11 time steps
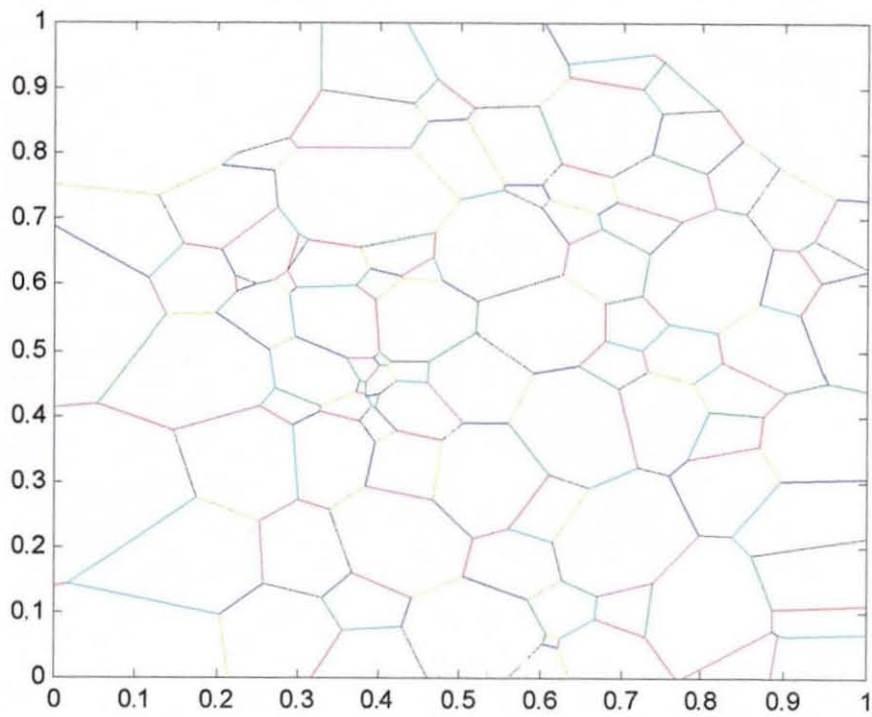
5.25(f)   After annealing 20 time steps

For the current experiment, 10 samples of Al films of the original non-annealed film of Fig5.22(a)-5.22(j) have been annealed for a duration of five time steps are shown in Fig.5.26(a)-5.26(j).
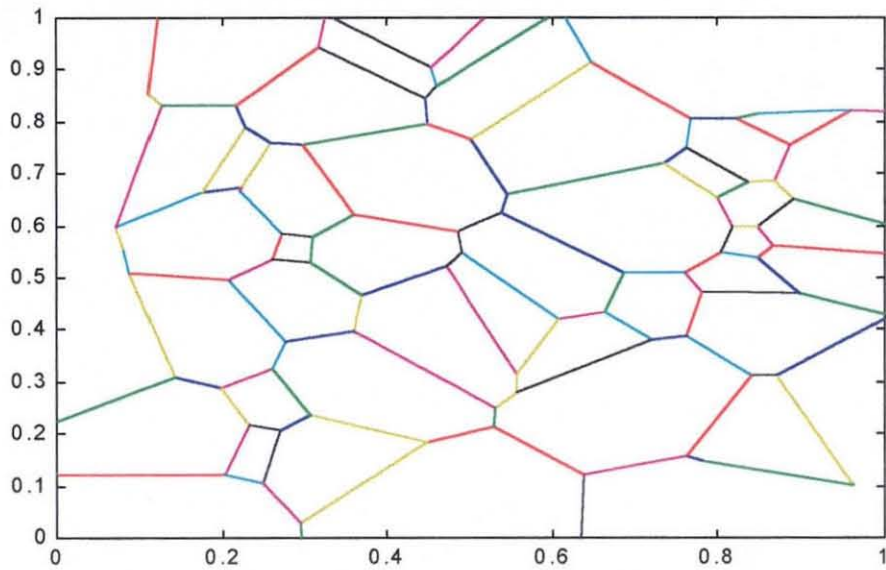
Fig 5.26(a) Voronoi network representing the annealed Al film sample no 1
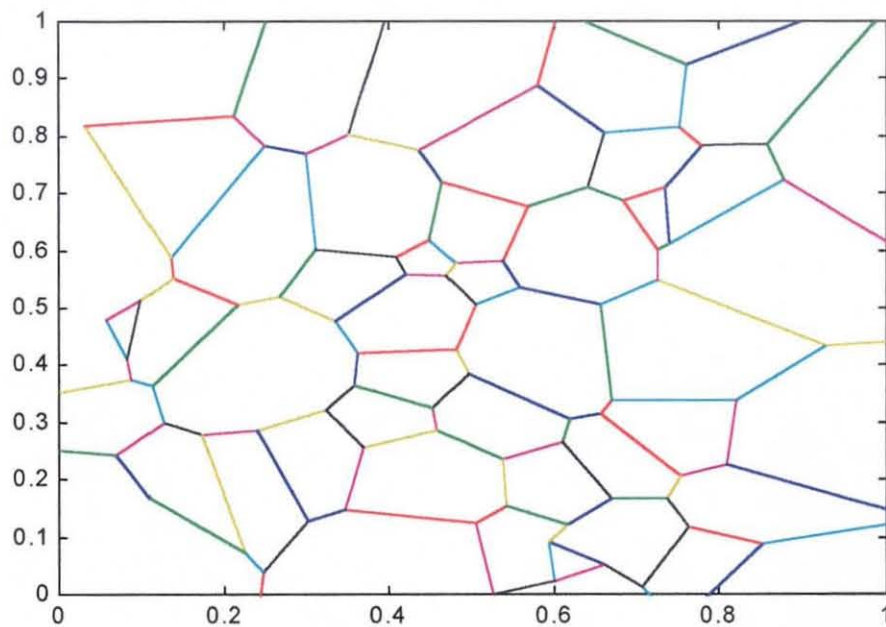
Fig 5.26(b) Voronoi network representing the annealed Al film sample no.2
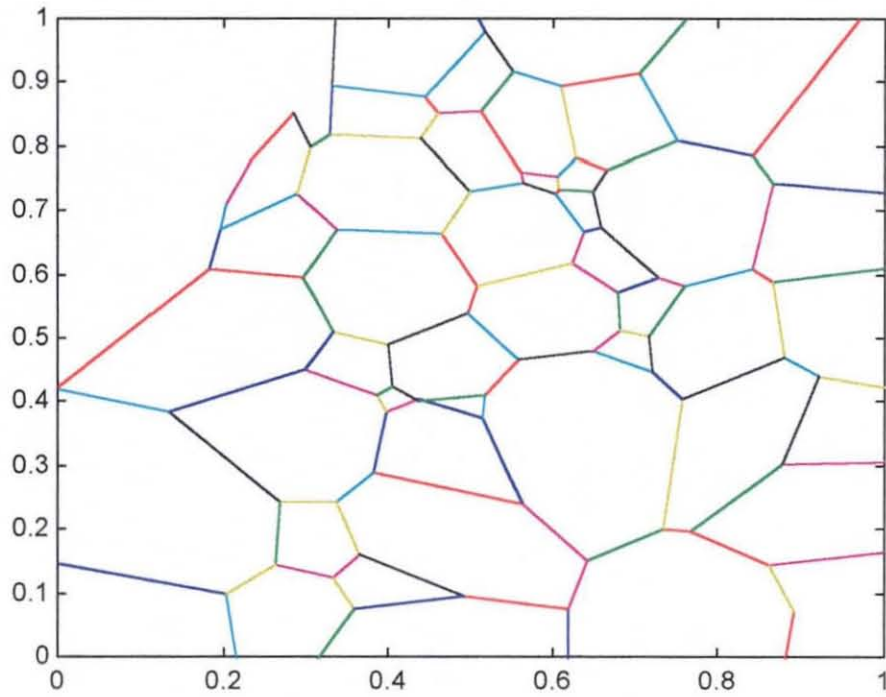
Fig 5.26(c) Voronoi network representing the annealed Al film sample no.3
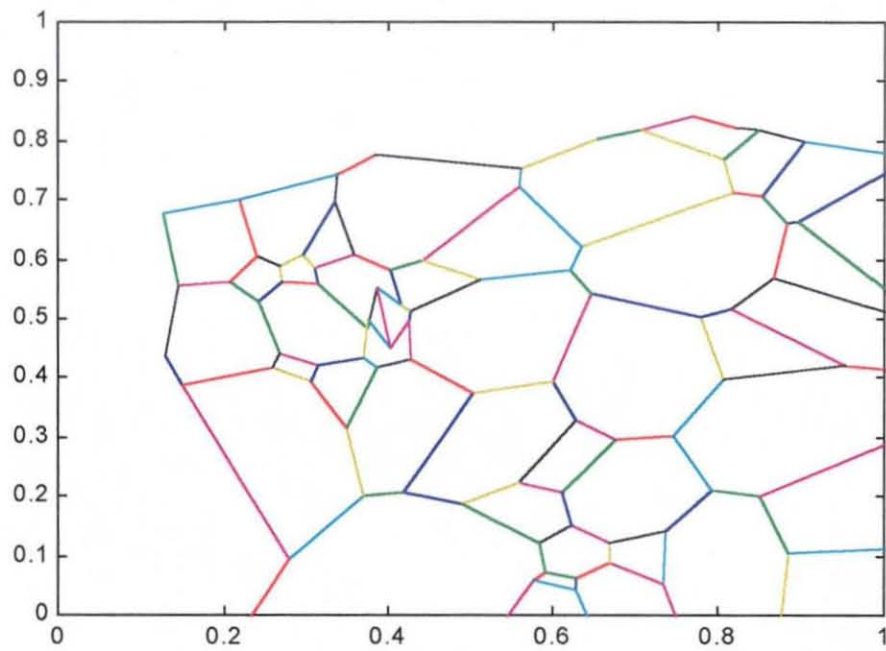
Fig 5.26(d) Voronoi network representing the annealed Al film sample no.4
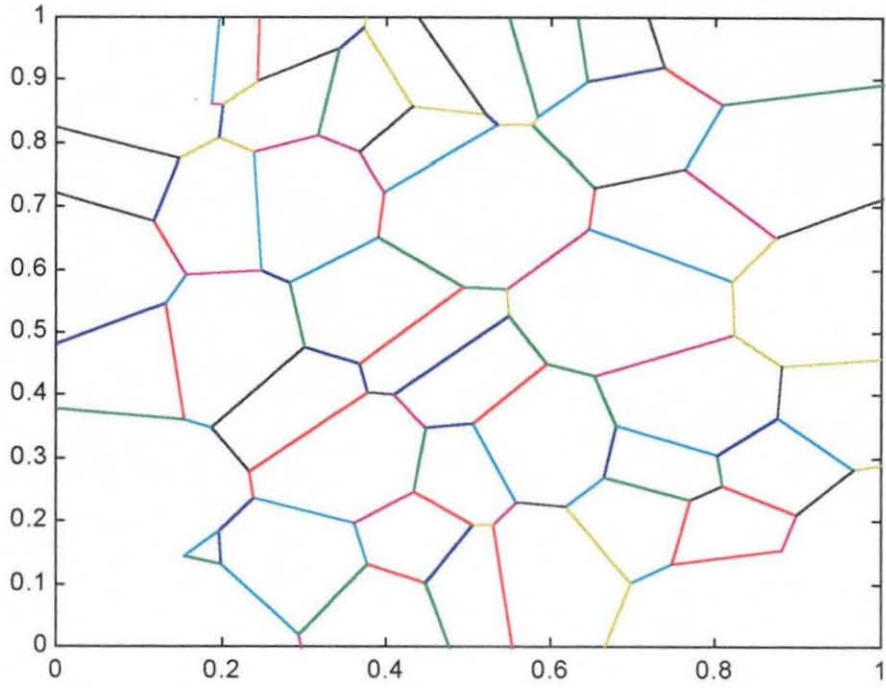
Fig 5.26(e) Voronoi network representing the annealed Al film sample no.5
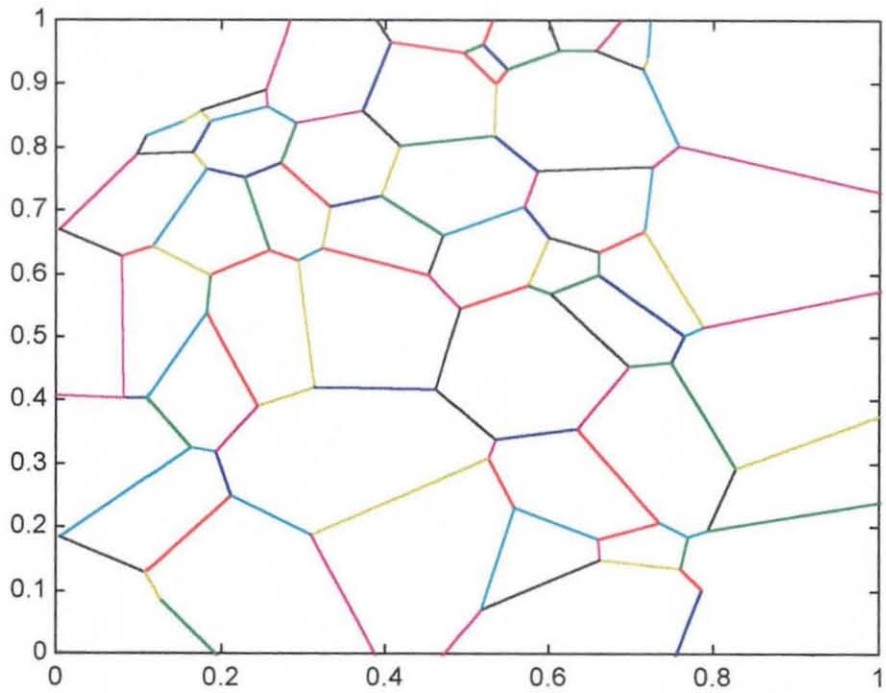
Fig 5.26(f) Voronoi network representing the annealed Al film sample no.6
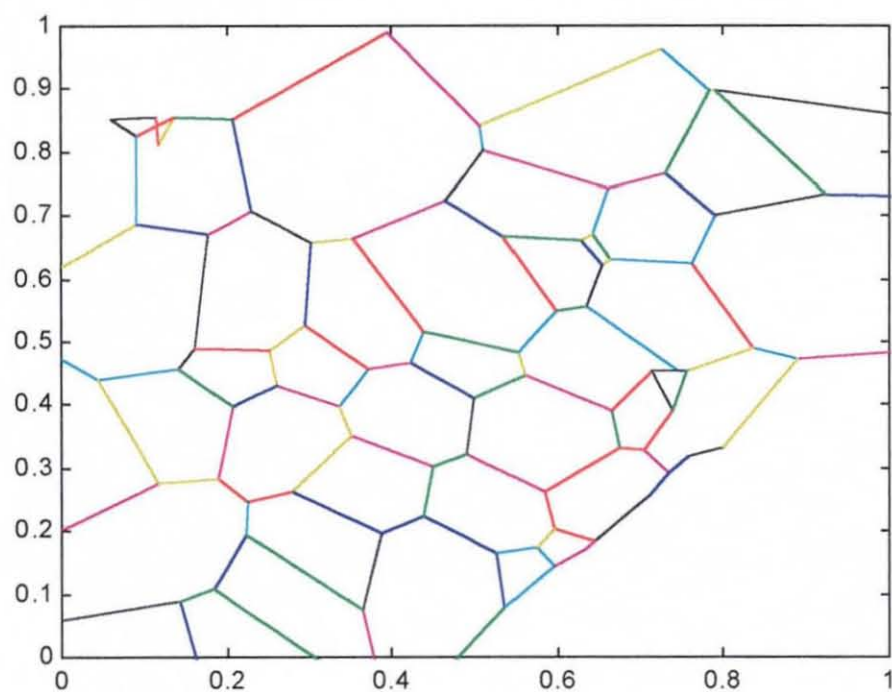
Fig 5.26(g) Voronoi network representing the annealed Al film sample no.7
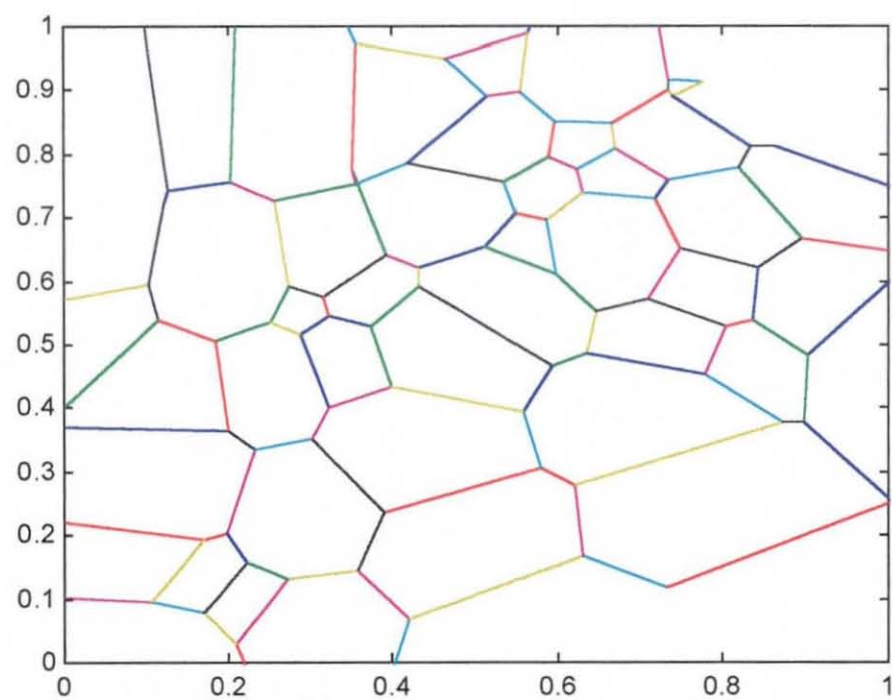
Fig 5.26(h) Voronoi network representing the annealed Al film sample no.8
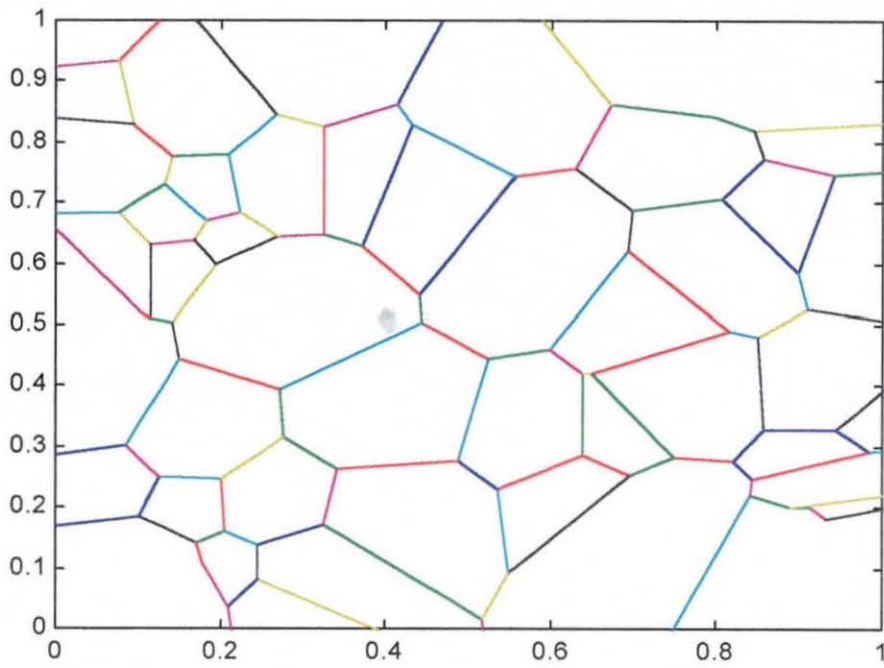
Fig 5.26(h) Voronoi network representing the annealed Al film sample no.9
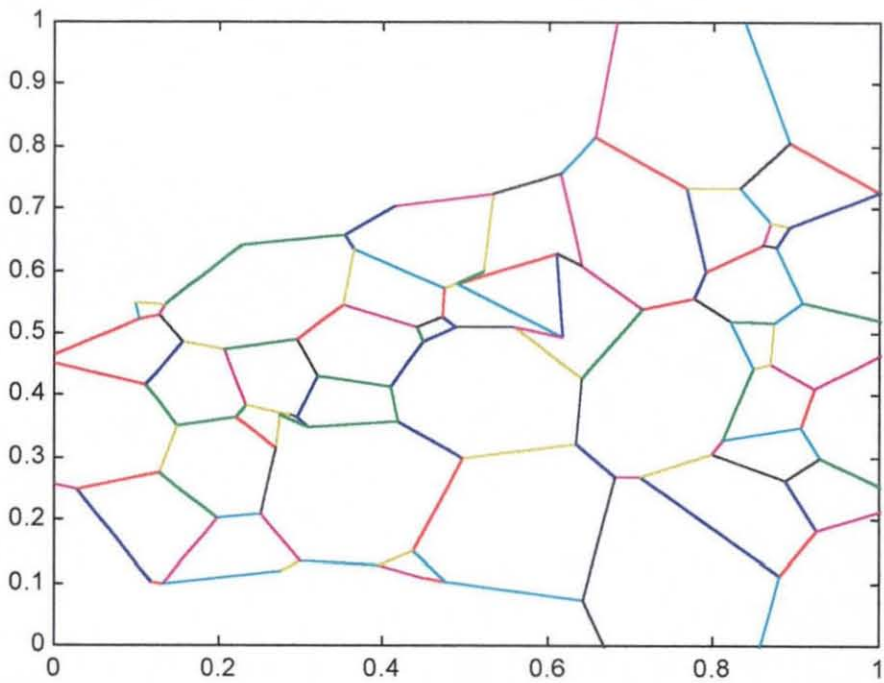
Fig 5.26(i) Voronoi network representing the annealed Al film sample no.10

5.3.6 The simulation to produce interconnects samples for experiment

The samples of IC interconnects for the experiments are produced from the 10 samples of Al films of Fig 5.22(a)-5.22(j) (non-annealed film) and of Fig 5.26(a)-Fig 5.26(j) (annealed film). Each sample of the Al films is sliced into equal samples to represent the IC interconnects depending on the size of the width of the interconnect . This simulation is performed by the program code **slice2.m** where the Voronoi diagram are being cut or slice into equal samples of interconnects. As the result of the slice, new nodes have to be recalculated as does the geometric information such as the length and angle of orientation of the grain boundaries. From this simulation, 100 samples of IC interconnects can be produced (for 0.1x1 scale). The interconnects samples will consist of a randomly distributed clusters of grain boundaries in which for each cluster will have its own characteristics consisting of:

    i)   The number of grain boundaries making up the cluster

    ii) The length of each grain boundary in the cluster

    iii) The length of the cluster (the spanning of the grain boundaries in the x direction i.e. the direction of the moving vacancies)

    iv) The angle of orientation of the grain boundaries.

These characteristics of the grain boundaries represent the complete microstructure of the interconnects which will be analysed to produce their Time to Failure. The interconnect samples under investigation are shown in Figures 5.27(a)-5.27(j) for non-annealed samples and Figures 5.28(a)-5.8(j) for annealed samples
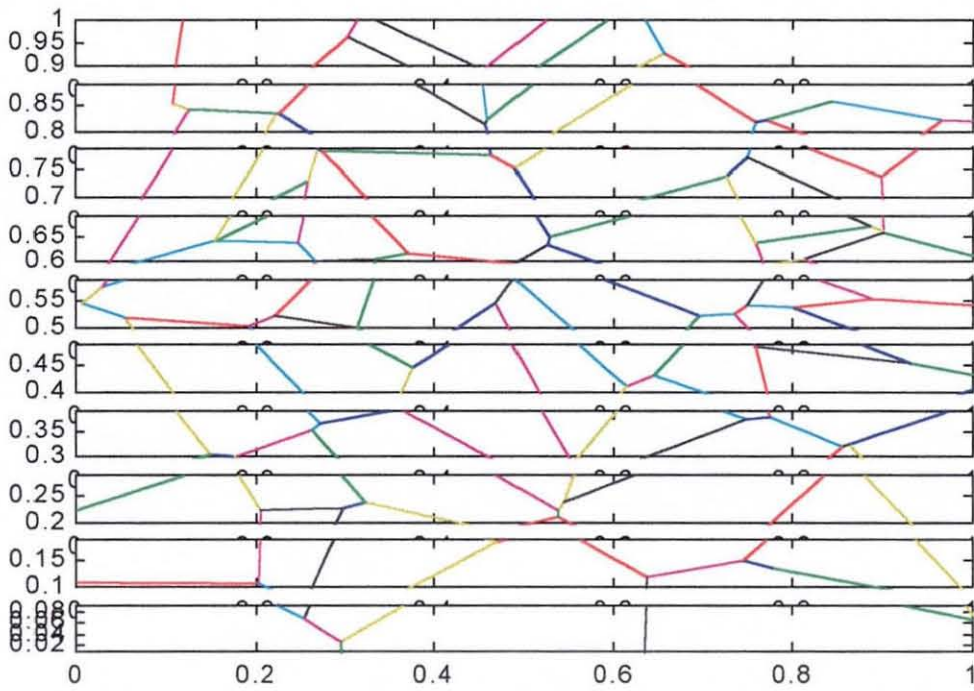
Fig.5.27(a) Interconnects samples (1-10) from non-annealed Al film sample no. 1
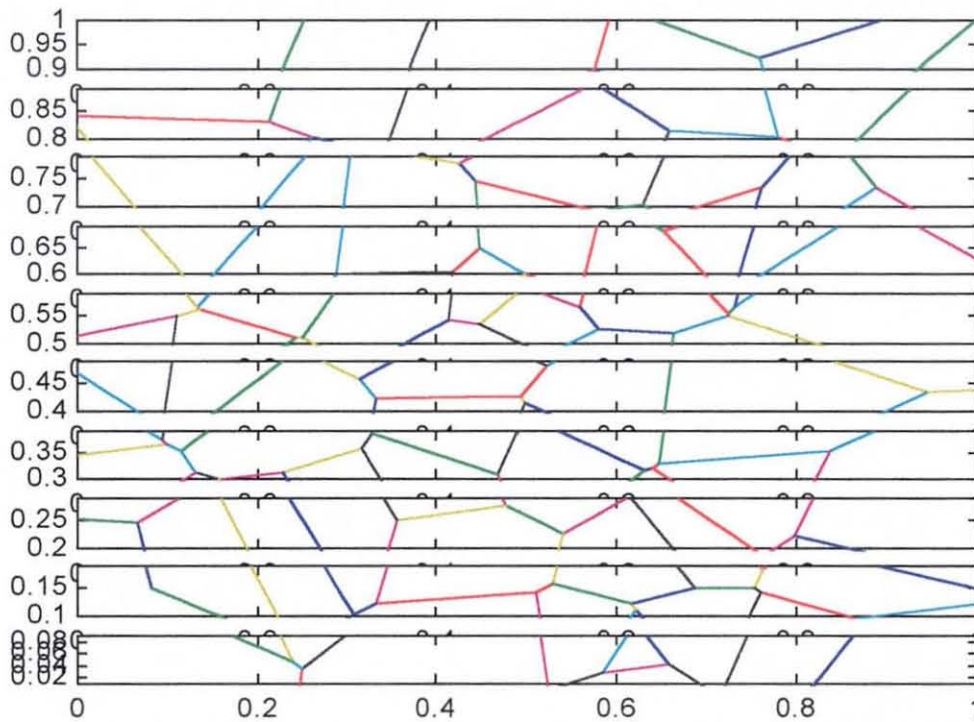
Fig 5.27(b)   Interconnects samples (11-20) from non-annealed Al film sample no 2
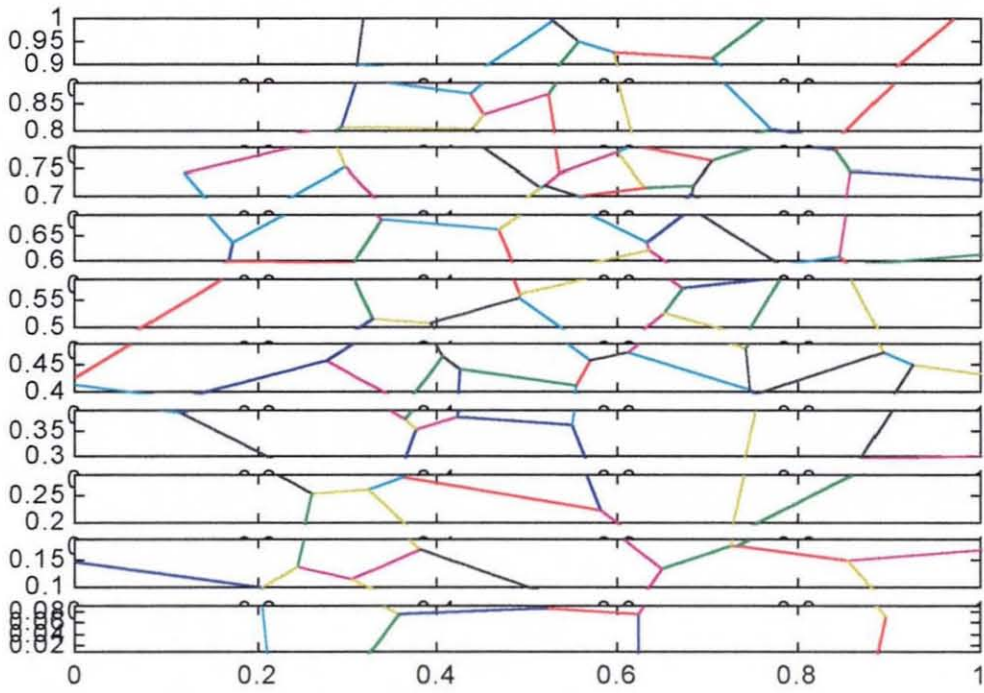
Fig 5.27(c) Interconnects samples (21-30) from non-annealed Al film sample no. 3
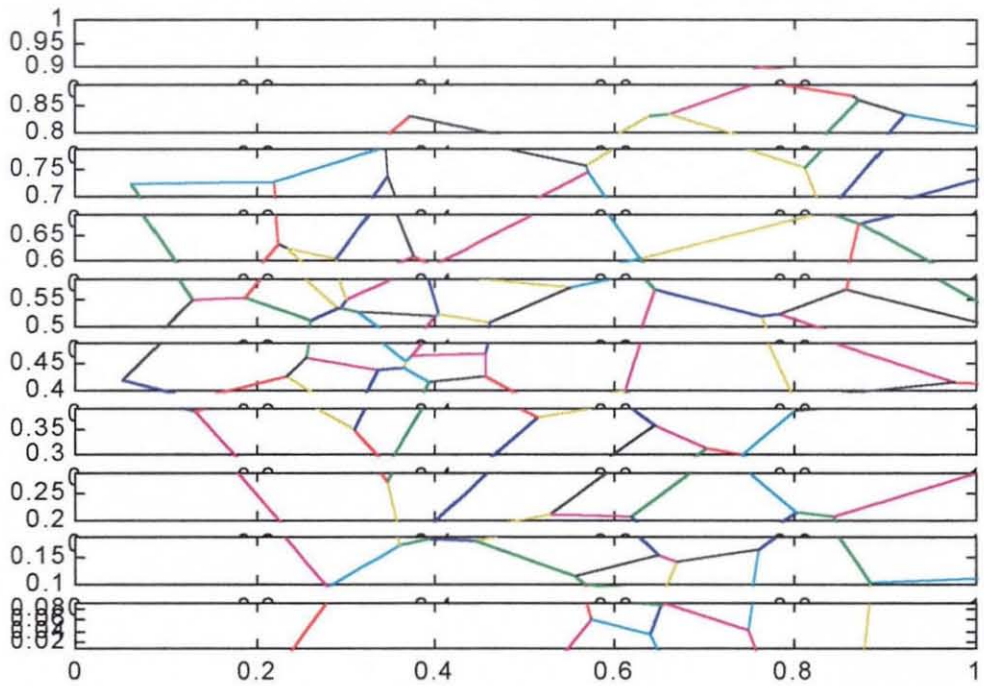
Fig 5.27(d)   Interconnects samples (31-40) from non-annealed Al film sample no. 4

217
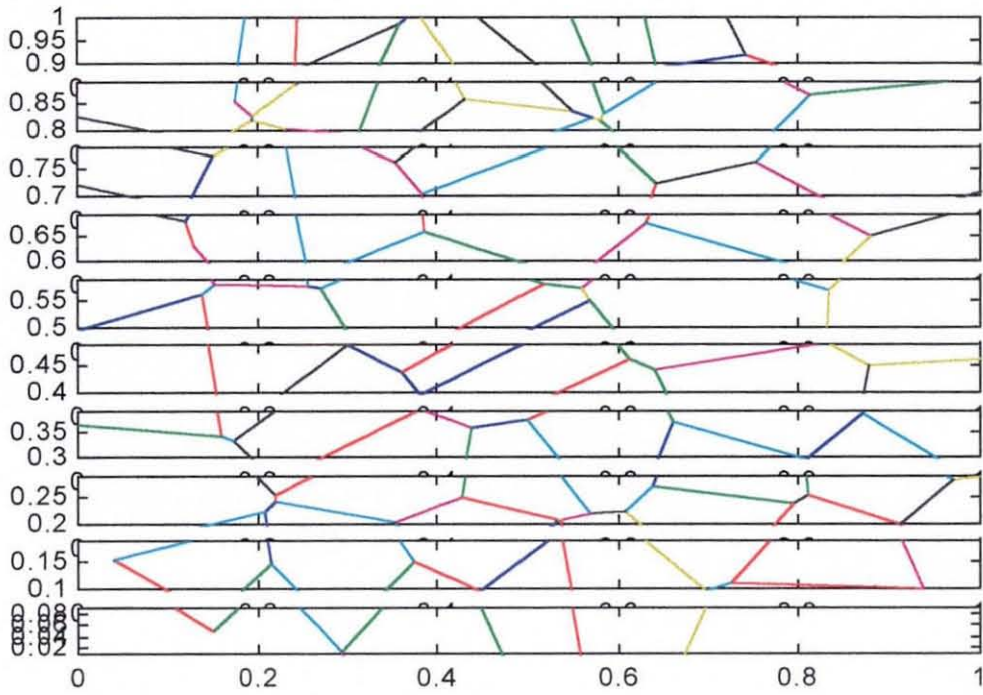
Fig 5.27(e) Interconnects samples (41-50) from non-annealed Al film sample no. 5
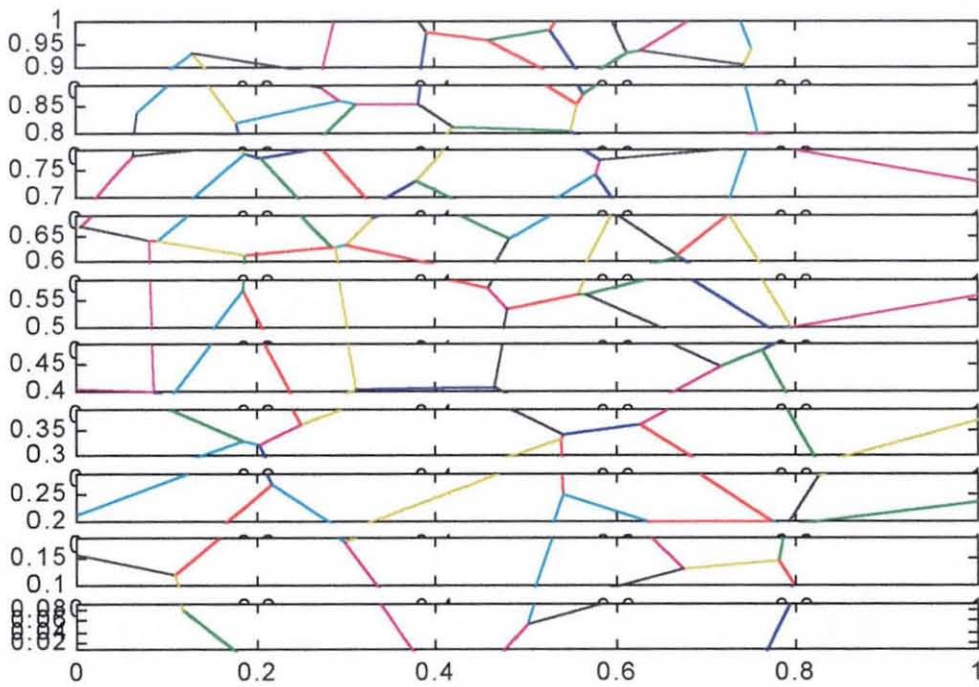
Fig 5.27(f) Interconnects samples (51-60) from non-annealed Al film sample no 6

218
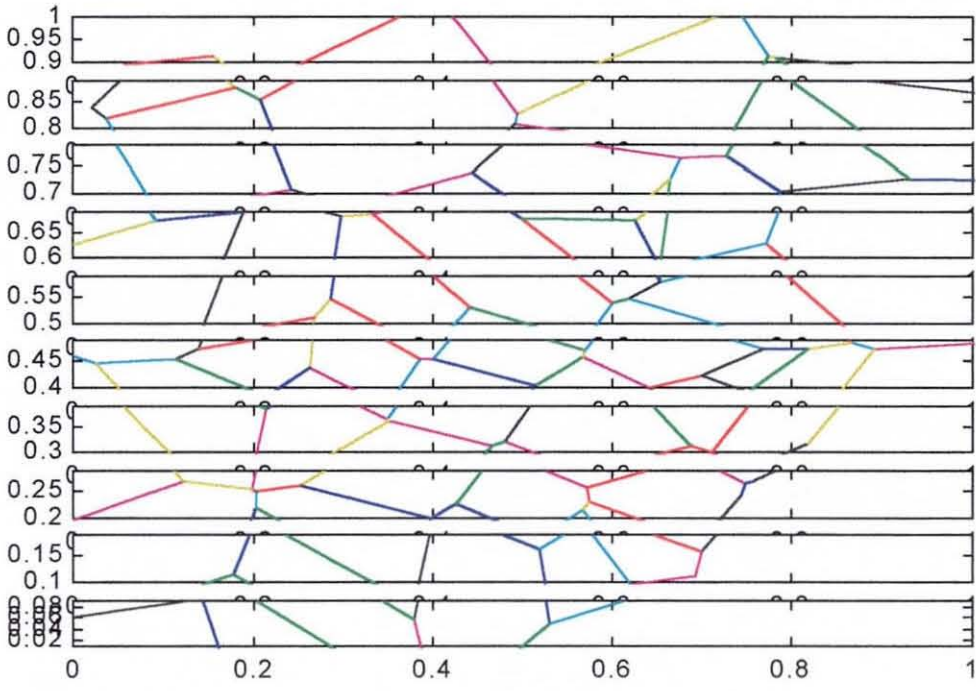
Fig 5.27(g) Interconnects samples (61-70) from non-annealed Al film sample no. 7
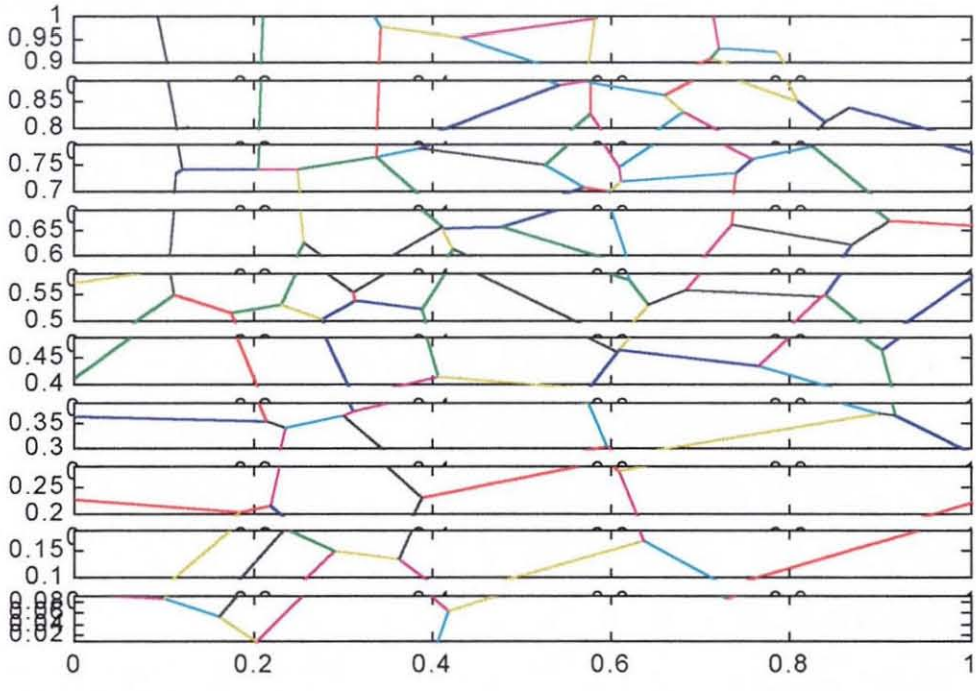
Fig 5.27(h) Interconnects samples (71-80) from non- annealed Al film no 8
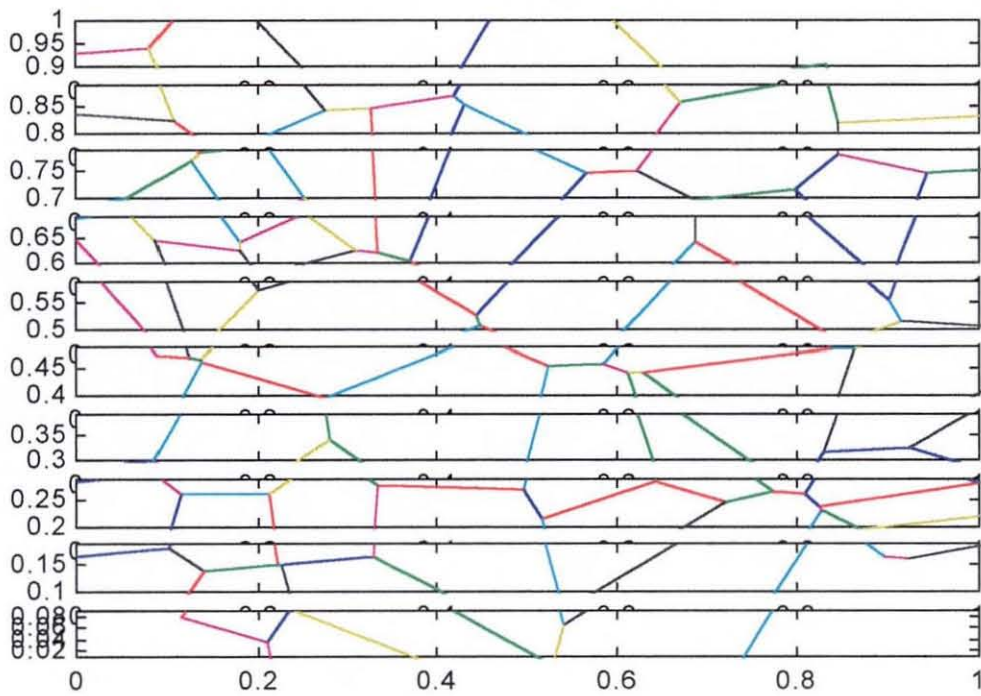
Fig 5.27(i) Interconnects samples (81-90) from non-annealed Al film sample no. 9
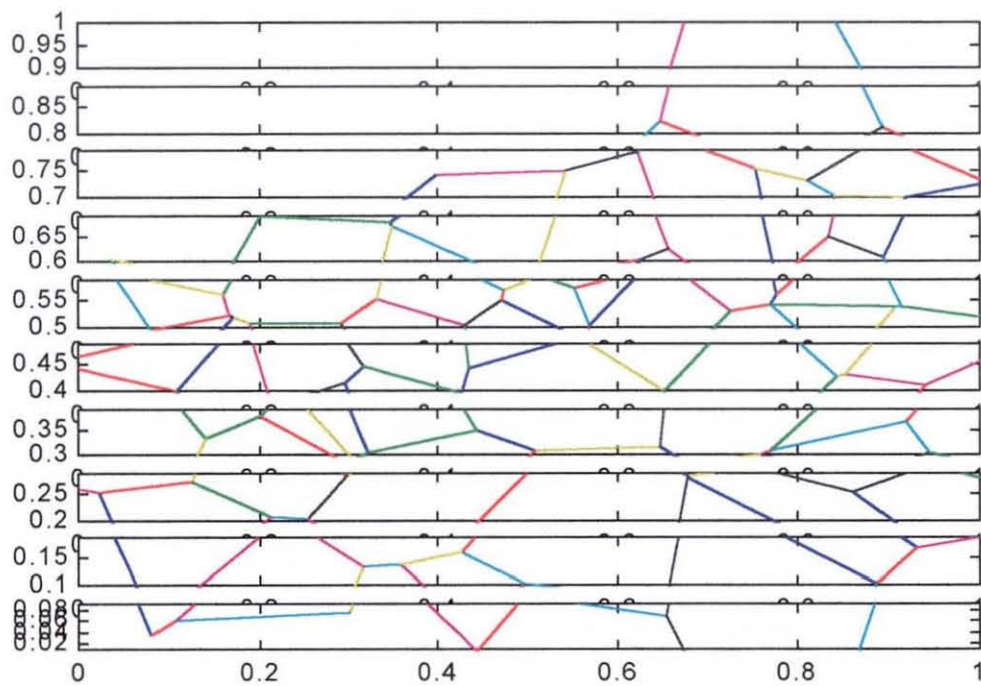
Fig 5.27(j) Interconnects samples (91-100) from non-annealed Al film sample no. 10
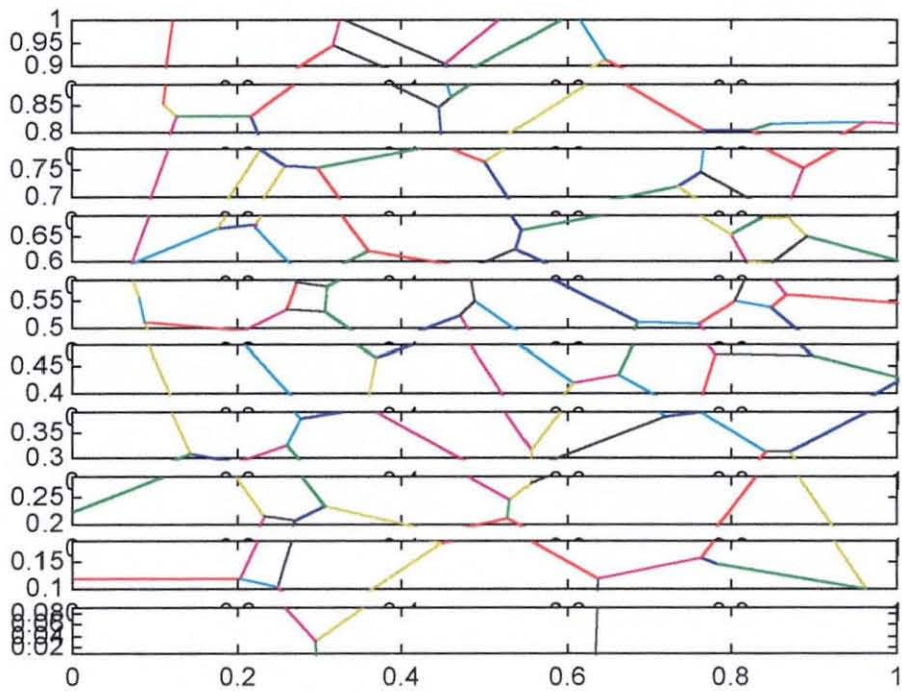
Fig.5.28(a)　　Interconnect samples (1-10) from annealed Al film sample no.1
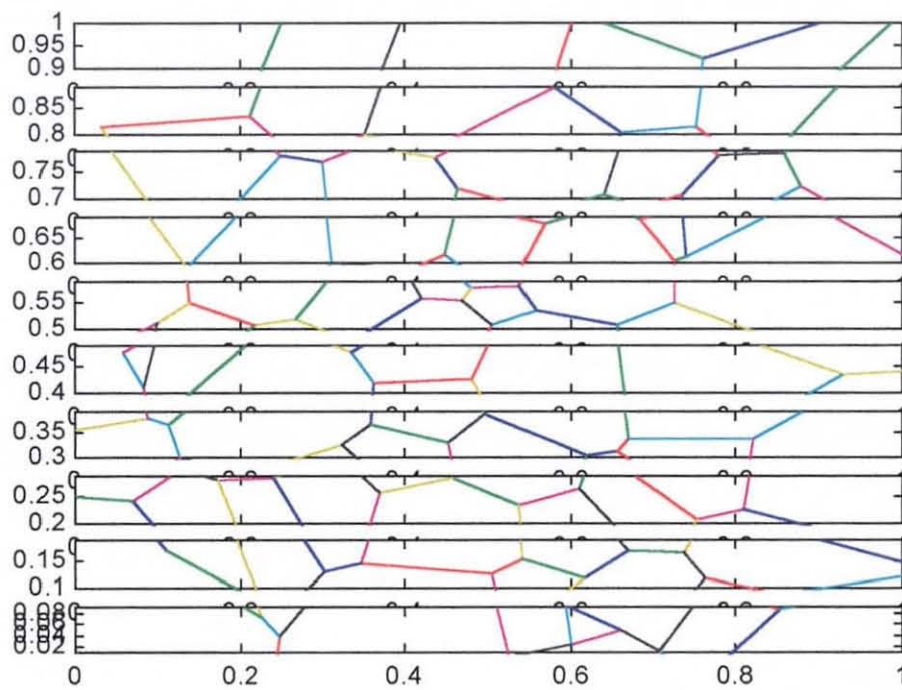
Fig 5.28(b)　　Interconnect samples (11-20) from annealed Al film no. 2

221
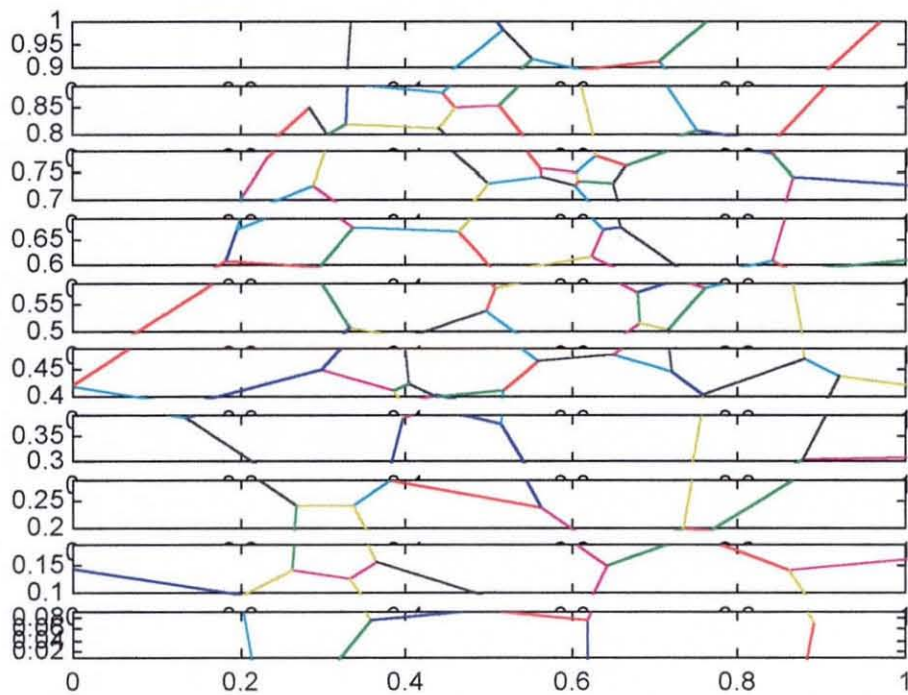
Fig.5.29(c) Interconnect samples (21-30) from annealed Al film no.3
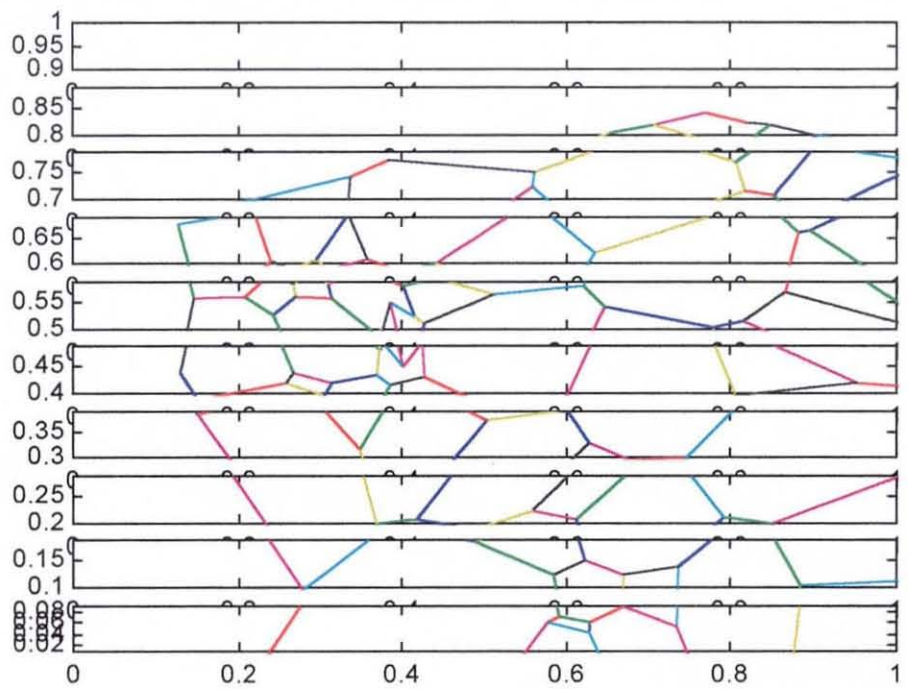
Fig.5.28(d) Interconnect samples (31-40) from annealed Al film no.4
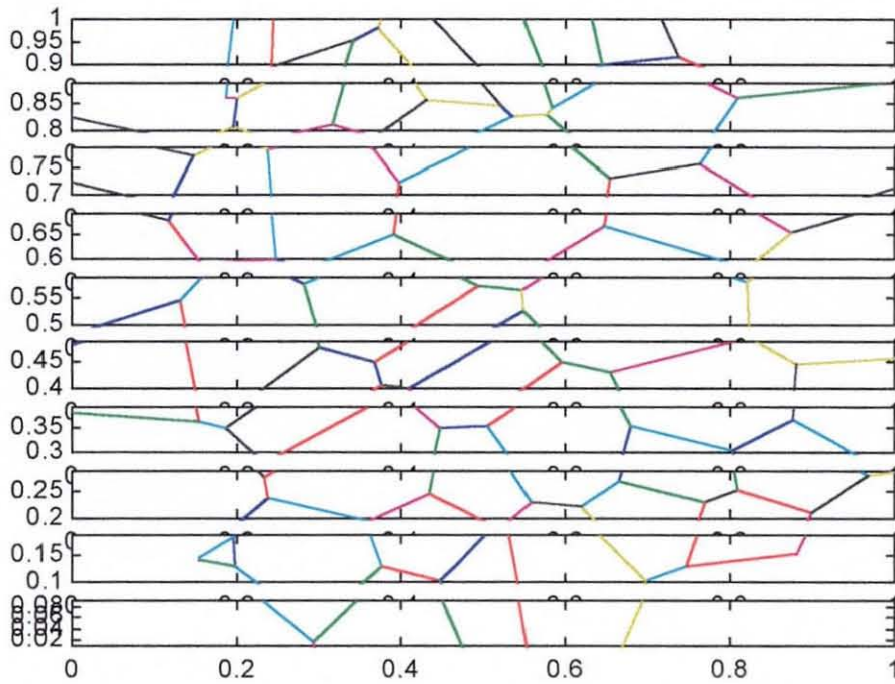
Fig.5.28(e) Interconnect samples (41-50) from annealed Al film no 5
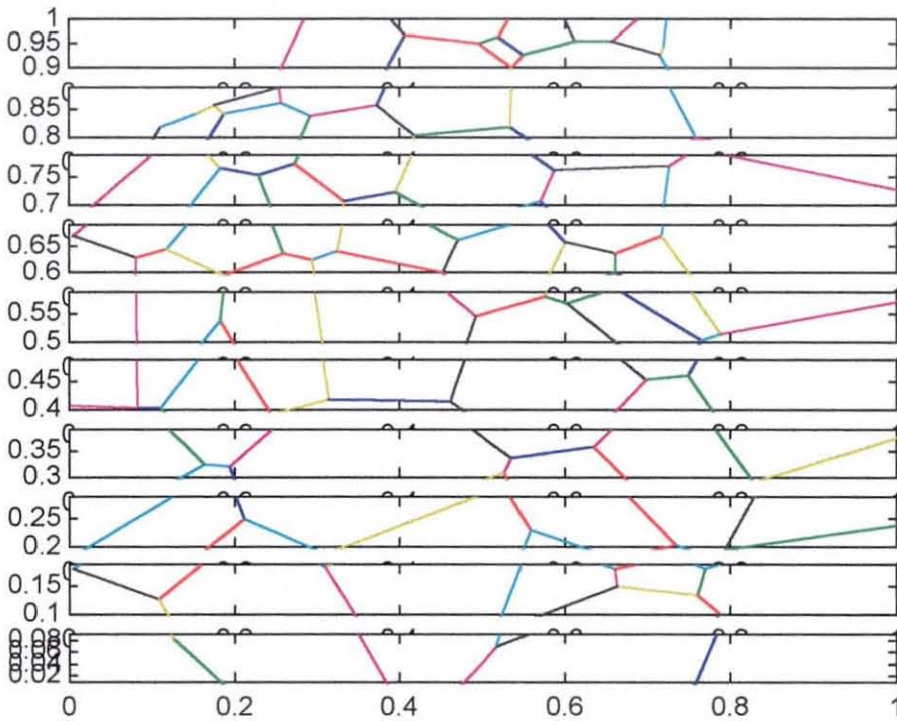
Fig.5.28(f) Interconnect samples (51-60) from annealed Al film no 6
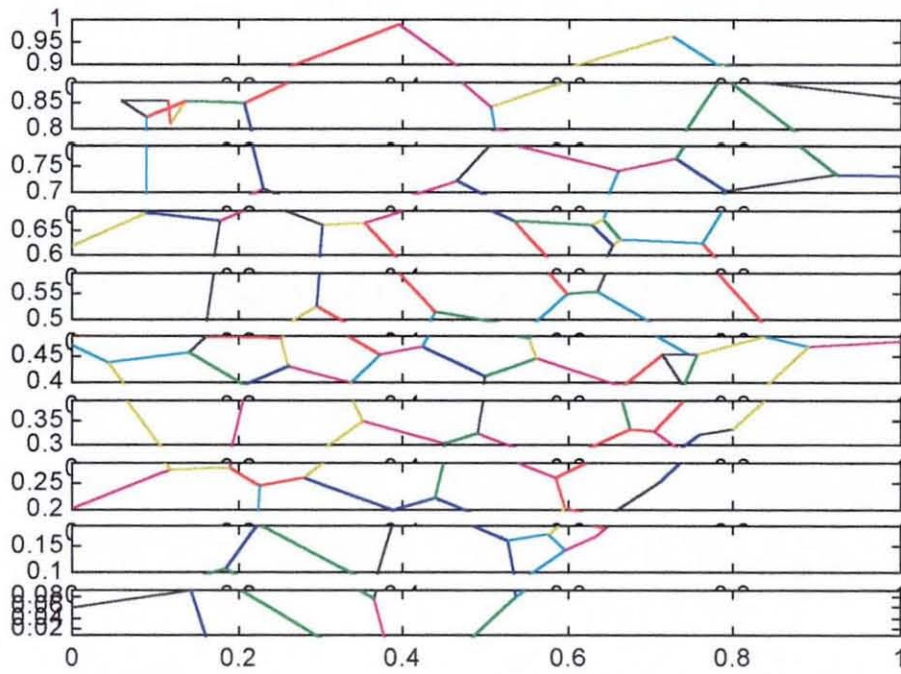
Fig.5.28(g) Interconnect samples (61-70) from annealed Al film no 7
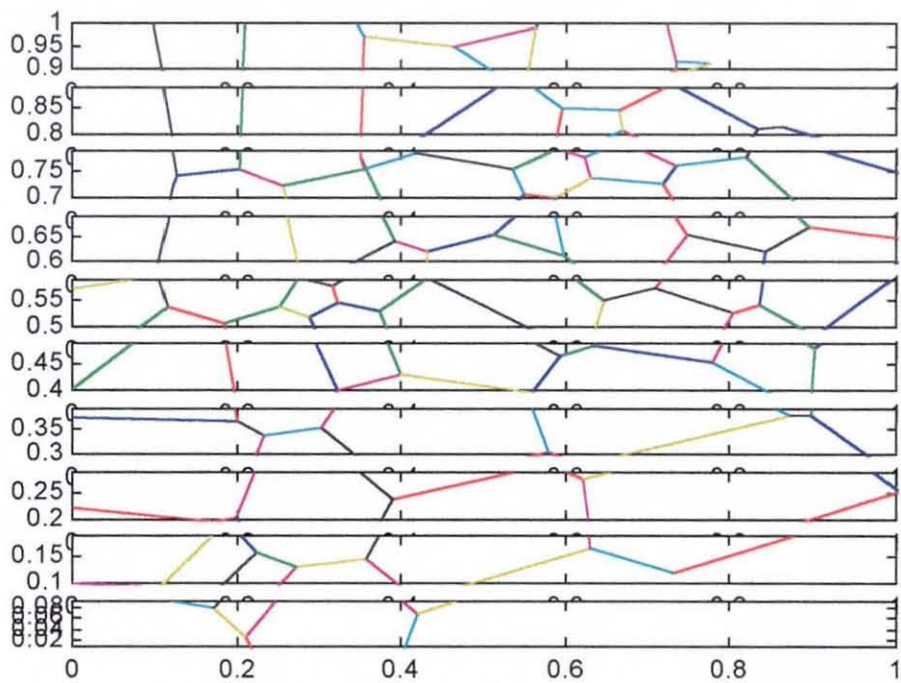
Fig.5.28(h) Interconnect samples (71-80) from annealed Al film no 8
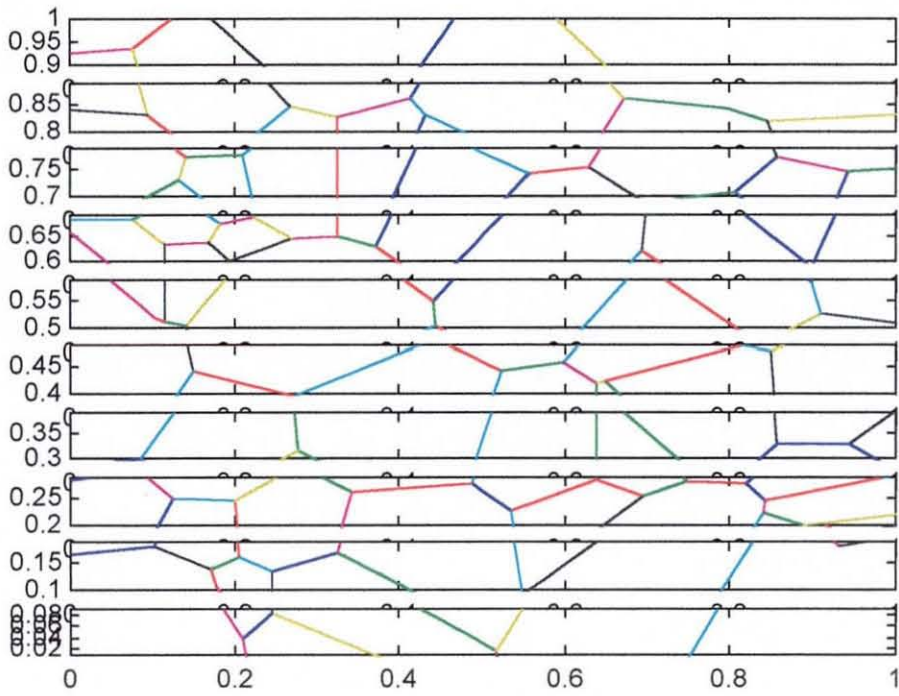
Fig.5.28(i) Interconnect samples (81-90) from annealed Al film no 9
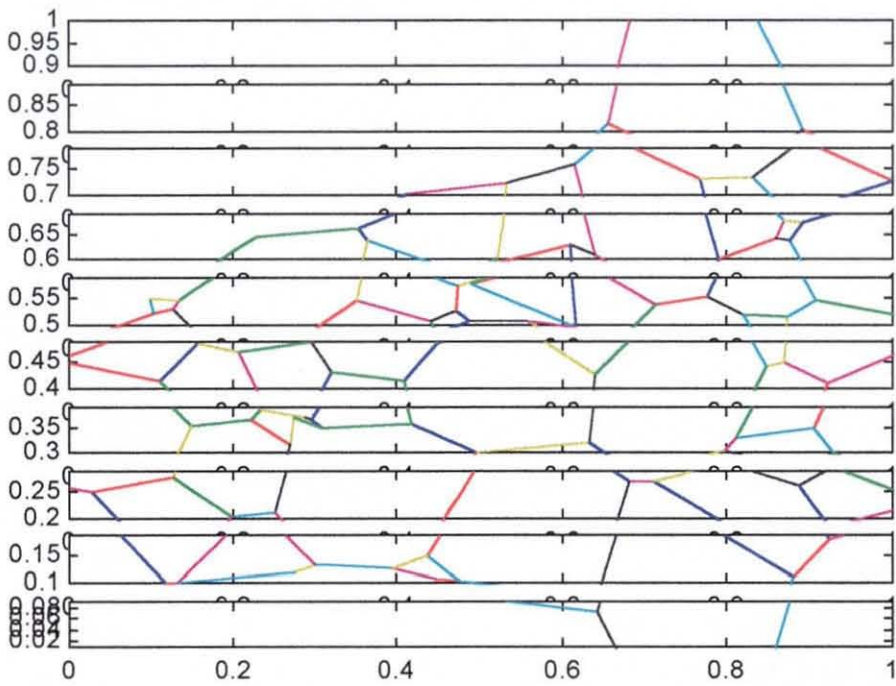
Fig.5.28(j) Interconnect samples (91-100) from annealed Al film no 10

5.3.7　The simulation of Time to Failure

In the present work, the simulation of Time to Failure is done by inputting the information (as shown in the detailed example in section 5.3.3) on the following parameters :-

  i)　Number of samples needed for the experiment

  ii)　Number of clusters present in the sample (by inspection)

  iii)　The length of the cluster(by inputting the start and end node of the cluster will automatically calculate the length of the cluster)

  iv)　The number of grain boundaries found in the cluster(by inspection)

  v)　The number of grain boundaries forming the longest path (by inspection)

  vi)　The length of the grain boundary (by inputting the grain boundary number will generate the length of each grain boundaries in the cluster)

  vii)　The angle of orientation of the grain boundary (by inputting the grain boundary number will generate the angle of orientation)

Once this information is fed into the system, the computer will calculate the TTF based on the lumped element model solution and the signal delay approximation. A grain boundary cluster will fail if it reaches a specified critical vacancy concentration value.

5.3.8 The experiments conducted

In the current work, there are three main experiments being conducted. The experiments are :-

1. An experiment on 100 samples of non-annealed interconnect
2. An experiment on 100 samples of annealed interconnect
3. An experiment on 5 samples of non-annealed Al films to determine the effect of varying the width of the interconnect on the Time to Failure, its Median Time to Failure (MTTF) and the Standard deviation . The width/length ratio selected for the experiment are a) w/l=0.04, b)w/l=0.075,c)w/l=0.1 and d) w/l=0.15 and e)w/l=0.2

with an average grain size ≈ 0.14. For (a) there will be 95 samples of interconnect, for (b) 65 samples, (c) 50 samples (d) 30 samples and (e) 25 samples

4. Finally we wish again to compare the data on Time to Failure between the lumped element model with the signal delay approximation

In all the experiments, the assumptions made and the boundary conditions are the same and are discussed in the following section. Basically the experiments objective is to obtain the distribution of the Time to Failure, its Mean Time to Failure and its standard deviation and to compare the results with existing references in the literature. This will provide a validity test on the lumped element model developed.

In all the experiments, the Time to Failure are calculated for every grain boundary cluster found in the samples of the interconnects. The shortest time of the TTF of the grain boundary will determine the Time to Failure of the interconnect samples. The data are then analysed to present in the form of graphs such as i) The Cumulative Distribution of the Time to Failure and ii) The Lognormal graph on the Time to Failure.

5.3.9 The assumptions and boundary conditions applied

In the current experiment, all the interconnect lines were initially assumed to be in a state of zero stress ($\sigma = 0$) at the beginning of the interconnect ,prior to the application of a current. This corresponds to a boundary condition at the anode end of the interconnect $\sigma(L = 0, t) = 0$. The boundary conditions at the cathode end of the interconnect is J(L,t)=0. These boundary conditions represent the real experimental situation where the interconnect is attached to a large contact pad at the beginning of the line and a stud attached at the end of the line. The chosen values used in the relevant parameters for the lumped element model is as follows:-

    i)   The number of section per grain boundary $s = 3$

    ii)   The critical vacancy concentration $c_{cr} = 2c_0$

    iii) The electromigration drift component $\alpha = 5$ (varies between grain boundaries where $\alpha_{eff} = \alpha.\cos(\theta)$, where θ is the angle of orientation)

    iv) The effective Diffusion coefficient $D = 5$ (varies between grain boundaries by eqn(3.1)in Chapter 3)

    v)   The total interconnect length $L = 1$

The values used in the simulation of the lumped element model will result in arbitrary values. In order to obtain the real physical data, some conversions have to be made to give a physical meaning of the results obtained. This will be discussed below.

5.3.10 The variables/parameters and data conversion

i) The parameters

The variables or parameters used in obtaining the actual experimental data for the results of the simulation are adopted from the references of [Korhonen , et,al,1993],[Knowlton,et.al.,1997],[Kircheim and Kaeber, 1991][Duan, and Shen, ,2000][Cho and Thompson,1997],[Joo et.al,1998]. All these references are based on the stress evolution model. The relevant variables or parameters and their values used in the current experiment are as follows:-

B= effective modulus = 50 GPa= $50 \times 10^9 Nm^{-2}$

Ω= atomic volume = $1 \times 10^{-29} m^3$

T = temperature = $227 \ ^0 C$= 500K

Z* = effective charge of atoms = 10

j= current density = $1 \times 10^6 A / cm^2 = 1 \times 10^{10} A / m^2$

ρ = aluminium resistivity = $5 \ \mu\Omega cm = 5 \times 10^{-8} \Omega m$

e= electron charge= $1.602 \times 10^{-19} C$

k=Boltzman contant = $1.38 \times 10^{-23} JK^{-1}$

D_a =effective diffusion coefficient of the entire cross section of interconnect

   = $3 \times 10^{-16} m^2 s^{-1}$

d = grain size = 1×10^{-6} m

δ = grain boundary thickness = $1 \times 10^{-9} m$

and from reference [Korhonen, et.al,1993]

$$D_a = \frac{\delta D_a^{GB}}{d}, \text{ therefore}$$

$$D_a^{GB} = \frac{d.D_a}{\delta} = \frac{1x10^{-6}.3x10^{-16}}{1x10^{-9}} = 3x10^{-13}\,m^2s^{-1}$$

ii)   **Conversion of the arbitrary values to the physical values**

a)   **The physical length of interconnect**

From the arbitrary values of $\alpha=5$ and $L=1$,

therefore

$\alpha L = 5$ 5.4

The electromigration drift component is given by the equation below:-

$$\alpha = \frac{Z^*e.\rho.j}{kT}$$ 5.5

substituting the values of the parameters in 5.3.8.2(i)

$$\alpha \;\; = \frac{10x1.602x10^{-19}.5x10^{-8}.1x10^{10}}{1.38x10^{-23}.500}$$

$\alpha \;\; = 1.1594 \times 10^5$

solving the length of interconnect

$$L = \frac{5}{\alpha} = \frac{5}{1.1594x10^5} = 43x10^{-6}\,m = 43\mu m$$

The calculation of the length of the interconnect will depend on the value of Z* in α. Z* values is not very well define, where the values used in the literature varies from 4-8 [Korhonen et al,1993] , Z*=15[Kirchheim and Kaeber,1991]. The various length of interconnect based on the different values of Z* are shown in Table5.10

Z*	α	L =length of interconnect
4	4.6377×10^4	107 μm
5	5.7971×10^4	86.25 μm
10	1.1594×10^5	43 μm
15	1.7391×10^5	28.7 μm

Table 5.10 The realistic length of interconnect

b) The physical effective Diffusion coefficient D

As derived earlier in Chapter 3 (eqn3.17& eqn3.18), the effective diffusion coefficient along the grain boundary is given by the equation below:-

$$D_{eff} = \left(\frac{\delta}{W}\right).\left(D_A^{GB}\right)\left(\frac{B\Omega}{kT}\right)$$

5.6

substitute the relevant variables values in equation 5.6 gives

$$D_{eff} = \left(\frac{1x10^{-9}}{1x10^{-6}}\right).\left(3x10^{-13}\right).72 \cdot$$

$$= 2.16 \times 10^{-14} m^2 s^{-1}$$

$$= 2.16x\ 10^{-2}(\mu m)^2 s^{-1}$$

On another reference[Joo ,1999], the value use for $D_{eff} = 4.32x10^{-3}(\mu m)^2 s^{-1}$

c)   The physical time scale of the Time to Failure (TTF)

In terms of the vacancy build-up equation

$$\frac{\partial C_V^{GB}}{\partial t} = D_{eff}\left(\frac{\partial^2 C_V^{GB}}{\partial x} + \alpha\frac{\partial C_V^{GB}}{\partial x}\right)$$

5.7

By introducing the scaling factor

let $LX = x$ and $t = \eta T$

substituting the scaling factors in equation 5.7

$$\frac{\partial C_V^{GB}}{\partial(\eta T)} = D_{eff}\left(\frac{\partial^2 C_V^{GB}}{\partial(LX)^2} + \alpha\frac{\partial C_V^{GB}}{\partial(LX)}\right)$$

$$\frac{\partial C_V^{GB}}{\partial(\eta T)} = \frac{D_{eff}}{L^2}\left(\frac{\partial^2 C_V^{GB}}{\partial X^2} + \alpha L\frac{\partial C_V^{GB}}{\partial X}\right)$$

$$\frac{\partial C_V^{GB}}{\partial T} = \frac{\eta D_{eff}}{L^2}\left(\frac{\partial^2 C_V^{GB}}{\partial X^2} + \alpha L\frac{\partial C_V^{GB}}{\partial X}\right) \qquad\qquad 5.8$$

now $\dfrac{\eta D_{eff}}{L^2} = 5$ (as use in the experiment)

Therefore the time scale is given by

$$\eta = \frac{L^2 x 5}{D_{eff}} \text{ in seconds} \qquad\qquad 5.9$$

$$\eta = \frac{L^2 x 5}{D_{eff} x 3600} \text{ in hours.} \qquad\qquad 5.10$$

The range of the time-scale based on the realistic interconnect length is given in Table 5.11 below

L(μm)	η at $D_{eff} = 2.16 \times 10^{-14}\, m^2 s^{-1}$	η at $D_{eff} = 4.32 \times 10^{-15}\, m^2 s^{-1}$
107	736 Hours	3680 Hours
86.25	478 Hours	2390 Hours
43	118 Hours	595 Hours
28.7	53 Hours	265 Hours

Table 5.11 The actual time-scale for various interconnect length and
effective diffusion constant

With the selection of $\alpha=5$ and $D=5$ produces a physical time-scale which is within the range of actual Time to Failure reported in [Knowlton et.al,1997],[Joo et.al,1999]

d) The critical vacancy/ critical stress

The critical vacancy use in the experiment for determining the Time to Failure is set at $c_{cr}=2c_0$ and this corresponds to the critical stress σ_{cr} given by the equation below of [Korhonen,et.al,1993]

$$c_r = c_0 e^{\left(\frac{\sigma_{cr}\Omega}{kT}\right)}$$

5.11

$$\log\frac{c_r}{c_0} = \frac{\sigma_{cr}\Omega}{kT}$$

$$\sigma_r = \frac{kT}{\Omega}\log\frac{c_r}{c_0} = \frac{1.38\times10^{-23}.500}{10^{-29}}\log(2) = \mathbf{478MPa}$$

The value of critical vacancy $c_{cr}=2c_0$ chosen reasonable because in the literature, the critical stress σ_r lies in the range of 100MPa-1 GPa [Knowlton et.al,1997]

5.3.11 Other relevant parameters used in the simulation and their justification

i.   The use of a 50 random point to construct the Voronoi network

The simulation to investigate the electromigration behaviour on the realistic interconnect was done on a Personal Computer with the Central Processing speed (cpu) of 166 Mhz and 32 Mbyte RAM. It is not the intention of the study to simulate actual Al films which may contains thousands of grain boundaries, the most important objectives is to investigate whether the model can exhibit the characteristics of the lognormal distribution of its Time to Failure. It is also must be realised that it is the first time that an attempt has been made to model the grain boundaries as a transmission line consisting of resistor and capacitor component to transport the vacancies along a the grain boundaries. Most of program codes developed involves searching algorithm which takes quite a lot of computer time too. The above reasons and the limitation of the programme codes are basis for choosing a 50 random point for a start.

ii. The time step dt and vertex size Δ use for annealing process

With respect to the simulation of the annealing process, the work of Kawasaki and co-workers are referred to since they outline in detail the rules and the equations relating to the movement of the vertices and it is suitable to be adapted to the programmes codes of MATLAB. However the only modifications that have been made are the values of the time step size dt of t and vertex size Δ. The original values used are 0.01 for step size dt and 0.1 for for vertex size Δ respectively[Kawasaki, et.al,1989]. These values are very critical since it will determine the success of the grain boundary recombination and the annihilation process and the annealing process as a whole. If this values are not correctly selected, the neighbouring line joining the vertices may overlap or overshoot due to the unbalance between the growth rate (determine by the time step size dt) and the recombination or annihilation process (determine by the vertex size).

235

For the actual simulation, the value chosen for the time step size dt is 0.001 and for the vertex size Δ is also 0.001. This value is chosen by trial and error since by using the original value the result is not good, a lot of overlap and overshoot occurs. The problem is minimised by making the time step size longer and the vertex size Δ shorter than the original values. The selection of this value seems reasonable because the original is used when simulating 48 000 vertices[Kawasaki et.al,1989] , but for the current simulation is only 94 vertices with 125 lines joining the vertices (the average value for 50 random point Voronoi diagram in a 1x1 scale).Also for the purpose of investigating the effect of annealed and non-annealed sample, the total amount of annealing time for all the samples is set to 5 time steps only to minimise the problem of overlapping of grain boundaries.

iii).   Number of grain boundaries

In the present work , the maximum number of grain boundaries in a cluster is limited to 11 grain boundaries. This is reasonable since other computer simulation of the Time to Failure only consider 10 grain boundaries connected in series [Kirchheim and Kaeber,1991]. These however show no structure where all the grain boundary orientation angle θ =0. The size of the matrices describing the cluster structure is also a limiting factor. For 3 sections per grain boundary, an eleven grain boundary clustres will require 34x34 matrix. In the case of more than 11 grain boundaries found in the cluster, the Time to Failure will be calculated only for the first 11 grain boundaries(the first 6 grain boundaries which form the longest path/length and 5 neighbouring / wing grain boundaries).

iv). Number of sections of components per grain boundary

The number of sections of the Π network is set to 3. This value is chosen instead of 5 to cut down the computer processing time during the calculation of Time to Failure. The difference in results between a 3 and a 5 section is very small (it has been shown earlier for single grain boundary for Case(b), one section is in fact adequate).

5.4 The simulation results of realistic interconnect

5.4.1 The experiment data

The detailed results of all the experiment are shown in Tables A.1(experiment no 1), Table A.2(experiment no.2) , TableA.3(experiment no 3) and TableA.4(experiment no.4) in Appendix A. The tables contain all the important and relevant data gathered during the simulation of the Time to Failure. The data of particular interest are:-

i) The number of cluster found in the interconnect samples

ii) The grain boundary cluster length

iii) The number of grain boundaries found in each cluster

iv) The Time to Failure for each cluster

v) The Time to Failure for the interconnect sample(the minimum value among the cluster)

5.4.2 Results of experiment no.1(a)- non-annealed grain boundary clusters

i) The length of grain boundary cluster and their Time to Failure

In experiment no.1 (a), 100 samples of interconnect are produced from 10 samples of non-annealed Al films as shown previously in Fig5.27(a)-Fig5.27(j). The data of the length of grain boundary cluster and the Time-to-failure in arbitrary units obtained are summarised in Table 5.12 and 5.13 below (data taken from Table A.1).

0.0202	0.0734	0.1061	0.1332	0.1691	0.2116	0.2516	0.3694
0.0204	0.0751	0.1083	0.1392	0.171	0.2141	0.2535	0.378
0.0235	0.0774	0.1103	0.1409	0.1712	0.2143	0.2587	0.3841
0.0274	0.0786	0.1104	0.1419	0.1721	0.2143	0.269	0.3985
0.0275	0.0797	0.1114	0.142	0.1745	0.2152	0.2754	0.4019
0.0316	0.0797	0.1115	0.1424	0.1777	0.2193	0.2776	0.4028
0.0366	0.0803	0.1118	0.1424	0.1783	0.22	0.2804	0.4054
0.038	0.0808	0.1127	0.1428	0.1795	0.2201	0.2831	0.4132
0.0381	0.0816	0.1135	0.1432	0.1808	0.2233	0.2838	0.4211
0.0393	0.0822	0.1139	0.1438	0.1817	0.224	0.2841	0.4213
0.0393	0.083	0.1146	0.1497	0.1818	0.2244	0.2844	0.4252
0.0403	0.0886	0.1146	0.1502	0.1833	0.2245	0.2868	0.4288
0.0443	0.0887	0.116	0.1506	0.1838	0.2253	0.2871	0.452
0.0447	0.0897	0.1165	0.1509	0.1852	0.2254	0.2908	0.4573
0.0448	0.0899	0.1167	0.1524	0.189	0.2268	0.2937	
0.0474	0.0901	0.1172	0.1529	0.1901	0.2289	0.2939	
0.0518	0.0908	0.118	0.1565	0.1919	0.2309	0.2962	
0.0531	0.0928	0.1185	0.1573	0.1946	0.2337	0.2982	
0.056	0.0943	0.1185	0.1586	0.1951	0.2343	0.3019	
0.058	0.0946	0.1203	0.1599	0.1954	0.2402	0.3053	
0.0617	0.0949	0.1214	0.1607	0.1967	0.2425	0.3076	
0.0621	0.0968	0.1215	0.1618	0.1972	0.244	0.3078	
0.0642	0.0995	0.1231	0.1631	0.1995	0.2442	0.3184	
0.0649	0.1019	0.1254	0.1636	0.2	0.2466	0.3204	
0.0659	0.1037	0.1255	0.1641	0.2	0.2478	0.322	
0.0668	0.1043	0.1259	0.165	0.2027	0.2483	0.3337	
0.0682	0.1049	0.1292	0.1663	0.2038	0.2487	0.3344	
0.0698	0.105	0.1297	0.1666	0.2045	0.2488	0.3359	
0.0707	0.1054	0.1304	0.1675	0.2057	0.2488	0.3459	
0.0733	0.1058	0.1311	0.1691	0.2105	0.2507	0.3497	

Table 5.12 The length of grain boundary cluster (arbitrary units) in the 100 samples of non-annealed interconnects arranged in ascending order.

0.0191	0.0388	0.0483	0.0559	0.0676	0.0809	0.096
0.0208	0.0392	0.0486	0.056	0.0684	0.0812	0.0964
0.0209	0.0401	0.0491	0.0578	0.0686	0.0817	0.0967
0.0255	0.0412	0.0494	0.0584	0.0689	0.0824	0.097
0.0318	0.0414	0.0505	0.0585	0.0691	0.0833	0.0971
0.0339	0.0416	0.0506	0.0587	0.0695	0.0835	0.0977
0.0343	0.0417	0.0513	0.0595	0.0699	0.0837	0.0985
0.0347	0.0425	0.0517	0.0606	0.07	0.084	0.1048
0.0349	0.0433	0.0518	0.0616	0.0708	0.0854	0.115
0.0349	0.0437	0.0523	0.0617	0.0709	0.0859	0.1251
0.035	0.0438	0.0526	0.0622	0.0723	0.0875	0.1266
0.0351	0.0438	0.0527	0.0626	0.0729	0.0876	0.1381
0.0352	0.044	0.0531	0.0626	0.0735	0.0878	0.1451
0.0363	0.0441	0.0536	0.0627	0.0746	0.0879	0.157
0.0366	0.0444	0.0538	0.0637	0.0756	0.0892	0.1686
0.0366	0.0456	0.054	0.0647	0.0758	0.0895	0.1738
0.0376	0.046	0.0541	0.065	0.0773	0.0905	
0.0376	0.0461	0.0547	0.0667	0.0778	0.0917	
0.0381	0.0471	0.0549	0.0667	0.0794	0.0946	
0.0386	0.0479	0.0555	0.0668	0.0802	0.0951	

Table 5.13 The Time to Failure(in arbitrary units) for the grain boundary clusters in the 100 samples of non-annealed interconnects arranged in ascending order.

From the summarised data shown in Table 5.12 and 5.13, the range of the length of the cluster obtained from the simulation is between 0.0202 (shortest length) - 0.4573 (longest length) and the Time to Failure obtained is between 0.0191(the fastest time) - 0.1738(the slowest time). Translating into the actual values, the length of the grain boundary cluster lies in the range of 0.87 μm – 19.6μm (scale = 43 μm) and the actual time lies in the range of 2.25 hrs-20.5 hrs (the time scale used is η=118hrs).

ii) The distribution of clusters and grain boundaries in the interconnect

Figure 5.29 shows the distribution of the simulated number of cluster found in the interconnect while Fig5.30, shows the simulated number of grain boundaries found in the cluster obtained from the non-annealed interconnect samples.

239
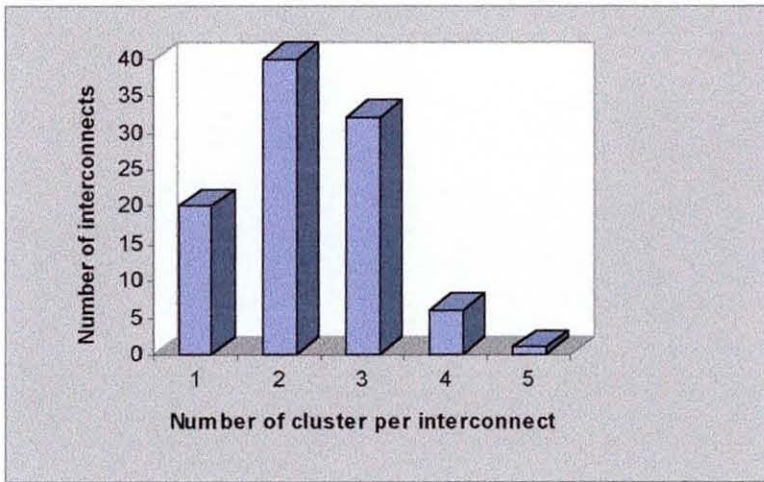
Fig 5.29 The distribution of the simulated number of cluster

found in the 100 samples of non-annealed interconnects
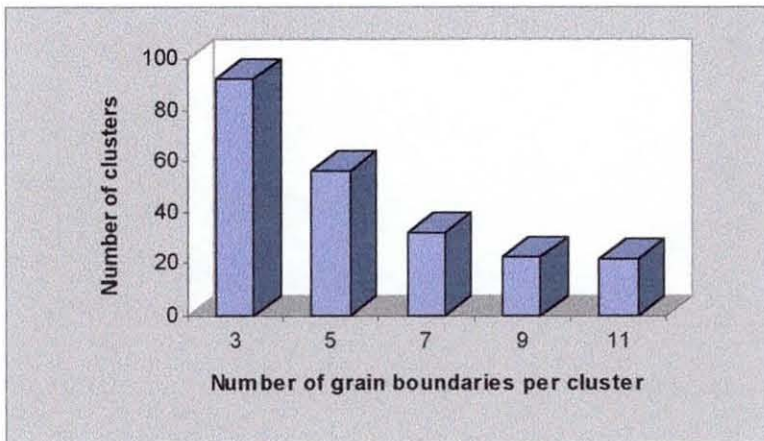
Fig 5.30 The distribution of the simulated number of grain

boundaries found per cluster obtained from 100 samples of interconnect

iii). The distribution of length of grain boundary cluster and Time to Failure

Fig 5.31 below shows the histogram and the cumulative distribution of the length of the grain boundary cluster, while Fig5.32 shows the cumulative distribution of the Time to Failure of the grain boundary clusters.
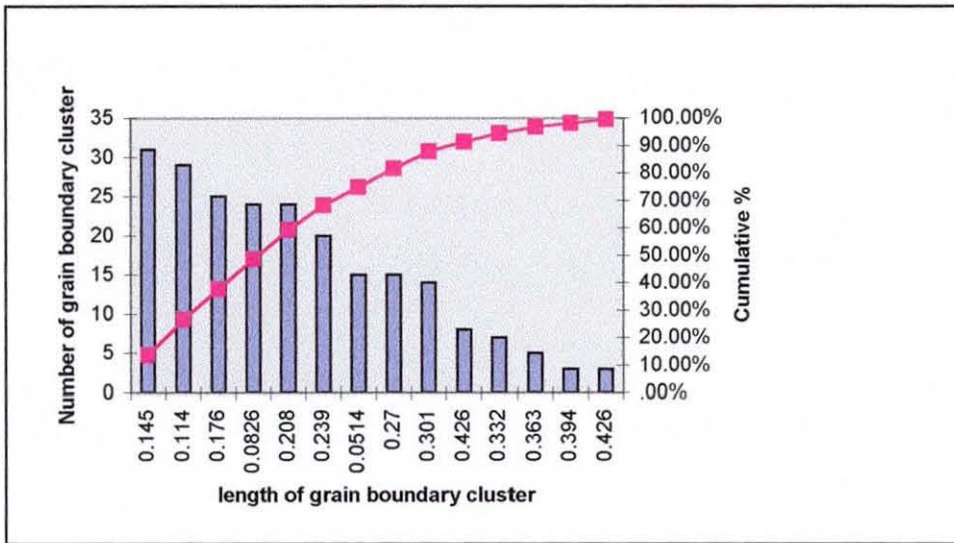
Fig 5.31 The histogram and the cumulative distributions of the simulated length of grain boundary cluster in 100 sample of non-annealed interconnect
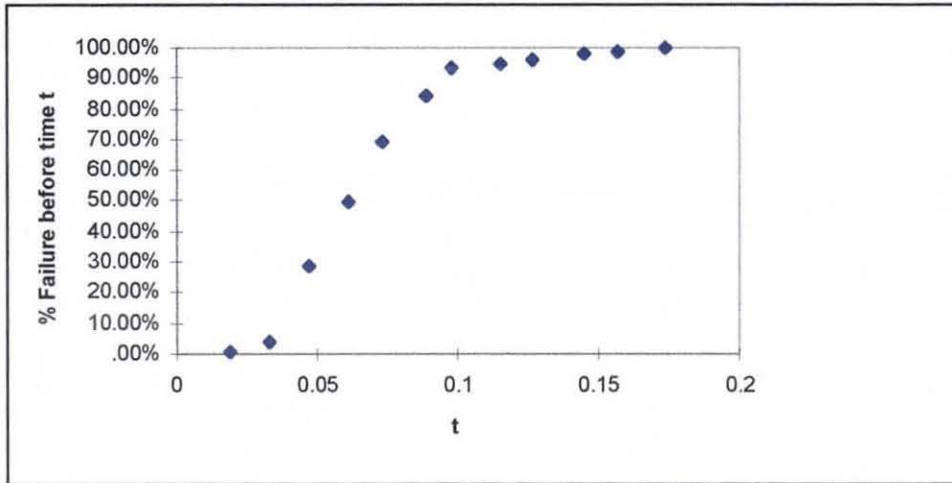
Fig 5.32 The cumulative distribution of the simulated Time to Failure in terms of the grain boundary cluster obtained from100 samples of non-annealed interconnects.

From both of the figure above, the cumulative distribution plotted follows the expected pattern i.e. in the form of nearly S-shape. The histogram of the length of grain boundary clusters are of similar in pattern to that of reference[Joo and Thompson ,1994]

iv)   The method used to obtain a log-normal distribution graph

One of the main tasks of this experiment is to test for the lognormality of the Time to Failure. To do this , normally , the data are plotted onto a special probability graph paper with logarithmic scale (the lognormal probability paper). However, the cumulative distribution graphs or function (CDF) can also be used instead ,by means of converting to the complementary error function(erfc) . This method have been used by others [Kircheim and Kaeber, 1991]. The conversion from cumulative distribution function to the complementary error function for a normal distribution is derived below:-

$$P(x < x_0) = 1 - P(x > x_0)$$

$$CDF_x = 1 - \frac{1}{2}erfc\left(\frac{x-\mu}{\sqrt{2}\sigma}\right)$$

$$CDF_x = 1 - \frac{1}{2}\left(1 - erf\left(\frac{x-\mu}{\sqrt{2}\sigma}\right)\right)$$

$$CDF_x = 1 - \frac{1}{2} + \frac{1}{2}erf\left(\frac{x-\mu}{\sqrt{2}\sigma}\right)$$

$$CDF_x = \frac{1}{2} + \frac{1}{2}erf\left(\frac{x-\mu}{\sqrt{2}\sigma}\right)$$

where

$P(x < x_0)$	=	The probabilty theat x is less than x_0 = CDF_x
CDF_x	=	cumulative distribution function of x
erfc	=	complementary error function
μ	=	Median of x
σ	=	standard deviation of x

By letting the CDF= y , the equation becomes

$$y = \frac{1}{2} + \frac{1}{2}erf\left(\frac{x-\mu}{\sqrt{2}\sigma}\right)$$

$$2y = 1 + \text{erf}\left(\frac{x - \mu}{\sqrt{2}\sigma}\right)$$

$$2y-1 = \text{erf}\left(\frac{x - \mu}{\sqrt{2}\sigma}\right)$$

therefore $\dfrac{x - \mu}{\sqrt{2}\sigma} = \text{erf}^{-1}(2y-1)$ 　　　　　　　　　　　　　　5.12

Plotting of the graph is done by making :-

Y axis = $\text{erf}^{-1}(2y-1)$ where y is in terms of cumulative % before the Time to Failure

X axis = the Time to Failure

Since the arbitrary values of the Time to Failure are less than 1 , all the TTF values are 'standardized' by a multiplying factor (in the current work it is x 10^3)so that when taking its logarithm will produce positive values in the lognormal distribution graph.

iv) **The lognormal distribution of Time to Failure**

Table 5.14 shows the 'treated' data on the Time to Failure for the grain boundary clusters found in the 100 samples of non-annealed interconnects. These data are use to obtain the lognormal distribution of Time to Failure as shown in Fig 5.33.

TTF	TTF(s)	Log(TTF(s))	efrinv(2y-1)	y	Cumulative %
0.0191	19.1	1.2810334	-1.7269	0.0073	0.73%
0.0208	20.8	1.3180633	-1.542	0.0146	1.46%
0.0209	20.9	1.3201463	-1.3383	0.0292	2.92%
0.0255	25.5	1.4065402	-1.2677	0.0365	3.65%
0.0318	31.8	1.5024271	-1.2079	0.0438	4.38%
0.0332	33.2	1.5211381	-1.1563	0.0511	5.11%
0.0339	33.9	1.5301997	-1.109	0.0584	5.84%
0.0343	34.3	1.5352941	-1.0667	0.0657	6.57%
0.0347	34.7	1.5403295	-1.0285	0.073	7.30%
0.0349	34.9	1.5428254	-0.9586	0.0876	8.76%
0.035	35	1.544068	-0.9276	0.0949	9.49%
0.0351	35.1	1.5453071	-0.8978	0.1022	10.22%
0.0363	36.3	1.5599066	-0.8426	0.1168	11.68%
0.0366	36.6	1.5634811	-0.7918	0.1314	13.14%

0.0376	37.6	1.5751878	-0.7454	0.146	14.60%
0.0388	38.8	1.5888317	-0.6809	0.1679	16.79%
0.0392	39.2	1.5932861	-0.6603	0.1752	17.52%
0.0412	41.2	1.6148972	-0.6215	0.1898	18.98%
0.0414	41.4	1.6170003	-0.6027	0.1971	19.71%
0.0417	41.7	1.6201361	-0.5663	0.2117	21.17%
0.0425	42.5	1.6283889	-0.5487	0.219	21.90%
0.0433	43.3	1.6364879	-0.5302	0.2263	22.63%
0.044	44	1.6434527	-0.465	0.255	25.55%
0.0441	44.1	1.6444386	-0.449	0.2628	26.28%
0.0444	44.4	1.647383	-0.4333	0.2701	27.01%
0.046	46	1.6627578	-0.4025	0.2847	28.47%
0.0461	46.1	1.6637009	-0.3874	0.2920	29.20%
0.0483	48.3	1.6839471	-0.343	0.3139	31.39%
0.0486	48.6	1.6866363	-0.3285	0.3212	32.12%
0.0491	49.1	1.6910815	-0.3142	0.3285	32.85%
0.0505	50.5	1.7032914	-0.2857	0.3431	34.31%
0.0506	50.6	1.7041505	-0.2719	0.3504	35.04%
0.0517	51.7	1.7134905	-0.2442	0.365	36.50%
0.0518	51.8	1.7143298	-0.2305	0.3723	37.23%
0.0527	52.7	1.7218106	-0.19	0.3942	39.42%
0.0531	53.1	1.7250945	-0.1766	0.4015	40.15%
0.0536	53.6	1.7291648	-0.1633	0.4088	40.88%
0.054	54	1.7323938	-0.1368	0.4234	42.34%
0.0541	54.1	1.7331973	-0.1236	0.4307	43.07%
0.0547	54.7	1.7379873	-0.1105	0.438	43.80%
0.0559	55.9	1.7474118	-0.0714	0.4599	45.99%
0.056	56	1.748188	-0.0582	0.4672	46.72%
0.0578	57.8	1.7619278	-0.0454	0.4745	47.45%
0.0585	58.5	1.7671559	-0.0195	0.4891	48.91%
0.0587	58.7	1.7686381	-0.0066	0.4964	49.64%
0.0595	59.5	1.774517	0.0064	0.5036	50.36%
0.0606	60.6	1.7824726	0.0193	0.5109	51.09%
0.0622	62.2	1.7937904	0.0582	0.5328	53.28%
0.0626	62.6	1.7965743	0.0842	0.5474	54.74%
0.0627	62.7	1.7972675	0.0973	0.5547	55.47%
0.0637	63.7	1.8041394	0.1103	0.5620	56.20%
0.0647	64.7	1.8109043	0.1235	0.5693	56.93%
0.065	65	1.8129134	0.1366	0.5766	57.66%
0.0667	66.7	1.8241258	0.1631	0.5912	59.12%
0.0668	66.8	1.8247765	0.1764	0.5985	59.85%
0.0676	67.6	1.8299467	0.1898	0.6058	60.58%
0.0686	68.6	1.8363241	0.2168	0.6204	62.04%
0.0691	69.1	1.839478	0.244	0.6350	63.50%
0.0695	69.5	1.8419848	0.2578	0.6423	64.23%
0.0699	69.9	1.8444772	0.2717	0.6496	64.96%
0.07	70	1.845098	0.2857	0.6569	65.69%
0.0708	70.8	1.8500333	0.2998	0.6642	66.42%

0.0709	70.9	1.8506462	0.314	0.6715	67.15%
0.0723	72.3	1.8591383	0.3283	0.6788	67.88%
0.0729	72.9	1.8627275	0.3428	0.6861	68.61%
0.0735	73.5	1.8662873	0.3575	0.69347	69.34%
0.0746	74.6	1.8727388	0.3708	0.7007	70.07%
0.0758	75.8	1.8796692	0.4023	0.7153	71.53%
0.0773	77.3	1.8881795	0.4176	0.7226	72.26%
0.0794	79.4	1.8998205	0.4488	0.7372	73.72%
0.0802	80.2	1.9041744	0.4648	0.7445	74.45%
0.0817	81.7	1.9122221	0.5141	0.7664	76.64%
0.0824	82.4	1.9159272	0.5311	0.7737	77.37%
0.0833	83.3	1.920645	0.5484	0.7810	78.10%
0.0837	83.7	1.9227255	0.5841	0.7956	79.56%
0.0859	85.9	1.9339932	0.6406	0.8175	81.75%
0.0875	87.5	1.9420081	0.6603	0.8248	82.48%
0.0876	87.6	1.9425041	0.6806	0.8321	83.21%
0.0895	89.5	1.951823	0.768	0.8613	86.13%
0.0917	91.7	1.9623693	0.8165	0.8759	87.59%
0.0946	94.6	1.9758911	0.8423	0.8832	88.32%
0.0964	96.4	1.984077	0.9271	0.9051	90.51%
0.0971	97.1	1.9872192	1.028	0.9270	92.70%
0.0977	97.7	1.9898946	1.0651	0.9343	93.43%
0.0985	98.5	1.9934362	1.109	0.9416	94.16%
0.115	115	2.0606978	1.2079	0.9562	95.62%
0.1251	125.1	2.0972573	1.2677	0.9635	96.35%
0.1381	138.1	2.1401937	1.4242	0.9781	97.81%
0.1451	145.1	2.1616674	1.542	0.9854	98.54%
0.157	157	2.1958997	1.7269	0.9927	99.27%

Table 5.14 The ' treated ' data of Time to Failure of grain boundary clusters
in 100 samples of non-annealed interconnect. TTF(s) is the standardize Time to Failure

The distribution of the Time to Failure is determined by many factors associated with the characteristics of the grain boundary clusters. The analysis of the distribution of the length of the grain boundary clusters is also important because it determines the distribution of the Time to Failure. To obtain the distribution of the length of grain boundary clusters, the similar approach of the Time to Failure is used. The lognormal distribution of the length of grain boundary clusters are shown in Fig5.34
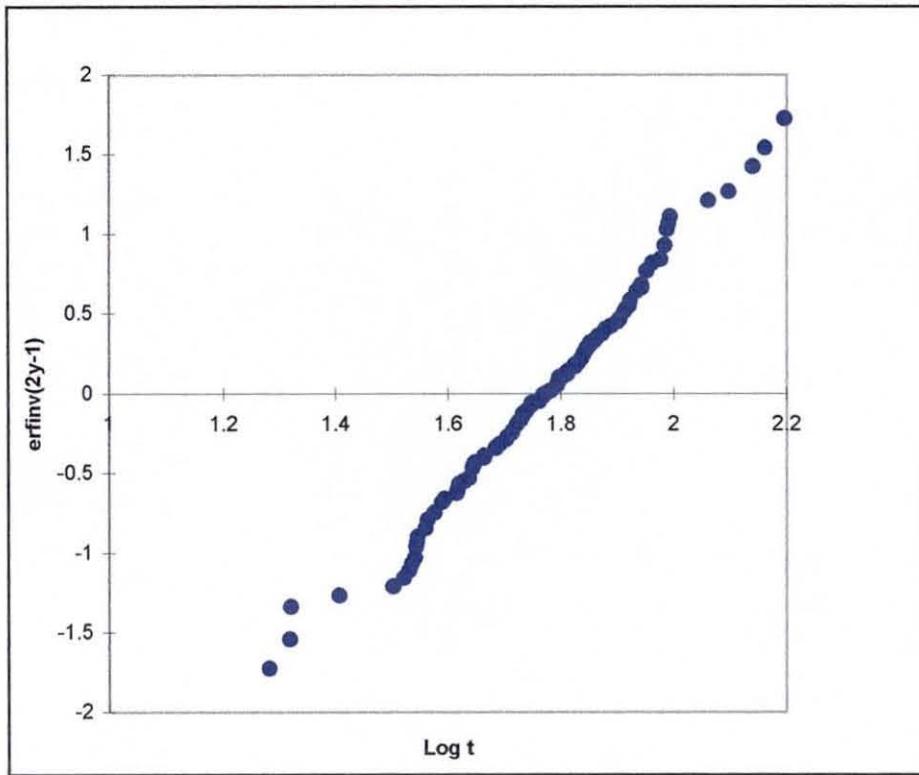
Fig 5.33 The plot of lognormal distribution of Time to Failure of
grain boundary clusters in 100 samples of non-annealed interconnects
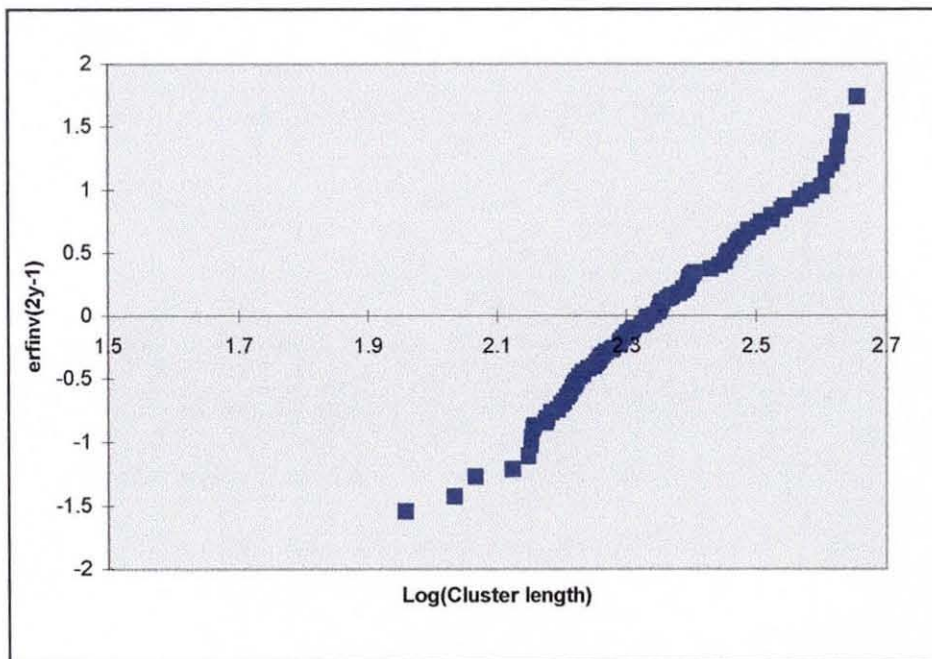
Fig. 5.34 Lognormal distributions of length of grain boundary clusters

Form the above figures, the distribution of the simulated Time to Failure and the grain boundary clusters obtained from the experiment involving 100 samples of non-annealed interconnects fit a lognormal distribution function well. The plots of the graphs are of typical of those observed in other computer simulations reported in the literature[Joo and Thompson,1994],[Kircheim and Kaeber,1991] [Knowlton, et.al,1997]

v) The Median Time to Failure (MTTF) and The Standard Deviation (DTTF)

From the lognormal distribution graph, the median and the standard deviation of the Time to Failure and the grain boundary cluster length can be obtained. Table 5.15 shows the arbitrary and the physical values for the MTTF, and the Median length of grain boundaries clusters and their respective standard deviations. The Standard deviation (σ_{sd}) is calculated from the slope of the graph and by using eqn(5.20) i.e gradient =

$$\frac{1}{\sqrt{2}\sigma}$$

Parameters	Scaling Factor	Median(arbitrary)	Median(actual)	Std deviation
Time To Failure	118Hours	0.059	6.962 Hours	0.188
Length of grain boundary cluster	43 μm	0.218	9.374 μm	0.154

Table 5.15 The median and the standard deviation of the Time to Failure and length of grain boundary cluster.

5.4.3 Results of experiment no.1(b)- non-annealed interconnect lines

i) 'Weakest link model' in determining the Time to Failure of interconnect

In the earlier experiment, the analysis done on the grain boundary clusters produced results which are very encouraging . It has been demonstrated that the distributions of the

simulated length of the grain boundaries clusters and the Time to Failure gave a very good fit on the lognormal distribution function. In this experiment, the Time to Failure of the interconnect is simulated. Basically the method used in determining the Time to Failure of the interconnect is by adopting the 'weakest link' model where the shortest/minimum failure time or (TTF) attain by a grain boundary cluster be the Time to Failure of the interconnect. The raw data of the Time to Failure obtained from 100 samples of interconnect are shown in Table 5.16. An example to demonstrate the weakest link model is shown below:-

The non-annealed interconnect sample no 5 (Fig 5.27(a)) has a total of 3 grain boundary clusters. The detail of the characteristics of the clusters is shown in the table below (taken from Table A.1) where Cluster no.1 has a total of 3 grain boundaries, Cluster no. 2 has 5 grain boundaries and Cluster no 3 also has 5 grain boundaries. Cluster no.1 did not fail because the vacancy concentration did not reach the critical vacancy concentration level. The reason may be because of the 'Blech length' effect where its total length is shorter than the critical length for failure to occur. Cluster no 2 and no.3 did fail, but since Cluster no 3, recorded a lower value of Time to Failure than Cluster No 2, therefore Cluster no 3 will fail first , it is the ' weakest link' in the line. Fig 5.35(a) and Fig 5.35(b) shows the vacancy profile of the grain boundary clusters.
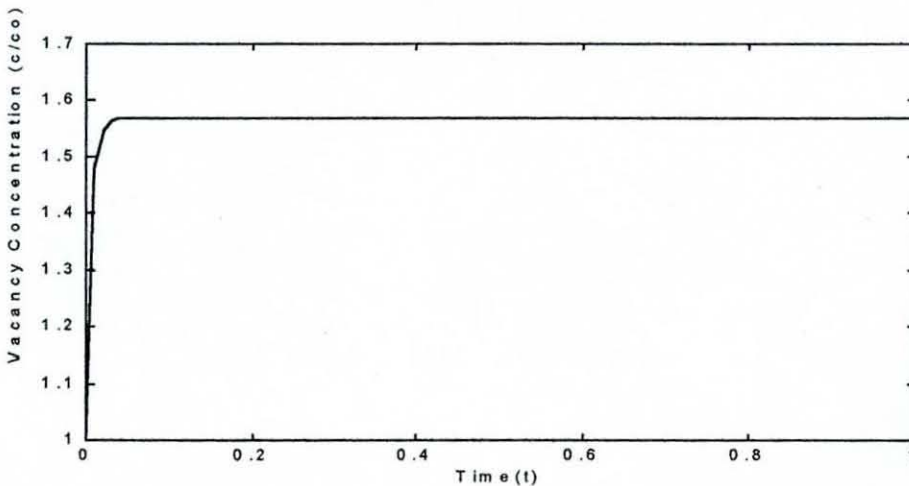
Fig.5.35(a)   The vacancy concentration response for Cluster no 1 of interconnect sample no 5. The vacancy concentration does not reach the critical vacancy concentration of 2co

248
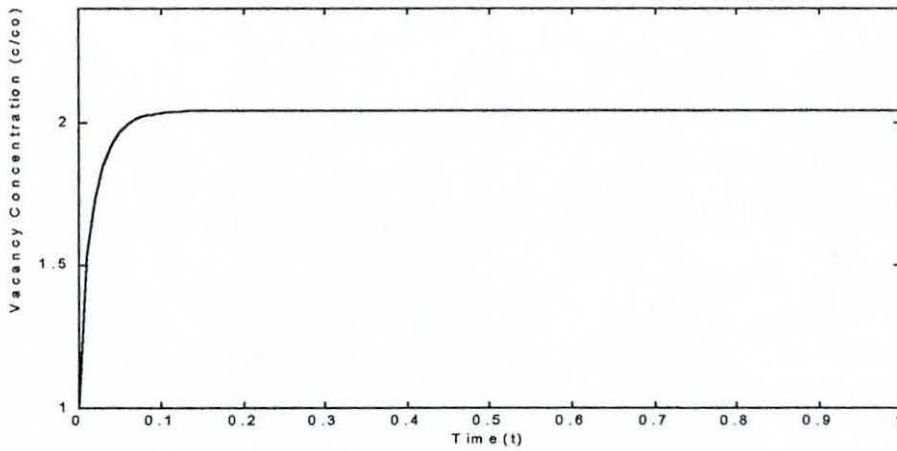
Fig. 5.35(a)　The vacancy concentration response for Cluster no 2 of interconnect sample no 5 .
　　　　　　　The vacancy concentration reach the critical vacancy concentration of 2co at t= 0.0967
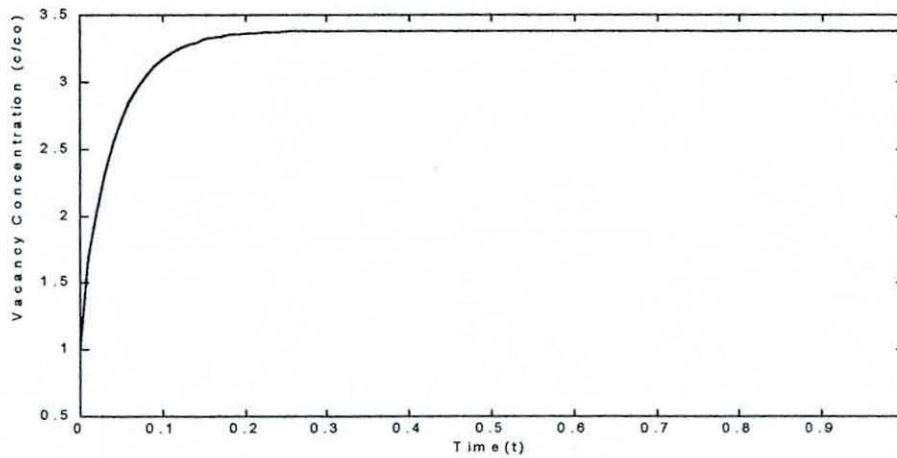
Fig. 5.35(a)　The vacancy concentration response for Cluster no 3 of interconnect sample no 5
　　　　　　　The vacancy concentration reach the critical vacancy concentration of 2co at t= 0.0191
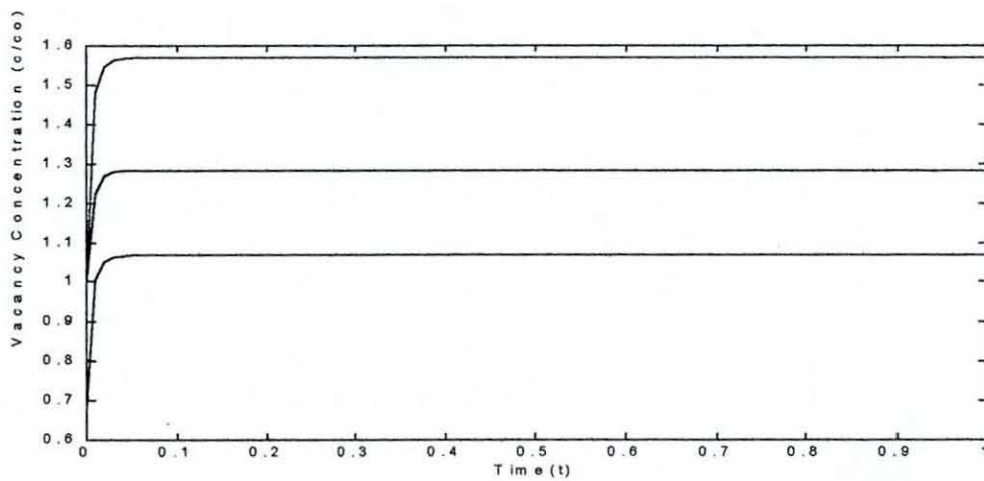
Fig.5.35(b)　The vacancy concentration response at all the nodes of Cluster No 1 of interconnect

249

sample no 5. The upper most line is the vacancy profile at the end of the grain boundary cluster
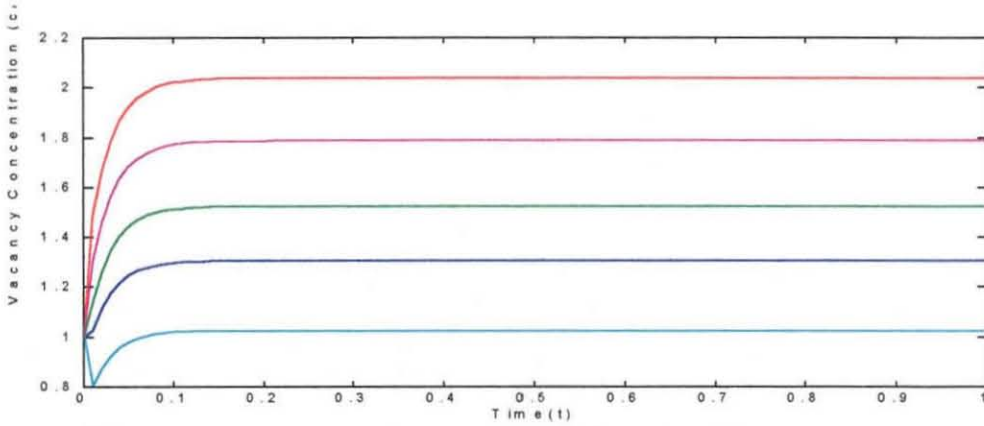
Fig.5.35(b)   The vacancy concentration response at all the nodes of Cluster No 2 of interconnect sample no 5. The upper most line is the vacancy profile at the end of the grain boundary cluster.
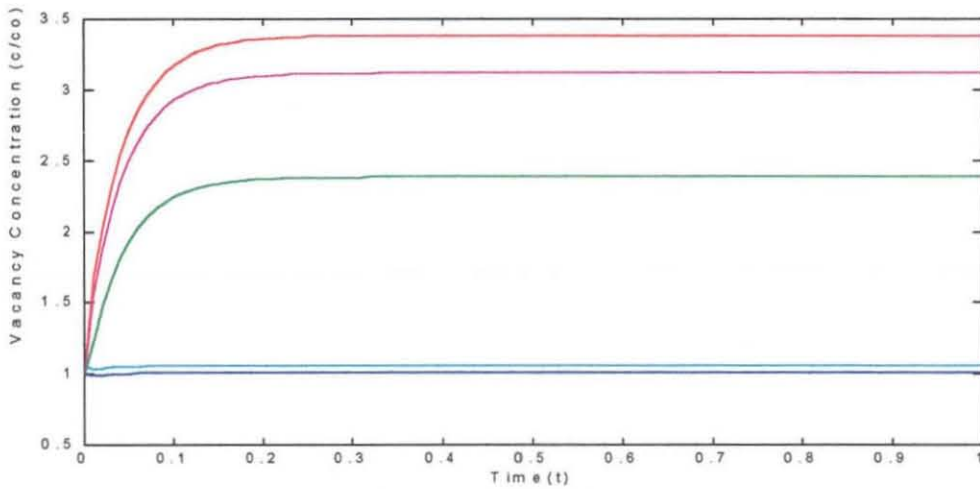
Fig.5.35(b)   The vacancy concentration response at all the nodes of Cluster No 3 of interconnect sample no 5. The upper most line is the vacancy profile at the end of the grain boundary cluster

CLIP	No of clusters	Cluster No	Cluster length	No. of GB	TTF	TTF OF SAMPLE
0.4-0.49	3	1	0.0901	3	-	-
		2	0.1428	5	0.0967	
		3	0.244	5	0.0191	**0.0191**

clipping from Table A.1

0.0191	0.0392	0.0517	0.0684	0.0892
0.0208	0.0412	0.0518	0.0686	0.0985
0.0209	0.0414	0.0523	0.0691	0.1048
0.0255	0.0416	0.0527	0.0695	
0.0318	0.0433	0.0531	0.0699	
0.0332	0.0437	0.0538	0.07	
0.0339	0.0438	0.0541	0.0709	

250

0.0349	0.0438	0.0547	0.0723	
0.0349	0.044	0.0549	0.0729	
0.035	0.0441	0.0559	0.0735	
0.0351	0.0444	0.0584	0.0746	
0.0352	0.0456	0.0585	0.0773	
0.0363	0.046	0.0626	0.0778	
0.0366	0.0461	0.0626	0.0802	
0.0366	0.0479	0.0627	0.0817	
0.0376	0.0483	0.0637	0.0835	
0.0376	0.0486	0.065	0.0854	
0.0381	0.0491	0.0667	0.0875	
0.0386	0.0494	0.0667	0.0876	
0.0388	0.0506	0.0676	0.0879	

Table 5.16 The raw data of the Time to Failure of interconnects obtained from 100 samples of non-annealed interconnects

ii) The distribution of the Time to Failure, Median Time to Failure and Deviation Time to Failure

The same procedure(as in the previous experiment) is applied to obtain the distribution of the Time to Failure . The 'treated' data of the Time to Failure of the interconnects is shown in Table A1.2 in Appendix A1. Fig 5.36 shows the distribution of the simulated Time to Failure of the interconnects which again fits a lognormal distribution function quite well. The Median Time to Failure (MTTF) calculated is 0.05175 which corresponds to 6.1 hours and the Deviation Time to Failure (DTTF) calculated is 0.148. The MTTF and DTTF from experimental results of [Cho and Thompson, 1989] for as-deposited interconnect line (without annealing) is 9.8 hours and 0.197 respectively.
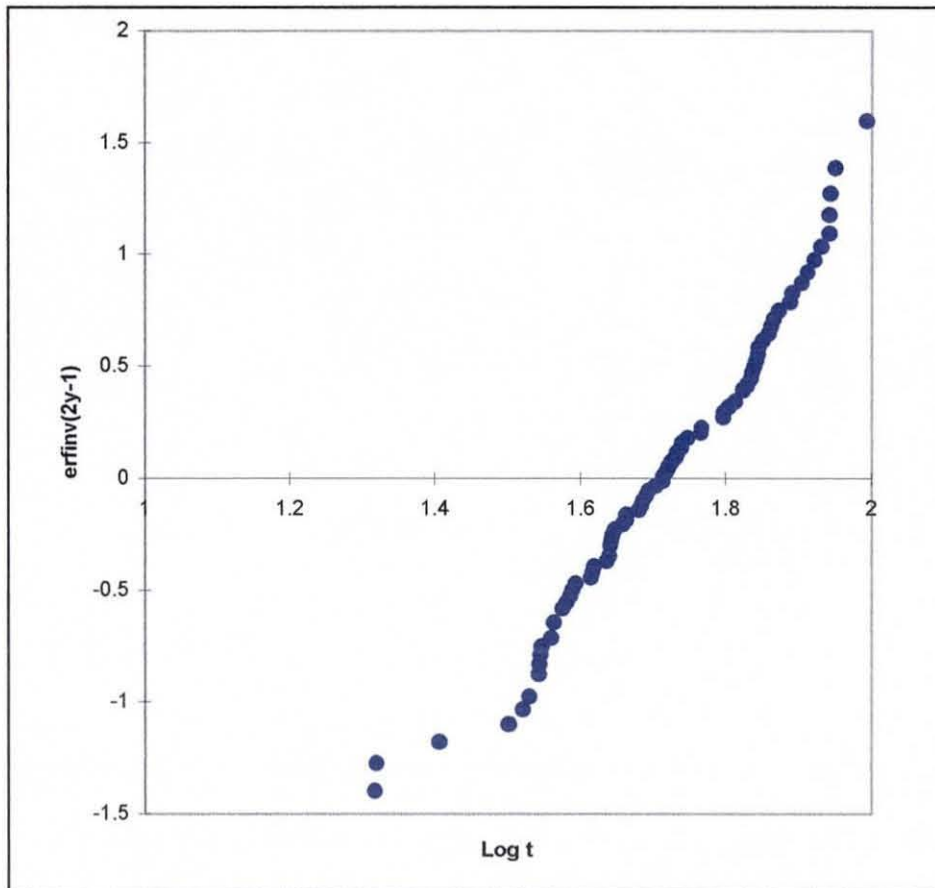
Fig 5.36 Lognormal distribution of the Time to Failure of the interconnects
obtained from 100 samples of non-annealed interconnects

5.4.4 Results of experiment no.2(a)- annealed grain boundary clusters

In the literature, normally the Al film which have been annealed will have a better
lifetime than non-annealed Al film. The effect of annealing of the Al film is to produce a
larger grain size and longer grain boundaries which has a direct effect on the
electromigration lifetime of interconnect. .In the current work, the annealing simulation
is not run as long as it would be as in a real experiments, however it is sufficient to make
an analysis of its effect on the grain boundary structure and the Time to Failure.

i) Data of the length of grain boundary cluster and its Time to Failure

In experiment no.2(a) , 100 samples of annealed interconnect are produced from 10 samples of annealed Al films as shown previously in Fig5.28(a)-Fig5.28(j). The results of the length of grain boundary cluster and the Time-to-failure in arbitrary units obtained are summarised in Table 5.16 and 5.17 below (data taken from Table A2.1).

0.0256	0.0743	0.118	0.1458	0.1668	0.2183	0.2771
0.0256	0.0815	0.1184	0.1477	0.1669	0.2187	0.2787
0.027	0.082	0.1189	0.1477	0.1696	0.2188	0.279
0.0317	0.0828	0.1213	0.1499	0.1699	0.2204	0.2791
0.0334	0.0844	0.1213	0.1505	0.172	0.2245	0.2805
0.034	0.0855	0.1217	0.1514	0.1751	0.227	0.2822
0.0372	0.086	0.1218	0.1515	0.1769	0.2286	0.2823
0.0378	0.0869	0.1232	0.1518	0.1772	0.2305	0.2913
0.0388	0.0889	0.1237	0.1525	0.1782	0.2308	0.2956
0.0405	0.0893	0.1256	0.1528	0.1832	0.2309	0.3084
0.0415	0.0894	0.1261	0.1536	0.1858	0.2349	0.31
0.0425	0.0926	0.1273	0.1536	0.1875	0.2364	0.3113
0.043	0.0931	0.1278	0.1542	0.1885	0.2373	0.3276
0.0451	0.0963	0.1294	0.1543	0.1902	0.2422	0.3282
0.0469	0.0981	0.1299	0.1551	0.1913	0.2425	0.3364
0.0469	0.0989	0.1306	0.1559	0.1939	0.2458	0.3418
0.0478	0.1	0.1307	0.1564	0.1967	0.2466	0.3536
0.0492	0.1022	0.1308	0.1564	0.1969	0.249	0.3609
0.0586	0.1026	0.1308	0.1569	0.198	0.2515	0.3631
0.062	0.103	0.131	0.1588	0.2003	0.2516	0.3645
0.0627	0.1085	0.1319	0.1591	0.2015	0.253	0.3662
0.0644	0.1089	0.1346	0.1608	0.2036	0.2568	0.3689
0.0645	0.1098	0.1351	0.1609	0.2076	0.2579	0.3746
0.067	0.1121	0.1357	0.1614	0.2082	0.2581	0.3958
0.0687	0.1124	0.1362	0.1619	0.2085	0.26	0.3959
0.069	0.1149	0.1387	0.1625	0.2094	0.2604	0.3964
0.071	0.1156	0.1393	0.1638	0.212	0.2656	0.4122
0.0722	0.1159	0.1395	0.165	0.2137	0.2669	0.4164
0.0725	0.1168	0.1403	0.1656	0.2164	0.2684	0.4417
0.073	0.1177	0.1452	0.1664	0.2182	0.2732	0.455

Table 5.16 The length of grain boundary cluster (arbitrary units) in the 100

samples of annealed interconnects arranged in ascending order.

0.0326	0.044	0.0549	0.0654	0.081	0.0916	0.19
0.0326	0.0442	0.055	0.0658	0.0811	0.0919	

0.0328	0.0443	0.0552	0.0658	0.0811	0.0925	
0.0331	0.0448	0.056	0.0661	0.0812	0.093	
0.0333	0.0453	0.056	0.0665	0.0823	0.0934	
0.0342	0.0458	0.056	0.0674	0.083	0.0947	
0.0342	0.0473	0.0563	0.0675	0.0837	0.0961	
0.0344	0.0494	0.0565	0.069	0.0848	0.0987	
0.0359	0.05	0.0568	0.0707	0.0849	0.0993	
0.0367	0.0501	0.0576	0.0716	0.085	0.1069	
0.0367	0.0501	0.0576	0.0737	0.0855	0.1126	
0.0385	0.0504	0.0603	0.0743	0.0855	0.1173	
0.0392	0.0511	0.0614	0.0743	0.086	0.1287	
0.0394	0.0515	0.0617	0.0749	0.0861	0.1299	
0.0416	0.0518	0.0619	0.0751	0.0866	0.1407	
0.0424	0.0524	0.0623	0.0768	0.0867	0.148	
0.0425	0.0526	0.0637	0.078	0.0868	0.1497	
0.0427	0.0527	0.0641	0.0799	0.0868	0.1524	
0.0435	0.0536	0.0647	0.0806	0.0896	0.1762	
0.0437	0.0539	0.0647	0.0808	0.0902	0.184	

Table5.17 The Time to Failure of grain boundary clusters in the 100 samples of
annealed interconnects arranged in ascending order.

From the summarised data shown in Table 5.16 and 5.17, the range of the length of the
cluster obtained from the simulation is between 0.0256 (shortest length) - 0.455
(longest length) and the Time to Failure obtained is between 0.0326(the fastest time) -
0.19(the slowest time). Translating into the actual values, the length of the grain
boundary cluster lies in the range of 1.1 $\mu m - 19.56\mu m$ (scale $= 43\,\mu m$) giving a physical
time in the range of 3.85 hrs-22.42 hrs (the time scale used is $\eta=118$hrs). From the raw
data observation, the initial results of the simulated annealed interconnects is in
agreement with the literature[Cho and Thompson,1989] where the values of the length of
grain boundary clusters and the Time to Failure indicates a higher value than the
simulated non-annealed interconnects as expected.

ii) **The distribution of the number of cluster and number of grain boundaries**

Fig 5.36 shows the distribution of the simulated number of cluster found per interconnect
while Fig 5.37 shows the distribution of the simulated number of grain boundaries found
in per cluster obtained from 100 samples of annealed interconnects.
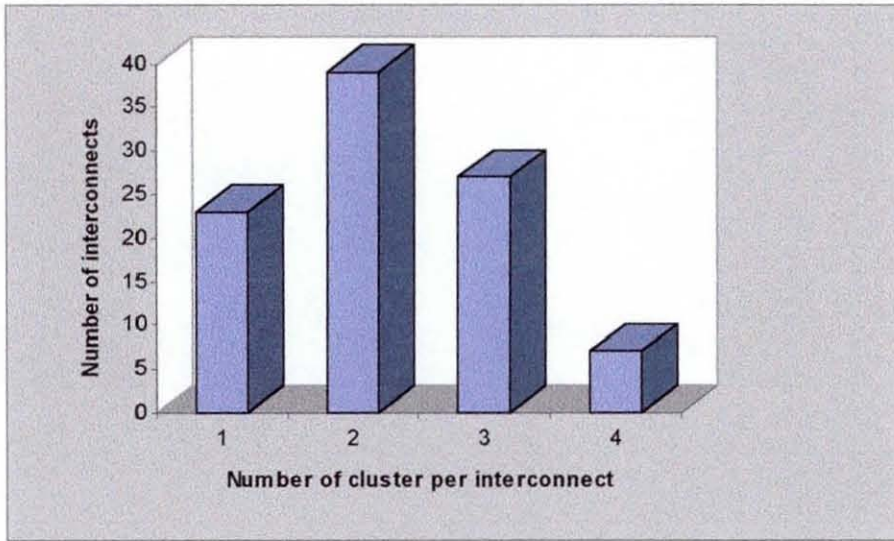
Fig 5.36 Distribution of the simulated number of cluster found per interconnect obtained from 100 samples of annealed interconnects
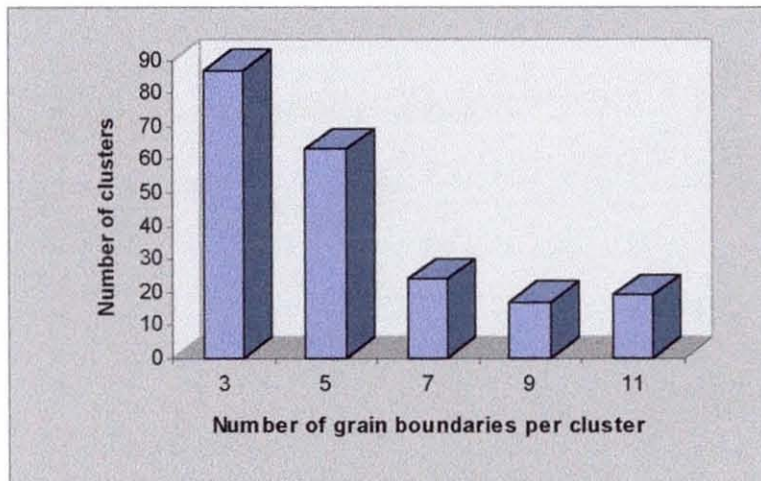
Fig 5.37 Distributions of the simulated number of grain boundaries found per cluster obtained from 100 samples of annealed interconnects

iii)   **The distribution of length of grain boundary cluster and Time to Failure**

Fig 5.38 below shows the histogram and the cumulative distribution of the length of the grain boundary cluster, while Fig5.39 shows the cumulative distribution of the Time to Failure of the grain boundary clusters.
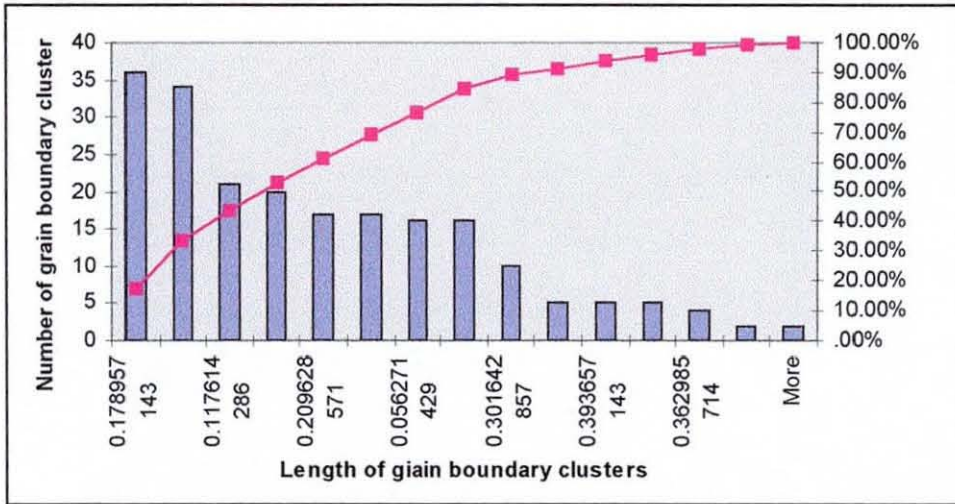
Fig 5.38 The histogram and the cumulative distributions of the simulated length

of grain boundary cluster in 100 sample of annealed interconnect
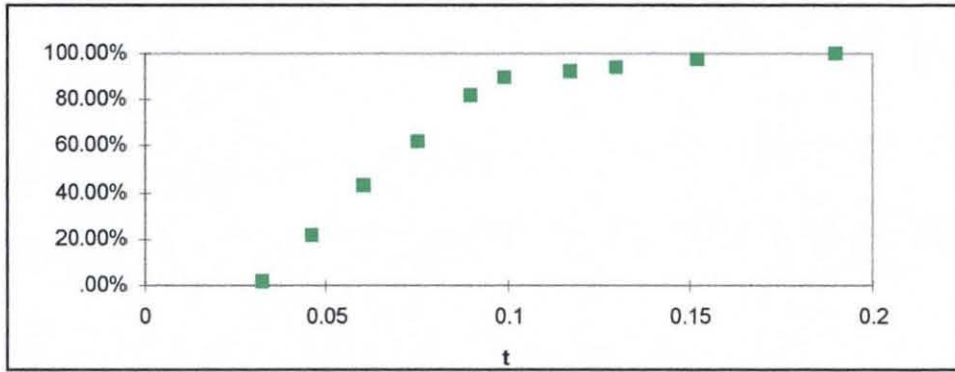
Fig5.39 The cumulative distribution of Time to Failure of grain boundary
clusters found in 100 samples of annealed interconnect

iv) The distribution of the Time to Failure, Mean Time to Failure and standard deviation

The same procedure(as in the previous experiment) is applied to obtain the distribution of the length of grain boundary clusters and Time to Failure . The 'treated' data of the Time to Failure of grain boundary cluster are shown in Table A2.1 of Appendix A . Fig 5.40 shows the distribution of the simulated length of grain boundary clusters and Fig

5.41 the distribution of the simulated Time to Failure of the grain boundary clusters interconnects which both fit well of a lognormal distribution
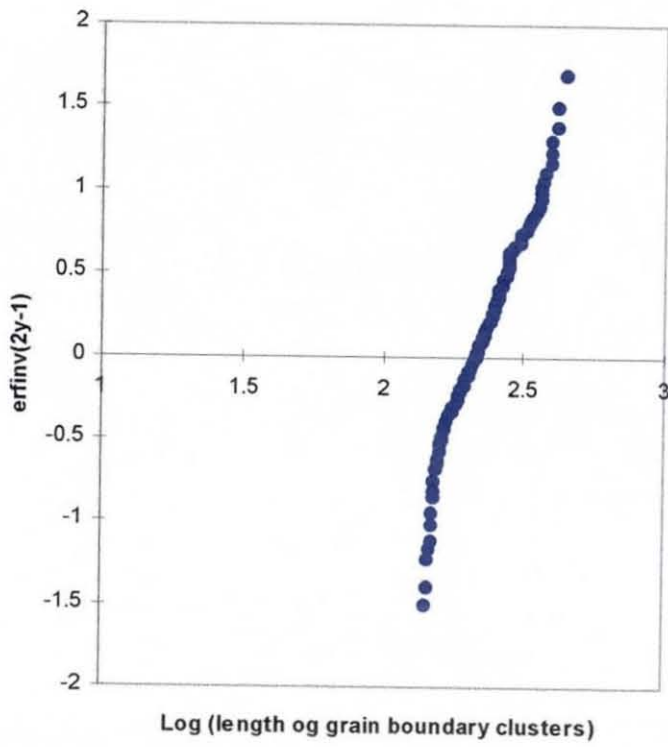
Fig5.40 Lognormal distribution of the length of grain boundaries obtained from 100 samples of annealed interconnects
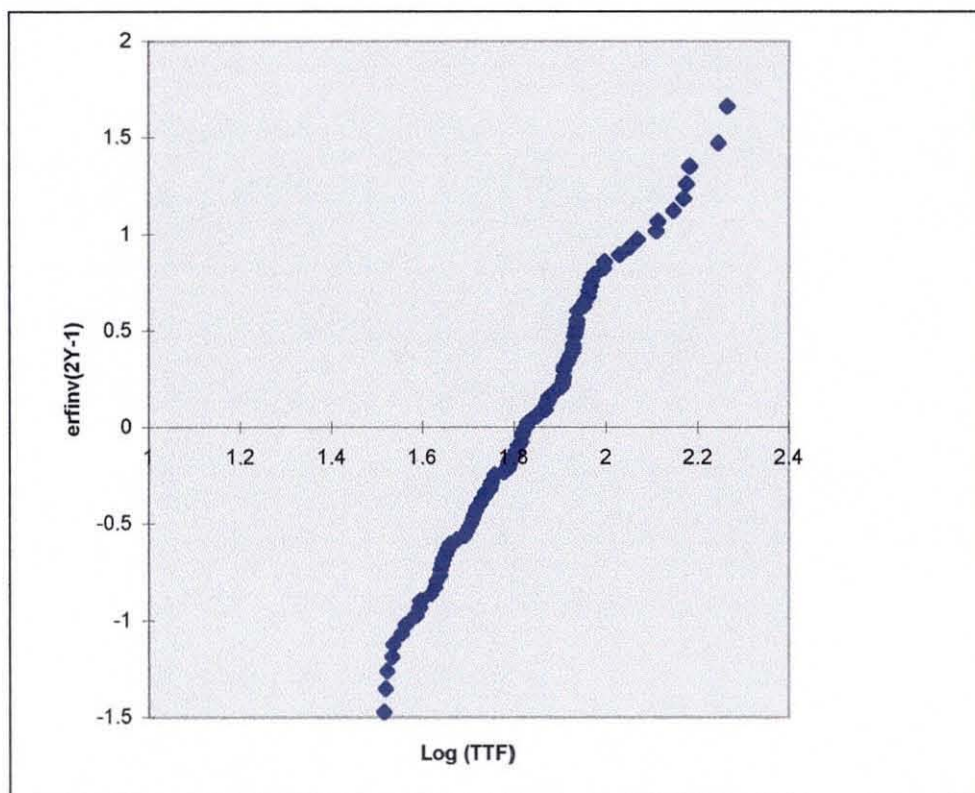
Fig 5.41 The lognormal distribution of the Time to Failure of grain boundary

clusters obtained from 100 samples of annealed interconnects

Parameters	Scaling Factor	Median(arbitrary)	Median(actual)	Std deviation
Time To Failure	118Hours	0.067	7.9 Hours	0.198
Length of grain boundary cluster	43 μm	0.218	9.374 μm	0.157

Table 5.18 The median and the standard deviation of the Time to Failure and length of grain boundary cluster.

From the simulation results obtained, the median Time to Failure is higher (1 hour) for the annealed interconnects than the non-annealed interconnects. The median length of grain boundaries is about the same for both the non-annealed and annealed interconnects.

5.4.5 Results of experiment no.2(b)- annealed interconnects

(i) Data of Time to Failure

The same approach is applied in determining the simulated Time to Failure of the interconnect by the 'weakest link model'. The raw data on the Time to failure of the interconnects are shown in Table5.19 below.

0.0326	0.0443	0.0565	0.078
0.0326	0.0448	0.0568	0.0799
0.0328	0.0453	0.0576	0.0811
0.0331	0.0458	0.0576	0.0849
0.0333	0.0494	0.0603	0.086
0.0342	0.05	0.0614	0.0866
0.0342	0.0501	0.0617	0.0867
0.0344	0.0501	0.0623	0.0868
0.0359	0.0504	0.0637	0.0868
0.0367	0.0515	0.0641	0.0896
0.0367	0.0518	0.0647	0.0919
0.0385	0.0524	0.0654	0.0934
0.0392	0.0526	0.0658	0.0947
0.0416	0.0527	0.0674	0.1069
0.0424	0.0539	0.0675	0.1126
0.0425	0.0549	0.069	0.1173
0.0427	0.0552	0.0716	0.1299
0.0435	0.056	0.0743	0.148
0.0437	0.056	0.0749	0.1497
0.044	0.0563	0.0768	

Table 5.19 The arbitrary Time to Failure of interconnects obtained from 100 samples of annealed interconnects.

From Table 5.19 , the raw data on Time to Failure suggest the range of the Time to Failure is between 0.0326 and 0.1497 which corresponds to the physical time of between 3.846 hours and 17.66 hours with the same time scale used(118hrs).

ii) The distribution of the Time to Failure, Mean Time to Failure and standard deviation

The same procedure(as in the previous experiment) is applied to obtain the distribution of the Time to Failure . The 'treated' data of the Time to Failure of the interconnects are shown in Table A.2.2 in Appendix A2 . Fig 5.42 shows the distribution of the simulated Time to Failure of the interconnects which fits well of a lognormal distribution function. The Median Time to Failure (MTTF) calculated is 0.0561 which corresponds to 6.63 Hours and the standard deviation calculated is 0.179
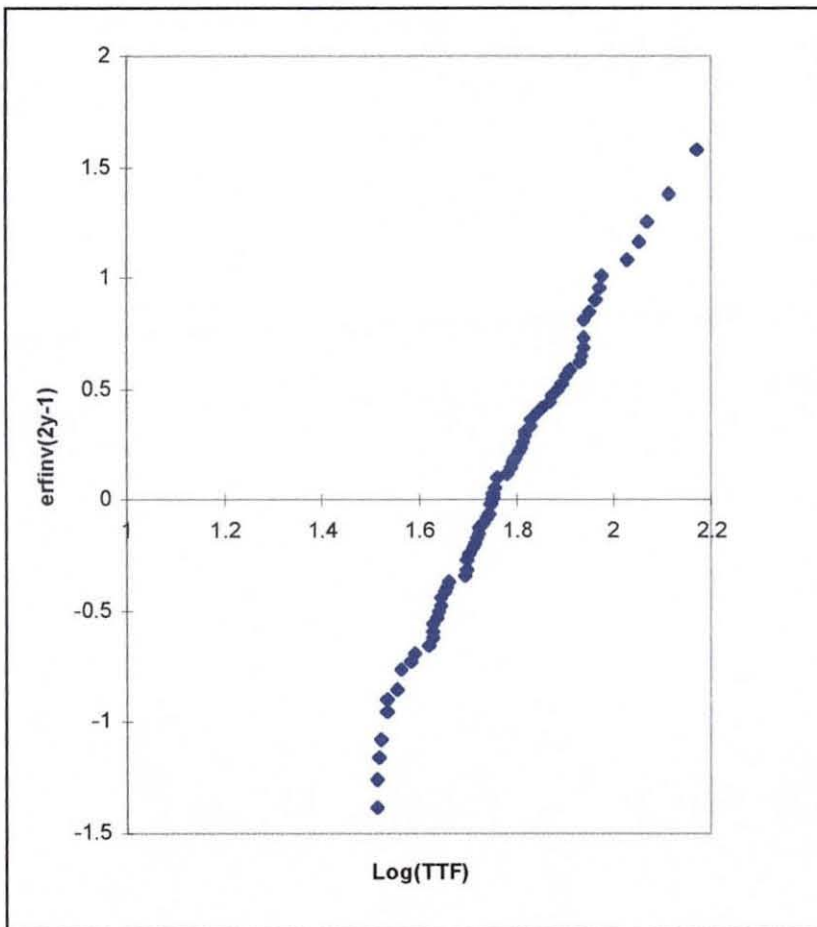
Fig 5.42 Lognormal distribution of the simulated Time to Failure

of interconnects obtained from 100 samples of annealed interconnects

Comparing the Medium Time to Failure between the non-annealed and annealed interconnects, the results shows that the annealed interconnect produce higher MTTF of about 0.6 hours than the non-annealed interconnects but both appear to display a log normal distribution. Although the values of the MTTF and DTTF is not as high compared to [Cho and Thomson,1989] which the MTTF is 26.3 hours and DTTF is 0.465 , the results may be reasonable because of the small time used in the annealing process. However the results shows that annealing process does improve the MTTF as expected. .

5.4.6 Results of experiment no.3 - The effect of Time to Failure with varying interconnect width.

i) The samples under investigation

In this simulation, the effect of varying the width of the interconnect by keeping the length of interconnect constant is analysed. The first five samples of non-annealed Al films [Fig 5.27(a)-5.27(e)] are again used in the study to investigate these effects. The width/length ratio of the interconnect under investigation are made up of a) 0.04, b)0.075 c) 0.1d) 0.15 e) 0.2 samples. The detailed results of the Time to Failure are shown in Table A.3 in Appendix A3. The distribution of the simulated number of clusters of all the samples are shown in Fig5.44(a)-5.44(e)
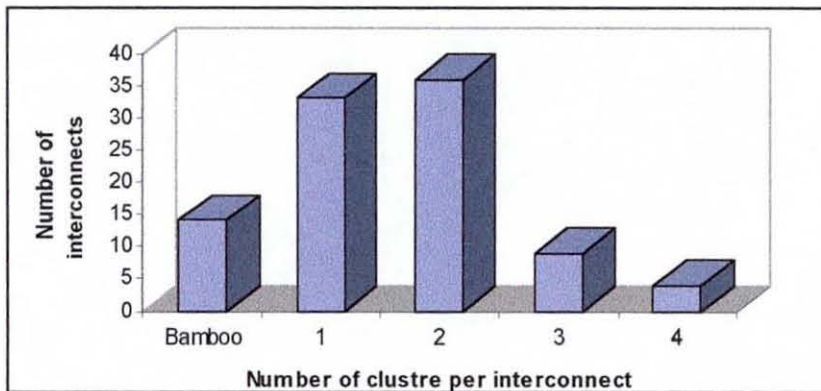
Fig5.44(a) The distribution of simulated number of cluster for sample a)0.04
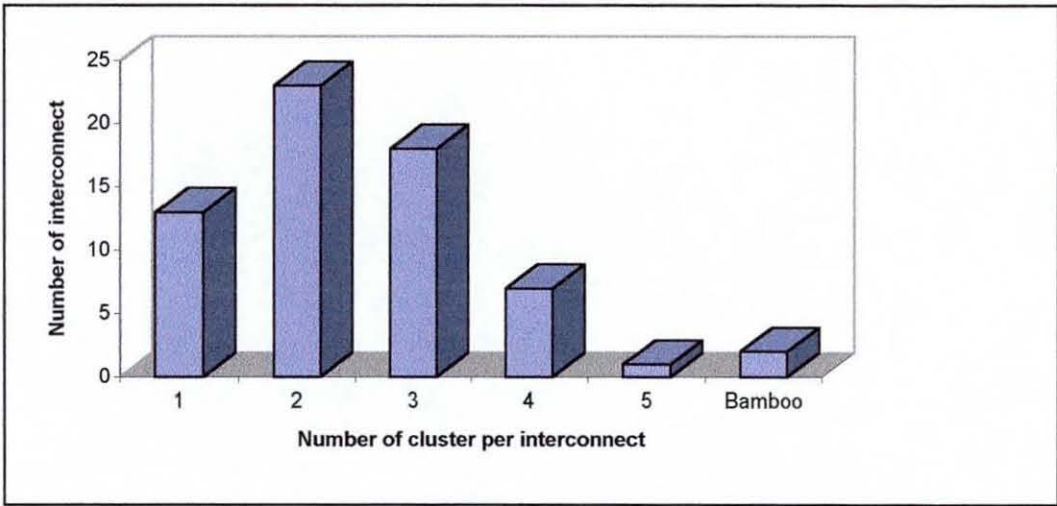
Fig 5.44(b) Distribution of simulated number of clusters in sample b)0.075
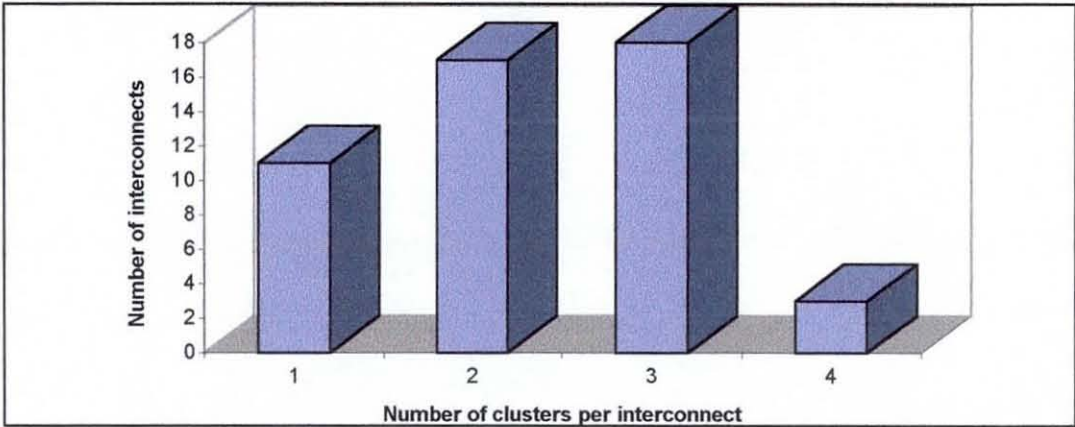
Fig 5.44(c) Distribution of simulated number of clusters in sample c)0.1
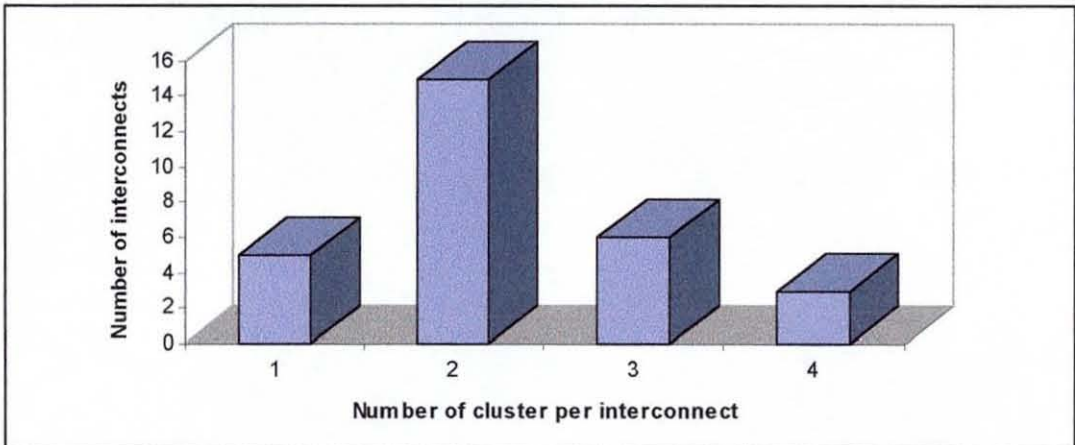
Fig 5.44(d) Distribution of simulated number of clusters in sample d)0.15
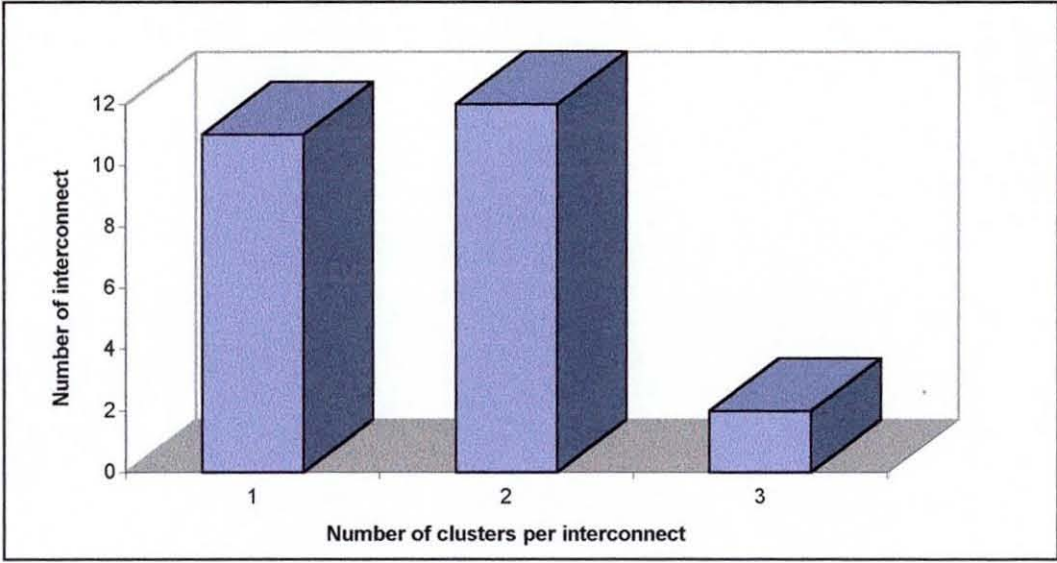
Fig 5.44(e) Distribution of simulated number of clusters in sample e)0.2
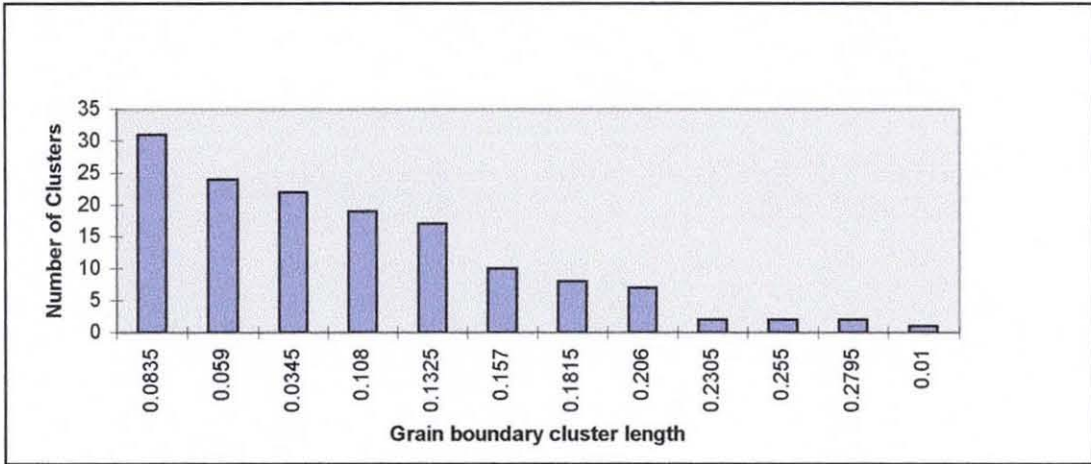
Fig 5.45 The distribution of cluster length of sample a)0.04

ii) Analysis of simulation results of Time to Failure

The raw data of the simulated Time to Failure for each set of the samples above are shown in Table5.20. The data of the Time to Failure are in terms of the percentages of interconnects which fails. The results obtained shows that only   30% of the interconnects of sample (a) fails , 70 % of sample (b), 90% of sample (c) and the other samples (d) and

(e) record 100 % failure. As the interconnect width/length ratio are decreased, less and less failure is observed because the interconnect are geared towards bamboo structure as can be seen from the distribution of the number of cluster in Fig 5.44(a). Another reason is the ' Blech length' effect, as can be seen from Fig5.45 where about 60% of the cluster lengths, is below the critical length for failure (cluster length ≤ 0.1325 more or less did not failed)

%	TTF(a)	%	TTF(b)	%	TTF(c)	%	TTF(d)	%	TTF(e)
1	0.0128	1.538462	0.011	2	0.0108	0.344828	0.0129	4.347826	0.0133
2	0.0129	3.076923	0.0127	4	0.0133	6.896552	0.0147	8.695652	0.0146
3	0.0132	4.615385	0.0136	6	0.015	10.34483	0.0157	13.04348	0.0154
4	0.0134	6.153846	0.0137	8	0.0172	13.7931	0.0163	17.3913	0.0173
5	0.0151	7.692308	0.014	10	0.0173	17.24138	0.017	21.73913	0.0195
6	0.0159	9.230769	0.0142	12	0.018	20.68966	0.0171	26.08696	0.0197
7	0.0169	10.76923	0.0142	14	0.0184	24.13793	0.0185	30.43478	0.02
8	0.0173	12.30769	0.0149	16	0.0186	27.58621	0.0193	34.78261	0.0203
9	0.0173	13.84615	0.0155	18	0.0187	31.03448	0.0212	39.13043	0.0221
10	0.0198	15.38462	0.016	20	0.0187	34.48276	0.0229	43.47826	0.0231
11	0.0199	16.92308	0.0169	22	0.0191	37.93103	0.0237	47.82609	0.0242
12	0.0207	18.46154	0.0172	24	0.0193	41.37931	0.0249	52.17391	0.0247
13	0.0218	20	0.0178	26	0.0194	44.82759	0.026	56.52174	0.0259
14	0.0218	21.53846	0.0182	28	0.0198	48.27586	0.026	60.86957	0.0262
15	0.0234	23.07692	0.0189	30	0.0201	51.72414	0.0267	65.21739	0.0311
16	0.0256	24.61538	0.02	32	0.0209	55.17241	0.0268	69.56522	0.0324
17	0.0257	26.15385	0.0209	34	0.0215	58.62069	0.0272	73.91304	0.0347
18	0.026	27.69231	0.0215	36	0.0217	62.06897	0.0296	78.26087	0.0518
19	0.0262	29.23077	0.022	38	0.0221	65.51724	0.0297	82.6087	0.0524
20	0.0263	30.76923	0.0221	40	0.0224	68.96552	0.0323	86.95652	0.0542
21	0.0279	32.30769	0.0229	42	0.0249	72.41379	0.0361	91.30435	0.06
22	0.029	33.84615	0.0231	44	0.0263	75.86207	0.0366	95.65217	0.0792
23	0.0295	35.38462	0.0233	46	0.0263	79.31034	0.0382	100	0.0833
24	0.0298	36.92308	0.0256	48	0.0273	82.75862	0.043		
25	0.0307	38.46154	0.0261	50	0.0275	86.2069	0.0435		
26	0.0442	40	0.0264	52	0.0277	89.65517	0.0456		
27	0.0741	41.53846	0.0265	54	0.0279	93.10345	0.0496		
28	0.0744	43.07692	0.0273	56	0.028	96.55172	0.0628		
29	0.0756	44.61538	0.0275	58	0.0286	100	0.0842		
		46.15385	0.0276	60	0.0307				
		47.69231	0.0288	62	0.0339				
		47.69231	0.029	64	0.0346				
		50.76923	0.0299	66	0.0346				
		52.30769	0.0309	68	0.0352				
		53.84615	0.0337	70	0.0361				
		55.38462	0.0365	72	0.0368				

		56.92308	0.0399	74	0.0407				
		58.46154	0.0403	76	0.0494				
		60	0.0413	78	0.05				
		61.53846	0.0414	80	0.0635				
		63.07692	0.045	82	0.0686				
		64.61538	0.0485	84	0.0716				
		66.15385	0.0505	86	0.078				
		67.69231	0.0511	88	0.0802				
		69.23077	0.0582						
		70.76923	0.0588						

Table 5.20 The Time to Failure for the 5 samples of Al films with different width/length ratio

The physical Time to Failure are shown in Table 5.21 below

Sample	Arbitrary range	Time scale	ActualTime range(hrs)
(a) 0.04	0.0128-0.0756	118	1.51-8.92
(b) 0.075	0.011- 0.0588	118	1.29 -6.94
(c) 0.1	0.0108-0.0802	118	1.27- 9.46
(d) 0.15	0.0129-0.0842	118	1.52- 9.94
(e) 0.2	0.0133-0.0833	118	1.56 - 9.83

Table 5.21 The physical Time to failure of samples

Fig 5.46 shows the simulated Time to Failure graphs of all the samples in terms of the percentage of the interconnects which have failed with its Time to Failure profile. From the graphs, sample (c),(d) and (e) have the highest percentage of interconnects that have failed and sample (a) has the lowest percentage failures. The reasons for this has been discussed earlier where sample(a) and (b) has few interconnects having bamboo structure which is resistant to electromigration along its grain boundaries. The only way that failure occurs through electromigration is by bulk diffusion which is not considered in the current work. The other reason is because of cluster length is not long enough for the stress/vacancy to reach the critical value for failure to occur. For sample c,d and e , their cluster length and their internal grain boundary structure supports the stress/ vacancy flow along its grain boundaries required to reach the critical value for failure to occur.
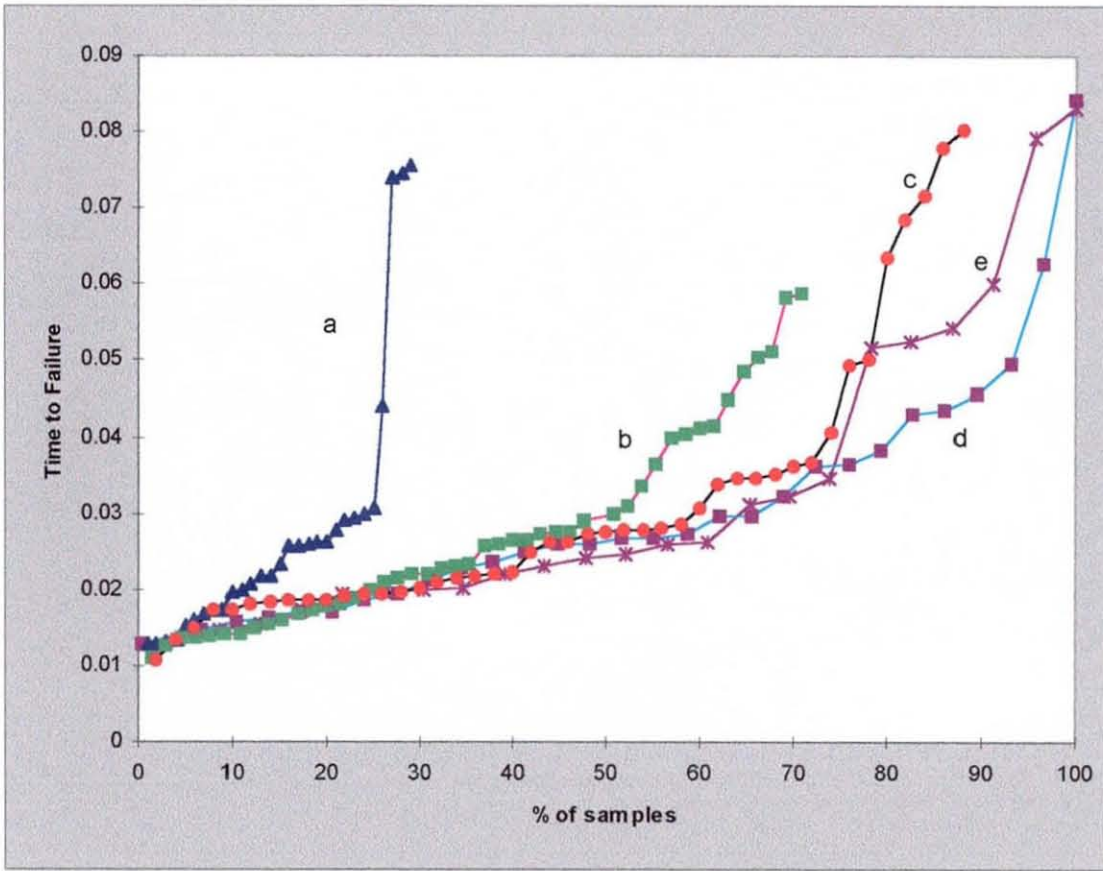
Fig 5.46 The % of samples with their simulated Time to Failure (arbitrary units) profile where sample a=0.04, b=0.075, c=0.1, d=0.15 and e=0.2

iii) The distribution of Time to Failure

The lognormal distributions of the simulated Time to Failure for the samples are shown in Fig5.47(sample(a)), Fig5.48(sample(b)), Fig5.49(sample (c)), Fig 5.50(sample(d)) and Fig5.51(sample(e)).
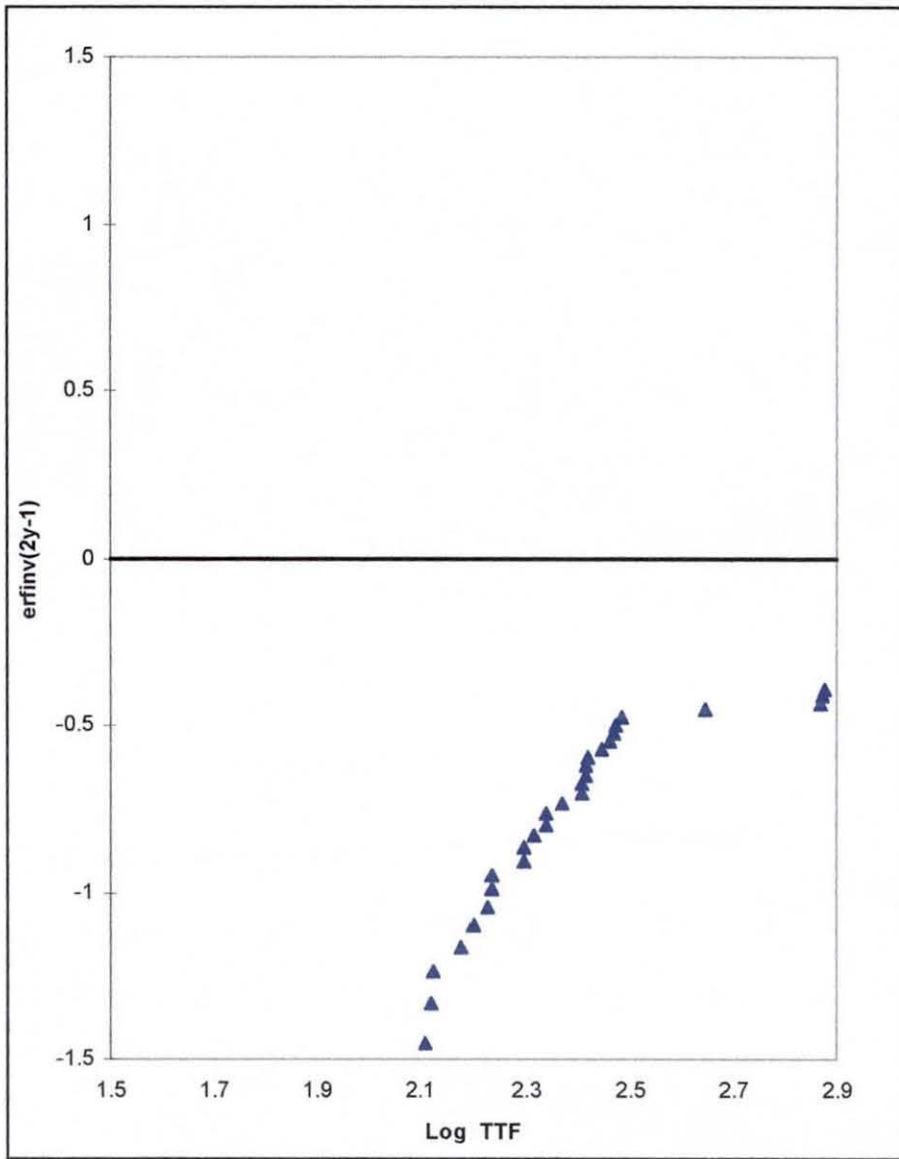
Fig 5.47 The lognormal distribution of simulated Time to failure of sample (a)
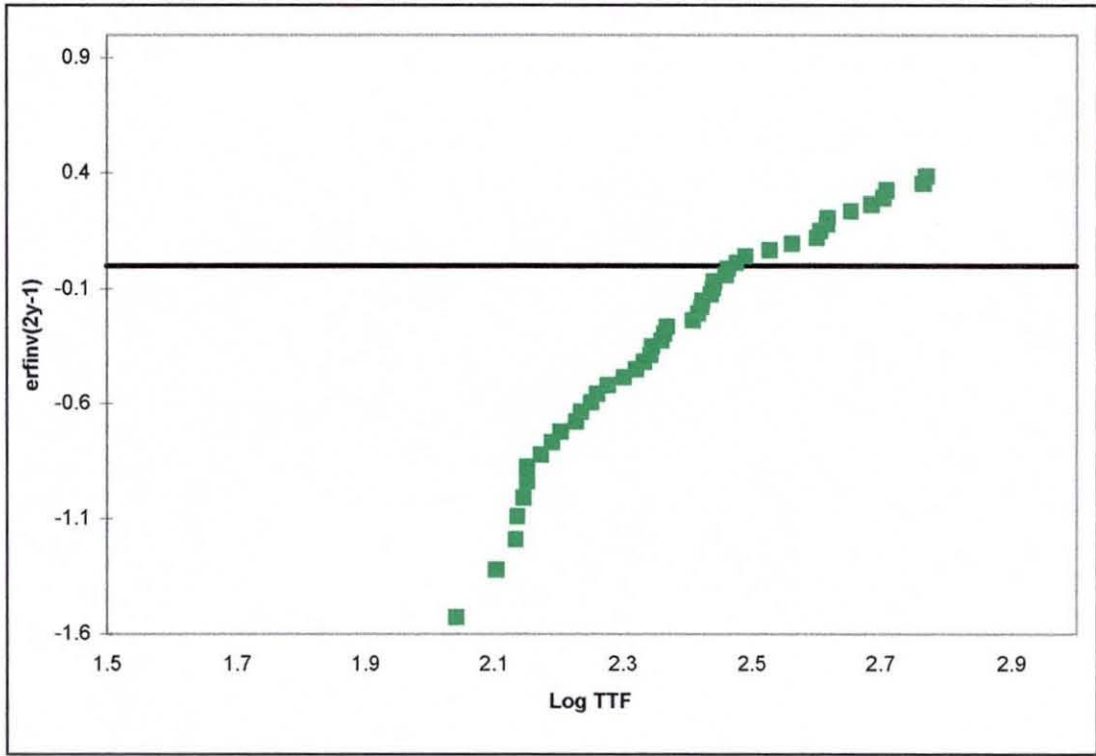
Fig 5.48 The lognormal distribution of simulated Time to failure of sample (b)
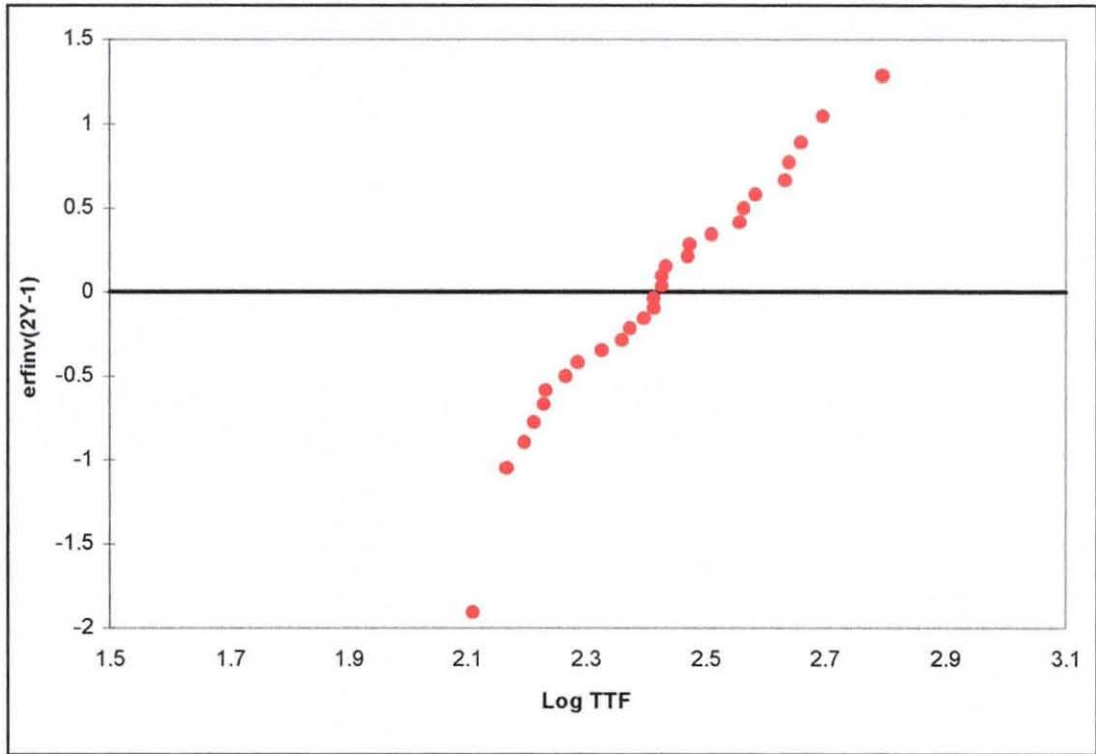
Fig 5.49 The lognormal distribution of simulated Time to failure of sample (c)
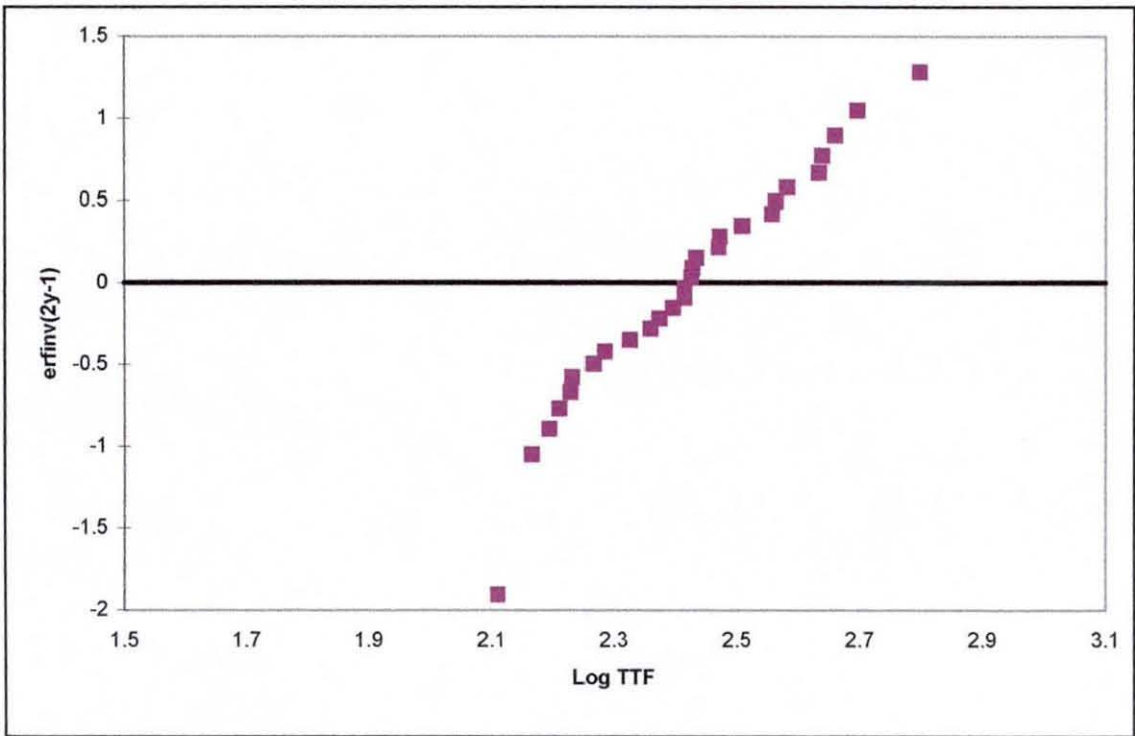
Fig 5.50 The lognormal distribution of simulated Time to failure of sample (d)
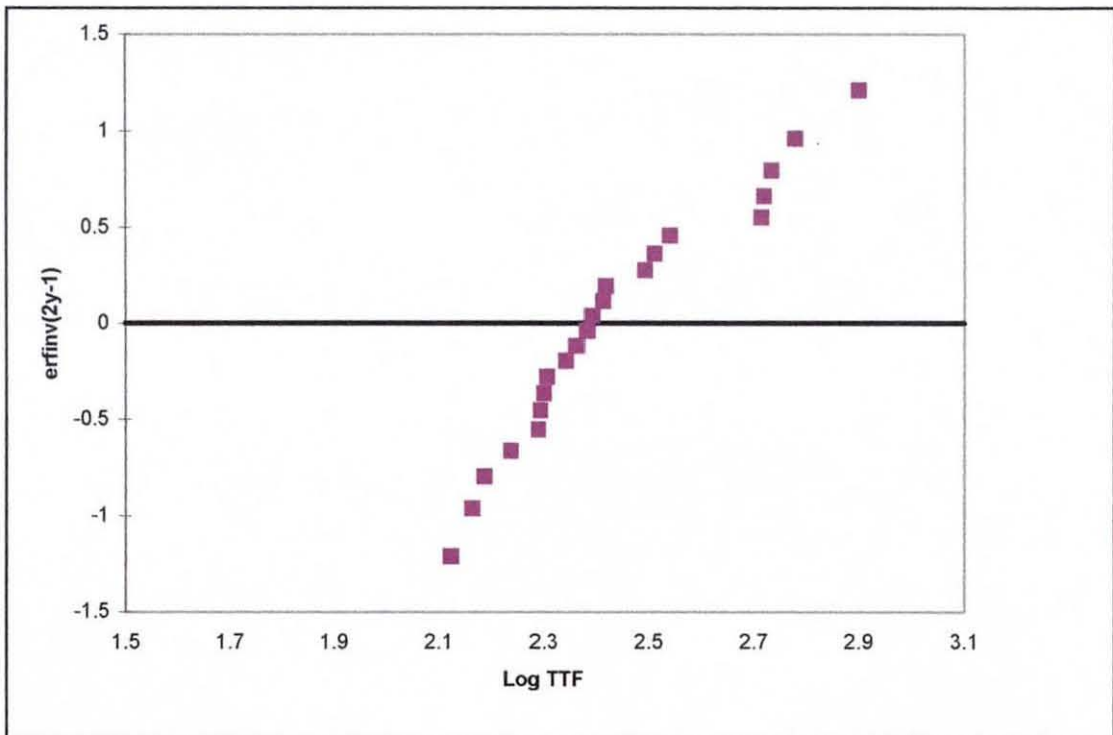
Fig 5.51 The lognormal distribution of simulated Time to failure of sample (e)

iv.   The Median Time to Failure and the Standard deviation

From the lognormal distribution graphs of the simulated Time to Failure, the Median Time to Failure and their standard deviation (calculating its slope gradient) can be obtained and are shown in Table 5.22

Sample	MTTF(arbitrary units)	MTTF(actual time)	DTTF
a (0.04)	0.052	6.1360	0.323
b(0.075)	0.0295	3.4810	0.261
c(0.1)	0.0275	3.2450	0.207
d(0.15)	0.0263	3.1034	0.177
d(0.2)	0.0245	2.891	0.165

Table5.22 The Median Time to Failure and standard deviation of Time to Failure
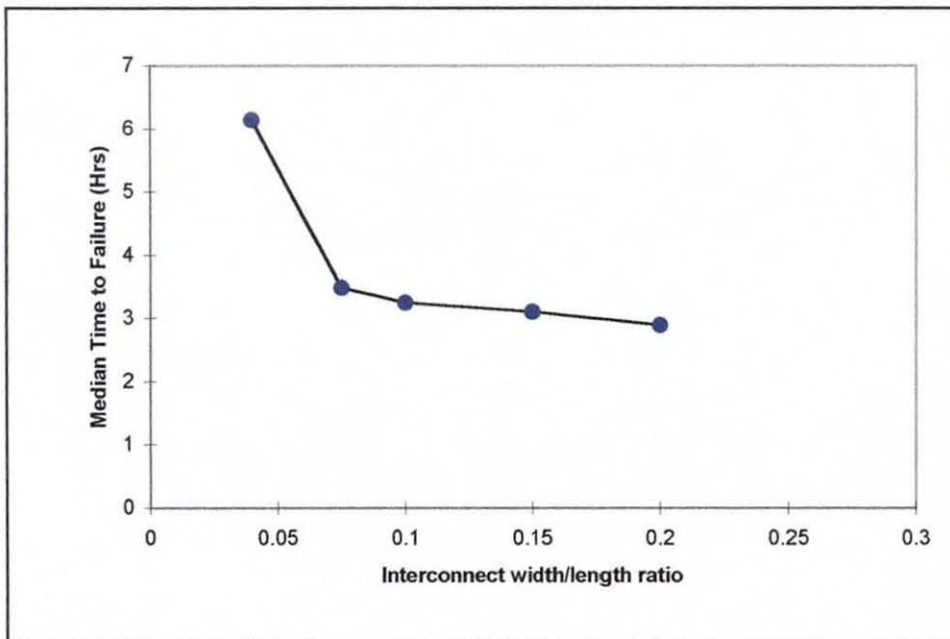
Fig5.52(a) The MTTF as function of interconnect width-to length ratio
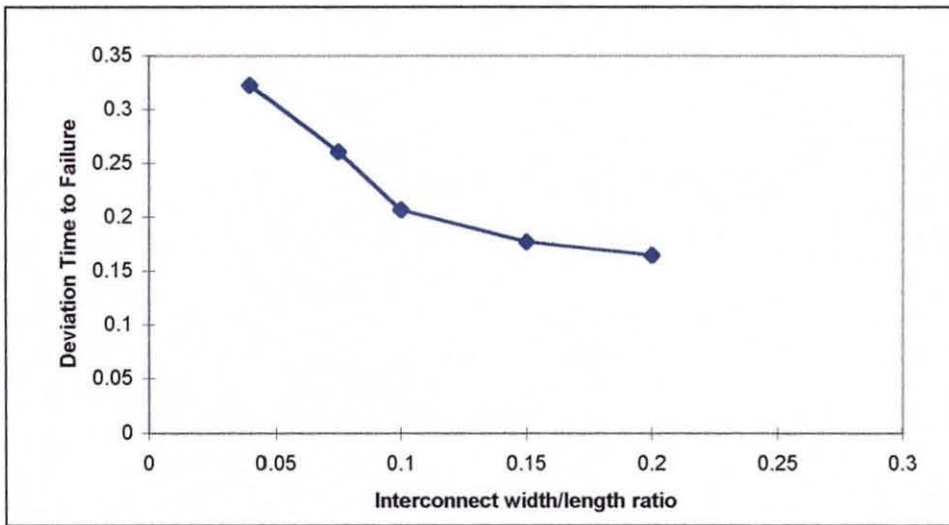
Fig5.52(b) The DTTF as a function of interconnect width-to-length ratio

Fig 5.52(a) and 5.52(b) show the Median Time to Failure and the standard deviation as the interconnect width/length ratio is varied. As the width/length ratio is decreased, the Median Time to Failure is observed to increase almost exponentially but the deviations of the Time to Failure are also increasing exponentially . This characteristic has been observed in the experiment by [Cho,and Thompson,1989] as shown in Fig 1.1 in Chapter 1. In the experiment [Cho and Thompson, 1989] have demonstrated that as the linewidth/grain size is decreased, at first the MTTF start to decreased, but as the linewidth/grain size ratio is decreased further to about w/d ≤3, a simultaneous increase of both MTTF and DTTF is observed. The sharp rise in the Time to Failure is observed as it approaches the width/length ratio of 0.04 as in sample (a) due to the bamboo effects as mentioned earlier. A sharp increase of the Deviation of the Time to Failure is also observed in the simulation results. The Deviation of Time to Failure is based on the calculation of the gradient of the slope. The slope of sample (a) in Fig 5.47 is seen to have sharper gradient than the other samples and this gives a higher values for the standard deviation. As can be seen in Fig 5.47, there are fever data points because there are fewer grain boundary clusters which fail. This constitute to the large deviation of Time To Failure between the large time and small time.

5.4.7 The effect of scaling of interconnect on the distribution of Time to Failure

One of the objectives of the current study is to analyse the effect of the scaling of the interconnect on the distribution of the Time to Failure. In this experiment, the same data of Time to Failure obtained from the interconnect sample (experiment no.1) are used, except the analysis are done for the first grain boundary cluster instead of analysing all the other cluster found in the interconnect. By using this method, the interconnect have been scaled by a (1/length of cluster no 1). The results are shown in Table 5.23 and the distribution of the Time to Failure in Fig 5.53

TTF	TTF(s)	Log(TTF(s))	erfinv(2y-1)	y	Cumulative %
0.0209	20.9	1.3201463	-1.3172	0.03125	3.13%
0.0318	31.8	1.5024271	-1.1851	0.046875	4.69%
0.0332	33.2	1.5211381	-1.0848	0.0625	6.25%
0.0339	33.9	1.5301997	-1.0025	0.078125	7.81%
0.035	35	1.544068	-0.932	0.09375	9.38%
0.0352	35.2	1.5465427	-0.8696	0.109375	10.94%
0.0363	36.3	1.5599066	-0.8134	0.125	12.50%
0.0366	36.6	1.5634811	-0.7142	0.15625	15.63%
0.0366	36.6	1.5634811	-0.7142	0.15625	15.63%
0.0376	37.6	1.5751878	-0.6273	0.1875	18.75%
0.0376	37.6	1.5751878	-0.6273	0.1875	18.75%
0.0386	38.6	1.5865873	-0.5873	0.203125	20.31%
0.0412	41.2	1.6148972	-0.549	0.21875	21.88%
0.0416	41.6	1.6190933	-0.5123	0.234375	23.44%
0.0425	42.5	1.6283889	-0.4769	0.25	25.00%
0.0433	43.3	1.6364879	-0.4427	0.265625	26.56%
0.0437	43.7	1.6404814	-0.4095	0.28125	28.13%
0.0438	43.8	1.6414741	-0.3772	0.296875	29.69%
0.044	44	1.6434527	-0.3456	0.3125	31.25%
0.0456	45.6	1.6589648	-0.3147	0.328125	32.81%
0.0483	48.3	1.6839471	-0.2844	0.34375	34.38%
0.0491	49.1	1.6910815	-0.2547	0.359375	35.94%
0.0494	49.4	1.6937269	-0.2253	0.375	37.50%
0.0506	50.6	1.7041505	-0.1964	0.390625	39.06%
0.0513	51.3	1.7101174	-0.1677	0.40625	40.63%
0.0523	52.3	1.7185017	-0.1394	0.421875	42.19%
0.0527	52.7	1.7218106	-0.1112	0.4375	43.75%
0.0531	53.1	1.7250945	-0.0833	0.453125	45.31%
0.0538	53.8	1.7307823	-0.0554	0.46875	46.88%
0.054	54	1.7323938	-0.0277	0.484375	48.44%

0.0541	54.1	1.7331973	0	0.5	50.00%
0.0547	54.7	1.7379873	0.0277	0.515625	51.56%
0.0549	54.9	1.7395723	0.0554	0.53125	53.13%
0.0555	55.5	1.744293	0.0833	0.546875	54.69%
0.0584	58.4	1.7664128	0.1112	0.5625	56.25%
0.0585	58.5	1.7671559	0.1394	0.578125	57.81%
0.0616	61.6	1.7895807	0.1677	0.59375	59.38%
0.0617	61.7	1.7902852	0.1964	0.609375	60.94%
0.0626	62.6	1.7965743	0.2253	0.625	62.50%
0.0647	64.7	1.8109043	0.2547	0.640625	64.06%
0.0667	66.7	1.8241258	0.3147	0.671875	67.19%
0.0667	66.7	1.8241258	0.3147	0.671875	67.19%
0.0684	68.4	1.8350561	0.3456	0.6875	68.75%
0.0686	68.6	1.8363241	0.3772	0.703125	70.31%
0.0695	69.5	1.8419848	0.4095	0.71875	71.88%
0.0729	72.9	1.8627275	0.4427	0.734375	73.44%
0.0778	77.8	1.8909796	0.4769	0.75	75.00%
0.0794	79.4	1.8998205	0.5123	0.765625	76.56%
0.0802	80.2	1.9041744	0.549	0.78125	78.13%
0.0817	81.7	1.9122221	0.5873	0.796875	79.69%
0.0837	83.7	1.9227255	0.6273	0.8125	81.25%
0.0854	85.4	1.9314579	0.6695	0.828125	82.81%
0.0859	85.9	1.9339932	0.7142	0.84375	84.38%
0.0875	87.5	1.9420081	0.7619	0.859375	85.94%
0.0878	87.8	1.9434945	0.8134	0.875	87.50%
0.0895	89.5	1.951823	0.8696	0.890625	89.06%
0.0905	90.5	1.9566486	0.932	0.90625	90.63%
0.0946	94.6	1.9758911	1.0025	0.921875	92.19%
0.0951	95.1	1.9781805	1.0848	0.9375	93.75%
0.0964	96.4	1.984077	1.1851	0.953125	95.31%
0.097	97	1.9867717	1.3172	0.96875	96.88%
0.0971	97.1	1.9872192	1.523	0.984375	98.44%

Table 5.23 The simulated Time to Failure of the first grain boundary cluster
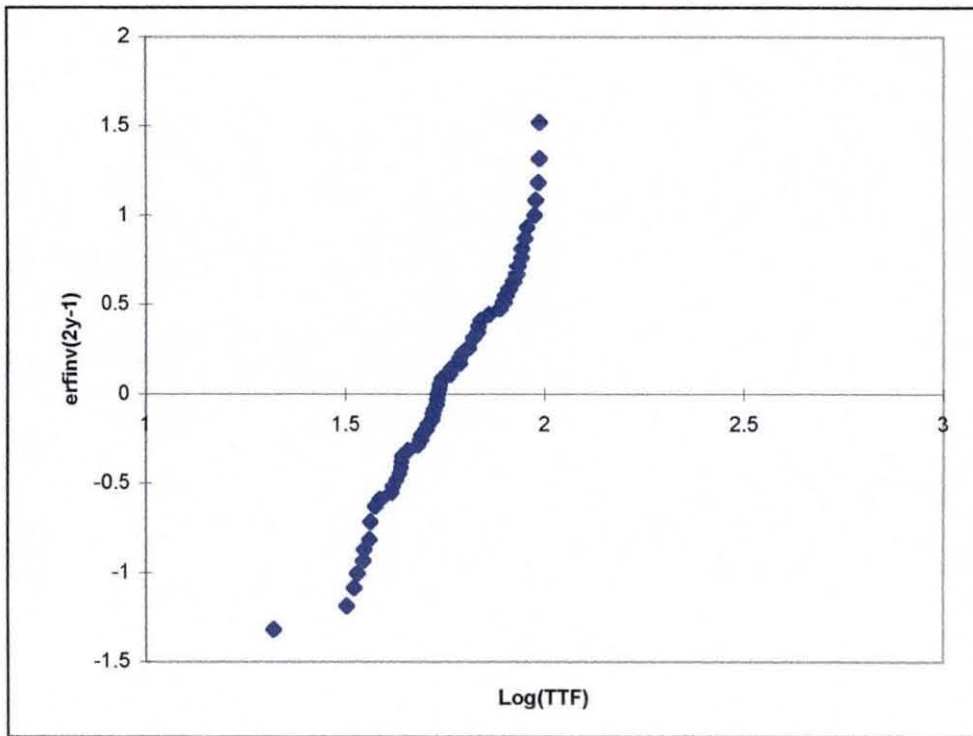
Fig 5.53 The lognormal distribution of simulated Time to Failure of the first
grain boundary cluster

Based on Fig 5.53, the distribution of the Time to Failure also follows the lognormal
distribution. The effect of scaling does not change the distribution of the Time to Failure
because one of the factor that determines the distribution is the distribution of the cluster
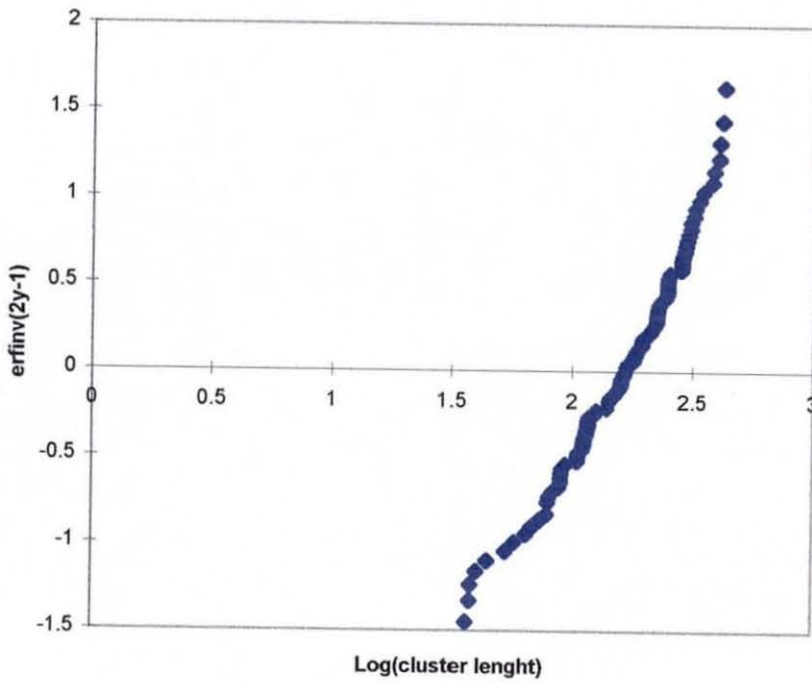length which in this experiment also produces a lognormal distribution function as shown
in Fig 5.54 below.

Fig 5.54 The lognormal distribution of simulated length of first grain boundary
cluster

5.4.8 The effect of the number of grain boundaries in a cluster(of different length) on the Time to Failure

The Time to Failure of interconnects depends on the microstructure of the grain boundaries in the interconnect. In this simulation of the Time to Failure, the effect of the number of grain boundaries which of various length in a cluster is analysed. The objective is to investigate whether the number of grain boundaries in a cluster produces shorter or longer electromigration lifetime. The results of the simulated Time to Failure is shown in Table 5.25 and in Fig 5.55 below.

% Cluster	TTF (GB=3)	% Cluster	TTF (GB=5)	% Cluster	TTF (GB=7)	% Cluster	TTF (GB=9)	% Cluster	TTF (GB=11)
1.25	0.0209	1.754386	0.0191	3.225806	0.0208	4.347826	0.0318	4.545455	0.0332
2.5	0.0255	3.508772	0.0209	6.451613	0.0339	8.695652	0.0349	9.090909	0.0349
3.75	0.0437	5.263158	0.0343	9.677419	0.0347	13.04348	0.0351	13.63636	0.035
5	0.0444	7.017544	0.0376	12.90323	0.0352	17.3913	0.0366	18.18182	0.0363
6.25	0.0479	8.77193	0.0414	16.12903	0.0381	21.73913	0.0376	22.72727	0.0366
7.5	0.0517	10.52632	0.0441	19.35484	0.0392	26.08696	0.0388	27.27273	0.0386
8.75	0.054	12.2807	0.0444	22.58065	0.0433	30.43478	0.0416	31.81818	0.0401
10	0.0616	14.03509	0.0461	25.80645	0.0438	34.78261	0.0417	36.36364	0.0412
11.25	0.0622	15.78947	0.0486	29.03226	0.0471	39.13043	0.0425	40.90909	0.0438
12.5	0.0627	17.54386	0.0491	32.25806	0.0494	43.47826	0.0456	45.45455	0.044
13.75	0.0667	19.29825	0.0523	35.48387	0.0506	47.82609	0.0505	50	0.046
15	0.0676	21.05263	0.0536	38.70968	0.0513	52.17391	0.0541	54.54545	0.0483
16.25	0.0684	22.80702	0.0559	41.93548	0.0518	56.52174	0.0547	59.09091	0.0526
17.5	0.0689	24.5614	0.0578	45.16129	0.0527	60.86957	0.0555	63.63636	0.0538
18.75	0.0756	26.31579	0.0584	48.3871	0.0531	65.21739	0.056	68.18182	0.0587
20	0.0809	28.07018	0.0595	51.6129	0.0617	69.56522	0.0585	72.72727	0.0606
21.2	0.0817	29.82456	0.0626	54.83871	0.0695	73.91304	0.0637	77.27273	0.0668
22.5	0.0837	31.57895	0.0626	58.06452	0.0735	78.26087	0.0691	81.81818	0.0729
23.75	0.084	33.33333	0.0647	61.29032	0.0778	82.6087	0.0699	86.36364	0.0758
25	0.0859	35.08772	0.065	64.51613	0.0794	86.95652	0.0746	90.90909	0.0824
26.25	0.0951	36.84211	0.0667	67.74194	0.0812	91.30435	0.0876	95.45455	0.0971
27.5	0.0964	38.59649	0.0686	70.96774	0.0835	95.65217	0.1048	100	0.1381
28.75	0.1266	40.35088	0.07	74.19355	0.0854	100	0.1251		
30	0.1451	42.10526	0.0708	77.41935	0.0875				
31.25	0.157	43.85965	0.0709	80.64516	0.0895				
		45.61404	0.0723	83.87097	0.0905				
		47.36842	0.0773	87.09677	0.0977				
		49.12281	0.0802	90.32258	0.115				
		50.87719	0.0833						
		52.63158	0.0854						
		54.38596	0.0878						
		56.14035	0.0879						
		57.89474	0.0892						
		59.64912	0.0917						
		61.40351	0.0946						
		63.15789	0.096						
		64.91228	0.0967						
		66.66667	0.097						
		68.42105	0.0985						
		70.17544	0.1686						

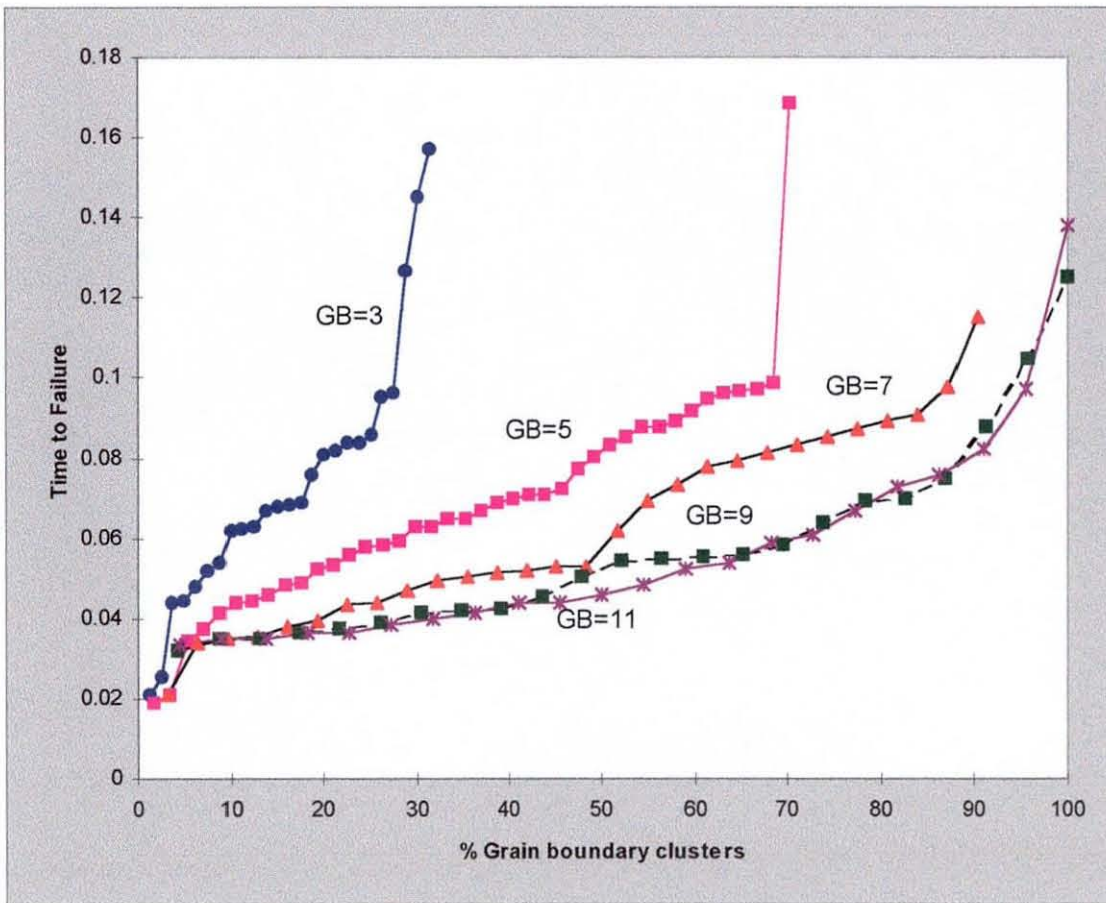Table 5.25 The Time to Failure of various number of grain boundaries

Fig 5.55 The Time to Failure profile of various number of grain boundaries

From the results shown above, for the grain boundary cluster with a total of 3 grain boundaries , the range of arbitrary Time to Failure is between 0.0209-0.157 which in physical time is between 2.46 hours-18.53 hours. For 5 grain boundary cluster, the range is between 0.0191(2.25hours)-0.1686(19.89hours), 7 grain boundary cluster it ranges from 0.0208(2.45hours)-0.115(13.57hours), 9 grain boundaries it ranges from 0.0318(3.75hrs)-0.1251(14.76hours) and for 11 grain boundaries the earliest failure time is 0.0302(3.56hours) and the latest failure time is 0.1381(16.29 hours). This result shows that the number of grain boundaries in a cluster does not have a great impact on deciding how fast or slow the Time to Failure. However from the data and the graph, it shows that the number of grain boundaries will affect the % failure of the interconnect where a smaller number of grain boundaries in a cluster will have a smaller percentage of failure because with a small number of grain boundaries in a cluster, the probability that it has a

longer cluster length than the critical length(Blech length) is small. It can be confirmed that the Time to Failure depends on a variety of factors which include i)the cluster length, ii) individual grain boundaries length, the diffusivities and the angle of orientation of the grain boundaries. The overall length of the grain boundary cluster has a direct effect on the number of failures (%) but does not have a direct effect on the Time to Failure. It is quite difficult at this stage to draw any conclusion which of these factors mentioned above are dominant it determining the Time to Failure.

5.4.9 Results of the simulation of Time to Failure between the lumped element model and the signal delay.

All the simulation results of the Time to Failure discussed earlier have been obtained by the lumped element model which has been very successful in demonstrating the behaviour of electromigration in the interconnects. Another method of obtaining the Time to Failure is by using the signal delay . This method has been used in the single grain boundary and the 'self generated' complex grain boundary and the analysis of the results shows that it is comparable with the lumped element model.

In this experiment, the same five samples of Al film as in the last experiment have also been used to make the comparison study and the detailed results of the Time to Failure recorded by both i.e. the lumped element model and the signal delay are shown in Table A.4 in Appendix A4. The summary of the results are shown in Table 5.26 below.

TTF cluster (model)	TTF cluster (elmore)	TTF sample(model)	TTF sample(elmore)
0.0686	0.0601	0.0686	0.0601
0.0111	0.0143	0.0111	0.0143
0.0207	0.0222	0.0212	0.0285
0.0212	0.0285	0.0182	0.0243
0.0302	0.0348	0.0276	0.0335
0.0182	0.0243	0.0169	0.021
0.0624	0.0534	0.0195	0.0231
0.0276	0.0335	0.0196	0.0209
0.0169	0.021	0.0324	0.0289

278

0.0516	0.0533	0.05	0.0501
0.0195	0.0231	0.0197	0.0334
0.0551	0.0522	0.0215	0.0258
0.0342	0.0401	0.0226	0.0339
0.0196	0.0209	0.0209	0.0186
0.0465	0.0438	0.0238	0.0263
0.0324	0.0289	0.0227	0.0227
0.05	0.0501	0.0184	0.0182
0.0197	0.0334	0.0167	0.0133
0.0215	0.0258	0.0163	0.0186
0.0295	0.0321	0.0274	0.0327
0.0226	0.0339	0.0181	0.0227
0.0209	0.0186	0.0241	0.0243
0.0282	0.0306	0.0316	0.0324
0.0238	0.0263	0.0189	0.0196
0.0407	0.0348	0.0864	0.0961
0.0227	0.0227	0.0405	0.0406
0.0184	0.0182	0.0171	0.0167
0.0167	0.0133	0.0444	0.0415
0.0336	0.0338	0.0344	0.0376
0.0163	0.0186	0.019	0.0267
0.0274	0.0327	0.0204	0.0172
0.0181	0.0227	0.0494	0.0412
0.0198	0.0273	0.0184	0.0236
0.0241	0.0243	0.088	0.0888
0.0316	0.0324	0.0136	0.0164
0.0189	0.0196	0.0288	0.0271
0.0341	0.0426	0.0133	0.0138
0.022	0.0243	0.0277	0.0282
0.0864	0.0961	0.0189	0.0206
0.0405	0.0406	0.0143	0.0182
0.0171	0.0167	0.0274	0.0296
0.0444	0.0415	0.0203	0.0204
0.0344	0.0376	0.0212	0.0222
0.019	0.0267	0.018	0.0184
0.0214	0.0215		
0.0204	0.0172		
0.0494	0.0412		
0.0184	0.0236		
0.0233	0.0277		
0.022	0.0275		
0.088	0.0888		
0.0136	0.0164		
0.0288	0.0271		
0.0133	0.0138		
0.0227	0.0282		
0.0189	0.0206		
0.0739	0.0667		

0.0298	0.028
0.0647	0.0572
0.0143	0.0182
0.0258	0.0245
0.0274	0.0296
0.0502	0.0494
0.0203	0.0204
0.0457	0.0514
0.0212	0.0222
0.0248	0.0265
0.0367	0.035
0.018	0.0184

Table 5.26 The Time to Failure of grain boundary cluster and interconnect sample between lumped element model and signal delay/elmore obtained from 50 samples of interconnect

Fig 5.56 and Fig 5.57 shows the graph of the simulated Time to Failure obtained by the lumped element model and the signal delay method
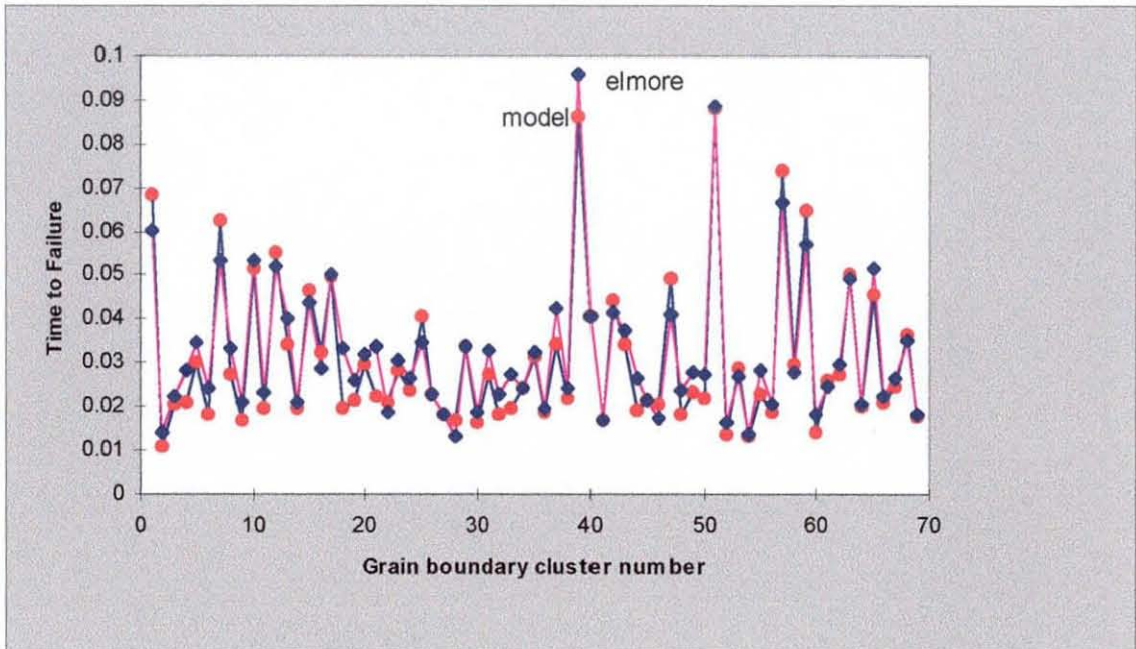
Fig. 5.56 The Time to Failure of the grain boundary cluster obtained by lumped element model (red) and signal delay/elmore(blue)
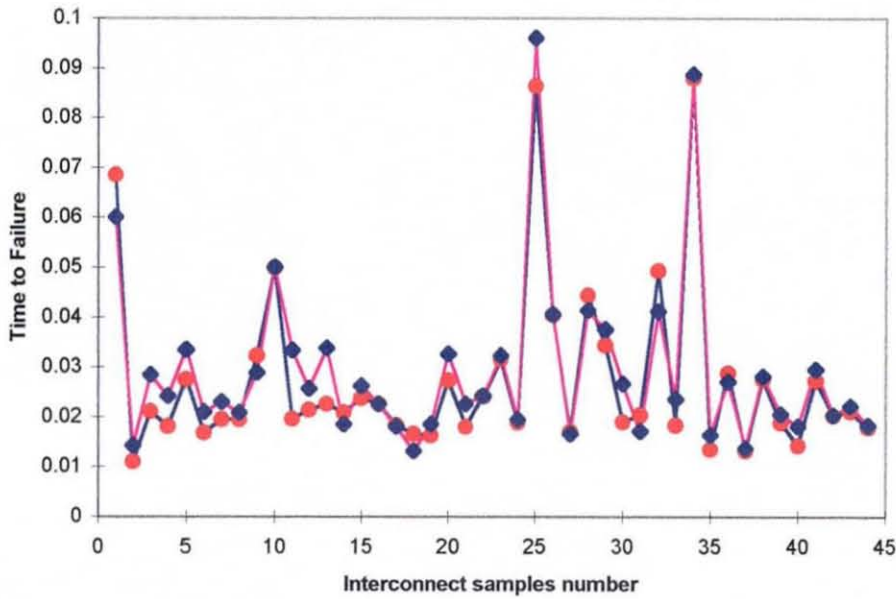
Fig. 5.57 The Time to Failure of the interconnect samples obtained by lumped element model (red) and signal delay/elmore(blue)

From the results shown in Table 5.26, Fig.5.56 and Fig 5.57 it is clear that the signal delay method is reliable and consistant in producing the Time to Failure. However , the signal delay method has not been analysed to see whether the Time to Failure exhibits the lognormal distribution.. The analysis will be carried out in the next section.

5.4.10 The Time to Failure distribution using signal delay method.

The Time to Failure distribution for the grain boundary clusters, for both the signal delay method and the Lumped element model are shown in Fig5.58(a) and Fig5.58(b) respectively. Also, the TTF distribution for the interconnect are shown in Fig 5.59(a) and 5.59(b).
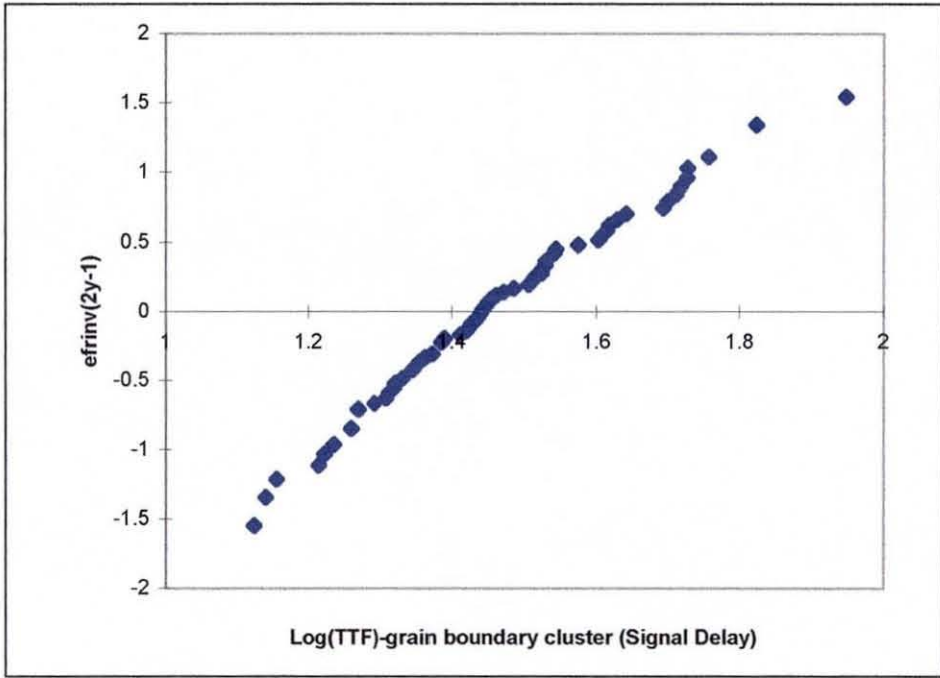
Fig5.58(a) The lognormal distribution of the simulated Time to Failure
of grain boundary clusters using the signal delay method
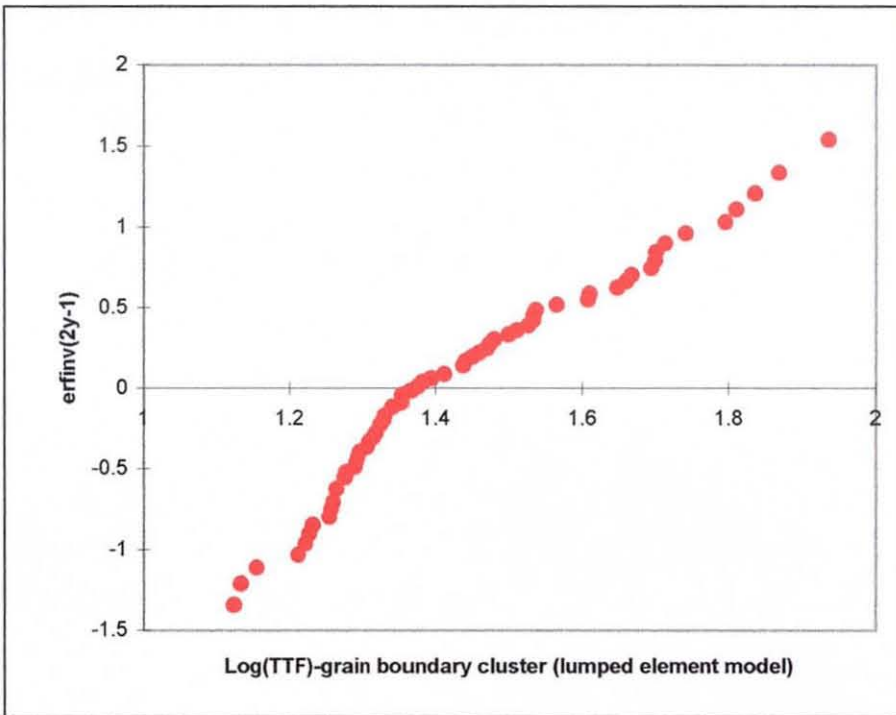
Fig5.58(b) The lognormal distribution of the simulated Time to Failure
of grain boundary clusters using the lumped element model
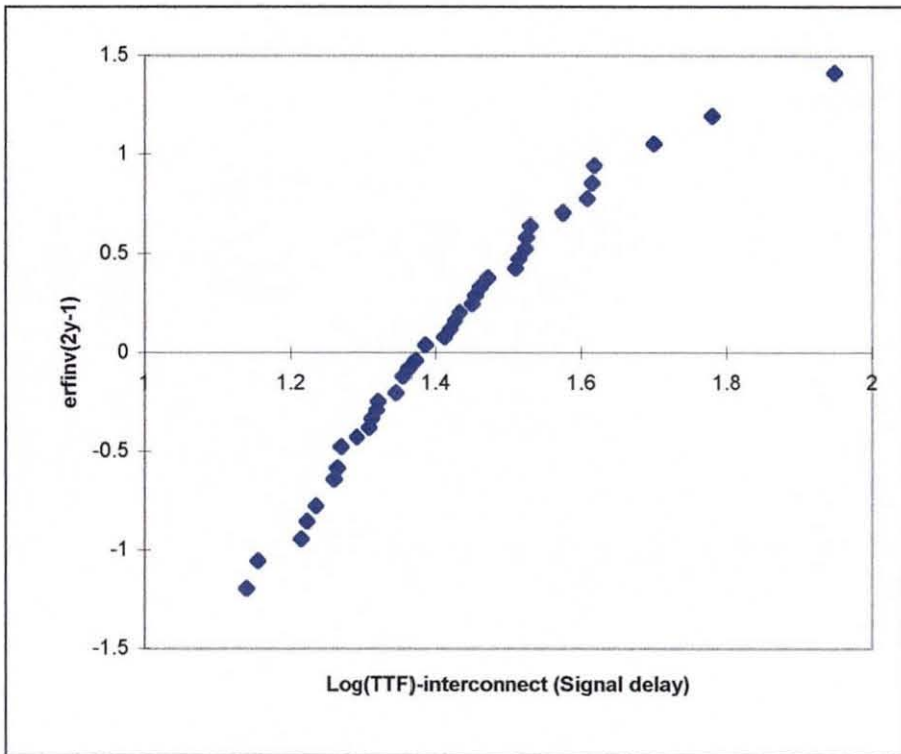
Fig5.59(b) The lognormal distribution of the simulated Time to Failure
of interconnect using the lumped element model
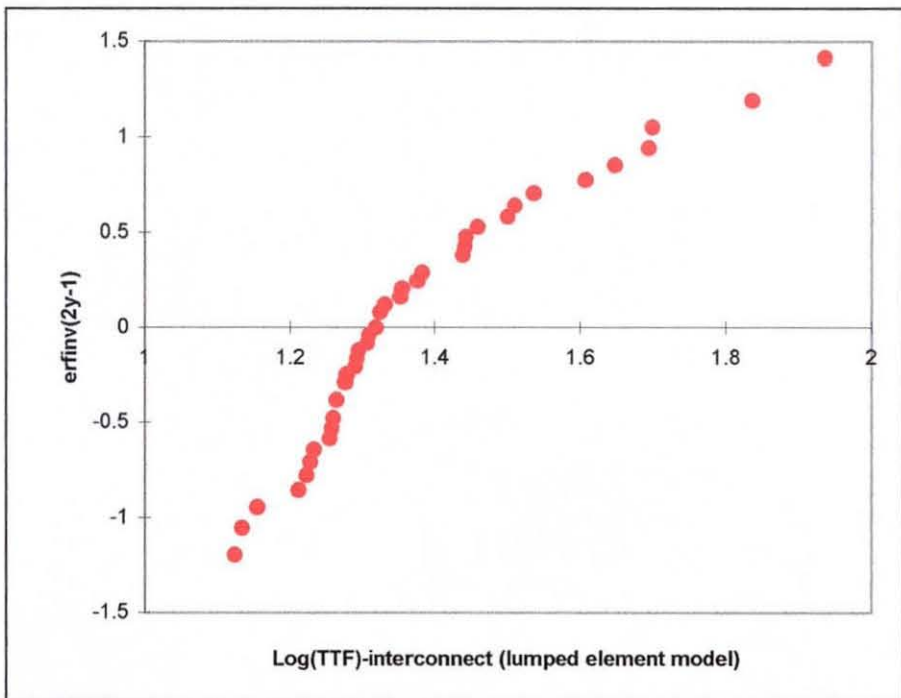
Fig5.59(b) The lognormal distribution of the simulated Time to Failure
of interconnect using the lumped element model

From these figures, it is observed that the Time to Failure using the lumped element model and the signal delay method both fit lognormal distribution. It is also observed that the distribution for the signal delay is in fact much better than the lumped element model particularly for the small times. From this results, it can be deduced that the lumped element model has been successfully proven valid in describing the behaviour of the electromigration where the Time to Failure is shown to closely approximates the lognormal distribution.

5.4.11 Other reliability distribution on the Time to Failure

We have assumed that the TTF is distributed lognormally however this may not be the case despite experimental evidence.[Lloyd and Kitchin, 1991] have proposed a different distribution for TTF that is well approximated by a multilognormal distribution. The simulation is based on the drift-diffusion model and the conductor stripe is modelled as a chain of links, each having its own derived failure distribution. Another distribution which is often used to described the lifetimes is the Weibull distributions. This distribution has been applied and tested for the Electromigration Time to Failure [Attardo et.al., 1971] and was found to fit equally well at relatively large percentage failures(greater than 5 %). However at percentage less than 1% it is not . The Weibull distribution is given by the equation below:-

$$F(t) = 1 - \exp\left(-\left(\frac{t}{a}\right)^b\right)$$

5.13

Where F(t) = the cumulative %

t = failure time

a = scale parameter

b = shape factor or standard deviation σ

Eqn(5.23) can be turned into a regression equation as follows

$$F(t) = 1 - \exp\left(-\left(\frac{t}{a}\right)^b\right)$$

$$\ln[(1-F(t)] = -\left(\frac{t}{a}\right)^b$$

$$\ln(-\ln[1-F(t)]) = b\ln(t) - b\ln(a) \quad OR \quad Y = mX + c \qquad\qquad 5.24$$

where $Y = \ln(-in(1-F(t))$, $m = b$, $X = \ln(t)$ $c = b\ln(a)$

A straight line plot of $\ln(-\ln(1-F(t))$ vs $\ln(t)$ will indicate that the data fits a Weibull distribution. Data from section 5.49 i.e. Table 5.26 are used in testing the fit to the Weibull distribution for the Time to Failure using both the Lumped element model and the signal delay method on the Time to Failure of the grain boundary clusters and the interconnect. The results are shown in Fig5.60(a) and Fig5.60(b)(for grain boundary clusters) and Fig5.61(a) and Fig5.61(b)(for interconnect)using the signal delay and Lumped element model respectively.
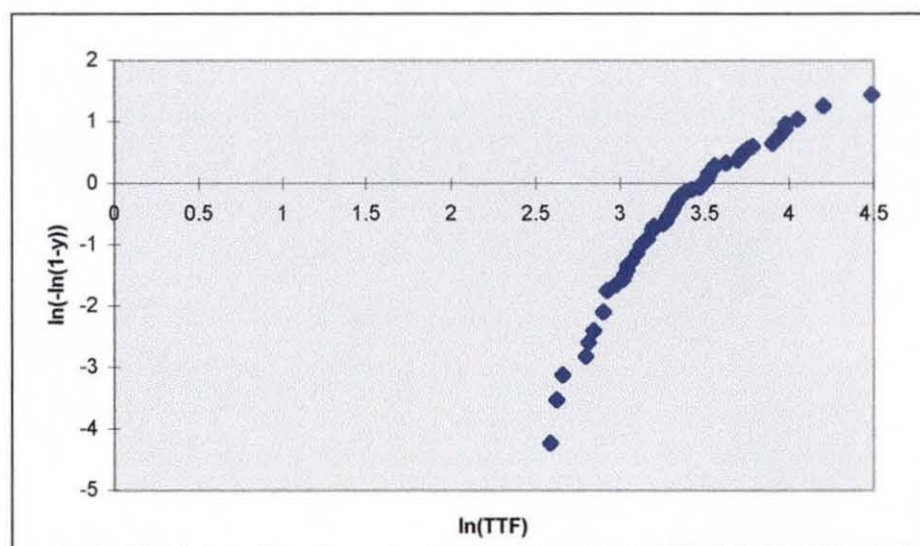
Fig5.60(a) The Weibull plot of the Time to Failure of the grain boundary clusters using the Signal delay method

285
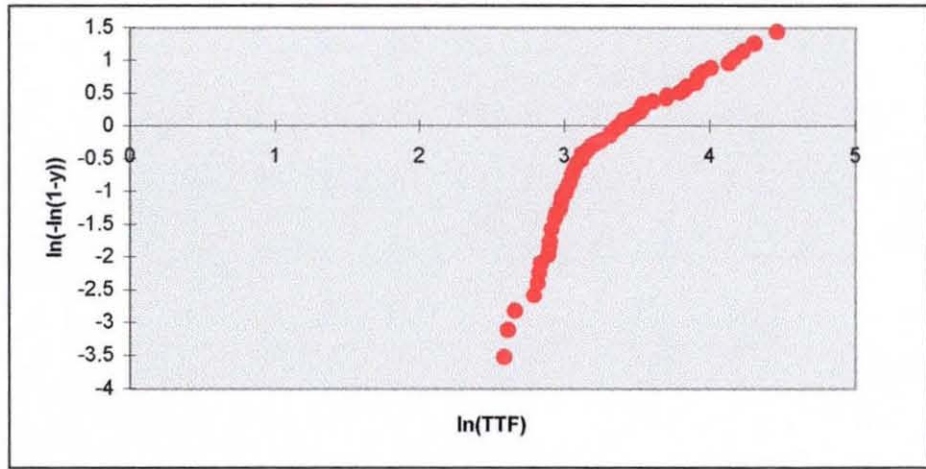
Fig5.60(b) The Weibull plot of the Time to Failure of the grain

boundary clusters using the Lumped element model
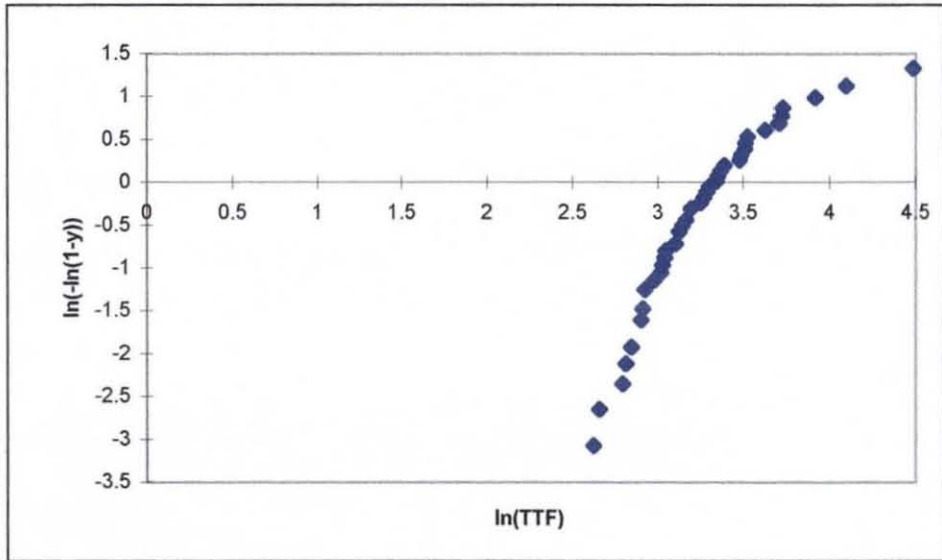
Fig5.61(a) The Weibull plot of the Time to Failure of the interconnect

using the signal delay method
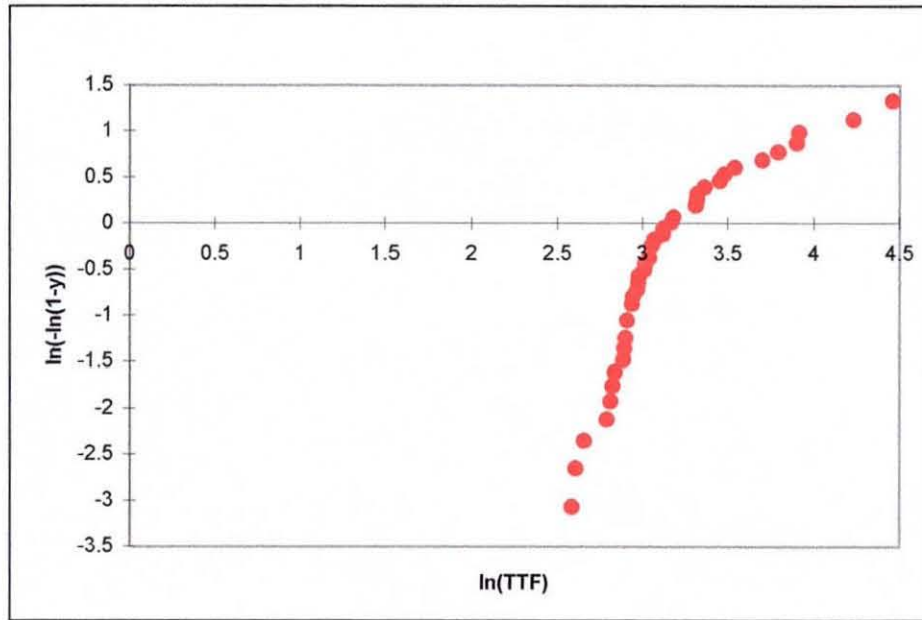
Fig5.61(b) The Weibull plot of the Time to Failure of the interconnect
using the Lumped element model

Based on the figures above, it is observed that the Time to Failure does not fit very well
for the Weibull distribution for both methods i.e. the Signal delay and the Lumped
element model. Therefore the lognormal distribution can be considered the best
approximation for the distribution of Time to Failure of Electromigration.

5.4.12 The analysis of small Time To Failure

The small Time to Failures or early failures are of great importance in the study of
interconnect reliability. From the results obtained in section 5.4.6, as linewidth decreases
(smaller than the grain size) the Time to Failure increases, but so does the deviation of
Time to Failure. From reliability point of view, the shape factor or the standard deviation
at least as important as the Mean Time to Failure, for early failures. In this analysis, the
configuration of the grain boundaries in a cluster are analysed.

Early failures data are analysed in detail from the non-annealed interconnect. Table 5.27 describes the features of the grain boundary clusters which have recorded the earliest failure time
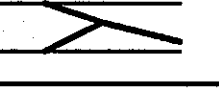
Sample	Cluster length	No of grain boundaries	TTF	Configuration
no.4	0.244	5	0.0191	
no.3	0.2478	7	0.0208	
no.13	0.1586	3	0.0209	

Table 5.27 Data of the grain boundary cluster which have the smallest failure times.

From Table 5.27, all the examples of grain boundary clusters which have the smallest failure time, have one common feature that is, the configuration allows fast diffusion of vacancies along the grain boundaries until it reaches the furthest/end point of the cluster(where in the current model ,all the Times to Failure are computed). From the table, the number of grain boundaries and the cluster length are seen to have little or no correlation to the Time to Failure. From the example shown here, it can be said that the Time to Failure is very complex , it depends on the combination of various microstructural parameters and geometrical properties of the grain boundaries that make up the cluster and not just the overall length.

5.5   Summary of simulation results of realistic interconnects

In the simulation of realistic interconnects, the arbitrary parameters used in the simulation of the lumped element model such as the values of $\alpha=5$,$D=5$ and $c_{cr}=2c_0$ have been shown to be suitable. This is based on the results of the simulation

where the time-scale of the Time to Failure, the length of interconnect and the grain boundary clusters are within the 'realistic values' reported in the literature where analytical or computer simulation is used.[Joo, et.al,1999].

The results obtained have shown that the Lumped element model is able to demonstrate the electromigration behaviour and characteristics obtained by other computer simulations in regarding with the distribution of the Time to Failure [Joo and Thompson,1994][Kirchheim and Kaeber,1991][Knowlton ,et.al,1997] but on much more complex interconnects i.e. a 2D-model is used and also on actual experimental such as the effect of annealing and the linewidth variation on the Time to Failure, Mean Time to Failure and the deviation of Time to Failure[Cho and Thompson,1989]

The validity of the Lumped element model has been successfully verified by the results of the Time to Failure distribution which fit quite well with the lognormal distribution, as found experimentally in the literature. The signal delay method of predicting the Time to Failure has been compared with the lumped element model , and a lognormal distribution is also obtained, and have a better fit.

The microstructure and the geometrical effects of the grain boundaries on the Time to Failure have also been analysed. The results show that the Time to Failure is a complex phenomenon, it depends on a collective of various parameters such as the length of grain boundaries, angle of orientation, diffusivities, number of grain boundaries and the configuration or geometrical properties.

CHAPTER 6

CONCLUSIONS

6.0   Introduction

This final chapter summarises the analysis and results recorded earlier in this thesis, and discusses their scientific significance in terms of their contribution towards the understanding of electromigration in general.

6.1   Summary

The 'state-of the art' physical model of electromigration is based on stress evolution which are introduced by Blech and co-workers and later 'finalised' by [Korhonen, et.al,1993]. Most of the previous stress evolution models are one-dimensional which effectively averages the microstructural effects and the electromigration current over the linewidth In the current work, attempts are made to develop a three-dimensional model based on the stress evolution model which includes some of the microstructural/geometrical effects (the vacancy diffusion coefficients, the lengths and orientations of the various grain boundaries) on the lifetime of IC interconnects in a realistic manner without averaging these effects over the interconnect cross-sections as in the standard one-dimensional model. By assuming both columnar grains and that vacancy flux is roughly uniform across the grain boundary width δ , the three-dimensional transport problem reduces to one along a stick-network of one-dimensional boundaries(this is sometimes referred to as a two-dimensional model). For a typical near-bamboo interconnect, consisting of both cluster and bamboo sections, there are two important time scales. The first, a short time scale, defines the time taken for the fast diffusion cluster regions to reach a quasi-steady state and the second, a longer time scale, defines the time for diffusion to occur through the grain bulk or along the metal/oxide sidewall. Therefore, for early failures transport occurs along the grain boundary networks, and ignoring transport through the grain bulk,

the problem reduces to that of solving the equations for stress evolution equation on the individual complex grain boundary networks which make up the cluster sections of the interconnect. This forms the basis of the current research.

The thesis describes the detailed stages involved in developing the current model i.e. the Lumped Element Model. In the first stage of the analysis, the equation describing the evolution of stress within an interconnect is shown to be equivalent to a slow non-linear drift-diffusion equation description of the vacancy build-up. Provided that the vacancy flow along the grain boundary network can be reasonably mapped on to an underlying network of one-dimensional grain boundaries, we are able to draw two very important conclusions. Firstly, the analysis of the steady state solution for an arbitrary grain boundary network, with arbitrary boundary conditions, can be treated as a similar network of random resistors. Secondly, in the analysis of the approach to the steady -state, the drift-diffusion equation may be represented by a distributed CR transmission line equivalent with inhomogeneous capacitance per unit length and resistance per unit length.

These two observations combine to demonstrate the possibility of treating vacancy build-up in a grain boundary network (approximately) by an equivalent electrical network of lumped elements. In the analysis that follows, it is shown that the vacancy build-up in a single grain may be approximated by a CR transmission line made up of five cascaded single C-R-C Π sections. Accuracy may always be improved by including more sections. At this early stage also, analysis to validate the model is performed by comparing with the existing references for "single grain" boundary sections and the results show good agreement. We also demonstrate the usefulness and the flexibility of the Transfer matrices in deriving the components values, and solving equivalent node voltages of the C-R-C Π network and hence the build-up of vacancies in a grain boundary network. Finally the lumped element model is used in the calculation of the Time to Failure when the vacancy concentration at a particular node along any grain boundary in the cluster reaches some threshold value.

The thesis introduces the idea of approximating the failure time on complex grain boundary networks using the concept of the signal or Elmore delay developed for CR networks by CMOS design engineers. With the introduction of this approximate technique we allow for rapid estimates of TTF for a given structure thus enabling statistics to be obtained quickly and efficiently. The technique has also been tested for its validity by comparing it with the 'exact solution' and the Lumped element model for a 'single grain' and the results show good agreement

The thesis also outlines in detailed the steps taken in implementing the software codes to produce the results based on the model developed. Since the solution to the model is in the form of matrix equations as described earlier, the best software package to handle such a problem is Matlab®. The main reason why Matlab® is used is that it is user friendly and it supports many built-in function. Some of the important built-in functions that are used in solving the mathematical equations are i)diag- use to diagonalise the matrix when solving the node voltage equation, ii) rot90 - use to rotate the matrix by 90° applied in the switching the grain boundaries during the annealing process and iii) Voronoi - use in producing the Voronoi network representing the realistic representation of the grain boundaries in an Al sample, etc. With these built-in tools, a great deal of time may be saved because the work put into the development of the software codes can be very time consuming. Another important factor which contributes to the choice of using Matlab® is that it is a Microsoft Window based language where transfer of data between software packages is easy (e.g data transfer between Matlab® and Microsoft Excel and Word) and also it is quite easy to troubleshoot for errors found in the code.

The software code developed is basically divided into 3 main categories to perform the necessary simulation such as the vacancy concentration profile, realistic grain boundaries , the calculation of the exact Time to Failure and signal delay approximation of TTF. These are based on i) single grain boundary ii) an example of a more complex grain boundaries and iii) the realistic grain boundaries in Al interconnects. To allow for easy understanding of the flow of the program codes, the thesis includes all the major Program Flow charts. As far as the program code is

concerned, it is designed to be 'structured' so that the code can be easily executed and debugged.

The only 'disadvantage' that may be considered in the software codes developed is the use of many subroutines that involve searching algorithms particularly in the program codes for the realistic grain boundaries. At the moment this cannot be avoided since the only available information produced by the Voronoi built-in function is the co-ordinates values of the vertices (grain boundaries nodes) which are randomly arranged. It is a major and time consuming task to produce a routine to rearrange and to label the nodes and the grain boundaries. Searching algorithms are also employed in much of the program code for the simulation of the annealing process and for the simulation of the production of realistic interconnects. Therefore as a result , the computing times are still quite long especially if one considers more than 100 random points to generate the Voronoi network. The other important point which at the moment is quite difficult to solve is in the simulation of the time to failure. Since the interconnect may have a few grain boundary clusters , it is a demanding task at the moment to calculate each cluster's TTF in an automatic mode. The best solution is to solve by inspection (determining the number of clusters and the grain boundaries contained) and then to do the calculation. These latter are calculated in automatic mode. The method employed have proven to be successful in producing the desired data although it will still take quite some time to produce all the grain boundary cluster TTFs in the interconnect samples.

Further simulations are done to validate the model by comparing with the other references available particularly for the single grain boundary. A comparison of results for the single grain boundary from three different method i.e. the exact solution, lumped element model and signal delay method confirms the validity of the developed lumped element model and suggest the suitability of the model for more complex grain boundary networks. Complex grain boundary networks enable more detailed analysis of electromigration to be carried out. The lengths of grain boundaries, angle of orientation and the diffusion coefficients have all been shown to have an effect on the Electromigration Time to Failure. In many references, it is been

assumed that the triple point is where failure normally occurs. In the current model, we show this is not necessarily the case. More important are the factors mentioned above (particularly the angles of orientation). These will determine where and when the first failure will occur. It is also been shown that these microstructural factors are the main contribution towards the variations of the Time to Failure. Signal delay approximations are compared to the lumped element model and results obtained are within acceptable level of error.

The validity of the stress evolution or the drift-diffusion model will not be complete if the distribution of the Time to Failure is not produced and analysed. Many experiments in the literature indicates that the Electromigration Time to Failure follows a log-normal distribution. To enable the distribution to be analysed, an adequate amount of data on Time to Failure is needed and it must come from a realistic representation of Al samples and the interconnect. The thesis has demonstrated a method (Voronoi technique, as has been used by others) of obtaining a realistic representation of the Al samples and also a means of simulating the annealing process. We demonstrate the various processes involved such as the growth of grains, the annihilation and the recombination/switching of grain boundaries.

The results of the analysis of the Time to Failure of the grain boundary clusters and that of interconnect draws two important conclusions with respect to the validity of the model. First it is shown that the distribution of the Time to Failure for both the grain boundary clusters and the interconnect samples for all the simulations undertaken exhibit an approximately log-normal distribution by using the lumped element model. Secondly the length of the grain boundary clusters also exhibit the lognormal distribution.

Using realistic experimental parameters, the analysis of the actual time scale of TTF and MTTF , realistic length of interconnect, the failure criterion (critical vacancy concentration/ critical stress) produced results which are comparable to other experimental and computer simulation results obtained by other researchers.

Analysis is also done on the effect of annealing of the Al samples on the Median Time to Failure and results confirms that annealing treatment increases the Electromigration lifetime of the interconnects. In analysing the detail of the microstructural parameters effects on the Time to Failure, it is observed that Time to Failure does not depend on a single parameter alone (for example the length of grain boundary clusters is shown to produce a random TTF results). We conclude that the factors affecting the Time to Failure of a grain boundary cluster are complex, that it involves more than one variable/parameters. Therefore it is quite impossible to segregate the parameters to analyse these parameters individually and independently because these factors work as a team

The advantages of the model can be seen from its ability to include the various distributions of the parameters which directly affect the distribution of the Time to Failure, such as the length of each grain boundary clusters, the distribution of the number of clusters in an interconnect and the distribution of the angle of orientation. These effects can be clearly observed by for example varying the width of the interconnect. The results obtained are similar to the other references i.e. as the width are reduced, the Median Time to Failure tends to increase, but the Deviation of Time to Failure also increases.

The thesis also includes a comparison between the results obtained by lumped element model and the signal delay. Analysis of the Time to Failure shows that the signal delay also exhibit the log-normal distribution (a better fit) and its Mean Time to Failure and Deviation of Time to Failure is within acceptable limits of error.

6.2 Scientific significance and Contribution to the understanding of Electromigration

The scientific significance of the research results obtained and their contribution to the understanding of Electromigration can be summarise as follows:-

i) A three dimensional model which includes the detailed microstructural/geometrical properties of the grain boundaries is developed. These are lacking in one-dimensional model available in the literature. Therefore analysis on Electromigration is more complete and detailed compared to the simplified/average micostructural effects considered in one-dimensional models.

ii) With the introduction of the equivalent C-R-C Π network representing the build-up of the vacancy concentration along the grain boundaries, fast and efficient Times to Failure can be estimated at every node along the complex grain boundary networks by both the lumped element model and by the signal delay method

iii) Detailed analysis on the effect of the microstructural properties on the Time to Failure can be performed.

iv) From the analysis observed , it is not necessarily the triple points that constitute the failure but more importantly the node which reach the stress/vacancy supersaturation first. That determines the Time To Failure.

v) The Electromigration Time to Failure is not determine by a single parameter alone but instead is a multi-variable function involving parameters such as the diffusion coefficient, the length of grain boundaries and the angle of orientation.

vi) The analysis can be done cheaply by using a common available software package such as Matlab® or PSpice since it involves an electrical circuit equations only and the results obtained are of acceptable quality.

6.3   Recommendation for Further work

The current research work can be improved or extended in the following areas:-

i) The program codes developed at present involves many search subroutines which have the effect on the run-time of the program and therefore limits the research to a small but reasonable number of realistic grain boundaries structures. The improvements to the program codes and a higher capability computer system will enable a larger number of realistic grain boundaries to be simulated.

ii) As discussed in Chapter 4, the program codes to produce the Time to Failure are based on the inspection of the number of grain boundary cluster and the grain boundary individual label number in a given interconnect sample. The program codes may be improved by automating this procedure, so that the results can be obtained faster and more reliably.

iii) The calculation of the Time-to Failure is based on the implicit assumption that the void formation time is dominated by the time for the vacancy build-up to reach some threshold. However there is some evidence that this might not be the case {Riege et al., 1996]. Further research needs to be done in modelling the periods (if they exist) between reaching the critical stress and voiding and between voiding and failure.

CHAPTER 7

REFERENCES

Agarwala , B.N., Attardo, M.J., and Ingraham,A.P., (1970)," Dependence of Electromigration-Induced Failure Time on Length and Width of Aluminium Thin-Film Conductors", Journal of Applied Physics, Vol 41(10), pp 3954-3960.

Agarwala,B.N., Patnaik,B.,and Schnitzel,R., (1972), " Effect of Microstructure on the Electromigration Life of Thin-Film Al-Cu Conductors", Journal of Applied Physics, Vol 43(40), pp 1487-1493.

Ainslie , N.G., d'Heurle,F.M., and Wells, O.C., (1971), "Coating, Mechanical Constraints, and Pressure Effects on Electromigration", Applied Physics Letters, Vol.20(4), pp 173-174.

Ames, I., d'Heurle,F.M.,Horstmann,R.E. ,(1970), "Reduction of Electromigration in Aluminium Films by Copper Doping", IBM Journal of Research and Development, pp 461-463.

Anderson M.P., Srolovitz D.J., Grest G.S., Sahni P.S.,(1984), " Computer Simulation Of Grain Growth - 1. Kinetics", Acta Metall, Vol 32, No.5 pp 783-791

Attardo, M.J., Rutledge, R.,and Jack, R.C., (1971), " Statistical Metallurgical Model for Electromigration Failure in Aluminium Thin-Film Conductors", Journal of Applied Physics, Vol. 42(11), pp 4343-4349.

Attardo,M.J., and Rosenberg,R., (1970), "Electromigration Damage in Aluminium Conductors", Journal of Applied Physics, Vol.41(6), pp 2381-2386.

Berenbaum,L., (1970), " Electromigration Damage of Grain-Boundary Triple Points in Al Thin Films", Journal of Applied Physics, Vol. 42, pp880-882.

Biran,A and Breiner,M,(1999) " MATLAB 5 for Engineers", Addison Wesley Longman Limited. PP 476-487

Black, J.R,(1969), "Electromigration Failure Models in Aluminium Metallization for Semiconductor Devices",Proceedings of The IEEE, Vol 57, pp 1587-1593.

Black, J.R.,(1969), "Electromigration - A brief survey and some results",IEEE Transaction on Electron Devices,Vol.ED-16,pp 338-347.

Blech, I.A., (1976), "Electromigration in Thin Aluminium Films on Titanium Nitrade", Journal of Applied Physics, Vol.47(4), pp 1203-1208.

Blech, I.A., and Meieran,E.S.,(1969), " Electromigration in Thin Films", Journal of Applied Physics, Vol. 40(2),pp 485-491.

Blech,I.A, and Herring,C,(1976), "Stress generation by Electromigration", Applied Physics Letters, Vol.29,No 3,pp131-133

Bobbio.A. and Saracco.O.,(1975)," A modified reliability expression for the Electromigration Time-To-Failure", Microelectronics and Reliability,Vol 14., pp 431-433.

Clement, J.J. and Thompson, C.V. ,(1995), " Modelling Electromigration-Induced Stress Evolution in Confined Metal Lines", Journal of Applied Physics, Vol. 78(2), pp 900-904

Clement, J.J.,(1997), " Reliability Analysis for Encapsulated Interconnect lines Under DC and Pulse DC Current Using a Continuum Electromigration Transport Model", Journal of Applied Physics, Vol 82(12). Pp 5991-6000

Clement, J.J,(1992), " Vacancy Supersaturation Model for Electromigration Failure Under DC and Pulse DC Stress", Journal of Applied Physics, Vol 71(9), pp4264-4268.

Clement, J.J., and Lloyd, J.R., (1992), " Numerical Investigation of The Electromigartion Boundary Value Problem", Journal of Applied Physics, Vol. 71(4), pp1729-1731

Cho, J, and Thompson, C.V.,(1989), "Grain Size Dependence of Electromigration-Induced Failures in Narrow Interconnects", Applied Physics Letters,Vol.54(25), pp2577-2579

d'Heurle,F., and Ames,I.,(1970), " Electromigration in Single Aluminium Films",Applied Physics Letter, Vol 16(2),pp 80-81.

d'Heurle,F., and Rosenberg,R.,(1973), "Electromigration in Thin Films", Physics of Thin Films, Vol. 7, pp257-310.

d'Heurle,F.,(1971), "Electromigration and Failure in Electronics", Proceedings of The IEEE, Vol.59(10), pp1409-1418.

d'Heurle,F.M. (1971), "The effect of copper additions on electromigration in aluminium films", Metallurgical Transactions2, pp 681-689

Dennard , H. R., Gaensslen, H. F, Yu,H.N.,Rideout,V.L.,Bassous,E., and LeBlanc,A.R., (1974), " Design of Ion-Implanted MOSFET's with Very Small Physical Dimensions", IEEE Journal of Solid-State, Vol SC-9(5), pp 256-267.

Domenicucci, A.G., Filippl, R.G., and Choi,K.W.,(1996) " Effect of Copper on the Microstructure and Electromigration lifetime of Ti-AlCu-Ti Fine Lines in the Presence of Tungsten Disffusion Barriers, Journal of Applied Physics, Vol 80(9),pp 4952-4959.

Duan,Q.F., and Shen,Y.-L,(2000) " On the prediction of electromigration voiding using stress-based modelling", Journal of Applied Physics, Vol 87(8), pp 4039-4041

Dwyer, V.M. (1996), " Electromigration Behavior Under a Unidirectional Time-Dependent Stress", Transactions on Electron Devices, Vol.43(6). Pp 877-882.

Dwyer, V.M., Wang, F.S., and Donaldson,P., (1994), " Electromigration Failure in A Finite Conductor with a Single Blocking Boundary", Journal of Applied Physics, Vol. 76(11), pp 7305-7309

Dwyer,V.M., and Wan Ismail,W.S.,(2001), " Electromigration voiding in nanoindented, single crystal Al Lines", Journal of Applied Physics, Vol 89(5), pp 3064-3066

English , A.T., Tai, K.L., and Turner, P.A.,(1974), "Electromigration of Ti-Au Thin-Film Conductors at 180^0 C", Journal of Applied Physics, Vol 45(9), pp 3757-3767.

English, A.T., and Kinsbron, E.,(1983), "Electromigration-Induced Failures by Edge Displacement in Fine-Line Aluminium 0.5% Copper thin films", Journal of Applied Physics, Vol.54(1), pp 268-274.

English, A.T., Tai, K.L., and Turner,P.A., (1972), "Electromigration in Conductor Stripes Under Pulse DC Powering", Applied Physics Letters, Vol.21(8), pp 397-398.

English,A.T., and Kinsbron,E., (1983),"Electromigration Transport Mobility Associated With Pulsed Direct Current in Fine-Grained Evaporated Al-0.5% Cu Thin Films", Journal Of Applied Physics,Vol.54(1), pp275-280.

Ferlazzo, L., and Reimbold,G, Gonchond,J.P., Heitzmann, M., and Demolliens,O.,Lormand,G., (1993), "Electromigration in AlCu Interconnections with W-Plug Contacts", Quality and Reliability Engineering International, Vol 9, pp 299-302.

Frankovic,R., Bernstein,G.H., and Clement,J.J.,(1996), "Pulsed-Current duty cycle dependence of Electromigration-induced stress generation in Aluminium Conductors", IEEE Electron Device Letters, Vol.17(5), pp244.

Frost H.J., Thompson C.V., Walton D.T., (1990), " Simulation of Thin Film Grain Structures - 1. Grain Growth Stagnation , Acta Metall Mater. Vol.38, No 8,pp 1455-1462

Gardner. D.S., Meindl., D.J., and Saraswat.K.S.,(1987), " Interconnection and Electromigration Scaling Theory",(1987), Transactions on Electron Devices, Vol-ED 34,No 3, pp633-642.

Gangulee, A., and d'Heurle,F.M. , (1973), "Anomalous Large Grains in Alloyed Aluminium Thin Film. Ii. Electromigration and Diffusion in Thin Films with very large grains" Thin Solid Films, Vol 16, pp 227-236.

Ghate, B. Prabhakar.,(1986), "Interconnections in VLSI", Physics Today,   pp 58-66.

Gupta.R., Tutuianu.B., Pileggi L.T.,(1997) " The elmore delay as a bound for RC trees with generalized Input Signals", IEEE Trans. On Computer-Aided Design of Integrated Circuits and Systems, Vol 16. No 1, pp95-104.

Gui, X., Haslett,J.W., Dew, S.K., and Brett, M.J., (1998) " Simulation of Temperature Cycling Effects on Electromigration Behavior Under Pulsed Current Stress, IEEE Transactions on Electron Devices,Vol 45(2), pp 380-385.

Gui, X., Dew, S.K., and Brett M.J, (1996), " Numerical Solution of Electromigration Boundary Value Problem Under Pulsed DC Conditions", Journal of Applied Physics, Vol 80(9), pp. 4948-4951.

Gleixner,R.J. and Nix W.D.(1998), " Effect of "bamboo" grain boundaries on the maximum electromigration-induced stress in microelectronic interconnect lines", Journal of Applied Physics, Vol 83(7), pp 3595-3599.

Gleixner,R.J. and Nix W.D.(1999), " A physically based model of electromigration and stress-induced void formation in microelectronic interconnectss", Journal of Applied Physics, Vol 86(4), pp 1932-1940.

Harrison, J.W,JR.,(1988), " A Simulation Model for Electromigration in Fine-Line Metallization of Integrated Circuits Due to Repetitive Pulse Currents", IEEE Transactions on Electrron Devices, Vol. 35(12), 2170-2170.

Ho,S.Paul.and Kwok,Thomas.,(1989), "Electromigration in metals", Report on Progress Physics, Vol 52, pp 301-341.

Howard, J.K.,and White,J.F. "Intermetallic Compounds of Al and Transitions Metals: Effect of electromigration in 1-2-μm-wide lines, Journal of Applied Physics.Vol. 49(7), pp 4083-4092.

Iyer, Subramanian S., and Ting,Chung-Yu, (1984) "Electromigration Lifetime Studies of Submicrometer-Linewidth Al-Cu Conductors", IEEE Transactions on Electron Devices, Vol-ED-31, pp 1468-1471.

Jones, B.K., and Xu, Y.Z., and Denton,T.C.,(1994) " Electrical Measurements as Performance Indicators of Electromigration", Quality and Reliability Engineering International, Vol. 10, pp 315-318.

Joo, Y-C, Thompson C.V.,(1994), " Analytic model for the grain structures of near-bamboo interconnect", Journal of Applied Physics, Vol.76(11), pp 7339-7346

Joo,Y-C,Baker,S.P.,and Arzt,E.,(1998), "Electromigration in Single-Crystal Alumuminium Lines with Fast Diffusion Paths by Nanoindention", Acta Matellurgical Materilia, Vol.46,No.6,pp 1969-1998.

Joo,Y-C, Thompson C.V., Baker,S.P., and Arzt,E.,(1999), " Electromigration proximity effects of two neighbouring fast-diffusion segments in single-crystal aluminium lines.", Journal of Applied Physics, Vol 85(4),pp 2108-2113.

Kinsbron, E., (1980), "A model for the width dependence of electromigration lifetimes in aluminium thin-film stripes", Applied Physics Letters, Vol.36(12), pp 968-970.

Kinsbron, E., Smith,C.M.M., and English, A.T., (1979), " Failure of Small Thin-Film Conductors Due to High Current-Density Pulses", IEEE Transactions on Electron Devices, Vol.-ED-26(1), pp 22-26.

Kirchheim,R,.(1992), " Stress and Electromigration in Al-lines of Integrated Circuits",Acta Metallurgica Materilia,Vol 40, No2, pp 309-323

Kirchheim,R.,(1993), " Electromigration, Models and Atomistic Interpretation", Quality and Reliability Engineering International, Vol 9, pp 287-293

Kirchheim, R., and Kaeber, U., (1991), " Atomistic and Computer Modeling of Metallization Failure of Integrated Circuits by Electromigration", Journal of Applied Physics, Vol. 70(1), pp 172-181.

Knorr, D.B., and Rodbell, K.P., (1996), " The Role of Texture in The Electromigration Behavior of Pure Aluminium Lines", Journal of Applied Physics, Vol.79(5), pp 2409-2417.

Korhonen,M.A., Paszkiet, C.A. and Li Che-Yu,(1991), " Mechanisms of thermal stress relaxation and stress-induced voiding in narrow aluminium-based metallizations", Journal of Applied Physics, Vol 69(12), pp 8083-8091

Korhonen, M.A., and Borgesen,P., Tu,K.N.,Li,Che-Yu, (1993(1)), " Stress evolution due to electromigration in confined metal lines", Journal of Applied Physics, Vol. 73(8), pp 3790-3799.

Korhonen, M.A., Borgesen, P., Brown,D.D., and Li,Che-Yu, (1993(2)) "Microstructure Based Statistical Model of Electromigration Damage in Confined Line Metallization in The Presence of Thermally Induced Stresses", Journal of Applied Physics , Vol. 74(8), pp 4995-5004.

Learn, Arthur J., (1971), " Effect of redundant microstructure on electromigration-induced failure", Applied Physics Letters, Vol. 19(8), pp 292-295.

Li.Z.,Bauer.C..L..,Mahajan,S, Mahajan.S,and Milnes A.G.,(1992), " Degradation and subsequent healing by electromigration Al-1 wt % Si thin films. Journal of Applied Physics,Vol.72(5), pp1821-1832.

Li, C.-Y., Borgesen,P., and Korhonen, M.A.,(1992) " Electromigration-Induced Failure in Passivated Aluminium-Based Metallizations- The Dependence on Temperature and Current Density", Applied Physics Letters, Vol.61(4), pp 411-413.

Lin T-M and Mead.C.A.,(1984), " Signal delay in general RC networks", IEEE Trans. On Computer -Aided Design, Vol.CAD-3.No 4., pp331-349

Liew,B.K.,Cheung,N.W., and Hu,C.(1990), "Projecting Interconnect Electromigration Lifetime for Arbitrary Current Waveforms",IEEE Transactions on Electron Devices, Vol.37(5), pp 1343-1350.

Liew,B.K.,Fang P., Cheung N.W. and Hu.C.,(1992) " Circuit Reliability Simulator for Interconnect, Via, and Contact Electromigration", IEEE Transactions on Electron Device, Vol.39(11),pp 2472-2478.

Liu, Y., Cox, C.L., and Diefendorf, " Finite Element Analysis of The Effects of Geometry and Microstructure on Electromigration in Confined Metal Lines", Journal of Applied Physics, Vol. 83(7), pp3600-3608.

Lloyd, J.R. and Koch,R.H., (1988), " Study of Electromigration Induced Resistance and Resistance Decay in Al Thin-Film Conductors", Applied Physics Letters, Vol. 52(3), pp 194-196.

Lloyd, J.R., and Koch, R.H., (1992) , " Electromigration-Induced Vacancy Behavior in Unpassivated Thin Films" , Journal of Applied Physics, Vol.71(7), pp 3231-3233.

Lloyd, J.R.,(1994), "Reliability modelling for electromigration failure",Quality and reliability and engineering international, Vol 10, pp 303-308.

Lloyd, J.R.,(1991), " Electromigration Failure", Journal of Applied Physics, Vol. 69(11), pp 7601-7604.

Lloyd,J.R., and Kitchin,J., (1991), "The Electromigration Failure Distribution: The Fine-Line case", Journal of Applied Physics, Vol.69(4), pp 2117-2127.

Malone,D.W., and Hummel,R.E.,(1997) " Electromigration in integrated circuits",Critical Reviews in Solid State and Material Science", pp 199-238.

Marcoux, P.J., Merchant,P.P.,Naroditsky,V., and Rehder,W.,(1989) " A New 2D Simulation Model of Electromigration, Hewlett-Packard Journal, pp 79-84.

MATLAB, High performance numeric computation and visualization software, 1992

Matsuoka, F., Iwai,H.,Hama, K.,Itoh, H., Nakata R., Nakakubo, T.,Maeguchi, K.,and Kanzaki,K.,(1990), " Electromigration Reliability for a Tungsten-Filled Via Hole Structure", IEEE Transactions on Electron Devices, Vol. 37(3),pp562-567.

Meeker, W.Q., and Escobar,L.A.,(1998), " Pitfalls of Accelerated Testing", IEEE Transactions on Reliability, Vol 47 (2), PP 114-118

Mulheran P.A. (1992), " On the statistical properties of the two-dimensional random Voronoi network", Philosophical Magazine Letters, Vol. 66, No.5, pp 219-224

Neri, B., Diligenti, A., and Bagnoli, P.E., (1987), "Electromigration and Low-Frequency Resistance Fluctuations in Aluminium Thin-Film Interconnections", IEEE Transactions on Electron Devices, Vol.Ed-34(11), pp 2317-2321.

Niehof, J., and Flinn, P.A., and Malonaey, T.J., (1993), "Electromigration Early Resistance Increase Measurements", Quality and Reliability Engineering International, Vol. 9, pp 295-298.

Ohfuji,S.,and Tsukada,M.,(1995) Journal of Applied Physics, Vol.78(6), pp 3769.

Ohring,Milton.,(1998), "Reliability and failure of electronic materials and devices",Academic Press.

Park, Y.J., and Thompson, C.V.,(1997), " The Effects of The Dependence of Atomic Diffusivity on Stress Evolution Due To Electromigration", Journal of Applied Physics, Vol. 82(9), pp 4277-4281.

Pasco, R.W., and Schwarz, J.A., "Temperature-Ramp Resistance Analysis to Characterise Electromigration" , Solid State Electronics, Vol.26(5), pp445-452.

Pierce, J.M.,and Thomas, M.E., (1981), "Electromigration in aluminium conductros which are chains of single crystals" , Applied Physics Letters, Vol. 39(2), pp 165-168.

Prybyla J.A, Riege,S.P., Grabowski,S.P., and Hunt. A.W. " Temperature dependence of Electromigration dynamics in Al interconnects by real-time microscopy",(1998), Applied Physics Letters, Vol.73, No.8, pp 1083-1085.

Riege, S.P. , Prybyla, J.A., and Hunt, A.W.(1996) "Influence of Microstructure on Electromigration Dynamics in Submicron Al Interconnects: Real-Time Imaging", Applied Physics Letters, Vol.69(16), pp 2367-2369.

Rosenberg, R., and Ohring, M.,(1971), "Void Formation and Growth During Electromigration in Thin Films", Journal of Applied Physics, Vol.42(13), pp 5671- 5679.

Rosenberg,R., and Berenbaum,L.,(1968), " Resistance monitoring and effects of nonadhesion during electromigration in Aluminium films", Applied Physic Letters, Vol 12(5), pp 201-204.

Rubinstein,J., Penfield P.JR., and Horowitz,(1983) " Signal Delay in RC Tree Networks". IEEE Transactions on Computer-Aided Design, Vol, CAD-2,No.3,pp 202-211

Sabnis, G.Anant, (1990), " VLSI Electronics Microstructure Science-VLSI Reliability",Vol. 22, Academic Press,Inc.

Sarychev, M.E., and Zhitnikov, Yu.V., Borucki,L., Liu,C.-L.,Makhviladze,T.M., (1999), " General Model for Mechanical Stress Evolution During Electromigration", Journal of Applied Physics, Vol 86(6),pp 3068-3074.

Schafft, H.A., Staton,T.C., Mandel, J., Shott, J.D., (1987), "Reproducibility of Electromigration Measurements", IEEE Transactions on Electron Devices, Vol.Ed-34(3), pp 673-681.

Schoen, J.M. (1980), "A model of Electromigration Failure Under Pulsed Condition", Journal of Applied Physics. Vol.51(1), pp 508-512.

Schoen, J.M. (1980), " Monte Carlo calculations of structure-induced electromigration failure", Journal of Applied Physics, Vol 51(1),pp513-521

Selikson, B.,(1969), "Void Formation Failure Mechanisms in Integrated Circuits",Proceedings of The IEEE, Vol. 57(9), pp 1594-1598.

Shatzkes, M., and Lloyd,J.R., (1986), " A model for conductor failure considering diffusion concurrently with electromigration resulting in a current exponent of 2", Journal of Applied Physics, Vol. 59(11), pp 3890-3893

Sigsbee,R.A.,(1973), " Electromigration and metalization lifetimes",Journal of Applied Physics, Vol 59(11),pp 2533- 2540.

Spitzer, Stuart M., (1969), " The Effects of Dielectric Overcoating on Electromigration in Aluminium Interconnections", IEEE Transactions on Electron Devices, Vol.ED-16, pp348-350.

Surh,M.P (1999)," Threshold stress behaviour in thin film electromigration", Journal of Applied Physics, Vol 85(12), pp8145-8154

Tammaro,M., and Setlik,B. (1999), " Variable Behavior of The Current Exponent in a Microscopic Nucleation Model for Electromigration", Journal of Applied Physics, Vol. 85(10), pp 7127-7129.

Thompson, C.V., and Cho,J., (1986) " A New Electromigration Testing Technique for Rapid Statistical Evaluation of Interconnect Technology", IEEE Electron Device letters, Vol.-EDL-7, No 12, PP 667-668.

Trattles, J.T., O'Neill,A.G., and Mecrow,B.C. ,(1994) "Computer Simulation of Electromigration in Thin-film metal conductors", Journal of Applied Physics.Vol 75(12), pp7799-7804.

Turnbull,D., and Hoffman R.E.,(1954), " The effect of relative crystal and boundary orientations on grain boundary diffusion rates", Acta Metalurgica, Vol. 2, pp419-426

Vaidya , S., Sheng, T.T., Sinha, A.K.,(1980), "Linewidth Dependence of Electromigration in evaporated Al-0.5%Cu", Applied Phys. Letters.Vol. 36(6), pp 464-466.

Vaidya, S., and Sinha, K.,(1981), "Effect of Texture and Grain Structure on Electromigration in Al-0.5% Cu. Thin Films", Thin Solid Films, Vol 75, pp 251-259.

Vaidya, S., Schutz, R.j., and Sinha,A.K., (1983), "Shallow Junction Cobalt Silicate Contacts with Enhanced Electromigration Resistance", Journal of Applied Physics, Vol. 55(10), pp 3514-3517.

Vandenberghe L., Boyd S. and Gamal.A.El., (1998), " Optimizing dominant Time constant in RC circuits", IEEE Trans. On Computer-Aided design of integrated circuits and Systems, Vol 17, No 2. Pp110-125

Verbruggen A.H.,(1988), " Fundamental questions in the theory of electromigration", IBM Journal Research Develpment., Vol 32. No 1. Pp93-98

Weaire D.,and Kermode J.P.,(1983), " Computer simulation of a two-dimensional soap froth. 1. Method and motivation", Philosophical Magazine B, Vol.48, No 3, pp 245-259.

Young.D, and Christou.A,(1994), " Failure Mechanism Models for Electromigration", IEEE Transactions on Reliability, Vol. 43, No 2,pp 186-191

NOTE: all appendices A& B are in the Floppy Disk enclosed

Appendix A1

Table A1(1-10)   Detailed results of experiment no.1: non-annealed interconnects

Table A1.1 - 'Treated data' of Time to Failure for grain boundary clusters
                (experiment .no1(a))

Table A1.2 - ' Treated data' of Time to Failure for interconnects
                (experiment no.1(b))

Appendix A2

Table A2(1-10)   Detailed results of experiment no.2: annealed interconnects

Table A2.1 - 'Treated data' of Time to Failure for grain boundary clusters
                (experiment no2(a))

Table A2.2 - ' Treated data' of Time to Failure for interconnects
                (experiment no.2(b))

Appendix A3

**Table A3(a1-a5)-A3(e1-e5) Detailed results of experiment no.3: The effect of the
                variation of interconnect width/length ratio on
                TTF,MTTF and DTTF**

Table A3.1 -   'Treated data' of Time to Failure for interconnect sample(a)

Table A3.2 -   'Treated data' of Time to Failure for interconnect sample (b)

Table A3.3-   'Treated data' of Time to Failure for interconnect sample (c)

Table A3.4-   'Treated data' of Time to Failure for interconnect sample (d)

Table A.3.5-   'Treated data' of Time to Failure for interconnect sample (e)

Appendix A4

**Table A4(1-5)   Detailed results of experiment no.4: Signal delay
                                                          vs Lumped element model**

Table A4.1.1 - 'Treated data' of Time to Failure of grain boundary clusters
                using Signal delay

Table A4.1.2- 'Treated data' of Time to Failure of grain boundary clusters
                using Lumped element model

Table A4.2.1 - ' Treated data' of Time to Failure of interconnects
                using Signal delay

Table A4.2.2 - ' Treated data' of Time to Failure of interconnects
                using Lumped element model

Appendix A5

Time to Failure using Weibull distributions

Table A5.1 - 'Treated data' of Time to Failure of grain boundary clusters
                using Signal delay.

Table A5.2- 'Treated data' of Time to Failure of grain boundary clusters
                using Lumped element model

Table A5.3- 'Treated data' of Time to Failure of interconnects using Signal delay

Table A5.4- 'Treated data' of Time to Failure of interconnects using Lumped element
                model

Appendix B1

**The program   code listings for single grain boundary with one end has vacancy
supply and the other end blocked**

(1) The script file: **simall1g.m**
(2) The function file: **rroot**
(3) The function file: **imroot.m**

Appendix B2

The Program code   listings for single grain boundary with both ends blocked

(1)The script file: **sg2ball.m**

Appendix B3

The program code listings for an example of complex grain boundary with one end has a vacancy supply c_0 and the rest blocked

(1).   The script file: **net1ball.m**

Appendix B4

The program code listings for an example of complex grain boundary with all ends blocked

(1)The script file: **net2ball.m**

Appendix B5

The program code for realistic interconnects

(1).The script file:	**vrnoittf.m**
(2)The function file:	**annealing.m**
(3)The function file:	**geometry.m**
(4)The function file:	**labgrain1.m**
(5)The function file:	**labgrain2.m**
(6)The function file:	**conmtrix.m**
(7)The function file:	**lamda1.m**
(8)The function file:	**grwth.m**
(9)The function file:	**trisw1.m**
(10)The function file:	**output.m**
(11)The function file:	**figvrnoi.m**
(l2The function file	**lablenode.m**
(13The function file:	**slices2.m**
(14)The function file:	**newgeometry.m**
(15)The function file:	**newnode.m**
(16)The function file:	**vrttf.m**
(17)The function file:	**vrmat4.m**

(18)The function file   **vres3.m**
(19)The function file: **vcmat3.m**
(20)The function file: **vnoicap3.m**
(21)The function file: **vcrgmat3.m**
(22)The function file   **vcrg3.m**
(23)The function file: **vumat3.m**
(24)The function file: **elmore3.m**

Appendix C

PUBLICATION

Electromigration voiding in nanoindented, single crystal Al lines

Electromigration voiding in nanoindented, single crystal Al lines

V. M. Dwyer[a] and W. S. Wan Ismail
Department of Electronic and Electrical Engineering, Loughborough University, Loughborough LE11 3TU, United Kingdom

We consider the interpretation of some theoretical and experimental work regarding electromigration voiding in nanoindented, single crystal aluminum lines. A recently suggested voiding criterion of a critical accumulated flux divergence is found, in fact, to be identical to the widely accepted critical stress criterion. The inclusion of the stress dependence of the atomic diffusion coefficient is shown to be vital when the steady state is characterized by $J \neq 0$, such as in the case of a void growing at a constant rate. It is found, for example, that the stress required for steady void growth, within single crystal Al lines, is probably significantly smaller than previously suggested. © *2001 American Institute of Physics.* [DOI: 10.1063/1.1342436]

In electromigration (EM), the total atomic flux density is generally taken to be

$$J_A = \frac{D_A C_A}{kT}(\Omega \nabla \sigma + Z^* q \rho j i), \tag{1}$$

where σ is the local tensile stress, C_A is the atomic concentration, D_A is the local atomic diffusion coefficient, Z^* is the effective electromigration charge and all other variables have their usual meanings.[1] Atomic diffusion occurs largely along a grain boundary network, as D_A is significantly larger on grain boundaries than it is through the bulk. Fluxes from Eq. (1) produce relatively small changes in local vacancy concentration so that continuity may be approximated by

$$\nabla . J_A + \gamma = 0, \tag{2}$$

where γ is the net rate of atomic recombination at sites other than vacancies. The process is typically considered to be one of dislocation climb within grain boundaries and gives rise to an increase in local tensile stress according to

$$d\sigma = -B \frac{dC_A}{C_A} = -\frac{B}{C_A} \gamma dt, \tag{3}$$

where B is an elastic (possibly bulk) modulus for aluminum.[1] In Eq. (3) averages have been taken over the cross section of the stripe.

Assuming a Maxwell–Boltzmann population for the vacancy concentration C_V and a hopping process for the diffusion mechanism, the atomic diffusion coefficient $D_A (= D_V C_V / C_A)$ has an exponential stress dependence, thus

$$D_A(\sigma) \approx D_{A_0} \exp\left(\frac{\sigma \Omega}{kT}\right). \tag{4}$$

Averaging Eq. (1) over the cross section of the stripe and combining the result with Eqs. (2)–(4) yields the final one-dimensional expression[1]

$$\frac{\partial \sigma}{\partial t} = \frac{\partial}{\partial x}\left[\frac{B D_A^{\text{eff}} \Omega}{kT}\left(\frac{\partial \sigma}{\partial x} + \frac{Z^* e \rho j}{\Omega}\right)\right] = B\Omega \frac{\partial J_A}{\partial x}, \tag{5}$$

where D_A^{eff} is the "effective" atomic diffusion coefficient caused by the averaging. For example, in polycrystalline regions $D_A^{\text{eff}} = \delta D_A / d$ for grain boundary thickness δ, and average grain size d. Void nucleation in polycrystalline and near bamboo aluminum lines occurs largely due to the dependence of D_A^{eff} on the position along the stripe and in typical structures this dependence is very complex. An artificial method of creating a "known" structure in single crystal aluminum lines is by nanoindentation[2,3] in which fast diffusing clusters are created by mechanically damaging the crystal at certain points. We consider here some recent results on such structures.

For voiding to occur, in the standard model of electromigration described above, the tensile stress evolves until it reaches some critical value σ_{cr} at some point; void nucleation then occurs. We first consider the countersuggestion of Duan and Shen[4] that nucleation occurs rather as the result of a critical accumulation (over time) of flux divergence as this is "a more feasible parameter for void formation," they claim that this gives a different nucleation point. To justify their view the authors analyze the experimental setup of Joo et al.[2,3] in which nanoindented single crystals are produced with a fast–slow–fast or similar pattern. Solving Eq. (5) they find that the two criteria give different voiding points. However, it is clear by integrating Eq. (5) that these two criteria are in fact rigorously identical, as

$$\sigma(x,t) = B\Omega \int_0^t \frac{\partial J_A}{\partial x} dt. \tag{6}$$

In following the work of Duan and Shen,[4] we are able to reproduce their figures for stress evolution and for the atomic flux but we have not been able to reproduce their figure for the accumulated flux divergence, which we find is proportional to the tensile stress and thus is in line with Eq. (6). We can only conclude that there are numerical errors in their integration of Eq. (6).

The position of maximum stress, and thus the theoretical voiding position, depends upon the extent of the SEM-invisible plastic regions created during the indentation process.[5] The nanoindented lines[2,3] are created in such a

---

[a]Electronic mail: v.m.dwyer@lboro.ac.uk

J. Appl. Phys., Vol. 89, No. 5, 1 March 2001

V. M. Dwyer and W. S. Wan Ismail   3065

manner that each indented segment may be considered to be continuous. This assumes that the plastic regions of each indentation overlap. As a consequence there will also exist a transition region of plastic damage between the fast and slow diffusing regions. Mechanical damage, due to indentation, appears in Eq. (5) as a position dependent diffusion coefficient $D_A^{\text{eff}}(x)$. Solving Eq. (1) in the steady state (with $J \neq 0$), for an unpassivated line, the position of maximum stress occurs at the point given by the solution to[6]

$$\frac{1}{D_A^{\text{eff}}(x)} = \frac{1}{L} \int_0^L \frac{dx}{D_A^{\text{eff}}(x)}, \tag{7}$$

and $\partial D_A^{\text{eff}}/\partial x > 0$. That is, the maximum steady state stress occurs where $D_A^{\text{eff}}(x)^{-1}$ is equal to its value averaged over the length L of the structure. Equation (7) predicts that the site of maximum steady state stress will usually lie within this transition region and thus somewhat outside the fast diffusing region. Time-dependent stress evolution for this structure also shows that, for reasonable values of the critical stress, the voiding position will occur close to the site of maximum steady state stress. Note that, as it is $D_A^{\text{eff}}(x)^{-1}$ rather than $D_A^{\text{eff}}(x)$ that is involved in the averaging process [Eq. (7)], the position of the voiding site within the transition region will tend to lie nearer to the slow (undamaged) region than to the fast (SEM-visibly damaged) region.

For systems with a steady state corresponding to $J = 0$, it is only the time to reach the steady state that is affected by D_A^{eff}. The final stress is independent of D_A^{eff} and hence it is unimportant whether or not stress dependence is included. This is not the case for a system whose steady state (as here) is characterized by $J \neq 0$. In the initial stage, where the stress is still small, inclusion of the stress dependence makes little difference as $D_A^{\text{eff}}(\sigma) \approx D_A^{\text{eff}}(\sigma=0) \equiv D_{A_0}^{\text{eff}}(x)$. However as time progresses and σ builds up the variation in D_A^{eff} has more obvious effects.

Consider the situation of Ref. 4, but without any transitional plastic damage zone and with a spatially uniform Z^* $= -15$. Equation (1) is solved for an unpassivated line with a slow–fast–slow structure of the same material constants as considered in Refs. 2–4 and the final stress is shown in Fig. 1(a). Note that the tensile stress gradient at the cathode end is very small. It is also true that the EM flux is much lower than the equivalent case in which the stress dependence is ignored. This is a result of the fact that compressive stress in the anode half of the interconnect reduces the effective D_A^{eff} values there, thus reducing the overall steady state flux. Now only a small tensile stress in the cathode half of the interconnect is required to match the EM current in the anode half. Figure 1(b) shows the situation with $Z^* = -4$, the asymmetry is reduced but still clear. In terms of stress profile Z^* is obviously an important, if a relatively unknown, parameter.

For this same structure (with $Z^* = -15$) we find that the maximum tensile stress in the line is $\sigma = 0.314$ GPa which occurs after ~1.75 h, after which time the maximum stress drops again until it reaches the steady state value of Fig. 1(a). If void nucleation has not occurred prior to 1.75 h it will never occur. The maximum compressive stress in the stripe however continues to increase in magnitude to a final steady
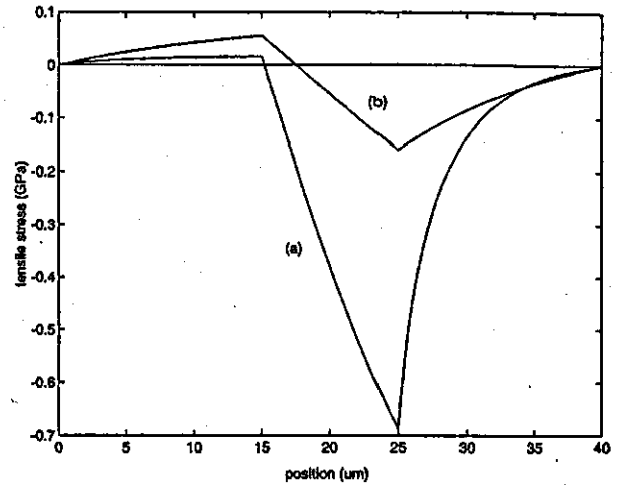

FIG. 1. Steady state tensile stress including the flux dependence of diffusion coefficient, (a) $Z^* = -15$, (b) $Z^* = -4$. Electron flow is from left- to right-hand side.

state value of $\sigma = -0.688$ GPa which may be sufficient to produce a hillock-related failure. This result is in contrast to the stress-independent case in which the value of both the maximum tensile stress and the maximum compressive stress increase as $t \to \infty$.

It is clear from the discussions above that, when the steady state is characterized by $J \neq 0$, it is not valid to use steady state stress profiles (as in Ref. 2 and references therein) which do not explicitly include the exponential term in D_A, Eq. (4). The departure from the $D_A \approx D_A(\sigma=0)$ profile, indicated above, occurs quickly (well before 1.75 h in the example above) so that it is not generally valid to use simple linear stress profiles, obtained through ignoring stress dependence, when modeling void growth. This latter situation is considered in Ref. 2 as a model for the possible interaction between two cluster sections, each below the critical Blech length. This example is similar to the one of Ref. 4 above but considers, instead, a slow region of length S separated by two fast (nanoindented) regions of lengths L_1 and L_2. Using linear steady state profiles, the authors[2] find that their results to be consistent with an assumed effective charge of $Z_f^* = -15$ for the fast regions and a derived Z_s^* $= -2$ for the slow region. Furthermore, because of the assumed linearity, their model only depends upon the difference in stress between the ends of the stripe $\Delta \sigma_{ss} = \sigma(x = L) - \sigma(x = 0)$ and not on the individual values. A value of $\Delta \sigma_{ss} = 0.51$ GPa is obtained by fitting the EM flux to the observed void growth rates. Naturally if the stress dependence of D_A^{eff} is included we obtain a rather different story as the EM current now also depends explicitly upon $\sigma(x = L)$ (through D_A^{eff}) but, in addition, the steady state stress profile itself is likely to be different. We set $\sigma(x = L) = 0.0$ GPa here to represent stress relaxation at the void surface as in Ref. 7. In the case of the 7-S-7 structure ($L_1 = 7$ μm, $L_2 = 7$ μm, and $S = 2$ μm), the stress profiles ignoring and including the σ dependence of D_A^{eff} are in fact very similar. Despite this there is a nearly 50% reduction in the steady state flux density J. This occurs as the presence of the void causes the

stress profile to be almost completely compressive,[7] thus reducing the diffusion coefficient (and mobility) through the exponential dependence on stress.

The quantitative analysis provided in Ref. 2 in order to obtain Z_s^* and $\Delta\sigma_{ss}$ may also be reinterpreted including the σ dependence. Their analysis is based on a linear fit between the segment separation S and a defined variable $Y(S)$ given as[2]

$$
Y(S) \equiv \left(\frac{J(S)kT}{D_f} - \frac{Z_f^* q\rho j}{\Omega} \right)\left(\frac{D_s}{D_f}(L_1 + L_2) + S \right)
$$

$$
= \frac{D_s}{D_f}\Delta\sigma_{ss} - S\left(\frac{Z_f^* q\rho j}{\Omega} - \frac{D_s}{D_f}\frac{Z_s^* q\rho j}{\Omega} \right). \tag{8}
$$

The authors find a remarkable straight-line fit between $Y(S)$ and S, after which the right-hand side of Eq. (8) is used to obtain Z_s^* and $\Delta\sigma_{ss}$. However the straight line obtained is erroneous. It occurs because $Y(S)$ so defined has an extremely weak dependence on the data $J(S)$, consequently the experimental results (i.e., the observed void growth rates) play an almost insignificant role in goodness of fit. $Y(S)$ is dominated by a linear term of slope $(-Z_f^* q\rho j/\Omega)(=9.4 \times 10^{13}\,\mathrm{J/m^3}$, equivalent to C_l in the notation of Ref. 2). It is this that accounts for the quality of the fit rather than any particular trend in experimental results. To see this we need only note that, after including the experimental data in $Y(S)$, the correction to the slope is $0.124\times 10^{13}\,\mathrm{J/m^3}$ ($\equiv \alpha C_u$ in the notation of Ref. 2) or substantially less than 2%. It is better to fit the variables Z_s^* and $\Delta\sigma_{ss}$ to the obtained experimental values of void growth rate against, e.g., S^{-1}, as shown in Fig. 2 for the 5-S-5 data. Figure 2(c) shows the best fit for stress-dependent D_A^{eff} (this corresponds to values of $Z_s^* = -4$, $\Delta\sigma_{ss} = 0.275\,\mathrm{GPa}$, $\sigma_L = 0.0\,\mathrm{GPa}$). Note that the effective EM charge in the slow region, $Z_s^* = -4$, is larger than the value of -2 suggested in Ref. 2 and perhaps in the more generally accepted range. Note also that the steady state stress across the crystal required for constant void growth rate, $\Delta\sigma_{ss} = 0.275\,\mathrm{GPa}$, is around half of the value of 0.51 GPa suggested in Ref. 2 and now substantially smaller than the value of $\Delta\sigma_{\mathrm{nucl}} \approx 0.75\,\mathrm{GPa}$ obtained in Ref. 2 for void nucleation. The latter value ($\Delta\sigma_{\mathrm{nucl}}$) is obtained from consideration of a $J=0$ steady state and is therefore independent of D_A^{eff}.

In summary, the recently proposed voiding criterion of Duan and Shen,[4] in which voiding occurs at the first point to have reached a critical accumulation (over time) of flux divergence, is in fact rigorously identical to the widely accepted critical stress criterion of the standard model, Eq. (6). For nanoindented single crystal aluminum lines the theoretical position of maximum stress lies outside the indented re-
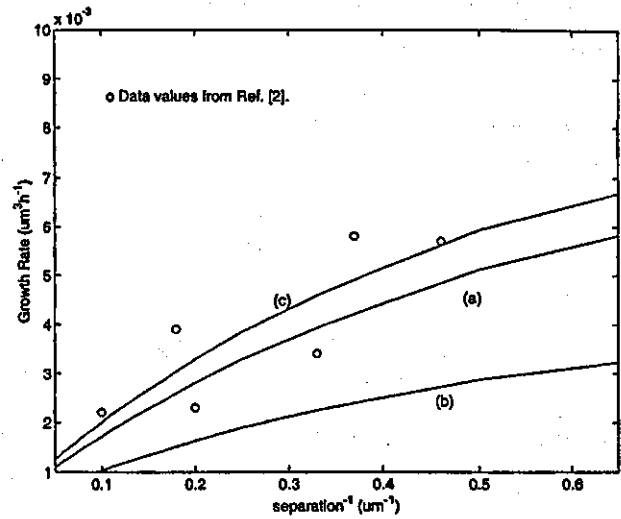

FIG. 2. Fitting of Z_s^* and $\Delta\sigma_{ss}$ to the experimental results (Ref. 2) for the void growth rate ($V = JA\Omega$) on the 5-S-5 structure. Curves correspond to (a) $Z_s^* = -2$, $\Delta\sigma_{ss} = 0.51\,\mathrm{GPa}$ ignoring stress dependence and as in Ref. 2; (b) $Z_s^* = -2$, $\Delta\sigma_{ss} = 0.51\,\mathrm{GPa}$, including stress dependence; (c) $Z_s^* = -4$, $\Delta\sigma_{ss} = 0.275\,\mathrm{GPa}$. Data points are taken from Ref. 2.

gion if standard EM models are to be assumed. The distance is of the order of the range that the plastic damage extends beyond the fast region. In the analysis of systems characterized by a $J \neq 0$ steady state it is vital to include the stress dependence of the diffusion coefficient. For example, on its inclusion in the analysis of the $L_1 - S - L_2$ structure[2] one finds that the stress required for steady state void growth is significantly smaller than previously suggested.[2] In addition, the effective EM charge in the slow region ($Z_s^* \approx -4$ in this example) is, perhaps, closer to a more generally accepted range. Finally, we note that $Y(S)$ given in Eq. (8) is an unsuitable parameter for fitting to the experimental data as it contains little information. The straight-line fit obtained in Ref. 2 should be disregarded.

[1] M. A. Korhonen, P. Børgesen, K. N. Tu, and C.-Y. Li, J. Appl. Phys. 73, 3790 (1993).

[2] Y.-C. Joo, C. V. Thompson, and S. P. Baker, J. Appl. Phys. 85, 2108 (1999).

[3] Y.-C. Joo, S. P. Baker, and E. Arzt, Acta Mater. 46, 1969 (1998).

[4] Q. F. Duan and Y.-L. Shen, J. Appl. Phys. 87, 4039 (2000).

[5] C. F. Robertson and M. C. Fivel, J. Mater. Res. 14, 2251 (1999).

[6] In order to separate effects we have ignored the stress dependence of D_A^{eff} in this calculation. This is in common with other authors (Refs. 2–4). Including the dependence leads to an expression different from Eq. (7) but does not alter the conclusion that the maximum stress is not at the end of the fast region.

[7] M. A. Korhonen, P. Børgesen, D. D. Brown, and C.-Y. Li, J. Appl. Phys. 74, 4995 (1993).